The role of the blood-brain barrier in a mouse model of Alzheimer's disease

Dissertation
zur Erlangung des Doktorgrades
der Naturwissenschaften

vorgelegt beim Fachbereich Biowissenschaften
der Johann Wolfgang Goethe-Universität
in Frankfurt am Main

von
Amaia Dominguez-Belloso
Master of Sciences

aus Pamplona (Spanien)

Frankfurt (2020)
(D30)

Vom Fachbereich 15 der
Johann Wolfgang Goethe-Universität als Dissertation angenommen.

Dekan:	Prof. Dr. Sven Klimpel
Gutachter:	Prof. Dr. Anna Starzinski-Powitz PD Dr. Stefan Liebner

Datum der Disputation:

Table of Contents

Table of Contents

1. Summary

The blood-brain barrier (BBB) is a function found in the brain vasculature formed by endothelial cells (ECs), pericytes (PCs) and astrocytic end-feet to separate and thus protect the microenvironment of the central nervous system (CNS). It was discovered in 1885 by Paul Ehrlich and first described as such by Lina Stern in 1921 when using coloured tracers that specifically did not stain the brain.

The ECs at the BBB express tight junctional proteins that reduce the space between EC membranes and hence, impair the extracellular cross of substances from blood to brain and vice versa. ECs also have reduced transcytosis to further decrease the passage of molecules. On the other hand, ECs express a wide variety of transporters to mediate the selective crossing of essential molecules necessary to sustain the CNS or to return substances to the circulation.

The specific BBB phenotype is orchestrated and maintained by the Wnt/β-catenin signalling pathway. Neural precursor cells during development and astrocytes (ACs) in the adult, secrete Wnt molecules that bind to specific receptors in the ECs, starting a molecular cascade that leads to β-catenin translocating to the nucleus, thereby activating the transcription of BBB genes. BBB dysfunction causes ion dysregulation, edema, and neuroinflammation, which can lead to neuronal dysfunction, increased intracranial pressure, neuronal degeneration, and ultimately death. Therefore, a correct BBB functioning is vital for brain homeostasis.

An increasing number of studies report BBB dysfunction in Alzheimer's disease (AD), although the topic is currently under debate as some researchers defend that no BBB permeability changes are detected in AD. AD is a debilitating syndrome characterized by memory loss, and deterioration in thinking, behaviour, and the ability to perform everyday activities. These symptoms are commonly known as dementia, which largely affects aged people. Other brain syndromes are known to cause dementia, such as vascular dementia, Lewy Body dementia, frontotemporal dementia, Parkinson's dementia, and Hungtington's dementia. However, AD is the main cause of dementia, accounting for around two thirds of all cases, and it currently has no cure.

The most accepted hypothesis of AD, called the amyloid hypothesis, formulates that Aβ, a segment of a bigger protein called amyloid precursor protein

(APP), accumulates as aggregations leading to synaptic disruption and ultimately neuronal cell death. This Aβ fragment is produced by sequential cleavage of APP by a β-secretase coded by ***BACE1*** and a γ-secretase, a multi-subunit protease complex with a catalytic subunit coded by ***PSEN1/2***. A second protein called Tau can be pathologically hyperphosphorylated in neurons, leading to Tau tangles known as neurofibrils, also causing further neuronal damage. Both Aβ aggregations and hyperphosphorylated Tau are AD hallmarks, although the amyloid hypothesis states that the primary cause is the aberrant production of Aβ, which eventually leads to Tau hyperphosphorylation. However, the cause of imbalance in Aβ production is largely not known, with only around 5% of all AD cases having a known genetic origin. Mutations in ***APP*** or ***PSEN1/2*** can lead to Aβ over-production and accumulation, causing familiar AD. The aetiology of AD remains a mystery and consequently, I studied the role of the BBB in AD, as the current knowledge of the brain vasculature in this context is not completely understood.

The aim of my thesis was to assess if a BBB dysfunction occurs in AD, and to identify by transcriptomic analysis novel gene regulations happening at the BBB in AD. The final objective was to evaluate the potential of identified BBB genes as therapeutical target.

Many research groups use known mutations in humans to generate mouse models of AD, in which mice accumulate Aβ and show cognitive deficits. In my research, I used transgenic mice expressing the human APP mutations ***Swiss***, ***Dutch*** and ***Iowa*** under the control of the neuronal promoter ***Thy1*** (***Thy1-APP^{SwDI}***) as AD model. In this AD mouse model, I could detect Aβ deposits and memory loss by immunofluorescence (IF) and behavioural tests. Importantly, I identified an increase of BBB permeability for 3-4 kDa dextrans in 6 months, 9-12 months, and 18 months or older AD mice compared to age-matched control wild types (WT), indicating BBB dysfunction in AD mice.

In order to study the BBB transcriptional changes in AD, I sequenced the RNA from 6 and 18 months old AD and WT mouse brain microvessels (MBMVs), as well as from FACS-sorted ECs, mural cells (MuCs), ACs, and microglia (MG) in collaboration with GenXPro, a company specialized in 3' RNA sequencing.

Importantly, no public transcriptomic datasets of ECs and MuCs are currently available in the context of AD.

The data analysis of MBMV and FACS-sorted samples revealed ageing as a strong regulator of gene transcription. Alterations in early AD and in healthy ageing shared a lot of regulated genes, whereas late AD compared to healthy ageing did not show great transcriptomic differences, highlighting the strong relationship between AD and ageing.

Thanks to recently published single-cell databases from homeostatic mouse brains, I could define genes expressed exclusively by each of the cell types present in mouse brains, and elaborate a list of cell type marker genes. The sequencing results from MBMVs identified genes coming from different cell types such as ***Cldn5*** from ECs, ***Pdgfrb*** and ***Acta2*** from MuCs, ***Aqp4*** from ACs, ***Itgam*** from MG, ***Mbp*** from oligodendrocytes, and ***Thy1*** from neurons, among others. As expected, the analysis of marker genes present at the MBMV sequencing dataset revealed an enrichment of EC markers, validating the sample quality. Unfortunately, FACS-sorted AC samples did not show AC marker genes and had to be discarded from data analysis. On the other hand, EC and MG samples showed pure expression of their correspondent marker genes, indicating a good purity and sample quality. MuC samples also showed a good exclusive expression of MuC marker genes, except 2 samples from the WT-6 group and 2 samples from the AD-6 group. Nevertheless, analysis of the remaining samples could still be done.

Further investigation into the specific markers present in each MBMV group identified a reduction of EC genes in healthy ageing (WT-18 compared to WT-6). A subsequent analysis of Erg^{+} cells in CD31 stained vessels demonstrated the reduction of ECs per vessel length in ageing and, importantly, in early AD (AD-6). Decreased brain capillary density in ageing and AD has been reported already. The finding, by marker analysis of MBMV samples, was thus a good indication of the validity of the method and served to obtain an overview of pronounced cell population swifts. Other changes detected by marker analysis were a trend of reduced PCs (p value = 0.05) and augmented ACs in ageing. The reduction of PCs with ageing has been demonstrated by other groups, and the increase of ACs might be due to astrogliosis, which is known to happen in ageing and involves abundant

transcriptional changes. Smooth muscle cells (SMCs) and MG markers were shown to be increased in both AD and ageing. This could be due to the loss of ECs, which increases the proportion of attached cells to MBMVs, such as SMCs and MG. Also, a thickened intima consisting of infiltrating SMCs and MG is known to develop with ageing and might explain the increased marker expression of those cell types.

An important finding in MBMV samples, later confirmed by the FACS-sorted EC samples, was the repression of the Wnt/β-catenin signalling pathway, along with an increase of inflammatory genes such as ***Ccl3***. A reduced Wnt/β-catenin signalling together with a pro-inflammatory state could explain the BBB dysfunction observed in AD mice. Along the same line, exclusive data from MuC samples revealed a set 11 genes strongly regulated in both AD groups. Three of those 11 genes are known to be involved in inflammatory processes, demonstrating that inflammation affects and plays an important role in MuCs and ECs during AD.

Many studies have been published in recent years about bulk or single-cell RNA sequencing of MG in AD from AD mouse models and human patients. Thanks to the published data, some up-regulated MG genes in AD are well known and recognized, such as ***Trem2*** and ***Apoe***. Those genes were found in the FACS-sorted MG data as well, validating the AD model and with it, the other novel sequenced datasets.

Importantly, one of the strongly AD-regulated genes in MBMV and MG samples was ***Dkk2***, a member of the Dickkopf family of secreted proteins known to be involved in Wnt signalling modulation. To test whether the Dkk2 protein would modulate canonical Wnt signalling, I performed a dual luciferase reporter assay with and without Dkk2. The results show a clear Wnt/β-catenin inhibition due to Dkk2 presence, therefore confirming its role as a Wnt signalling repressor. The ***Dkk2*** up-regulation in MG could as well explain the BBB dysfunction observed in AD. An immunohistochemistry (IHC) examination of DKK2 in human brain autopsy tissue from an AD patient and age-matched control revealed a stronger DKK2 immunoreactivity in the AD brain. This is however a preliminary result and a bigger n number is needed to confirm the discovery.

In order to answer the question whether a rescue of BBB function would ameliorate AD symptoms, I made use of a tamoxifen-inducible transgenic mouse

line to activate the Wnt/β-catenin pathway specifically in ECs, leading to a gain of function (GOF) condition. ***Cdh5***-CreERT2$^{+/-}$/***Ctnnb1***(Ex3)$^{fl/fl}$ mice express the Cre recombinase only in ECs, where it deletes the exon three of β-catenin, which encodes the phosphorylation sites and prevents protein labelling for proteasomal degradation. Therefore, β-catenin is constitutively active, promoting Wnt/β-catenin signalling. This mouse line was then crossed with the AD line, creating AD/GOF and AD/control groups.

AD/GOF mice performed better in a Y-maze memory test than AD/controls when the Wnt/β-catenin pathway was induced before AD onset (before 3 month-of-age), indicating a protective effect. Moreover, the finding implies that shielding BBB functioning in AD further protects the brain from AD toxic effects, suggesting an important role of brain vasculature in AD and its potential as therapeutic target.

Overall, the data produced in this project offer novel opportunities for the study of AD. The transcriptomic changes in ECs and MuCs prove that the role of the BBB in AD should not be disregarded. Likewise, the protective effect that the vasculature has in the AD brain supports the current search of new treatment strategies, offering novel potential candidates.

2. Zusammenfassung

Die Blut-Hirn-Schranke auf Ebene der Mikrovaskulatur des Gehirns ist aufgebaut aus Endothelzellen (ECs), Perizyten (PCs) und Astrozyten-Endfüßchen und schützt das Hirnparenchym vor äußeren Einflüssen. Die Blut-Hirn-Schranke wurde im Jahre 1885 von Paul Ehrlich durch eine Fabrstoffinjektion mit ausbleibender Anfärbung von Hirnparenchym entdeckt und zuerst 1921 durch Lina Stern beschrieben.

Die Endothelzellen der Blut-Hirn-Schranke exprimieren tight junctions die den Interzellulärspalt zwischen den Endothelzellmembranen reduzieren und den extrazellulären Transport von Substanzen aus der Blutbahn in das Hirnparenchym und vice versa beeinträchtigen. Endothelzellen weisen zudem eine reduzierte Transzytose auf, was die Molekülpassage weiter reduziert. Andererseits exprimieren Endothelzellen eine große Anzahl an Transportern, welche den selektiven Übertritt von essentiellen Molekülen in das zentrale Nervensystem (ZNS) oder vom ZNS in die Blutbahn vermitteln.

Die Integrität der Blut-Hirn-Schranke wird durch den Wnt-/Beta-Catenin-Signalweg aufrechterhalten. Sowohl Astrozyten (im Erwachsenen) als auch neuronale Vorläuferzellen (während der Entwicklung) sezernieren Wnt-Moleküle, die an spezifische Rezeptoren auf den Endothelzellen binden und dadurch eine Signalkaskade, die in die Translokation von Beta-Catenin in den Zellkern mündet, in Gang setzen, wodurch die Transkription von Blut-Hirn-Schranken-relevanten Genen initiiert wird. Eine dysfunktionale Blut-Hirn-Schranke kann zu Ionenverschiebungen, Ödemen und einer Neuroinflammation führen; dies wiederum kann zu einer neuronalen Dysfunktion, einem erhöhten intrakranialen Druck, einem neuronalen Untergang und letztendlich zum Tode führen. Aus diesem Grund ist eine funktionierende Blut-Hirn-Schranke unabdingbar für die Homöostase des Hirnparenchyms.

Immer mehr Studien zeigen eine Assoziation zwischen einer dysfunktionalen Blut-Hirn-Schranke und der Alzheimerschen Erkrankung auf, obschon diese Thematik gegenwärtig kontrovers diskutiert wird, da manche Autoren der Ansicht sind, dass im Kontext des Morbus Alzheimer keine Veränderungen der Blut-Hirn-Schranken-Permeabiliät beobachtet werden können. Der Morbus Alzheimer ist eine

Erkrankung, welche durch einen Gedächtnisverlust, Denkstörungen, Verhaltensauffälligkeiten sowie einer abnehmenden Fähigkeit zur Verrichtung alltäglicher Aktivitäten charakterisiert ist. Diese Symptomatik ist im Allgemeinen als Demenz bekannt, die überwiegend die alternde Bevölkerung betrifft. Neben der Alzheimerschen Demenz sind weitere Demenz-Erkrankungen, wie die vaskuläre Demenz, die Lewy-Body-Demenz, die frontotemporale Demenz, die Demenz im Rahmen des Morbus Parkinson sowie die Demenz im Rahmen der Chorea Huntington bekannt. Die Alzheimersche Demenz wird mit etwa zwei Dritteln aller Demenzfälle als Hauptursache eines demenziellen Syndroms angesehen und ist gegenwärtig nicht heilbar.

Die meist akzeptierte Hypothese zur Ursache des Morbus Alzheimer ist die sogenannte Amyloid-Hypothese, gemäß derer es im Rahmen von Amyloid-Beta-Akkumulationen, hervorgehend aus dem Amyloid-Precursor-Protein (APP) zu einem neuronalen Zelluntergang sowie einem Synapsenverlust kommt. Die Amyloid-Beta-Fragmente werden durch die sequentielle enzymatische Spaltung des APP durch die ß-Sekreatase, kodiert durch das BACE1-Gen und die γ-Sekretase, kodiert durch unter anderem PSEN1/2 produziert. Daneben kann die Hyperphosphorilierung vom Tau-Protein zu intraneuronalen, fibrillären Tau-Tangles, sogenannten Neurofibrillen führen, welche ebenso den neuronalen Zelluntergang fördern. Sowohl die Aß-Aggregate als das hyperphosphorilierte Tau sind wesentliche Charakteristika des Morbus Alzheimer, obschon gemäß der Amyloid-Hypothese die primäre Ursache der Alzheimer-Erkrankung in der Aß-Überproduktion liegt, welche nachfolgend in eine Tau-Hyperphosphorilierung mündet. Die eigentliche Ursache des Ungleichgewichts bezüglich der Aß-Produktion ist weitgehend unbekannt und nur etwa 5% der Alzheimer-Fälle sind auf eine genetische Ursache zurückzuführen. Mutationen in den Genen APP oder PSEN1/2 können zu einer Aß-Überproduktion und -Akkumulation führen, welche die familiäre Form des Morbus Alzheimer verursachen. Die genaue Ätiologie der Alzheimerschen Erkrankung bleibt mysteriös; der Fokus der vorliegenden Arbeit lag auf der Rolle der Blut-Hirn-Schranke im Kontext der Alzheimer-Erkrankung, da der Einfluss der Vaskulatur des Gehirns in diesem Kontext nicht vollständig verstanden ist.

Zusammenfassung

Das Ziel der vorliegenden Arbeit lag in der Untersuchung einer Assoziation zwischen einer dysfunktionalen Blut-Hirn-Schranke und dem Morbus Alzheimer und der Identifikation neuartiger Genregulationen auf Ebene der Blut-Hirnschranke im Kontext der Alzheimerschen Erkrankung auf Basis von Transkriptomanalysen. Das übergeordnete Ziel bestand in der Aufdeckung potentiell therapierelevanter Blut-Hirn-Schranken-Gene.

In vielen Arbeitsgruppen werden bekannte humane Mutationen zur Generierung von transgenen Mausmodellen, welche den Morbus Alzheimer abbilden und in denen es zur Akkumulation von Aß und zur Ausbildung kognitiver Defizite kommt, benutzt. Für die vorliegende Arbeit wurden transgene Mäuse, welche das humane APP mit den sogenannten schwedischen, niederländischen sowie der Iowa-Mutation unter der Kontrolle des neuronenspezifischen Thy1-Promoters benutzt (Thy1-APPSwDI). In diesem Tiermodell konnten in dieser Arbeit fluoreszenzmikroskopisch Aß-Ablagerungen sowie ein Gedächtnisdefizit in Verhaltensexperimenten gezeigt werden. Bemerkenswert ist eine beobachtete Zunahme der Permeabilität der Blut-Hirn-Schranke für 3-4 KDa Dextrane in den sechs, 9-12 sowie 18 und mehr Monate alten AD-Mäusen im Vergleich zu altersangepassten Kontrolltieren (Wildtyp); dies deutet auf eine dysfunktionale Blut-Hirn-Schranke im Kontext des M. Alzheimer hin.

Um potentielle transkriptionale Veränderungen auf Ebene der Blut-Hirn-Schranke zu detektieren, wurde einerseits eine RNA-Sequenzierung der Hirn-Mikrovaskulatur von sechs und 18 Monate alten AD- und Wildtyp-Mäusen und andererseits eine RNA-Sequenzierung von FACS- (fluorescence activated cell sorting) sortierten ECs, muralen Zellen (MuCs), ACs und Mikroglia (MG) in Kollaboration mit GenXPro, einem Unternehmen mit Spezialisierung auf die 3‘-RNA-Sequenzierung, durchgeführt. Gegenwärtig sind keine Transkriptomdaten zu Endothelzellen oder muralen Zellen im Kontext des Morbus Alzheimer öffentlich zugänglich.

Im Rahmen der Auswertung der Sequenzierungsdaten der MBMV und FACS-sortierten Zellen konnte das Alter als starker Regulator der Genexpression identifiziert werden. Insgesamt zeigte sich eine Überlappung unterschiedlich regulierter Gene zwischen einerseits jungen AD-Mäusen und andererseits

gesunden, alternden Mäusen im Vergleich zu jungen Wildtyp-Mäusen. Diese Überlappung war zwischen gealterten AD-Tieren und gesunden, gealterten Tieren nicht mehr zu beobachten, was auf eine starke Korrelation zwischen dem Altern und dem Alzheimer-Phänotyp hinweist.

Auf Basis von kürzlich veröffentlichten Single-Cell-Datensätzen von homöostatischen Mausgehirnen war es möglich, Zelltyp-spezifische Gene im Mausgehirn zu definieren. In den Sequenzierdaten der MBMVs konnten Zelltyp-spezifische Gene wie beispielsweise Cldn5 aus ECs, Pdgfrb und Acta2 aus MuCs, Aqp4 aus ACs, Itgam aus MG, Mbp aus Oligodendrozyten und Thy1 aus Neuronen, neben weiteren Zelltyp-spezifischen Markern, identifiziert werden. Erwartungsgemäß konnte in den MBMV-Sequenzierdaten eine Anreicherung von Endothelzell-spezifischen Markergenen gezeigt werden; dies unterstreicht eine hohe Probenqualität. Da in den FACS-sortierten AC-Proben keine AC-Markergene gefunden werden konnten, wurden diese von den weiteren Analysen ausgeschlossen. Darüber hinaus konnte in den EC- und MG-Datensätzen eine Expression der korrespondierenden Markergene, hinweisend auf eine hier gute Probenqualität und -reinheit, nachgewiesen werden. In den MuC-Proben zeigte sich eine exklusive Expression von MuC-Markergenen, abgesehen von zwei Porben aus der WT-6-Gruppe und zwei Proben aus der AD-6-Gruppe. Unabhängig davon konnte eine Analyse der verbleibenden Proben durchgeführt werden.

In den weiterführenden Analysen bezüglich spezifischer Markergene konnte eine Reduktion von EC-Genen in den gesunden, gealteren Tieren gezeigt werden (WT18 im Vergleich zu WT6). In einer darauffolgenden A656nalyse von Erg+-Zellen in mit CD31 gefärbten Gefäßen konnte eine Reduktion der EC bezogen auf die Gefäßlänge in den alternden Tieren und in den jungen AD-Tieren demonstriert werden (AD6). Eine verminderte Kapillardichte in alternden Tieren und transgenen AD-Tieren konnte bereits gezeigt werden. Im Rahmen der Markergenanalyse, welche die Validität der Methodik aufzeigte, war es möglich, sich einen Überblick über übergeordnete Zellpopulationsveränderungen zu verschaffen. Zu den Veränderungen, welche im Rahmen der Markergenanalyse aufgedeckt werden konnten, gehörten der Trend zu einer PC-Reduktion (p-Wert = 0,05) und eine Zunahme an AC in den alterenden Tieren. Eine Reduktion der PCs im Alter wurde

auch von anderen Arbeitsgruppen gezeigt; die Zunahme von ACs könnte in der Entwicklung einer Astrogliose begründet sein, welche bekanntermaßen im Alter zunehmend auftritt und mit verschiedenartigen transkriptionalen Veränderungen einhergeht. Glattmuskuläre Zellen (SMCs) und MG-Markergene zeigten sowohl in den AD-Tieren als auch in den alternden Tieren eine Zunahme. Diese Beobachtung könnten an dem Verlust von EC liegen, wodurch eine proportionale Zunahme an adhärenten Zellen der Mikrovaskulatur, wie beispielsweise SMCs und MG, hervorgerufen werden könnte. Daneben ist eine Verdickung der Intima, welche aus infiltrierenden SMCs und MG besteht im Alter beschrieben; dies ist eine mögliche zusätzliche Erklärung für die Zunahme der entsprechenden Markergene.

Eine wichtige Entdeckung in den MBMV-Proben, später auch in den FACS-sortierten Proben bestätigt, war die Inhibition des Wnt-Beta-Catenin-Signalweges sowie die Zunahme inflammatorischer Gene wie beispielsweise Ccl3. Eine reduzierte Aktivität des Wnt-Signalweges sowie ein pro-inflammatorischer Status könnte die beobachtete dysfunktionale Blut-Hirn-Schranke in AD-Mäusen erklären. In den Daten der MuC-Proben konnten elf Gene mit unterschiedlicher Genregulation in den AD-Tieren aufgezeigt werden. Drei dieser elf Gene sind bekanntermaßen bedeutsam für inflammatorische Prozesse; dies deutet auf einen Einfluss inflammatorischer Abläufe auf MuCs und ECs im AD-Kontext hin.

Innerhalb der letzten Jahre wurden viele Publikationen über die Gesamt- oder Single-Cell-RNA-Sequenzierung von MG in AD-Tieren und Alzheimerpatienten veröffentlicht. Gemäß dieser veröffentlichten Datensätze sind bestimmte MG-assoziierte Gene wie beispielsweise Trem2 oder Apoe im AD-Kontext aufreguliert. Diese Gene wurden auch in den FACS-sortierten MG-Datensätzen gefunden, was die Validität des für diese Arbeit benutzten AD-Modells unterstreicht.

Eines der in den AD-Mäusen unterschiedlich regulierten Gene in den MBMV- und MG-Datensätzen war Dkk2, welches ein Mitglied der sogenannten Dickkopf-Familie aus sezernierten Proteinen, die in die Modulation des Wnt-Signalweges involviert sind, gehört. Um zu testen, ob das Dkk2 tatsächlich den kanonischen Wnt-Signalweg beeinflusst, wurde ein Luciferase Reporter Assay mit Dkk2 und ohne Dkk2 angewandt. Aus diesem Experiment ging eine eindeutige Inhibition des Wnt-Signalweges durch die Präsenz von Dkk2 hervor; dies bestätigt die Wnt-

repressive Funktion des Dkk2. Die Dkk2-Aufregulation in den MG könnte die dysfunktionale Blut-Hirn-Schranke im AD-Kontext erklären. Im Rahmen einer immunhistochemischen Analyse der Dkk2-Expression in humanem Autopsiegewebe eines Alzheimerpatienten und einem altersangepassten Kontrollgewebe konnte eine stärkere Immunreaktivität gegenüber Dkk2 im Alzheimergewebe gezeigt werden. Dies stellt allerdings ein vorläufiges Resultat dar, welches in einer größeren Kohorte bestätigt werden sollte.

Zur Adressierung der Frage, ob eine Verbesserung der Blut-Hirn-Schranken-Integrität möglicherweise eine Alzheimer-Symptomatik positiv beeinflussen kann, wurde eine transgene AD-Mauslinie mit Expression eines Tamoxifen-induzierbaren Cre-Rekombinase-Estrogenrezeptor-Ligandenbindungsdomänen-Fusionsproteins unter der Kontrolle des Endothelzell-spezifischen Cdh5-Promoters nach dem Prinzip des Cre-LoxP-Rekombinationssystems als AD-Gain-of-Function (AD-GOF) Mausmodell benutzt; der LoxP-flankierte Genabschnitt ist in diesem Modell das Exon 3 des Beta-Catenin-Gens, welches durch die Tamoxifen-induzierbare Translokation der Cre-Rekombinase in den Nukleus exzidiert wird (Cdh5-CreERT2+/–/Ctnnb1(Ex3)fl/fl). Das entsprechende Beta-Catenin-Produkt wird durch den Beta-Catenin-Degradationskomplex nicht abgebaut und akkumuliert im Zytosol, wodurch der Wnt-Signalweg überaktiviert wird.

Die AD-GOF-Mäuse zeigten eine Gedächtnisverbesserung in dem Y-Maze-Verhaltensexperiment im Vergleich zu den AD-Kontrolltieren, sofern die Überaktivierung des Wnt-Signalweges bereits vor Ausbruch der Alzheimersymptomatik und des Alzheimer-Phänotyps (in Tieren jünger als drei Monate) induziert wurde; dies zeigt einen potentiellen protektiven Effekt auf. Diese Erkenntnis zeigt darüber hinaus einen protektive Wirkung einer intakten Blut-Hirn-Schranke in Bezug auf toxische Effekte im Rahmen des Morbus Alzheimer auf; dies suggeriert eine bedeutende Rolle der Gehirnvaskulatur im AD-Kontext sowie einen potentiellen therapeutischen Angriffspunkt.

Insgesamt eröffnen die im Rahmen dieser Arbeit generierten Daten neuartige Ansätze zum Verständnis des Morbus Alzheimer. Die transkriptionalen Veränderungen in den ECs und MuCs zeigen, dass der Einfluss der Blut-Hirn-Schranke auf den Morbus Alzheimer nicht unterschätzt werden sollte. Der

protektive Effekt der Vaskulatur auf das Alzheimer-Gehirn unterstreicht die Dringlichkeit zur Suche nach neuartigen Therapiemöglichkeiten auf dieser Ebene und eröffnet mögliche neue Kandidaten für einen Therapieansatz.

3. Introduction

The present section focuses on the literature knowledge about the blood-brain barrier and Alzheimer's disease, in an effort to offer an up-to-date view that serves as a basis to follow the rest of the thesis.

3.1. The blood-brain barrier

The BBB, or its evolutionary equivalent (see 3.1.2 Evolution of the BBB), is an essential cellular function of all metazoans with a CNS. It exists to separate and thus protect the microenvironment of the CNS (brain) from the rest of the body (blood/hemolymph).

3.1.1. Discovery

The BBB was first described in 1885 by Paul Ehrlich although he did not use the same terminology to refer to the BBB. He injected rats subcutaneously with alizarin blue and observed that, while the tissues were stained in blue, the brains were always tracer-free (**Figure 1**; Ehrlich 1885). After this first study others followed with similar observations, however it was not until 1921 when the name "blood-brain barrier" was first used by Lina Stern and Raymond Gautier. They injected dogs, cats, rabbits and guinea pigs intravenously with different compounds and measured the concentration in the blood and the cerebrospinal fluid (CSF). They found that those compounds with known effect in the nervous system, such as morphine, were detectable in both blood and CSF while others, like India ink, were found only in blood. Consequently, Stern and Gautier coined the term "blood-brain barrier" that we still use nowadays (Stern and Gautier 1921).

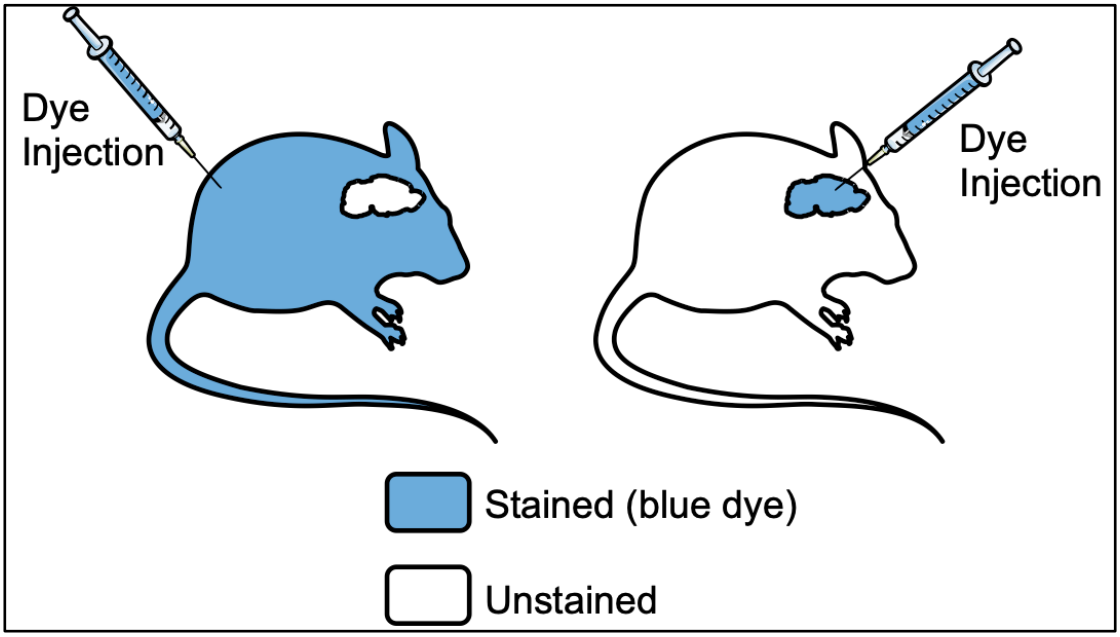

Figure 1: Representation of original experiments by Paul Ehrlich with alizarin blue. The dye cannot cross the BBB and shows the separation between brain and body. From https://brainbarriers4you.eu

3.1.2. Evolution of the BBB

Highly specialized structures compel highly specialized functions. The BBB is no exception and hence, throughout evolution, it is possible to observe the intimate link between its structure and function. In invertebrates such as flies, the nervous system consists of a primitive brain, and the circulatory system is open with hemolymph surrounding all cells except the nerve cells of the brain (**Figure 2**). This separation is achieved by glial cells, that express nutrient transporters and have specialized septate junctions, forming the hemolymph–brain barrier (O'Brown, Pfau, and Gu 2018). In vertebrates, a closed vascular system has already evolved. As CNS complexity advances through taxa, so does the brain-barriers complexity. Thus, in numerous cartilaginous fish like sharks, where the neuronal complexity is still not high, the BBB is still maintained by glial cells expressing tight junctions (**Figure 2**). These glial cells evolved to surround the blood vessels of the brain, which are composed by ECs and PCs, but they are not different from the ECs of the rest of the body (O'Brown, Pfau, and Gu 2018). In hagfish, teleost ray-finned fish, and amniotes (mammals, reptiles, and birds), their CNS has increased total neuronal abundance, complexity, and displays stereotypic neuronal migration away from the ventricular surface during development. The BBB of those organisms is

made of ECs expressing tight junctions, with PCs supporting them and a layer of glial cells around (O'Brown, Pfau, and Gu 2018). Thus, all animals require a separation between their CNS and the periphery, highlighting the importance of having an isolated CNS with the correct homeostasis control (**Figure 2**). Losing this separation leads to brain damage and ultimately death (see 3.1.5. The BBB in disease). Alzheimer's disease is an example of a condition in which BBB impairment has been described. Consequently, understanding the structure and regulation of the BBB is essential to prevent and/or treat Alzheimer's and other diseases.

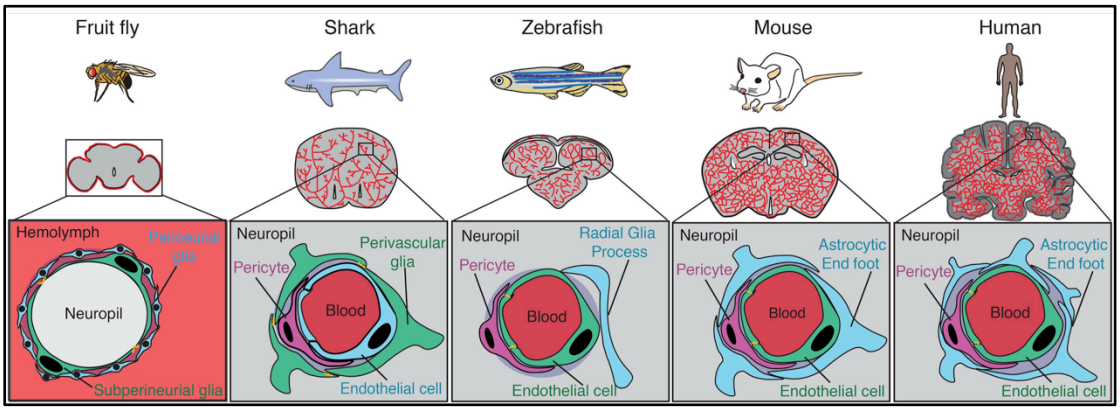

Figure 2: Functional conservation of the brain barrier across organisms (O'Brown, Pfau, and Gu 2018).

3.1.3. Structure of the mammal BBB

Many experiments have been performed to understand the nature of the BBB since its discovery. Now we know that we can distinguish two levels of specialization: the cellular level and the molecular level.

3.1.3.1. Cellular components

The CNS contains not only neurons but also other cell types such as ACs, MG or oligodendrocytes (OLs). All these cells constantly demand oxygen and nutrients but at the same time they require protection to maintain the special brain homeostasis. The biological structure of the BBB comprises three main cell types: ECs, PCs and ACs. See below a schematic representation in **Figure 3** (Zenaro, Piacentino, and Constantin 2017).

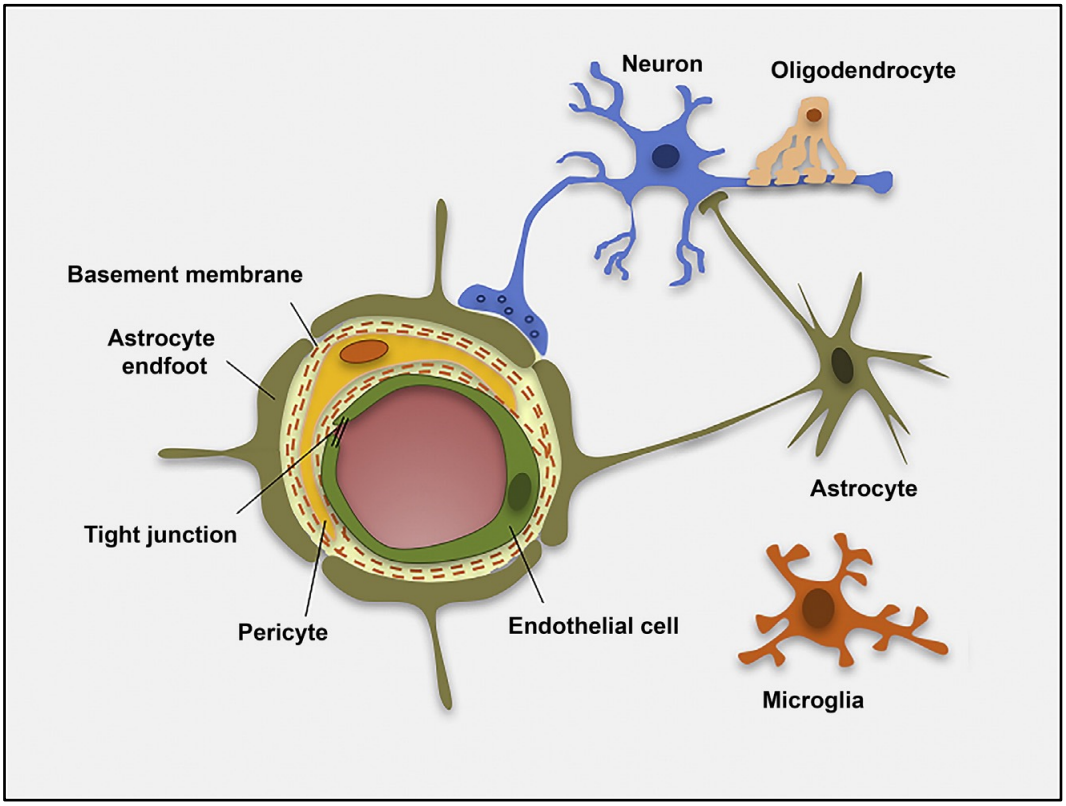

Figure 3: The cellular components of the BBB (Zenaro, Piacentino, and Constantin 2017).

3.1.3.1.1. ECs

The blood vessels of the entire body are made of ECs, which adopt an elongated shape to build, like bricks, the vessel wall. In humans, the endothelium weighs approximately 1 kg in average and covers a total surface area of 4000 to 7000 m^2 (the equivalent to a football field; Kitchens 2013). The exchange of substances between the blood and tissues occurs at the capillary level, which is the smallest vessel diameter (less than 10 μm) where a sequence of single ECs stretches out to form the lumen. Some authors have estimated the number of capillaries in the human brain to be around 100 million with a surface area of ~12 m^2 (Newman et al. 2002). This means that virtually every neuron has its own capillary, with an approximated distance from a capillary to a neuron of 8 to 20 μm (Schlageter et al. 1999). It is clear that for a molecule or cell to cross from the blood to the tissue parenchyma or vice versa, they need to traverse the EC layer. They can do it either between the borders of the ECs – paracellular way – or through an EC – transcellular way (**Figure 4**; Engelhardt and Wolburg 2004). Both processes are

highly regulated and thus, ECs express a series of junctions and transporters that are tissue-specific, allowing ECs to be selective or permissive according to tissue and conditions.

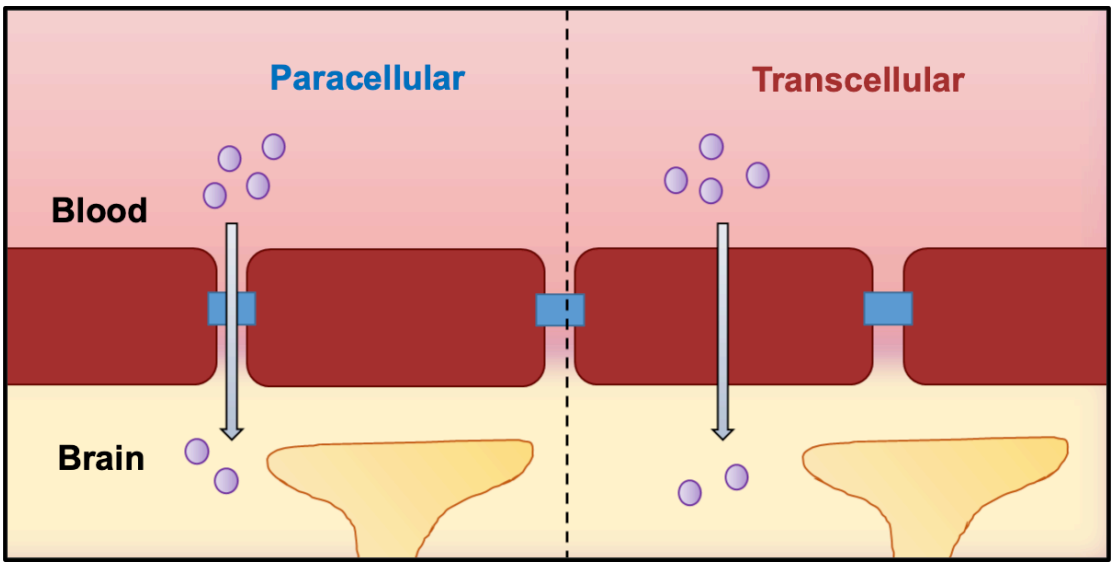

Figure 4: Paracellular vs. transcellular way across the endothelial barrier of the BBB. From https://brainbarriers4you.eu

ECs are polarized, adopting different properties at the luminal membrane (in contact with the blood stream), at the abluminal membrane (in contact with the parenchymal tissue), and at the basolateral membrane (in contact with other ECs), highlighting the specialized function of ECs. Specific structural proteins are expressed at the basolateral membrane that attach the endothelial membranes to each other, closing the gap between them and therefore, impairing the passage of substances. This is particularly important in the CNS and thus, it is explained in more detail at the "Junctions" section (3.1.3.2.1). At the luminal membrane, a network of membrane-bound proteoglycans, glycosaminoglycans and glycoproteins form the so-called glycocalyx (from Greek ***glykys*** meaning "sweet" and ***kalyx*** meaning "husk"). It was first visualized by Luft in 1966 using the electron microscope with ruthenium red staining (Luft 1966), but the concept originates from the initial observations by Danielli (Danielli 1940) and Chambers and Zweifach (Chambers and Zweifach 1947), who saw a thin, non-cellular layer on the endothelial surface (**Figure 5**). The glycocalyx has a thickness ranging from 0,5 to 1 μm and is involved in many important functions such as regulation of blood flow,

inflammatory responses, blood coagulation and endothelial permeability (Pries, Secomb, and Gaehtgens 2000; Hayden 2019). Hence, it plays an important role in diseases like atherosclerosis, stroke, hypertension and chronic kidney disease (Tarbell and Cancel 2016). By contrast, the abluminal membrane is characterized by the absence of a glycocalyx and the presence of transporters and structural proteins, which anchor the cell to the surrounding basement membrane (BM). The BM is an essential structure present in all metazoans. During evolution, it appeared at the same time as multicellularity, suggesting a crucial role in tissue establishment (Jayadev and Sherwood 2017). The BM is defined as a thin but dense, sheet-like specialized and self-assembled type of extracellular matrix that surrounds the majority of animal tissues. Certainly, it is present at the endothelium level, surrounding the ECs (**Figure 5**). In blood vessels, the BM is made of two independent polymeric networks: laminin and type IV collagen; they form a stable intertwining mesh which stops the transmigration of most cells (except leukocytes). Additionally to its tissue separation and barrier function, the BM serves as an adhesive substrate and signalling platform for migration, polarization, differentiation, tissue shaping, and growth (Sekiguchi and Yamada 2018).

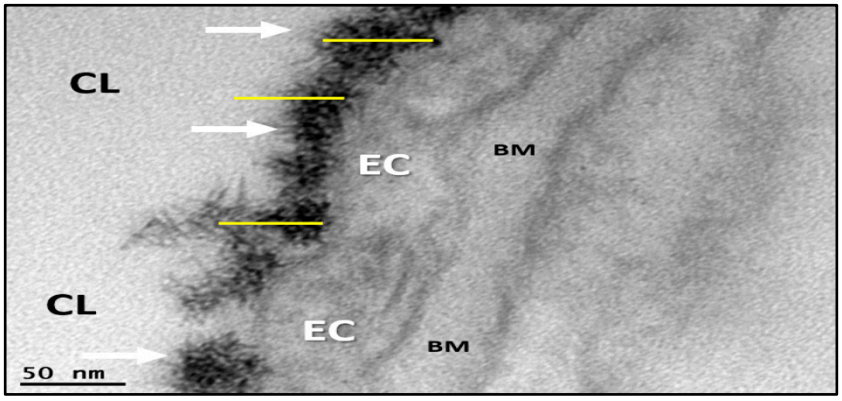

Figure 5: electron microscopy image of ECs showing the capillary lumen (CL), glycocalyx (arrows), and the basement membrane (BM). Yellow bars represent 50 nm (Hayden 2019).

Depending on the tissue where the vessels are, they acquire different and specialized properties. One of the main differences is the change in permeability, i.e., how permissive or restrictive is the endothelium to the passage of substances (Augustin and Koh 2017; Potente and Mäkinen 2017). In fact, the endothelium is

discontinuous in liver, spleen, and bone marrow– allowing the free crossing of molecules (but not cells) – while in the kidneys, endocrine glands, circumventricular organs, and choroid plexus of the brain, the ECs are fenestrated – letting the passage of small peptides through membrane pores (**Figure 6**). In the rest of the body, the endothelium is continuous and therefore, only permits the diffusion of water, small solutes, and lipid-soluble materials without any loss of circulating cells and plasma proteins (Augustin and Koh 2017; Potente and Mäkinen 2017).

An even more specialized type of continuous endothelium exists in the CNS (**Figure 6**), where the ECs of the BBB express exclusive junctional proteins, which firmly close the spaces in between the ECs, restricting the crossing of polar and water soluble substances (see 3.1.3.2.1. Junctions). Another distinctive characteristic of the BBB endothelium is the low rate of transcytosis, i.e., the vesicle transport of macromolecules across the ECs is reduced. This, together with the expression of specific transporters that only permit the passage of selected molecules (see 3.1.3.2.2. Transporters), allow the ECs to provide the CNS cells with the required substances and at the same time protect them from external pathogens and toxic elements (Obermeier, Daneman, and Ransohoff 2013; Zhao et al. 2015).

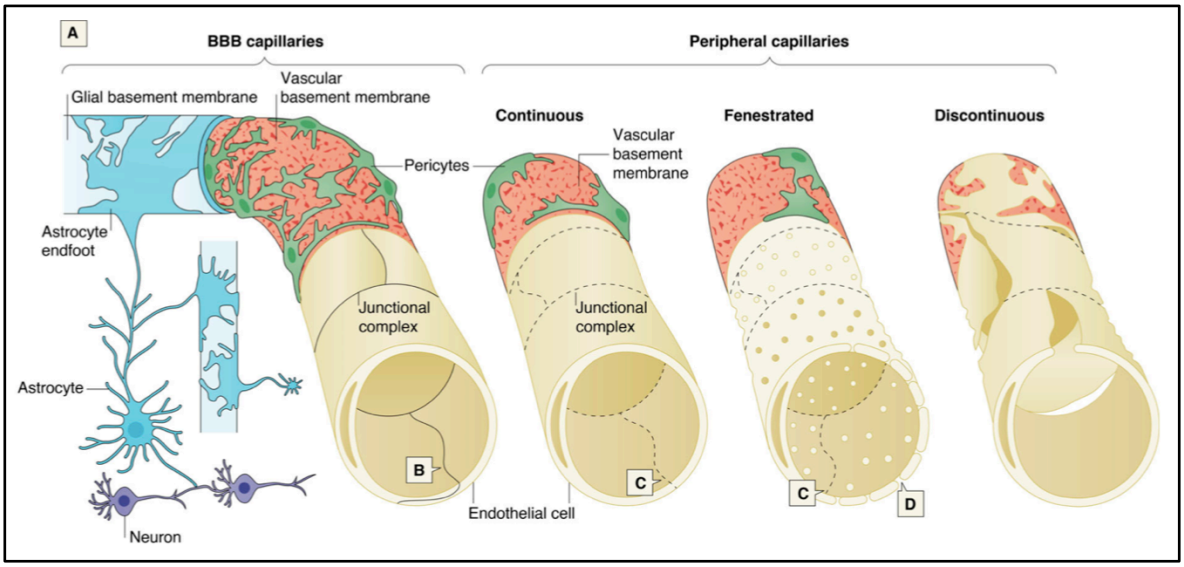

Figure 6: endothelium types. (A) BBB capillaries with (B) tight junctions. (C) Adherens junctions. (D) Fenestrations (Profaci et al. 2020).

Due to the specialized properties of brain ECs, they are considered to form the basis of the barrier. Nonetheless, PCs and ACs play a vital role too, as it is explained below (**Figure 7**).

3.1.3.1.2. PCs

The term pericyte comes from the Greek words ***peri*** (meaning "around") and ***cyte*** ("cell"), indicating the morphology of PCs as the cells surrounding ECs. This term was first used in 1923 (Zimmermann 1923) and although the discovery of PCs is commonly attributed to Charles-Marie Benjamin Rouget (Rouget 1873) – who described a population of contractile cells surrounding ECs of small blood vessels – it was two years before that their presence was first noticed (Eberth 1871). With the development of new techniques such as the electronic microscope, the PC was defined as a cell embedded within the vascular BM, which in fact is produced by both cell types ECs and PCs. This definition is controversial though, since the periendothelial location of PCs is frequently confused with the periendothelial location of other cell types like vascular SMCs, fibroblasts (FBs), macrophages, and even epithelial cells (Armulik, Genové, and Betsholtz 2011).

Both PCs and SMCs are mural cells, i.e., the cells lining the vascular wall at the abluminal side (**Figure 7**). The distinction between PCs and SMCs is not so sharp and for years researchers have tried to find good markers to distinguish them. It is accepted that microvessels – composed by capillaries and small arterioles and venules – are covered by PCs and the rest of bigger vessels by SMCs (Holm, Heumann, and Augustin 2018). Therefore, PCs and not by SMCs are part of the BBB (**Figure 7**). The SMCs surround the surface of the vascular wall completely and, thanks to their contraction, they regulate the blood flow. PCs however, only surround the vessel wall partially and whether they contract or not is still nowadays a matter of debate (Hill et al. 2015; Attwell et al. 2016). Some authors defend that these cells contract and help regulate blood flow in the smallest vessels but, in opposition, others argue that those studies come from misidentified SMCs, and PCs are not able to contract. One point that seems to reunite opinions is the fact that ***ACTA2*** (or Actin Alpha 2) is expressed exclusively by SMCs and it is used as a marker gene to identify this cell type. In contrast to SMCs, due to the lack of

proper marker genes for PCs, it is common to use a combination of two markers to correctly label PCs, e.g., ***PDGFRB*** and ***ANPEP***. It was only recently and thanks to the advances in single-cell RNA-Sequencing (scRNA-Seq) that it was possible to accurately characterise brain mural cells, and define their transcriptional profile according to their position in the vascular tree (Vanlandewijck et al. 2018). See **Table 1** below with the main marker genes for the individual BBB cell types.

PCs regulate angiogenesis, vessel stabilization, and support the formation of the BBB and retinal barrier. Their role is vital; a mouse lacking ***Pdgfrb***$^{+}$-PCs dies at birth, and defects in brain PCs demonstrate that they are needed to inhibit "leaky properties" – transcytosis and leukocyte adhesion molecule (LAM) expression – in ECs at the BBB (Daneman et al. 2010; Armulik et al. 2010). Brain PCs are also required for the proper astrocyte endfeet recruitment, which is the third and last but not least component of the BBB.

3.1.3.1.3. ACs

The term "glia" defines those non-neuronal cells that support neurons both in the CNS or the peripheral nervous system (PNS). ACs belong to this group and as such, they actively participate in CNS homeostasis with functions as diverse as neurotransmission, energy metabolism, modulation of blood flow, and ion and water homeostasis. They adopt a particular morphology that allows them to perform all those important roles: the cell body stretches out to form many ramifications from a central area where the nucleus is located (**Figure 7**). This star-like shape is what inspired Michael von Lenhossék to coin the name astrocyte (from Greek ***astro*** meaning "star", and ***cyte*** meaning "cell") in 1891 (von Lenhossék 1891). However, the first visualization of ACs took place twenty years before, when Camillo Golgi developed his technique of Golgi staining (Golgi 1871). Later on, Santiago Ramón y Cajal published detailed drawings that allowed the appreciation of the diversity and complexity of human astrocytes (Ramón y Cajal 1911).

ACs can reach many different neurons and blood vessels thanks to their elongations. At the connection with a vessel wall, the astrocytic ramification spreads over the ECs and PCs, comparable to a foot (the tip of the AC) stepping on

the ground (the vascular wall), and therefore this specific structure is called the astrocytic end-foot (**Figure 7**). The combination of all astrocytic end-feet completely surrounds the blood vessels, including the ECs, the PCs and the BM (Mathiisen et al. 2010). This astrocytic layer – also known as the ***glia limitans*** – reduces even further the permeability of molecules and cells, creating a small space between the BM and the ACs called the perivascular space (or Virchow–Robin space). This space can contain surveillance cells such as antigen-presenting cells. Hence, substances crossing from the blood to the CNS or vice versa must endure two cellular barriers and a surveyed space, making the BBB the highly specific and restrictive barrier that it is (Engelhardt, Vajkoczy, and Weller 2017).

Additionally, ACs are able to regulate the CNS osmotic pressure through water channels expressed specifically at their end-feet, called aquaporin-4 (***AQP4***). The unambiguous expression of ***AQP4*** makes it a useful marker for ACs, together with other genes like transporters such as Glast (***SLC1A3***), and the glial fibrillary acidic protein (***GFAP***; see **Table 1**). Postnatally, ACs regulate the maintenance of the barrier by secreting Wnts and norrin (see section 3.1.4. The Wnt pathway) and, moreover, they secrete sonic hedgehog (Shh), retinoic acid (RA), and other important factors that contribute to the BBB phenotype (Liebner et al. 2018). Thus, ACs are not only in close contact with ECs and PCs, but they also communicate and regulate their behaviour, supporting the BBB phenotype and maintaining it.

Table 1: important BBB marker genes

Cell type	Marker gene
EC	***CDH5***, ***CLDN5***, ***ERG***, ***OCLN***, ***PECAM1***
PC	***ANPEP***, ***PDGFRB***, ***VTN***
SMC	***ACTA2***, ***CNN1***, ***MYH11***
AC	***AQP4***, ***GFAP***, ***SLC1A3***

3.1.3.1.4. The NVU concept

The BBB can recognize signals coming from the blood and the brain cells, changing its behaviour to satisfy their needs. Hence, in 2001 at the 'Stroke Progress Review Group' meeting of the 'National Institute of Neurological Disorders and Stroke', a new concept was introduced to include the interaction between the brain parenchyma and the vascular compartment: the neuro-vascular unit (NVU). Since then, it has gained attention within the vascular and neuroscientific community due to the growing evidence linking neural activity with vascular activity, a.k.a. neurovascular coupling. The interactions between neurons, glia and vascular cells (**Figure 7**) have been shown to regulate many processes such as blood pressure, shear stress, body temperature, blood sugar level, and gas tension (Furtado et al. 2018). Moreover, the NVU is involved in neurodegenerative diseases like Alzheimer's dementia, frontotemporal dementia, amyotrophic lateral sclerosis, Parkinson's dementia, and dementia with Lewy bodies (Iadecola 2017). These findings highlight the complexity of the BBB regulation and its importance maintaining the CNS homeostasis.

3.1.3.1.5. MG

Microglia are considered to form the immune system of the CNS and – due to the BBB – the CNS is considered to be an immune privileged organ, i.e., immune isolated (**Figure 7**). Thus, under homeostatic conditions, there is no infiltration from blood cells and MG are in charge of functions such as phagocytosis of cellular debris, immune surveillance and synapse stripping. Furthermore, MG undergo transcriptomic and phenotypic changes according to the conditions that they sense, being able to activate the immune response and even recruit blood immune cells through interaction with the BBB (Deczkowska, Amit, and Schwartz 2018). The importance of MG in the modulation of many brain diseases, such as multiple sclerosis and Alzheimer's disease, is becoming increasingly evident and it cannot be disregarded as a mere inflammatory reaction from the injured tissue.

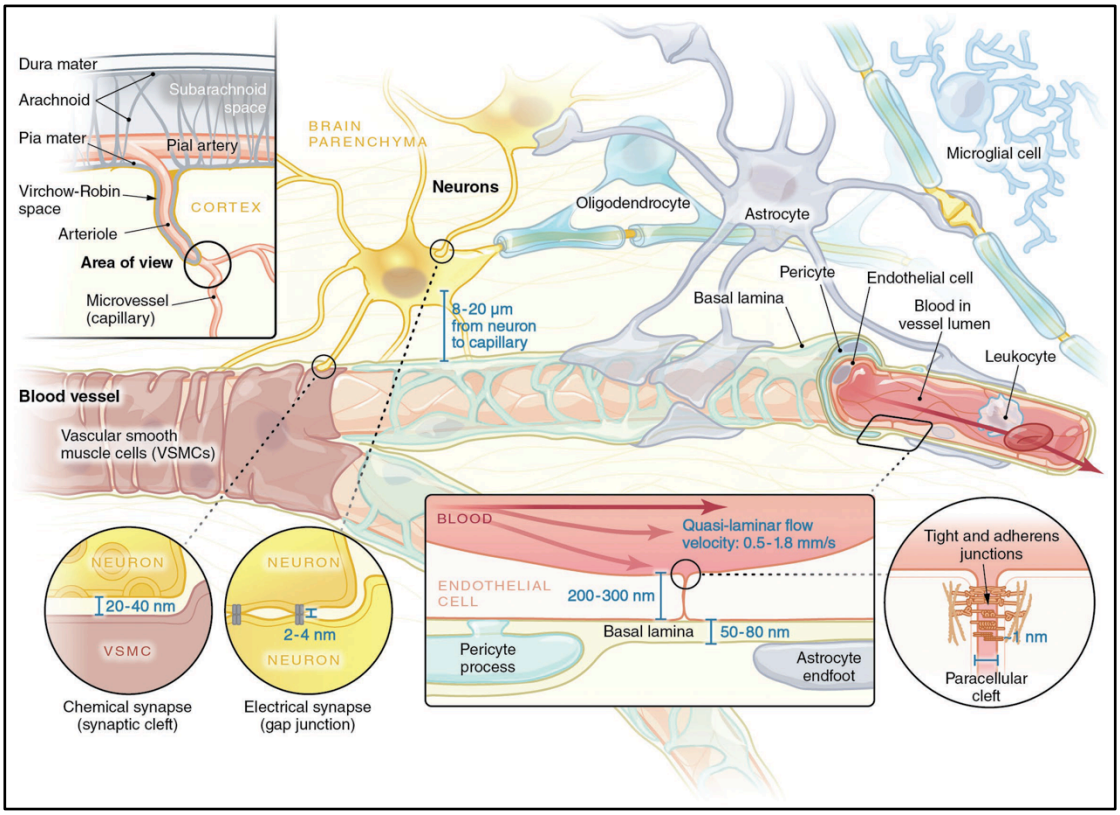

Figure 7: The NVU (Furtado et al. 2018).

3.1.3.2. Molecular components

As it is explained above, brain ECs are forming a physical barrier preventing substances to freely cross from blood, and at the same time allowing specific molecules or even cells to go through. They are able to do so thanks to the expression of specialized transporters, junctions and other adhesion molecules.

3.1.3.2.1. Junctions

ECs express many different junctional proteins that link adjacent membranes in order to stop substances passing in between them (paracellularly; **Figure 8**). According to how close the two membranes are joint, they are classified as tight junctions – with a pore of about 1 nm of diameter, preventing the passage of very small molecules (<1 kDa) and even restricting the flow of small inorganic ions (e.g., Na^+) – or adherens junctions – around 3 nm of pore diameter and therefore impermeable to albumin (69 kDa and molecular radius 3.6 nm) and other large proteins (Abbott, Rönnbäck, and Hansson 2006; Yuan and Rigor 2011).

The adherens junctions expressed by ECs are mainly formed by cadherins, but other adhesion molecules like Pecam-1 (***PECAM1/CD31***) are needed for a correct assembly (**Figure 8**). All ECs throughout the body express VE-cadherin (***CDH5/CD144***) at high levels to maintain the vessel wall integrity and restrict the general paracellular crossing of substances (Dejana and Orsenigo 2013). Moreover, adherens junctions are contemplated as a requirement for the establishment of tight junctions. The intracellular domain of VE-cadherin is anchored to the actin cytoskeleton either by β- or γ-catenin (also known as junction plakoglobin or ***JUP***), and at times with zona occludens-1 (ZO-1, also called tight junction protein 1, ***TJP1***), desmoplakin (***DSP***), or by γ-catenin together with the armadillo family protein p120^{ctn} (catenin delta-1, or ***CTNND1***). This interactions are summarized in **Figure 8** (Abbott, Rönnbäck, and Hansson 2006).

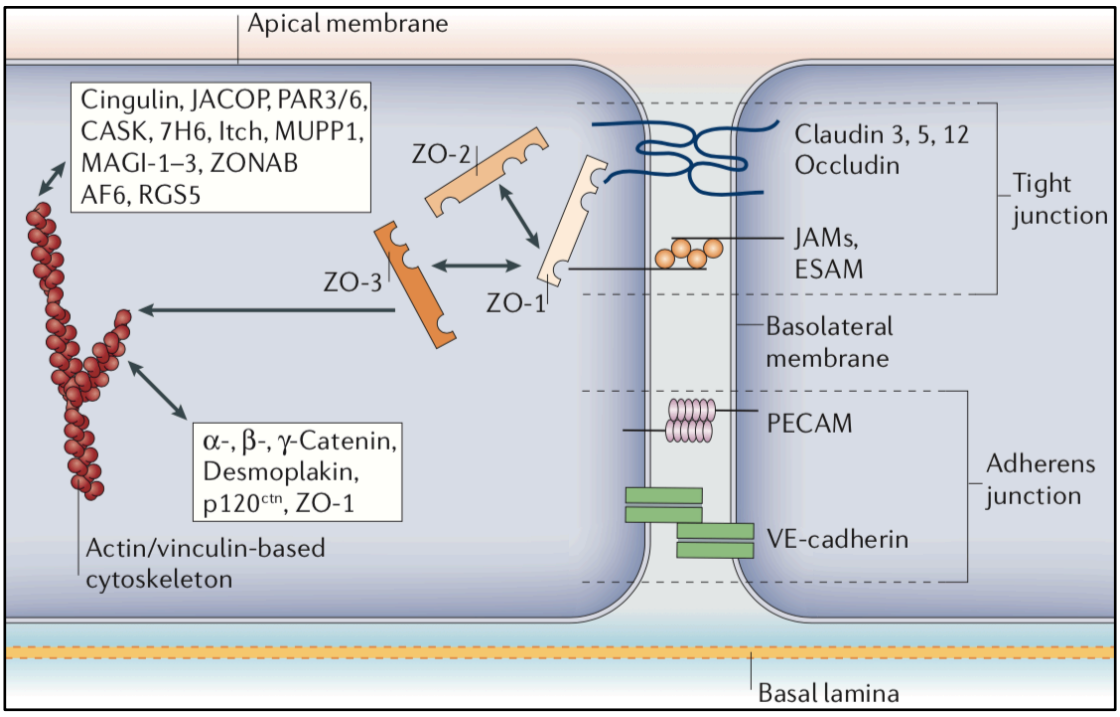

Figure 8: EC junctions (Abbott, Rönnbäck, and Hansson 2006).

Tight junctions are intercellular adhesion complexes expressed by ECs or epithelial cells under very specific conditions. Throughout the body, they are found in the distal convoluted tubule and the collecting duct of the nephron in the kidney, the bile ducts ramifying through liver tissue, the BBB, and the blood cerebrospinal fluid barrier. At the BBB, ECs express high levels of claudin-5 (***CLDN5***) and

occluding (***OCLN***), both localized at the basolateral membrane and close to the lumen, and they are the main molecules responsible for the reduced paracellular transit between brain ECs (**Figure 8**), although other molecules such as the endothelial cell adhesion molecule (***ESAM***) and junctional adhesion molecules (JAMs) contribute to tighten the EC membranes together (Liebner et al. 2018). Some authors reported that other claudins (claudin-3 and -12) are also part of the TJ machinery of brain ECs. This information is controversial with other scientists claiming otherwise (Castro Dias et al. 2019; Winkler et al. 2020). In any case, the intracellular domains of TJs are linked by protein complexes comprised of either of ZO-1 and -2 (***TJP2***), or ZO-1 and -3 (***TJP3***). These complexes are further anchored to the actin cytoskeleton by different proteins, summarized in **Figure 8**.

Claudin-5 and VE-cadherin are expressed specifically by ECs and they are widely used as endothelial markers (see **Table 1**).

3.1.3.2.2. Transporters

ECs express a battery of transporters to mediate the selective crossing of all the essential molecules necessary to sustain the CNS, or to return substances to the circulation. Broadly, brain endothelial transporters can be classified as efflux, or solute transporters.

Efflux transporters are expressed at the luminal membrane and work against the concentration gradient, returning molecules back to the blood circulation. The most known transporter of this kind is the Mdr1/P-glycoprotein (Pgp, or gene ***ABCB1***), which plays an important role limiting the entry of many xenobiotics but also endogenous molecules, and hence offering protection to the brain. It is also known to be dysregulated in Alzheimer's disease and to contribute to its pathology (Profaci et al. 2020).

Solute transporters work in favor of the concentration gradient ensuring barrier passage to specific nutrients that are vital for energy and homeostasis. The most studied transporter is glucose transporter isoform 1 (Glut-1, or gene ***SLC2A1***), which provides glucose transport to the CNS. Due to the inability of the CNS to obtain energy from circulating fatty acids, it is dependent on glucose since the brain consumes 20% of the body's glucose-derived energy but it comprises only the

2% of the body weight. Therefore, the brain relies heavily on the correct functioning of glucose transporters (Gras et al. 2014; Yazdani et al. 2019). Another example is the receptor for advanced glycation endproducts (RAGE or gene ***AGER***). RAGE belongs to the immunoglobulin super family and binds advanced glycation endproducts such as amyloid-β, one of the hallmarks in AD. Some reports show an up-regulation of RAGE in AD, which drives some of the pathophysiological changes of the disease (Cai et al. 2016). Solute transporters are also important for removing molecules from the CNS. The lipoprotein receptor-related protein-1 (***LRP1***) is a receptor for Apolipoprotein E – a lipid carrier important in AD – and is expressed by mural cells and astrocytes at the BBB. It is dysregulated in AD as well, which emphasizes the importance of transporters in diseases like AD and the need of understanding their role and regulation (Profaci et al. 2020).

3.1.3.2.3. Other molecules

The BBB expresses a diverse set of molecules that are not transporters, or do not form tight/adherens junctions. Selectins are an example of this; they belong to the cell adhesion molecule (CAM) superfamily but, unlike cadherins, they do not interact with their own extracellular structure from adjacent cells, and instead they bind to sugar polymers. The ECs of the BBB can up-regulate the expression E-selectin (***SELE***), P-selectin (***SELP***) and P-selectin glycoprotein ligand-1 (***PSGL-1***) under inflammatory conditions to mediate leukocyte and platelet adhesion. Another key molecule up-regulated during inflammation is Vcam-1 (***VCAM1***) and, together with Pecam-1, helps to initiate the BBB extravasation of blood-born cells like leukocytes to the brain (Profaci et al. 2020). The regulation of these molecules is very important in brain conditions such as multiple sclerosis and stroke, while in others like AD is not well known.

3.1.4. The Wnt pathway

Understanding the mechanisms controlling the development and maitenance of the BBB is key to treat conditions like neurodegenerative diseases, brain tumours or stroke, where BBB impairment is observed. The most important pathway orchestrating the correct BBB functioning is the Wnt/β-catenin pathway (**Figure 9**). During development, the sprouting angiogenic vessels vascularizing the brain

acquire BBB properties induced by the growth factors Wnt7a and Wnt7b secreted by neural progenitor cells. As development advances, ACs and PCs are formed and take over the duty of secreting Wnt7a and Wnt7b and hence, maintaining the endothelial BBB phenotype.

The Wnt7 molecules are recognized at the EC membrane by the receptors Frizzled 4 (***FZD4***) and reversion-inducing cysteine-rich protein with Kazal motifs (***RECK***). They form a receptor complex with the co-receptors LDL-receptor related protein 5/6 (***LRP5*** or ***LRP6***) and G-protein coupled receptor 124 (***GPR124***). This protein complex induces the polymerization of Dishevelled (***DSH***) and the Lrp5/6 intracellular tail phosphorylation, which in combination lead to the final sequestration of Axin. In contrast, the vessels formed outside the CNS do not receive Wnt signaling and consequentely Axin is free in the cytoplasm where it can interact with Adenomatous polyposis coli (***APC***), Casein kinase 1a (CK1a), and Glycogen synthase kinase-3β (***GSK3B***), forming a destruction protein complex that recognizes and phosphorylates free soluble β-catenin (***CTNNB1***). This phosphorilation allows E3 ubiquitin ligase β-TrCP1 (***BTRC***) to ubiquitinate β-catenin and thereby mark it for proteasomal degradation. Therefore, the absence of Wnt ligands leads to β-catenin degradation – also called the “off-state” – whereas the presence of Wnts permits the concentration of free soluble β-catenin to rise in the cytoplasm – the “on-state”. β-Catenin is then able to translocate to the nucleus where it acts as a cofactor of the transcription factors T-cell factor/lymphoid enhancer factor (TCF/LEF), activating the transcription of BBB genes as it is pictured in **Figure 9** (Liebner et al. 2008; Stenman et al. 2008; Daneman et al. 2009; Yulian Zhou and Nathans 2014; Yulian Zhou et al. 2014; Cho, Smallwood, and Nathans 2017; Hupe et al. 2017; Eubelen et al. 2018; Benz and Liebner 2020).

A multitude of nuclear players cooperate with β-catenin to generate a transcriptional program. They compose a flexible colection of proteins that might interact with β-catenin in order to activate the "right" targets in each tissue, developmental stage, or disease context (Söderholm and Cantù 2020). A complete list of target genes of the Wnt/β-catenin pathway can be found at the Standford web-page (https://web.stanford.edu/group/nusselab/cgi-bin/wnt/target_genes). Importantly, the Wnt/β-catenin direct target genes in ECs are not completely identified. Some target genes have been documented, such as the Sex Determining Region Y (SRY)-Box Transcription Factor 17 (***SOX17***) – a transcription factor known to be required for endothelial regeneration. Nonetheless, the exact molecular mechanism by which β-catenin activates the genes responsible for the BBB phenotype (***CLDN5***, ***ABCB1***, ***SLC2A1***; **Figure 9**) remains unknown (Liebner and Plate 2010).

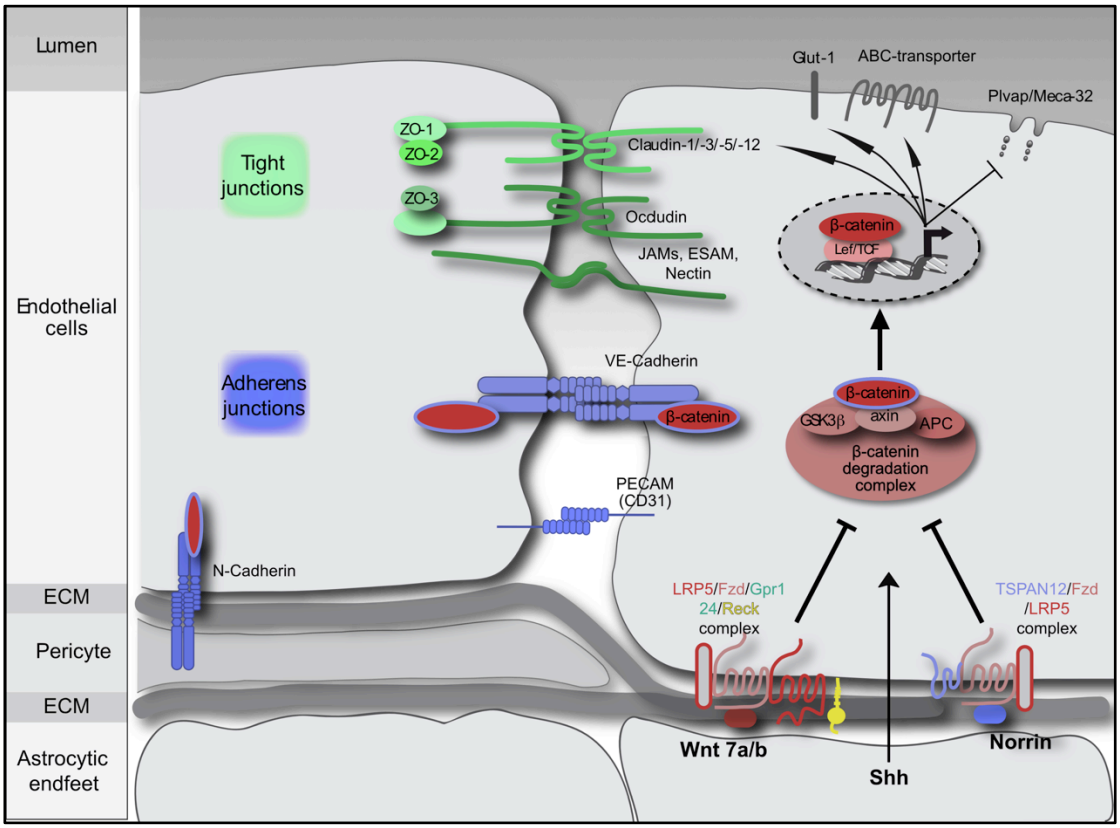

Figure 9: The Wnt/β-catenin pathway at the BBB. Figure modified from Benz and Liebner 2020.

The Wnt-signaling pathway can be further modulated by secreted antagonists such as Dickkopf homologs (DKK1-4), Notum, the Adenomatosis polyposis coli

down-regulated 1 protein (APCDD1), the Sclerostin/SOST family, and Wnt inhibitory factor 1 (WIF1), secreted frizzled-related protein families (sFRPs, 1-5), and atypical Wnt receptors such as the receptor-like tyrosine kinase (RYK) and receptor tyrosine kinase-like orphan receptors (ROR). More specifically, the Dickkopf family of Wnt modulators acts by inhibiting the Wnt co-receptors Lrp5/6, and is thus up-stream of β-catenin (Liebner and Plate 2010). DKK1-4 are implicated in bone formation and bone disease, cancer, and AD although the exact mechanism remains unknown.

3.1.4.1. Other important pathways

An important characteristic of the BBB is the reduced transcytosis, without which the BBB would still be "leaky". The major facilitator super family domain containing 2a protein, or Mfsd2a (***MFSD2A***), is a sodium-dependent lipid trasporter with a higher specificity for lysophosphatidylcholine (LPC) with unsaturated fatty acyl chains. Mfsd2a is involved in various biological processes such as transport, cell fusion, cell cycle, inflammation, regeneration, and tumor growth (Eser Ocak et al. 2020). Mfsd2a is highly expressed by brain ECs, where it transports docosahexaenoic acid (DHA) bound to LPC from the blood to inside the ECs. DHA is therefore enriched at the plasma membrane of ECs, where it supresses the caveolae mediated transcytosis. Hence, Mfsd2a is contributing to inhibit the "leaky" properties of ECs and maintain the BBB phenotype (**Figure 10**). PCs further contribute to maintain the BBB as their presence is required for ECs to express Mfsd2a (Nguyen et al. 2014; Ben-Zvi et al. 2014; Andreone et al. 2017).

Other molecular pathways and signals are able to induce and/or to modulate BBB properties such as RA, Shh, Notch, VEGF and angiopoietin/Tie2 (Liebner, Czupalla, and Wolburg 2011). Neuronal activity has been shown to additionally modulate BBB function although the mechanisms behind it remain unclear. Furthermore, external stimuli like exercise, diet or the circadian rhythm can regulate BBB characteristics (Profaci et al. 2020). Last but not least, pathological conditions creating inflammation can alter the BBB phisiology generating a new state in which the gene & protein expressions are different. This "inflammed" state

can lead to futher complications and hence, a good understanding of the phisiology of the BBB and its regulation is imperative to offer reliable medical solutions.

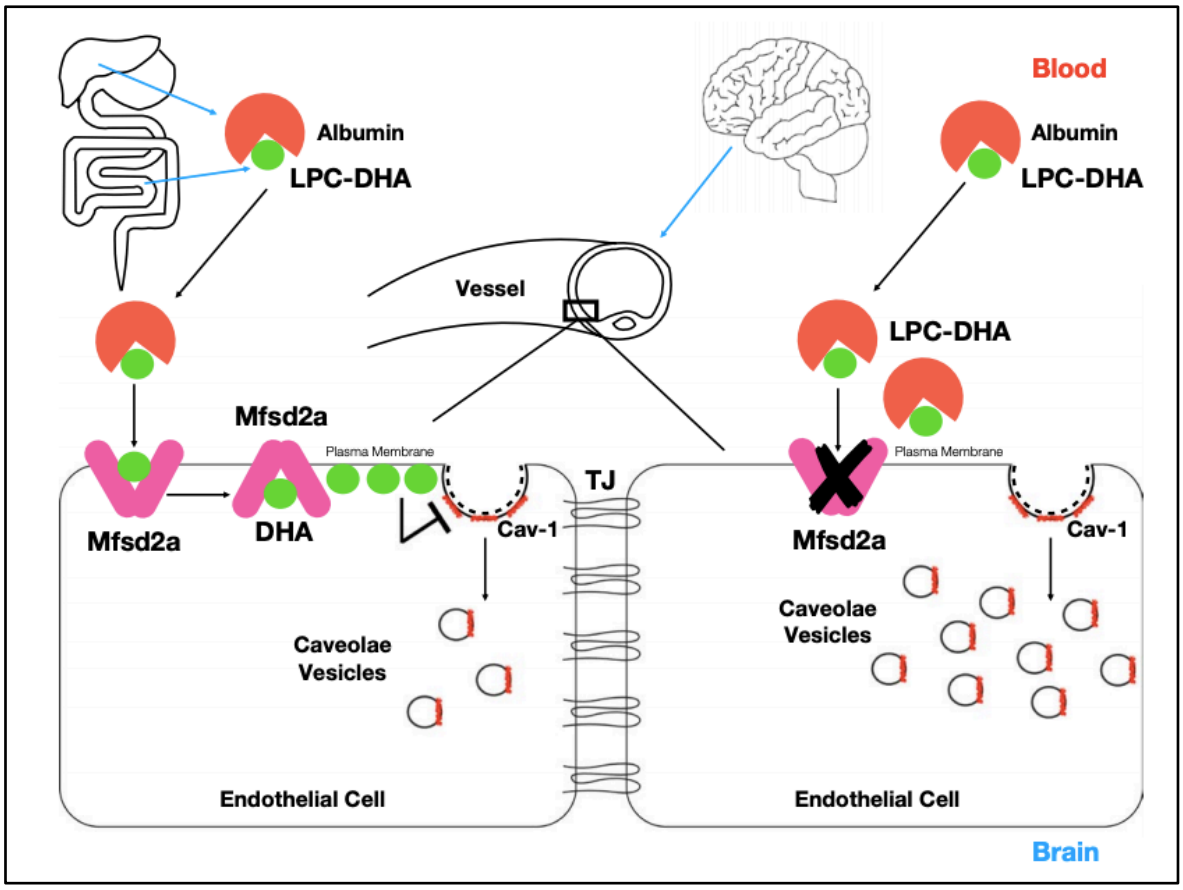

Figure 10: Regulation of BBB permeability by Mfsd2a-mediated suppression of caveolae-mediated transcytosis in endothelial cells (Eser Ocak et al. 2020).

3.1.5. The BBB in disease

Dysfunction of the BBB can be a cause or a consequence of diseases. Either way, BBB disruption causes ion dysregulation, edema, and neuroinflammation, which can lead to neuronal dysfunction, increased intracranial pressure, neuronal degeneration, and ultimately death (Profaci et al. 2020).

Complete destruction or genetic ablation of the BBB phenotype is fatal; mice lacking Claudin-5 (***Cldn5***^{KO}) exhibit normal vasculature formation but the BBB is leaky and the pups die a few hours after birth (Nitta et al. 2003). Dysregulation of any BBB characteristics such as transcytosis or transportation are sufficient to change the neural environment and cause disorders like seizures, autism, or psychomotor retardation syndrome. Along the same line, conditions affecting blood

vessels primarily such as cholesterolemia, hyperlipidemia, atherosclerosis, or hypertension are linked to increased risk of neurodegeneration (Profaci et al. 2020).

On the other hand, a growing amount of neurological diseases and disorders have been shown to affect the BBB to a greater or lesser extent. The impact of multiple sclerosis, stroke, cancer, and epilepsy on BBB function is easily discernible, whereas in other diseases like AD, the BBB dysfunction is still for some authors a matter of debate (Liebner et al. 2018; Profaci et al. 2020). In any case, correctly identifying all the components of a disease or condition is essential for treating it accurately. Henceforth, in the next section I put the focus on AD, describing the current knowledge regarding the disease, and how the BBB plays an important role.

3.2. Alzheimer's disease

AD is considered as the disease of the 21st century because of the high amount of people affected and the lack of effective treatment. AD is the main cause of dementia, contributing to 60–70% of cases. In numbers, there are about 40-50 million people currently living with dementia, and this is expected to almost double every 20 years, reaching an estimated number of 75 million by 2030 and 131.5 million by 2050. The total estimated worldwide cost of dementia in 2015 is US$ 818 billion and by 2030, dementia will become a 2-trillion dollar disease. If global dementia care was a country, it would be the 18th largest economy in the world, exceeding the market values of companies such as Apple and Google (Alzheimer's Disease International et al. 2015; Alzheimer's Disease International 2019; Nichols et al. 2019). Clearly, the global socio-economic repercussions of dementia are huge and only worsening; therefore, finding a cure has become crucial.

3.2.1. Description

AD is a debilitating syndrome affecting mainly aged people, and characterized by memory loss and deterioration in thinking, behaviour, and the ability to perform everyday activities.

3.2.1.1. Discovery & first hypothesis

The name "Alzheimer's disease" comes from Alois Alzheimer (**Figure 11**), a German medical doctor who worked in an asylum in Frankfurt am Main, and who was the first person to describe the disease. He observed in the patient Auguste Deter (**Figure 11**) that she suffered from memory loss, disorientation, hallucinations, and ultimately death at age of only 55. In 1906 he gave a lecture describing what he called an "unusual disease of the cerebral cortex" and showed, thanks to a new stain developed by Max Bielschowsky (Bielschowsky 1902), that the brain had neuritic plaques and neurofibrillary tangles (**Figure 12**), the latter had not been described previously. His findings were published a year later (Alzheimer 1907).

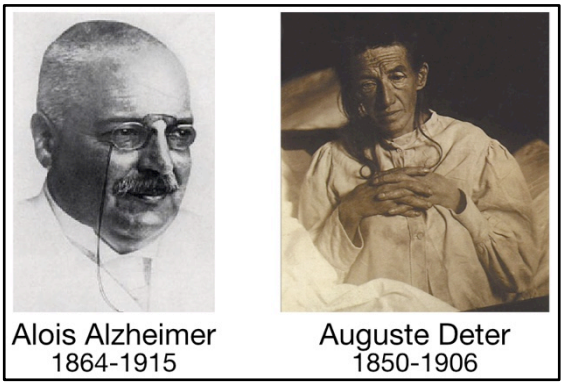

Figure 11: Alois Alzheimer and Auguste Deter (public domain).

After Alzheimer described the, at the time, novel condition, further professionals observed the same symptoms and cerebral pathology in other patients and realized that AD and senile dementia where identical diseases (Blessed, Tomlinson, and Roth 1968; Katzman 1976). Suddenly, AD dementia went from a relatively rare condition to a major public health issue, being the fourth leading cause of death in the elderly (Katzman 1976). In the same year, the first hypothesis was formulated to explain the cause of AD, the "cholinergic hypothesis". Post-mortem biochemical analysis of brains from AD patients identified a loss in neocortical choline acetyltransferase (ChAT), the enzyme in charge of the synthesis of acetylcholine (ACh), causing a presynaptic cholinergic deficit (Bowen et al. 1976; Davies and Maloney 1976). ACh was recently discovered to play a role of in

learning and memory (Drachman and Leavitt 1974), and the nucleus basalis of Meynert was pointed as the source of cortical cholinergic innervation. Around that time, the nucleus basalis of Meynert was found to suffer from heavy neurodegeneration in AD (Mesulam 1976; Whitehouse et al. 1981), which served to link the disease's biochemical dysfunction with dementia. Thus, it was proposed that degeneration of cholinergic neurons largely contributed to the deterioration in cognitive function seen in patients with AD (Bartus et al. 1982). Those findings led to the development of cholinesterase inhibitors – they increase the availability of ACh at synapses – as a treatment solution for AD patients, and proving to significantly ameliorate symptoms (Summers et al. 1986).

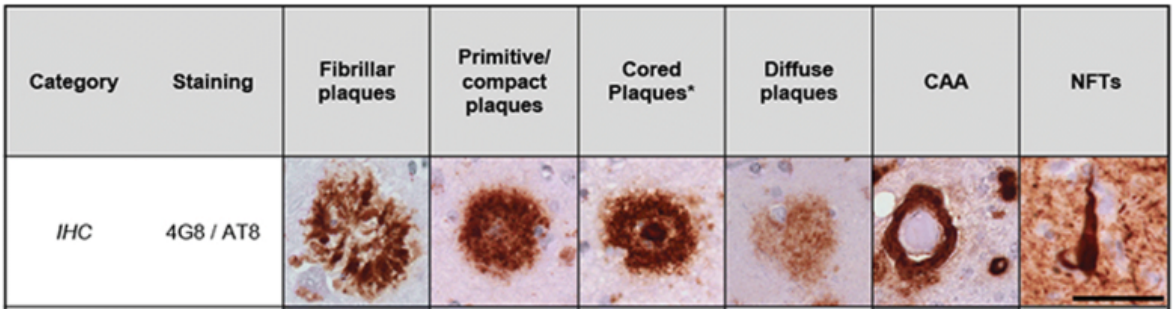

Figure 12: Plaques and tangles. Classification of Aβ-plaques in fibrillar, compact, cored or diffuse. Cerebral amyloid angiopathy (CAA) and neuro-fibrillar tangles (NFTs) are also shown (den Haan et al. 2018).

Subsequent studies revealed inconsistencies in the cholinergic hypothesis of AD, such as deficient cholinergic activity in regular ageing and in other neurodegenerative diseases like inherited olivo-ponto cerebellar atrophy, which progress without dementia. Furthermore, evidence linking amyloid-β (Aβ) and hyperphosphorylated tau protein with the development of the disease, and the fact that cholinergic deficits appeared to be a secondary effect of Aβ toxicity, finally led to the substitution of the hypothesis of AD (Hardy and Allsop 1991; Selkoe 1991). Nevertheless, cholinesterase inhibitors remain as the only approved drugs to treat AD (tacrine, donepezil, rivastigmine and galantamine) together with memantine (NMDAR antagonist), although none of them can counteract or significantly delay the disease's progression, they are given as symptomatic relief (Contestabile 2011).

3.2.1.2. Current hypothesis of AD: amyloid cascade

Understanding the aetiology of AD is of vital importance, as it would presumably help to find novel and hopefully successful treatment concepts. Now we know that although a cholinergic dysfunction happens in AD and cholinesterase inhibitors are therapeutically valuable in modestly ameliorating dementia, the cause behind the disease is of a different origin.

Since Alzheimer first described the pathological changes in the brain of A. Deter, it has been shown that brains of AD patients contain senile plaques and neurofibrillary tangles (**Figure 12**). Further research identified the plaques as accumulations of Aβ (Glenner and Wong 1984) – a segment of a bigger protein called amyloid precursor protein (APP; Kang et al. 1987) – and the tangles as accumulations of hyperphosphorylated tau protein (Brion et al. 1985; Grundke-Iqbal et al. 1986). Additionally, the Aβ peptide was found to be toxic in cultured neurons (Yankner, Duffy, and Kirschner 1990) and mutations in the ***APP*** gene cause autosomal-dominant cerebral amyloid angiopathy (CAA; **Figure 12**) and AD (Levy et al. 1990; Goate et al. 1991). This accumulated evidence, together with the first ***APP*** transgenic mouse (Quon et al. 1991), led to the formulation of the amyloid cascade hypothesis of AD (**Figure 13**; Selkoe 1991; Hardy and Allsop 1991; Hardy and Selkoe 2002).

APP is a gene coding for a transmembrane protein ubiquitously expressed by neurons, ACs, and MG. It is also expressed outside the brain by a great variety of tissues, such as thymus, heart, muscle, lung, kidney, adipose tissue, liver, spleen, skin, and intestine. Its physiological function is still not clear, but some studies report that it plays a role in protecting synaptic integrity, anterograde neuronal transport, iron export, and hormonal regulation (Cirrito et al. 2005; Satpute-Krishnan et al. 2006; Porayette et al. 2007; McCarthy, Park, and Kosman 2014). APP can be cleaved at the C-terminal side by γ-secretase – a protein complex with two catalytic subunits coded by the ***PSEN1*** and ***PSEN2*** genes – and at the N-terminal side by either α- or β-secretase (***ADAM10*** and ***BACE1***, respectively). The peptide resulting from the cleavage of the α- & γ-secretase (named p3) has 24 or 26 amino acids and is considered healthy, i. e., not prone to aggregate, although its physiological function is still not understood. On the other hand, if APP is cleaved

by β- & γ-secretase, the product is a longer peptide of 40 or 42 residues with fibrillar morphology and thus called amyloid-β or Aβ (**Figure 14**; Gandy 2005). Soluble Aβ easily forms oligomers, which in turn can generate non-soluble deposits of bigger aggregations known as plaques. These plaques are found in the brain parenchyma and often surround brain vessels, creating what is known as CAA, which is present in many (up to 80%) cases of AD (**Figure 12**; Brenowitz et al. 2015).

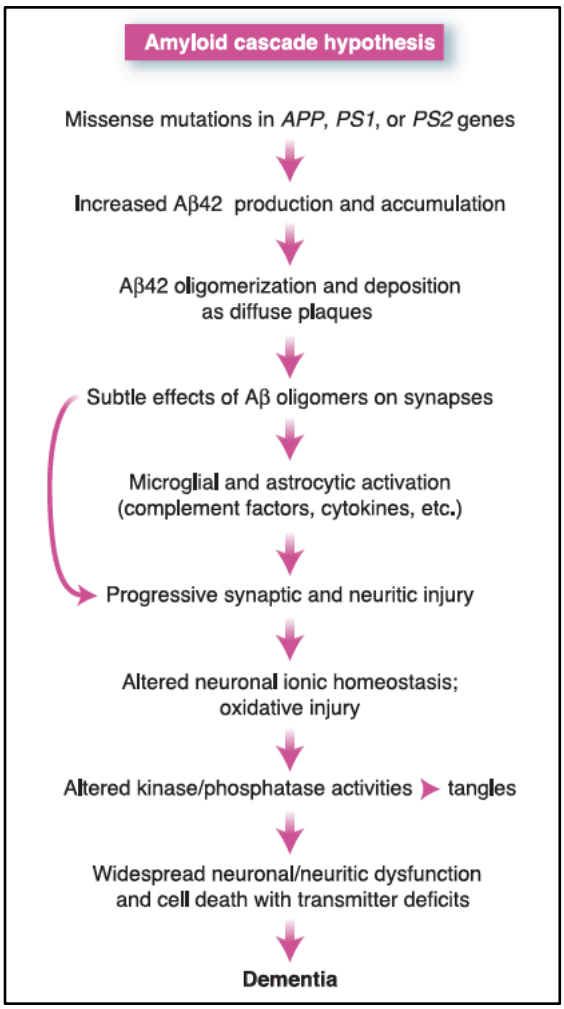

Figure 13: the amyloid cascade hypothesis of AD (Hardy and Selkoe 2002).

The amyloid cascade hypothesis of AD (**Figure 13**) states that Aβ production gets dysregulated – either because of genetic mutations in ***APP*** or ***PSEN1/2***, or because of an imbalance during ageing – resulting in an accumulation of Aβ-forming plaques. The excess of Aβ causes neurotoxicity, preventing synaptic activity

and leading to neurodegeneration (Yankner, Duffy, and Kirschner 1990). It also causes astrocytic and microglial activation, and an increasing number of studies are showing effects at the BBB and even systemically, such as disorders of systemic immunity, cardiovascular disease, hepatic dysfunction, microbiota disturbance and infection, metabolic disorders, respiratory and sleep disorders, blood abnormalities, and renal dysfunction (J. Wang et al. 2017). Many pharmacological drugs have attempted to target Aβ (with antibodies) or the β-secretase (with inhibitors), but all of them have failed. These fiascos, together with the increasing amount of evidence showing that AD effects are broader than the classical neuronal degeneration, have motivated the formulation of new hypothesis to explain AD. Nevertheless, the amyloid cascade is still the most accepted hypothesis within the scientific community.

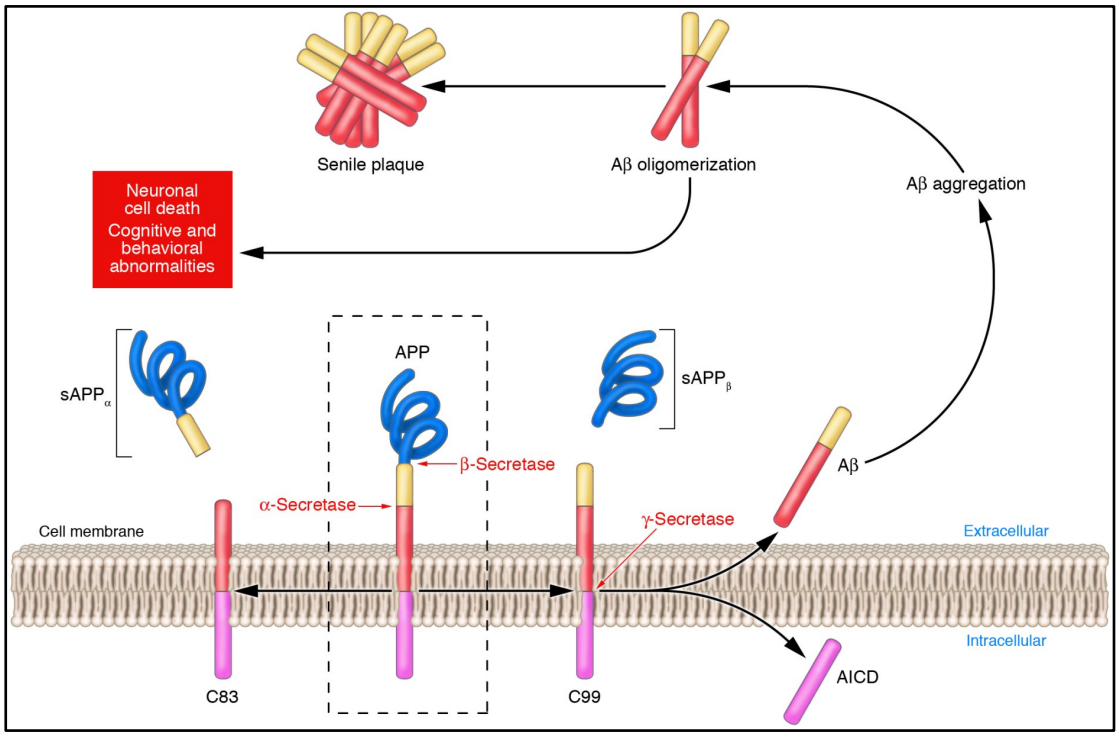

Figure 14: APP processing (Gandy 2005).

3.2.1.3. The neurovascular hypothesis of AD

Since Alzheimer described the now widely known disease, it has been known that Aβ can accumulate around brain blood vessels (called CAA). However, only in recent years researchers started to pay attention to this fact. Already at the end of last century, some studies showed the presence of vascular alterations in AD (Buée

et al. 1994; Iadecola et al. 1999). Some years later, the concept of the "neurovascular unit" was introduced (see 3.1.3.1.4. The NVU concept), opening new possibilities and generating new questions. The Alzheimer's field was no exception and soon, more studies followed linking neuronal dysfunction with vascular dysfunction (**Figure 15**), leading to the formulation of the neurovascular hypothesis of AD (Iadecola 2004; Zlokovic 2005).

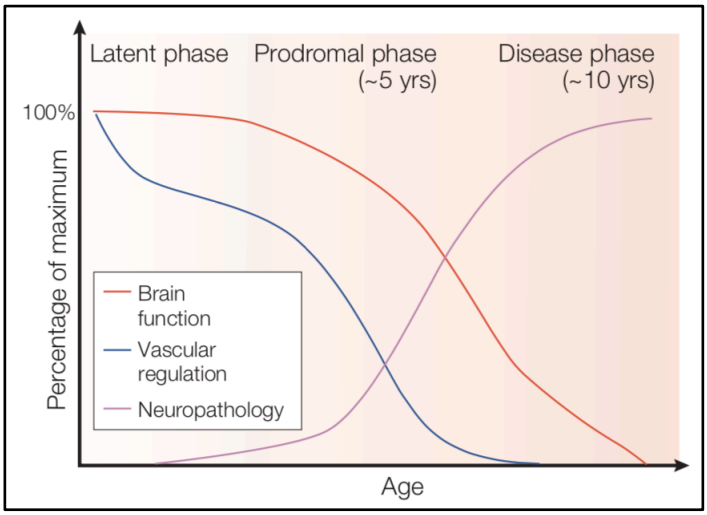

Figure 15: time-course of the interplay between vascular dysregulation, neuropathological alterations and decline in brain function in AD (Iadecola 2004).

Briefly, this hypothesis theorizes that the elevated levels of Aβ are a result of insufficient clearance through the BBB, and lead to the formation of vascular amyloid lesions and higher fibrillar Aβ levels. The insufficient clearance can occur due to aberrant angiogenesis, endothelial senescence, low levels of Aβ clearance receptors (LRP), or increased levels of Aβ influx receptors (RAGE). These changes can also produce neurovascular uncoupling, vessel regression, brain hypo-perfusion, and neurovascular inflammation; all of them observed in brains of AD patients (Iadecola 2004). Moreover, cardiovascular risk factors associated with AD (see 3.2.4.3. Cardiovascular risk factors), such as atherosclerosis or hypertension, alter cerebral arteries leading to CAA and disintegration of the NVU (Zlokovic 2005). The original scheme of the neurovascular hypothesis of AD is depicted below in **Figure 16**.

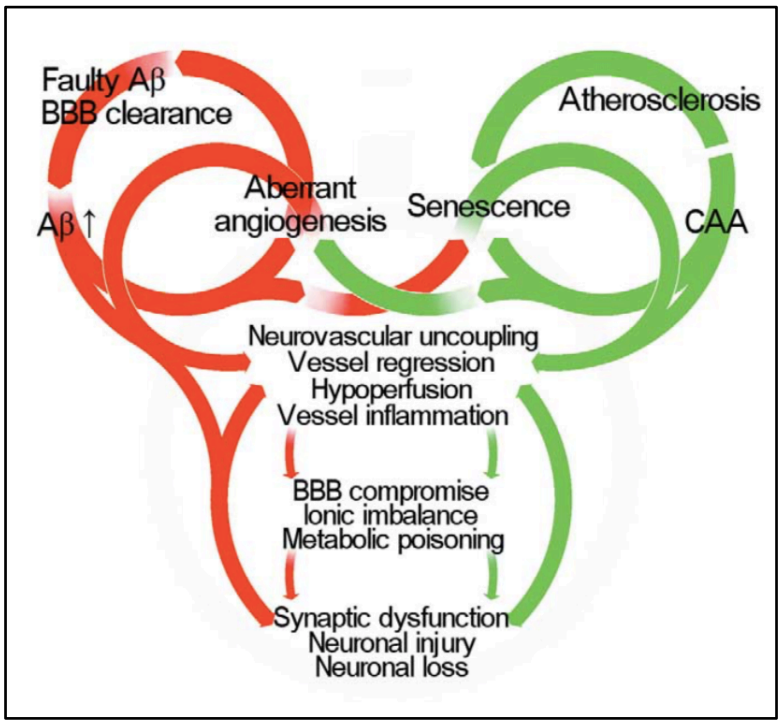

Figure 16: original neurovascular hypothesis figure (Zlokovic 2005).

This hypothesis, however, does not change the supposition that Aβ is the major cause of neuronal cell death. Dementia cases caused exclusively by vascular factors are classified as 'vascular dementia' and are considered a different disease. Some authors disagree with this division (Iadecola 2004) and propose that vascular dementia and AD are two extremes of the same disease, which in many cases runs with features from both sides, i.e., with strong vascular dysfunction, and with Aβ deposits. However, those unclear cases are classified as 'mixed dementia', and even though they are much more common than "pure" AD or vascular dementia (Barker et al. 2002; Franklin et al. 2015), they do not have a clear treatment, and they often receive the same medication as AD patients. Unfortunately, the role of the brain vasculature in AD is not yet well understood. More research is needed to understand if indeed vascular dementia and AD are two sides of the same coin, or what are the specific differences between the two diseases.

3.2.1.4. The tau hypothesis of AD

A different approach is to focus on the other AD hallmark, the neurofibrillary tangles. They are composed of hyperphosphorylated tau, which is encoded by the

gene ***MAPT***, and is a microtubule-associated, scaffolding protein that is enriched in axons. Tau's degree of phosphorylation changes its affinity for microtubule filaments, resulting in their stabilization or disassembly. Under pathological conditions tau is hyperphosphorylated, which yields to aggregation and loss of affinity for microtubules, ultimately leading to axon damage, neuronal dysfunction, and eventually neurodegeneration. Some studies have shown that tau aggregates can exhibit prion-like behaviour, propagating through the brain and causing further aggregation and damage (Frost, Jacks, and Diamond 2009; Clavaguera et al. 2009; Liu et al. 2012; De Calignon et al. 2012). This tau-mediated neurodegeneration is considered as another hypothesis of AD by some authors, although tau abnormalities only appear after Aβ dysfunction and many studies already demonstrated that Aβ increase causes tau malfunction but not vice versa (Selkoe and Hardy 2016).

3.2.1.5. The inflammation hypothesis of AD

The last relevant AD hypothesis deals with the immune element of the disease. The role of MG in phagocytosis and neuronal pruning has been well characterized under homeostatic conditions. Likewise, the role of MG in Aβ clearance has emerged since the discovery that MG actively degrade Aβ (Lee and Landreth 2010) and activated MG are found surrounding Aβ deposits already at prodromal stages of AD (Bolmont et al. 2008). MG become reactive upon the presence of Aβ, changing their morphology and the way they behave. Furthermore, Aβ-induced toxicity requires micromolar concentrations of the soluble Aβ forms, and the concentrations in the brain are a million times lower, i.e. in the picomolar range. What the inflammation hypothesis of AD suggests, is that increasing soluble Aβ in the brain initiates an inflammatory response in MG, which becomes amplified later on by tau aggregates. Activated MG are the cause of neuronal damage owing to the persistent and chronic brain inflammation (McGeer and McGeer 2013).

New sequencing technologies have allowed the study of single cell transcriptomics, revealing that MG are composed of heterogeneous subpopulations that react differently during AD. This means that some cells could be fighting against the progression of AD and others supporting its progression, making the

search of a therapeutic target very complicated. Understanding what drives these cell types to develop into each subgroup is therefore fundamental, and many researchers are currently focusing on this topic (Keren-Shaul et al. 2017; Mathys et al. 2017; Friedman et al. 2018; Kelley et al. 2018; Sala Frigerio et al. 2019; Mathys et al. 2019; Grubman et al. 2019; Habib et al. 2020; Yingyue Zhou et al. 2020). More specifically, a set of up-regulated microglial genes that correlates with AD progression is now well recognized, which includes genes like ***ITGAX***, ***TYROBP***, ***CST7***, ***GPNMB***, and ***SPP1***. Some of the microglial up-regulated genes are also known risk factor genes for AD (see 3.2.4.2. Genetics), such as ***APOE*** and ***TREM2***. Moreover, rare heterozygous variants in ***TREM2*** are associated with a significantly increased risk of developing AD (Guerreiro et al. 2013; Y. Shi and Holtzman 2018).

Currently, the role of MG and inflammation in AD is well recognized and some therapies are being developed to target it. Very recently, a direct link between Aβ production and inflammation has been discovered, emphasising the importance of inflammation in AD (Hur et al. 2020). However, the association between MG and the brain vasculature is not well characterized in the AD context.

3.2.2. The biology of AD

Despite its unclear aetiology, AD is deeply studied and the changes that occur during its curse are well characterized. Macroscopically, the brain of a person with AD has shrunk due to atrophy, causing the ventricles to expand, and emphasizing the gyri & sulci (**Figure 17**). Brain atrophy in AD strongly affects the cortical and hippocampal areas of the brain, where the neuronal loss is more pronounced. This damage manifests clinically as dementia, but it can also affect the ability to move, talk and even eat (J. Allen, J. Watson, and Dawbarn 2011; Gaugler et al. 2016).

There is no discussion about the fact that Aβ affects neurons. Many studies have proven the harmful effects of increasing the extracellular Aβ concentration. However, before neuronal degeneration occurs, other alterations can be seen such as synaptic and dendritic injury, disturbances in the process of adult neurogenesis, circuitry dysfunction, and aberrant innervation. Soluble Aβ oligomers trigger early damage to synapses, which is followed by retrograde degeneration of the axons, and eventual atrophy of the dendritic tree and perikaryon (Serrano-Pozo et al.

2011). Recent advances in positron emission tomography (PET) with the tracer UCB-J can detect synapse loss in AD cortex (Chen et al. 2018). Volumetric magnetic resonance imaging (MRI) also serves to identify macroscopic changes early on. Nevertheless, those tools alone are insufficient for a final diagnosis and AD case confirmations can still only be achieved postmortem.

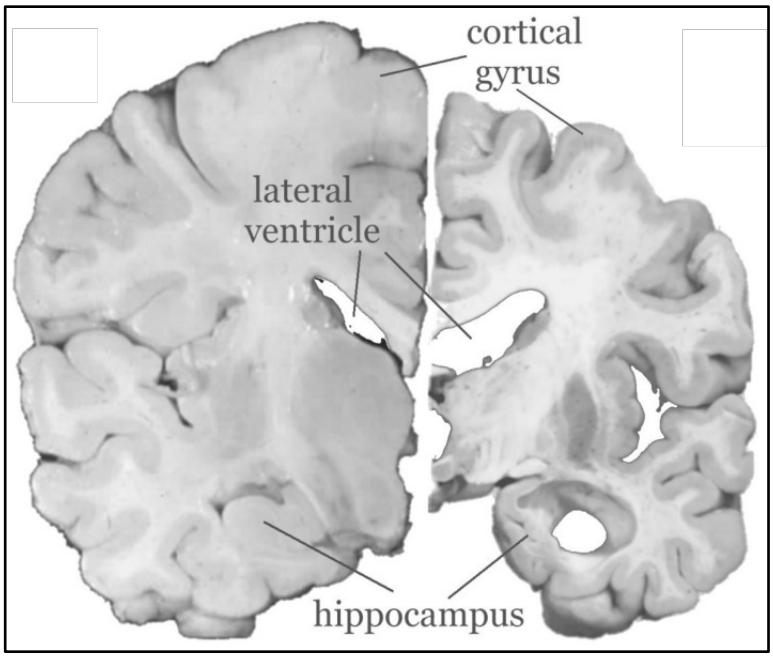

Figure 17: AD vs healthy brain. Brain section of a healthy human brain (left) compared to AD (right) where the brain atrophy is clearly visible (Allen et al., 2011 J. Allen, J. Watson, and Dawbarn 2011).

All the described changes come accompanied by astrogliosis, vascular abnormalities, and MG activation, as seen in 3.2.1.3. The neurovascular hypothesis of AD and 3.2.1.5. The inflammation hypothesis of AD. Importantly, the common factor causing all the pathophysiological alterations, according to the amyloid cascade hypothesis of AD, can be found at the molecular level, explained below.

3.2.3. AD at a molecular level

There are two main hallmarks to be considered at a molecular level in AD: Aβ depositions, and tau tangles. Both contribute to the disease and thus, a greater description of them is offered hereunder.

3.2.3.1. APP/Amyloid beta

The amyloid cascade hypothesis states that Aβ is responsible for the onset of AD. Therefore, many studies have focused on deciphering the physiological and pathophysiological role of APP/Aβ (see 3.2.1.2 Current hypothesis of AD: amyloid cascade). Despite of not having a perfectly defined function, Aβ has served to model AD in mice, rats and other animals, and many groups use these tools for their experiments. The first AD model was generated in 1991 by overexpressing a human ***APP*** isoform in mice (Quon et al. 1991). Since then, many different models have been generated, including those that express known human mutations in ***APP*** such as the ***Dutch*** mutation (Herzig et al. 2004), mutations in ***PSEN*** (Duff et al. 1996), mutations in ***MAPT*** (Lewis et al. 2000), and combinations of them (Davis et al. 2004; Jawhar et al. 2012).

Thanks to AD models ***in vivo*** and cell cultures ***in vitro***, the study of Aβ and its effect has advanced considerably. Aβ levels have been shown to be modulated or related to many different factors. We now know that Aβ can be influenced by lipids; high cholesterol levels are associated with increased brain Aβ (Reed et al. 2014). Along this line, apolipoprotein E (***APOE***), an important lipid carrier, is the main genetic risk factor associated to AD (see 3.2.4.2 Genetics), and gets up-regulated in MG after Aβ exposure, further underlining the role of Aβ & AD with lipids.

APP processing by secretases has alternative (previously not known) cleavage sites. One of these secretases, the so-called η-secretase, cleaves APP at its N-terminus further away from the β-secretase, producing a peptide of 92 or 108 amino acids that finishes at β- or α-secretase site, respectively (**Figure 18**). In healthy brains, these fragments are ten times more abundant than Aβ, and the longer peptide (Aη-α) suppresses synaptic activity ***in vitro*** and neuronal activity ***in vivo*** (mouse). Moreover, β-secretase inhibition increases Aη-α concentration in the brain, which raises the question whether β-secretase targeting drugs are the correct choice of treatment (Willem et al. 2015).

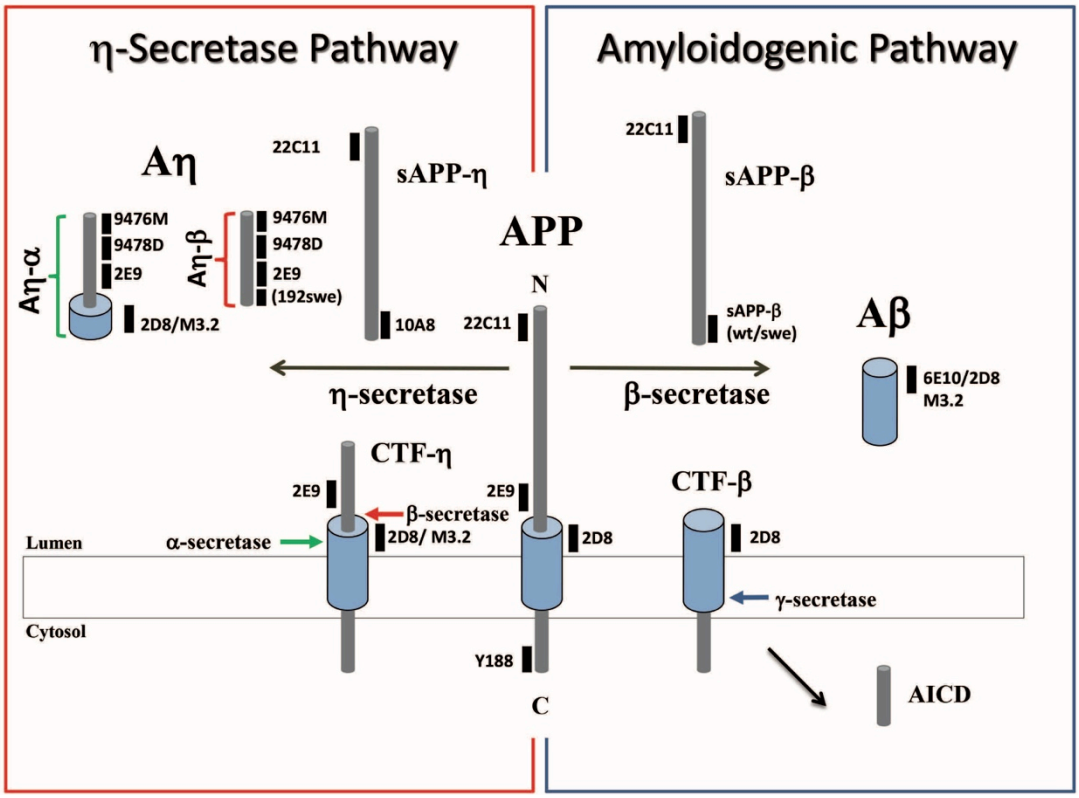

Figure 18: APP cleavage by η-secretase vs β-secretase. Antibodies used in the study are indicated (Willem et al. 2015).

Furthermore, β-secretase inhibitors effectively suppress Aβ production; however, they suppress the production of other β-secretase targets, such as neuregulin and jagged 1 & 2 proteins, impairing a correct myelination and notch signalling respectively (Willem et al. 2006; He et al. 2014). The current view about β-secretase suppressors is that a full inhibition is not wise, due to the previously explained reasons, but a partial inhibition seems to still show beneficial effects in mouse models of AD. Nevertheless, human trials keep failing and some experts criticize that the Aβ hypothesis might not be the dogma after all, pointing at the lack of pharmacological success as an evidence example.

3.2.3.2. Tau

Hyperphosphorylation of the tau protein is recognized as an AD hallmark that occurs after Aβ dysregulation, according to the amyloid cascade hypothesis. There is no question that tau tangles lead to neuronal cell death, and that tau alone can lead to neurodegeneration (Ghetti et al. 2014). In fact, the group of conditions that develop with tau dysfunction are called tauopathies and are classified as

neurodegenerative diseases. As such, AD can be considered a tauopathy too. However, neurofibrillary tangles alone are not sufficient to clinically qualify as AD pathology since the presence of Aβ deposits is required as well (den Haan et al. 2018). Therefore, many AD mouse models mimic AD by overexpressing or mutating ***APP***, but without any changes in ***MAPT***. Nevertheless, tau aggregation is an important event in AD and it should not be underestimated.

As explained previously at the tau hypothesis of AD (see 3.2.1.4 The tau hypothesis of AD), tau aggregates behave like prions and spread over the brain, causing further damage. However, tau fibrils in the brain of AD patients are known to contain a mixture of 3- and 4-repeats of tau, while those in other tauopathies tend to contain only one kind (Crowther and Goedert 2000). Recent advances at cryo-electron microscopy allowed to uncover the ultrastructure at 3.4 Å resolution of both straight and paired helical filaments of tau (Fitzpatrick et al. 2017). Still, the reason why tau aggregates as semi-ordered filaments remains a mystery. Nonetheless, tau tangles can be used as markers of AD evolution. According to the distribution of those aggregates throughout the brain, different stages were defined already in 1991 by Eva and Heiko Braak (H. Braak and Braak 1991) and they are still used nowadays to describe the disease's progression (**Figure 19**).

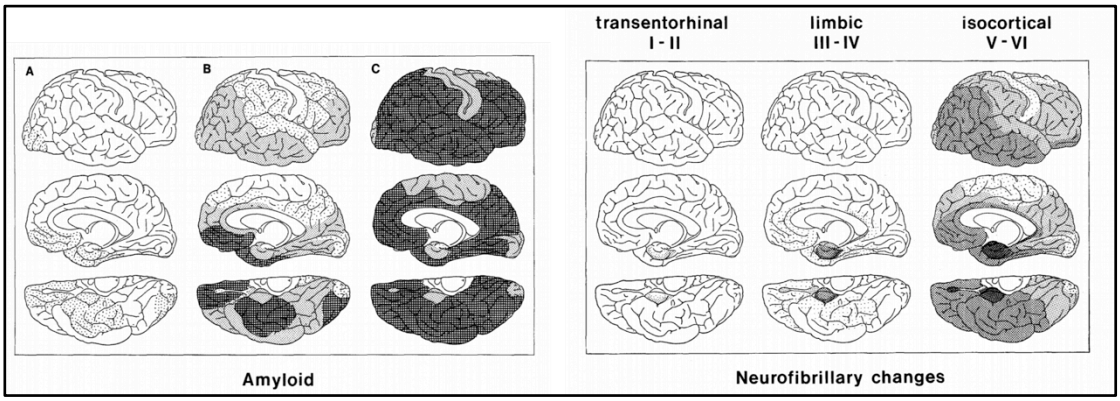

Figure 19: Braak stages. Left panel, amyloid deposition starts in (A) basal portions of the isocortex, continues to (B) isocortical association areas until the entire cortex is covered (C) and becomes denser. Right panel, tau aggregation is divided in six stages: it starts at a single layer of the transentorhinal region (I-II), spreads throughout the transentorhinal and entorhinal regions (III-IV) and at the end it covers the isocortex (V-VI; H. Braak and Braak 1991).

3.2.4. Factors contributing to AD

Albeit Aβ and tau are the hallmarks of AD, other factors are involved and play an important role (see **Table 2** for a complete list). Hereunder I offer an overview of the three most important factors.

3.2.4.1. Ageing

Aging is the time-dependent physiological and functional decline that every living organism experiences. Many non-infectious diseases are associated with ageing, and AD or other forms of dementia are no exception. The prevalence in the USA for AD is 3%, 17%, and 32% in people of age 65-74, 75-84, and >85, respectively (Hebert et al. 2013). The percentages are a bit lower in the rest of the world, but the increase of cases with age is nonetheless indubitable (Qiu, Kivipelto, and Von Strauss 2009). Therefore, ageing is globally considered as the AD top risk factor (**Figure 20**).

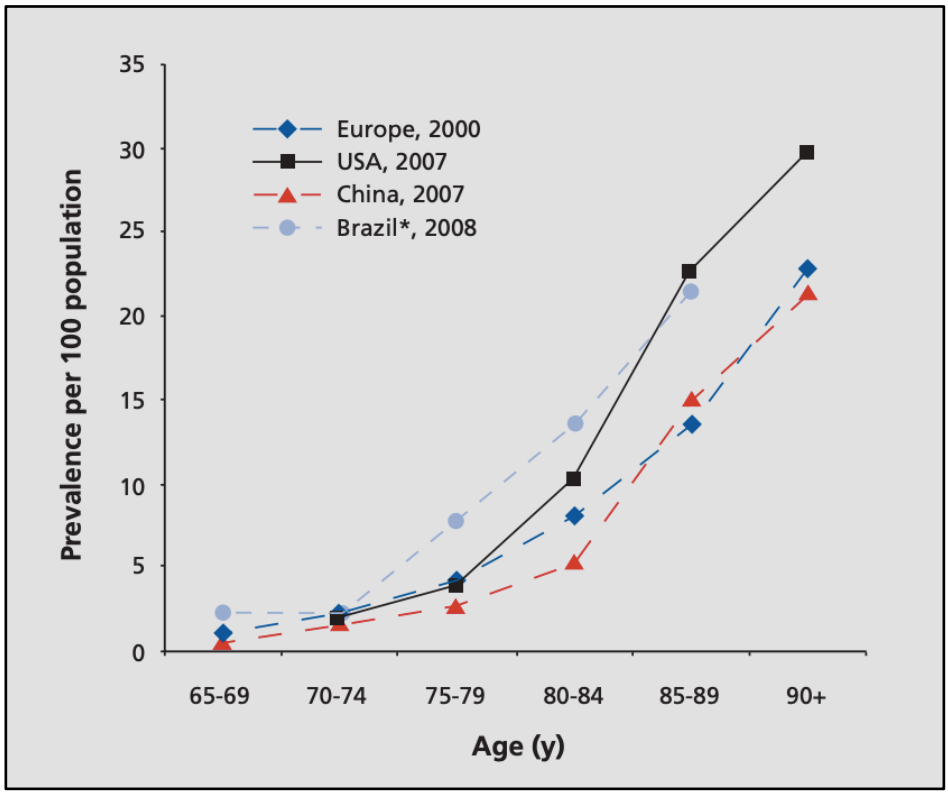

Figure 20: AD prevalence in the world (age-specific cases per 100 population). *Prevalence of all types of dementia (Qiu, Kivipelto, and Von Strauss 2009).

As it was explained in previous sections, the two pathophysiological hallmarks of AD are cerebral Aβ deposits and tau neurofibrillary tangles. Interestingly, healthy

brains from individuals of all ages can contain hyperphosphorylated tau (Heiko Braak and Del Tredici 2011). Along the same line, amyloid plaques are common in healthy aged people (Chételat et al. 2013). Moreover, brains of healthy aged individuals present symptoms of inflammation, reasonably similar to the inflammation observed in AD, e.g. astrogliosis and microglial activation. Furthermore, mitochondrial dysfunction, reduced proteostasis, stem cell exhaustion, and epigenetic changes are alterations observed in both healthy ageing and AD (Xia et al. 2018). The prevalent current of thought accepts that although physiological ageing and AD are two different processes, they are not mutually exclusive and every aging adult is existing in a spectrum between them (Kerchner and Wyss-Coray 2015).

Along the same line, sirtuins are conserved NAD^+-dependent enzymes that display beneficial effects in age-related disorders. Sirtuin 1 (***SIRT1***) deacetylates histones and transcription factors, and is a known modulator of stress response, energy metabolism, and cellular senescence/death pathways. Some studies in animal models of AD have showed that overexpression of ***SIRT1*** has protective effects against the disease. Furthermore, ***SIRT1*** activation has been linked to the induction of non-amyloidogenic APP cleavage and reduction of Aβ levels. Interestingly, the role of ***SIRT1*** in vascular ageing is becoming increasingly recognized with several reports showing that overexpression of ***SIRT1*** in the endothelium prevents cellular senescence, enhances vasodilatory responses, and attenuates ageing-induced vascular damages. However, the role of vascular ***SIRT1*** in AD is not well understood (Potente et al. 2007; Lalla and Donmez 2013; Wong and Tang 2016; Kida and Goligorsky 2016; Guo, Xu, and Wang 2016).

3.2.4.2. Genetics

Despite that >95% of AD patients do not carry an AD-related mutation, the remaining <5% of cases served to understand, define, and model AD. The first studies that identified a genetic mutation leading to AD appeared in 1990 (Levy et al. 1990; Van Broeckhoven et al. 1990), although the mutation had already been discovered in a Dutch family but without linking it to AD (Wattendorff et al. 1982). The mutation, a single nucleotide exchange in ***APP*** that shifts glutamic acid for

glutamine (GAA>CAA codon change), is enough for APP dysfunction that leads to the development of a severe form of CAA, known as hereditary cerebral haemorrhage with amyloidosis, Dutch type (HCHWA-D). As the name implies, individuals accumulate extensive Aβ around cerebral vessels leading to cell death and loss of vessel wall integrity, which in turn makes the vessels prone to obstruction and rupture, manifesting clinically as haemorrhages and infarcts. This mutation is used in animal models that aim to study Aβ-mediated vascular effects in AD (Herzig et al. 2004; Davis et al. 2004).

After the first link of an APP mutation to AD was discovered, others followed reinforcing the amyloid cascade hypothesis of AD. Moreover, mutations in the catalytic parts of the γ-secretase (***PSEN1/2***) and in tau (***MAPT***) were discovered too. A complete list of AD-related mutations can be found on the webpage https://www.alzforum.org/mutations with a description and literature links. It is important to notice that some of these mutations cause autosomal-dominant AD (Goate et al. 1991) while others cause autosomal-recessive AD (Wingo et al. 2012). In any case, the age at which the mutation-carriers develop AD is much lower – less than sixty years old (early-onset) – than in the sporadic AD patients – more than sixty-five years old (late-onset) – (Wingo et al. 2012). This suggests that the sporadic form of AD differs from the genetic form. Unfortunately, the only available methods to study AD are genetic models that mimic the early-onset form of the disease. This might explain why the clinical trials fail, and is one of the arguments that some authors highlight to question the validity of the amyloid cascade hypothesis of AD (Ricciarelli and Fedele 2017).

Many groups have thus focused on finding genetic risk factors that correlate with AD. The first gene discovered to increase the risk to develop AD was Apolipoprotein E or ***APOE*** (Strittmatter et al. 1993; Saunders et al. 1993; Corder et al. 1993; Poirier et al. 1993; Corder et al. 1994). This gene can exist as the polymorphic alleles ε2, ε3, and ε4, which have a worldwide frequency of 8.4%, 77.9% and 13.7%, respectively. However, in AD patients, the frequency of the ε4 allele is 36.7% – increasing significantly the risk to develop AD – and 3.9% for the ε2 allele – decreasing the risk for AD. Nowadays ***APOE*** remains as the top genetic risk factor for AD, although more risk genes and loci have been identified (**Figure**

21) thanks to the numerous genome-wide association studies (GWAS) performed (Sims, Hill, and Williams 2020).

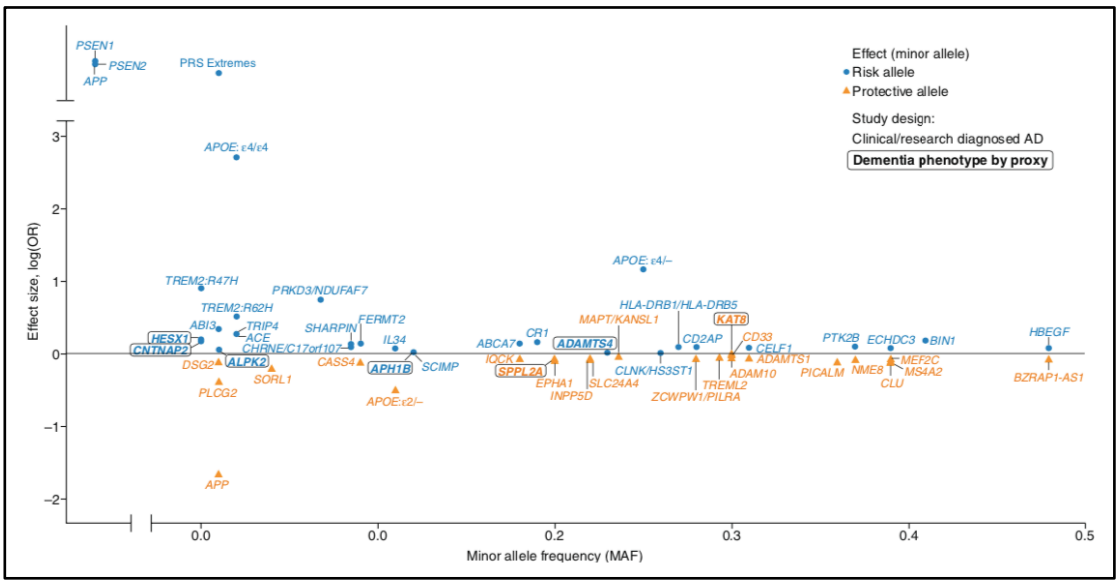

Figure 21: Schematic of Mendelian disease-causing genes and loci reaching GWS for single-variant (not gene-wide) association with sporadic AD. Blue circles and orange triangles represent risk and protective association, respectively. Associations identified in AD-diagnosed cohorts are not in boxes, while associations identified in meta-analysis of AD-diagnosed and proxy-diagnosed cohorts are indicated by black box outlines (Sims, Hill, and Williams 2020).

One of the genes discovered to be associated with AD is ***TREM2*** (Triggering Receptor Expressed On Myeloid Cells 2), in which a rare variant – R47H – triplicates the risk to develop AD (Guerreiro et al. 2013). Homozygous mutations of this gene were already known to produce Nasu-Hakola disease, characterized by bone cysts and dementia (Paloneva et al. 2002). The discovery emphasized the role of inflammation in AD, given the fact that TREM2 is expressed by MG, and it is up-regulated by MG in AD (see 3.2.1.5. The inflammation hypothesis of AD). The latest studies with inducible transgenic mice suggest that the non-pathologically associated isoform of ***TREM2*** protects against AD, but only at the beginning of the disease, while later on it loses its protective effect. The R47H variant – AD-associated – worsens the AD pathology independently of the stage of the disease (Zhong et al. 2019). This finding stresses the importance of the timing of therapeutic strategies, and bides scientists not to forget the multi-factorial aspect of AD.

3.2.4.3. Cardiovascular risk factors

Even though ageing is the most important risk factor associated to AD, we all age and this is inevitable. Consequently, targetable risk factors are therapeutically more interesting. Cardiovascular risk factors are long known to be associated to AD; fact that helped devising the neurovascular hypothesis of AD (see 3.2.1.3. The neurovascular hypothesis of AD).

The first evidence about neurovascular dysfunction in AD came already in 1994 (Buée et al. 1994) but it was not until the new millennium started that the first association of a cardiovascular disease risk factor – hypertension – and AD was made (Launer et al. 2000; Kivipelto et al. 2001). Moreover, people that received a treatment for hypertension in their midlife had a better cognition in their old age than those who did not (Gottesman et al. 2014). This finding goes hand by hand with the association of atherosclerosis/cholesterol and other vascular disease factors with AD. It was shown that midlife vascular disease was linked to late-life dementia, and more specifically, individuals in their 50s with two or more vascular risk factors had a triplicated risk of developing Aβ depositions in their 70s (Gottesman et al. 2017). Similarly, diabetes and obesity – known risk factors for cardiovascular disease – have been individually linked to AD (Biessels and Kappelle 2005; Chuang et al. 2016). Likewise, it has been proven that cerebrovascular and neurodegenerative diseases often occur together (Jellinger and Attems 2008).

The mechanisms by which the cardiovascular factors contribute to AD are not entirely clear. Some authors point out that they lead to cerebral artery alterations, which in turn could potentiate CAA (Zlokovic 2005). In any case, a good cardiovascular health and care during adulthood is advised to preserve the cognitive function later in life.

3.2.4.4. Others

Many other factors have been linked to AD. Because explaining them individually would be a complete thesis and it is not the aim of this one, and for the sake of space, I created a table with the list of all known associated factors referenced to get a clear overview (see **Table 2** below).

Table 2: AD associated factors

AD-associated factors	References
Ageing	Section 3.2.4.1
Genetic risk	Section 3.2.4.2
Cardiovascular risk	Section 3.2.4.3
Lipid imbalance	(Di Paolo and Kim 2011)
Mitochondrial dysfunction & oxidative stress	(Albensi 2019; Butterfield and Boyd-Kimball 2019)
Glucose metabolism dysfunction	(Croteau et al. 2018)
Viral infections & inflammation	(Devanand 2018)
Sleep dysregulation	(Musiek, Xiong, and Holtzman 2015)
Hormonal imbalance	(Pike 2017)
Alcohol consumption	(Piazza-Gardner, Gaffud, and Barry 2013)
Poor diet: vitamin B insufficiency	(Luchsinger et al. 2007)
Biometal dysregulation	(Mezzaroba et al. 2019)
Aluminium and mercury exposure	(Colomina and Peris-Sampedro 2017; Siblerud et al. 2019)
Cognitive inactivity	(Sajeev et al. 2016)
Head injuries	(Li et al. 2017)
Gut microbiome imbalance	(Cryan et al. 2020)
Neurotransmitter dysfunction	(Snowden et al. 2019)
Epigenetic dysregulation	(Qazi et al. 2018)
Lysosomal dysfunction	(Chung et al. 2019)
Excitatory-inhibitory imbalance	(Vico Varela, Etter, and Williams 2019)
Dysfunctional myelination	(Nasrabady et al. 2018)

Noticeably, AD has been related to many different factors. This thesis focuses on the vascular part, which is one of the topics taking off due to the increasing amount of studies linking it to AD. In the next section I deepen into this matter.

3.3. The BBB in AD

Whether the neurovascular hypothesis reflects the real aetiology of AD is a matter of debate (see 3.2.1.3. The neurovascular hypothesis of AD). What is clear though is the increasing amount of evidence supporting an important role of the vascular compartment in AD. Some of this evidence comes from alterations in the vascular morphology observed from brains of AD patients, such as microvascular damage, microbleeds, white matter lesions, and arterial atherosclerosis (more than age matched healthy brains). Also, neurovascular changes like reduced CBF appear before symptoms (Aβ & tau deposition, and dementia), and hemodynamic responses to neural activation are attenuated in the pre-symptomatic phase of AD. Moreover, AD and cerebrovascular diseases share risk factors (diabetes, hypertension, and obesity), and Aβ hinders a correct cerebral circulation by impairing the ability of endothelial and mural cells to relax. The fact that vascular abnormalities appear before obvious AD classical changes speak in favour of an early pathogenic role (Iadecola 2017).

Other reported vascular changes are a bit more controversial, with studies showing opposite results. The most marked example is the change in BBB permeability reported by some authors. Classically, BBB permeability has been assessed by different methods such as quantification in brain parenchyma of (A) blood-born proteins, (B) endogenous or blood-administered exogenous antibodies, and (C) blood-administered inert molecules. More recently, advances in MRI have allowed ***in vivo*** vascular permeability quantification. The increase in BBB permeability in AD has been reported using all the mentioned techniques (Blennow et al. 1990; Montagne et al. 2015; Van De Haar et al. 2016) although, on the other hand, some authors have not detected any changes using the same methods (Frölich et al. 1991; Starr et al. 2009; Bien-Ly et al. 2015). This topic remains an open debate nowadays that waits to be clarified (Profaci et al. 2020).

Within the BBB, PCs seem to undergo critical changes; in patients with prodromal AD, soluble Pdgfr-β is increased in the CSF, and PC loss has been demonstrated in some studies (Sengillo et al. 2013; Montagne et al. 2015; H. Shi et al. 2020). Also, BBB breakdown is associated to the reported PC degeneration, supporting other studies that claim that the BBB dysfunction seen in AD is independent of Aβ or tau accumulation (Nation et al. 2019). Furthermore, the loss of PCs has been shown to influence AD, and PC dysfunction driven by brain metabolic imbalances triggers BBB malfunction (Sagare et al. 2013; Sheikh et al. 2020). All of these reports highlight PCs as new important players in the disease pathology, although they remain vastly understudied in comparison to other neurovascular cells.

ECs too have been described to suffer from changes during AD progression. Vascular injury is a known pathophysiological feature in AD brains (Zipser et al. 2007) and ***APOE*** has been shown to control the cerebrovascular function, leading to BBB breakdown and cognitive dysfunction in the ***APOE4*** carriers (Bell et al. 2012; Montagne et al. 2020). Brain microvascular degeneration has been reported in AD by way of reduced capillary length, decreased tight junctional protein expression, alterations at the basement membrane, and even EC degeneration (Sweeney et al. 2019). Additionally, the group of Stefan Liebner previously demonstrated that brain microvessels from an AD mouse model not only express ***Bace1*** but also up-regulate its expression, potentially worsening the disease pathology (Devraj et al. 2016).

Altogether, many changes are described to occur at the BBB in AD, but very few studies are done to inquire deeper. No transcriptomic, epigenetic, metabolomic, lipidomic or proteomic data of the vascular compartment in AD is available yet. There is a lack of knowledge that needs to be filled to understand how these cells affect and are affected by AD.

3.4. Aim of the thesis & research questions

Certainly, research about the role of the BBB in AD has still many open questions to be answered. The aim of this thesis is to dwell into them in an effort to shed light upon a research topic that is full of potential. Furthermore, achieving a

better understanding of how the BBB is contributing to AD might allow the discovery of crucial therapeutic targets that will benefit millions of people. Improving the life-quality of AD patients is the ultimate objective of all AD research, and this study is no exception.

Currently, how the BBB is affected by AD, and how it contributes to AD pathology is not clear. Some studies report a BBB leakage in AD and others contradict this observation. In this thesis I hypothesize that the BBB is impaired in AD, resulting in an increased vascular permeability. Moreover, previous experiments in the Liebner research group where I worked during my thesis showed an up-regulation of ***Bace1*** in mouse brain microvessels (MBMVs). I therefore hypothesize that the BBB contributes to the AD pathology through APP cleavage and Aβ generation around vessels, which in turn causes BBB dysfunction and further worsening of the disease. Lastly, due to the lack of success of clinical trials, novel therapeutic targets to treat AD are needed. I hypothesize that targeting the BBB might prevent and/or ameliorate AD symptoms.

Additionally, this project is part of the Brain Barriers Training European PhD Training Network "BtRAIN" (H2020-MSCA-ITN-2015 675619), a Marie Skłodowska Curie research fellowship program. The aim of this collaborative project is to obtain knowledge on the vertebrate brain barrier signature genes and their specific role in regulating brain barriers function in development, health, ageing and disease. More specifically, my project contributes by analyzing 3' RNA-Seq data coming from MBMVs and FACS-sorted BBB cell types of an AD mouse model compared to age-matched wild type controls, in an effort to identify BBB regulated genes specific for AD.

4. Methods

4.1. Animal models

Mice were housed under standard conditions with 12 hours light dark cycle, with water and mouse chow available ad libitum. All experiments were performed according to the 3R principle (reduction, refinement, replacement). The handling and use of mice were approved by the Regional Council Darmstadt, Germany (V54-19c20/15-FK/1052). My work includes WT (C57BL6/J) as well as transgenic mice. The following mouse strains were used: AD model ***Thy1-APP***^{SwDI} (Davis et al. 2004), EC-specific inducible line ***Cdh5***(PAC)-CreERT2 (Y. Wang et al. 2010), β-catenin loxP-flanked line ***Ctnnb1***(Ex3)$^{fl/fl}$ (Harada et al. 1999), and reporter line mT/mG (Muzumdar et al. 2007).

Some of these mouse lines are based on the Cre/loxP model. Briefly, the Cre-recombinase is expressed under the control of a specific promotor and gets activated after induction with Tamoxifen (estrogen derivative). It recognizes loxP binding sites and cuts them, eliminating all the genetic information that was in between. By crossing the EC-specific inducible line with the β-catenin loxP-flanked line, a new mouse line is obtained – ***Cdh5***(PAC)-CreERT2:***Ctnnb1***(Ex3)fl/fl – in which the exon 3 of ***Ctnnb1*** is cleaved away in ECs specifically upon Tamoxifen induction. The exon 3 of ***Ctnnb1*** encodes the region of β-catenin that is phosphorylated and recognized by the destruction complex. Thus, β-catenin without exon3, cannot get phosphorylated and destroyed, and is free in the cytoplasm to translocate to the nucleus and activate transcription (see 3.1.4. The Wnt pathway). This mouse line is therefore a Wnt/β-catenin gain-of-function (GOF) model. Homozygous ***Thy1-APP***^{SwDI} mice were crossed with ***Cdh5***(PAC)-CreERT2:***Ctnnb1***(Ex3)fl/fl to obtain 50% AD/GOF (or simply GOF) and 50% AD/***Ctnnb1***(Ex3)$^{fl/-}$ (AD control or simply control) mice, according to Mendelian genetics.

The reporter line mT/mG is a regular WT mouse line that expresses either red fluorescence, or green if it received Tamoxifen. In my studies it was only used as a WT equivalent, with no Tamoxifen induction. This was necessary due to the difficulty of obtaining healthy aged mice, and owing to the 3R principle, I made use

of mice that would otherwise have been sacrificed. The use of mT/mG mice as WT is indicated appropriately in the respective experiements.

4.2. Tamoxifen preparation and induction

To activate the Cre-recombinase in the GOF lines, Tamoxifen (500 μg/vial; central pharmacy, Steinbach, Germany) was dissolved in corn oil (concentration of 5 μg/μl) and intraperitoneally injected in a final volume of 100 µl for five consecutive days. As control, mice without the Cre allele (Cre^-) were used and treated the same way as the GOF (Cre^+) mice.

4.3. Behavioural tests

All behavioural tests were performed in the afternoon, after at least one day of habituation to the new room. Mice were kept in individual cages with food and water ***ad libitum***. The nesting and burrowing tests were set three hours before the night cycle. All the tests were blind; random numbers were given to the mice and only after analysis of all the data, the different mouse groups were revealed.

4.3.1. Nesting test

The mice were changed to a new cage lacking the normal material that they usually have to build their nests. Instead, a nestlet was placed in each cage so that the mouse had to break it to build its nest. Mice were left overnight until the next morning, when pictures of the nests were taken. These pictures were analysed according to a pre-defined scale by colleagues and me separately. The average score was used as final output, and the Mann Whitney test for statistical analysis.

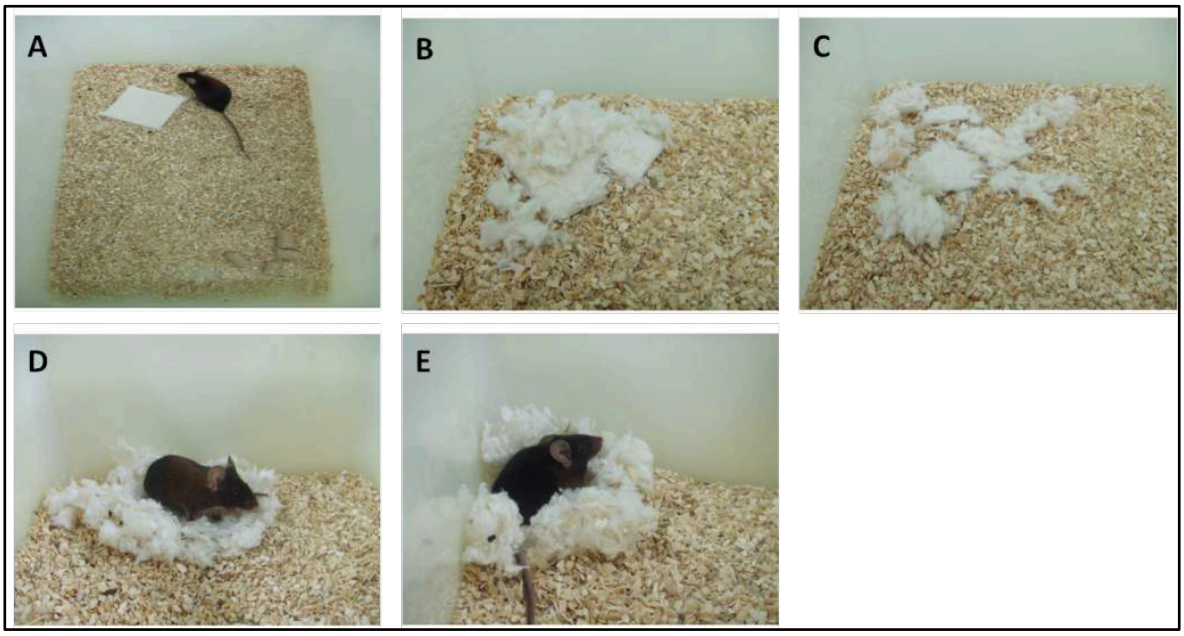

Figure 22: nesting test scores from worse (A or 1) to perfect (E or 5).

4.3.2. Burrowing test

Mice were transferred to rat cages containing a tube with 200 or 300 g (depending on the tube) of their regular food. The rest of the elements of the cage were left undisturbed (bedding, water, and nesting material). Mice were kept overnight, and on the next morning the food left in the tubes was measured. This food was subtracted from the initial food to obtain the burrowed food. To obtain percentages, the burrowed food was divided by the initial food and multiplied by 100.

$$\frac{food\ left - initial\ food}{initial\ food} \times 100 = \%\ burrowed\ food$$

4.3.3. Y-maze test of spontaneous alternations

Before and after every test, the maze was always wiped with 80% ethanol to clean and cover any odour cues. Once inside, the mouse had five minutes to freely explore, and its movements were either videotaped or manually annotated. The three arms of the Y-maze are named “A”, “B” and “C”. Each time that the mouse enters in one, it gets annotated. For an entry to be valid, the mouse needs to have crossed with its four paws. The final sequence of entries is analysed as follows: the combination of three different consecutive letters make an “alternation”, e.g., “ABC”, “BCA”, etc. The total alternations are divided by the total entries minus two

– for the last two entries cannot form an alternation – and multiplied by one hundred to obtain the percentage of alternations.

$$\frac{Total\ alternations}{Total\ entries - 2} \times 100 = \%\ alternations$$

Mice that did not make nine or more entries were excluded from the analysis.

4.3.4. Elevated-plus maze test

Before and after every test, the maze was always wiped with 80% ethanol to clean and cover any odour cues. Once inside, the mouse had five minutes to freely explore, and its movements were manually annotated. The elevated-plus maze has two closed arms and two open arms at a distance of 50 cm from the floor (**Figure 23**). The time spent in each arm as well as the entries were annotated. There are two final outputs: % time in the open arms, and % entries to open arms. The percentage of time in the open arms is obtained dividing the sum of time spent in the open arms by the total time and multiplying by 100. The percentage of entries to open arms is obtained dividing the entries to open arms by the total entries and multiplying by 100.

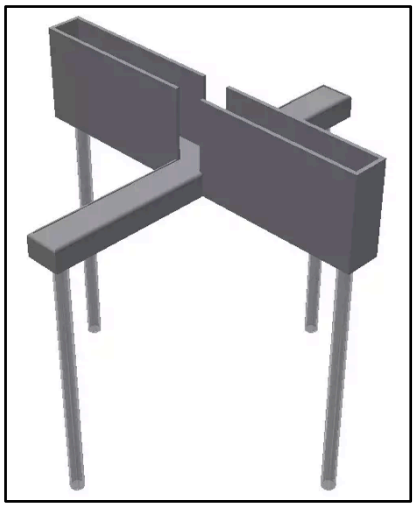

Figure 23: Elevated plus maze

4.4. BBB permeability assays

Anaesthesia (mixture of 2,5ml NaCl 0.9%, 500μl Ketavet, and 125μl Rompun) was IP injected ($\sim$ 200 μl but adjusting to body weight) 15 min before perfusion and reflexes were always tested before starting. Isofluorane was administered if the mouse was still showing reflexes. IP injected tracers were left in the circulation for 20 min, and IV injected tracers for 3-5 min. A sham control with PBS injection was always included.

Before starting the perfusion, blood was collected in a serum separating tube and stored on ice until further use. At the end of all the perfusions, the tubes were spin down to separate the serum and stored on -80˚C with no light until further use.

Perfusion was done transcardially with PBS for 3 min and the mouse was killed by cervical dislocation. The brain, cerebellum and kidneys were collected afterwards. One hemi-brain, one kidney, and the cerebellum were placed on 2 ml tubes, froze with dry ice and stored at -80˚C. Samples were always protected from light. The next day they were thawed on ice and weighted. 300 μl, 150 μl, and 100 μl of PBS were added to each kidney, hemi-brain and cerebellum, respectively. Then, they were homogenized with an electric overhead stirrer and dounce homogenizer, and spin down (13,000 rpm for 15 min at 4 ˚C). The supernatant was loaded to a 384 well-plate reader and the serum was diluted 1:10 and loaded too. Fluorescence was measured with a fluorescence plate reader (Tecan) at excitation / emission wavelength of 550 / 577 nm for TMR and 494 / 521 nm for FITC. The permeability index (μl/g) was calculated as follows:

I. Background correction: subtraction of sham fluorescence values to all the other samples.
II. Fluorescence per tissue gram: division of tissue fluorescence values by the respective tissue weight.
III. Normalization to serum: division by serum values. (Adjust to amount loaded and dilution made as well.)

The final formula is:

$$permeability\ index\ (\mu l/g) = (\frac{tissue\ fluorescence}{tissue\ weight})/(\frac{serum\ fluorescence}{\mu l\ serum\ loaded})$$

4.5. Brain microvessel isolation

Anaesthesia (mixture of 2,5ml NaCl 0.9%, 500μl Ketavet, and 125μl Rompun) was IP injected ($\sim$ 200 μl but adjusting to body weight) 15 min before perfusion and reflexes were always tested before starting. If the mouse was still showing reflexes, Isofluorane was administered. Perfusion was performed transcardially with PBS for 3 min and then, the mouse was killed by cervical dislocation.

All buffers and procedures were maintained at 4˚C unless stated otherwise. The brain was collected and placed in microvessel buffer (MVB; 4ml/brain). The cerebellum and olphactory bulbs were removed with a scalpel and the meninges peeled off by rolling the brain on Whatman paper. The choroid plexus was removed too and the "clean" brain placed in new MVB. For a primary detaching of cells, a mechanical homogenization was made with an electric overhead stirrer and dounce homogenizer (4 ml/brain to the pestle – of PTFE – and give 13-15 strokes, 100% machine intensity). Centrifuge 15 min, 4˚C, 1500rpm and suck the supernatant. Vortex the pellet in 3-4 times more volume of BSA 25% (in PBS) than the pellet and centrifuge (4˚C, 3000 rpm, 30 min): the myelin is lighter so it stays in the upper fraction. The cells & vessel fragments are denser than the BSA so they stay in the bottom (BSA in the middle, separating the 2 fractions). The pellet should appear reddish due to the erythrocytes, and the myelin white; otherwise the separation has not been successful. Aspirate the myelin and BSA fraction, and resuspend the pellet in clean MVB (2 ml/brain). Apply the suspension to a 100 μm pore mesh. Capillaries have a smaller diameter so they go through the mesh, leaving the bigger vessels on top. Apply the capillary fraction (flow-through) to a 40 μm pore mesh. This step is important to get rid of single cells (microglia, blood cells, etc.) and fragments of cells. Place the mesh upside-down on a sterile bacterial Petri dish. Use 350μl RLT&DTT buffer (lysis buffer from Quiagen) to scratch the mesh and to make sure that all the mouse brain microvessels are lifted and lysated. Collect it on a 2 ml tube and repeat it (700μl total/sample). Store at -80˚C until further use (for RNA isolation). **Figure 24** shows a schematic representation.

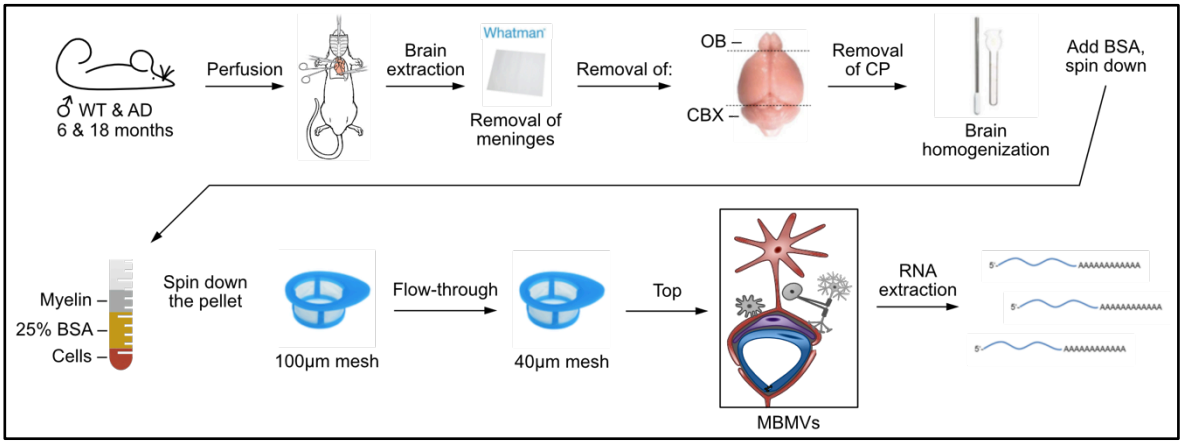

Figure 24: schematic representation of MBMV isolation protocol.

4.6. Brain single cell suspension & FACS

All buffers and procedures were maintained at 4˚C unless stated otherwise. All mice were treated with Isofluorane before cervical dislocation. The brain was then collected and placed in DPBS. The cerebellum and olphactory bulbs were removed with a scalpel and the meninges peeled off by rolling the brain on Whatman paper. The choroid plexus was removed too and the "clean" brain placed in new DPBS. With a scalpel, the brain was minced and incubated at 37˚C for 45 min and 600 rpm, in a mix containing DNase I & Papaine (4 ml/brain pair). Afterwards 8 ml of DPBS were added, mixed and spin down. The pellet was re-suspended in 4 ml DPBS and passed through a 10 μm pore mesh. The flow-through contains glial and non-vascular cells and was kept on ice until further use. The top of the mesh containing the vascular compartment was taken with buffer A and homogenized with an electrical overhead stirrer and dounce homogenizer. Then, an incubation at 37˚C, for 1 h, and 600 rpm was made with Collagenase II. At the end, both glial and vascular samples were spin down and re-suspended in 25% BSA (in DPBS) to separate the myelin by density gradient. The samples were spin down, myelin and BSA sucked away, and re-suspended in 1 ml DPBS for the glial sample, and a mix of 4 ml buffer A, 40 μl collagenase/dispase, and 4 μl DNase for the vascular sample. Subsequently, this vascular sample underwent a last incubation at 37˚C for 15min and 600 rpm. At the end, 8 ml DPBS were added, and the mix spin down and re-suspended with the glial sample. An extra spin down was performed and the pellet re-suspended in 200 μl FACS buffer. 20 μl were taking for the

unstained FACS control, the rest was incubated with 250 μl FACS antibody mix (Acsa2 1:50, Pdgfrβ 1:25, VE-Cad 1:50, Ng2 1:20, Cd11b 1:100, and Cd45 1:100) for 45 min. At the end, the mix was washed two timed with FACS buffer and finally re-suspended in 450 μl. A scheme of the protocol is pictured in **Figure 25**.

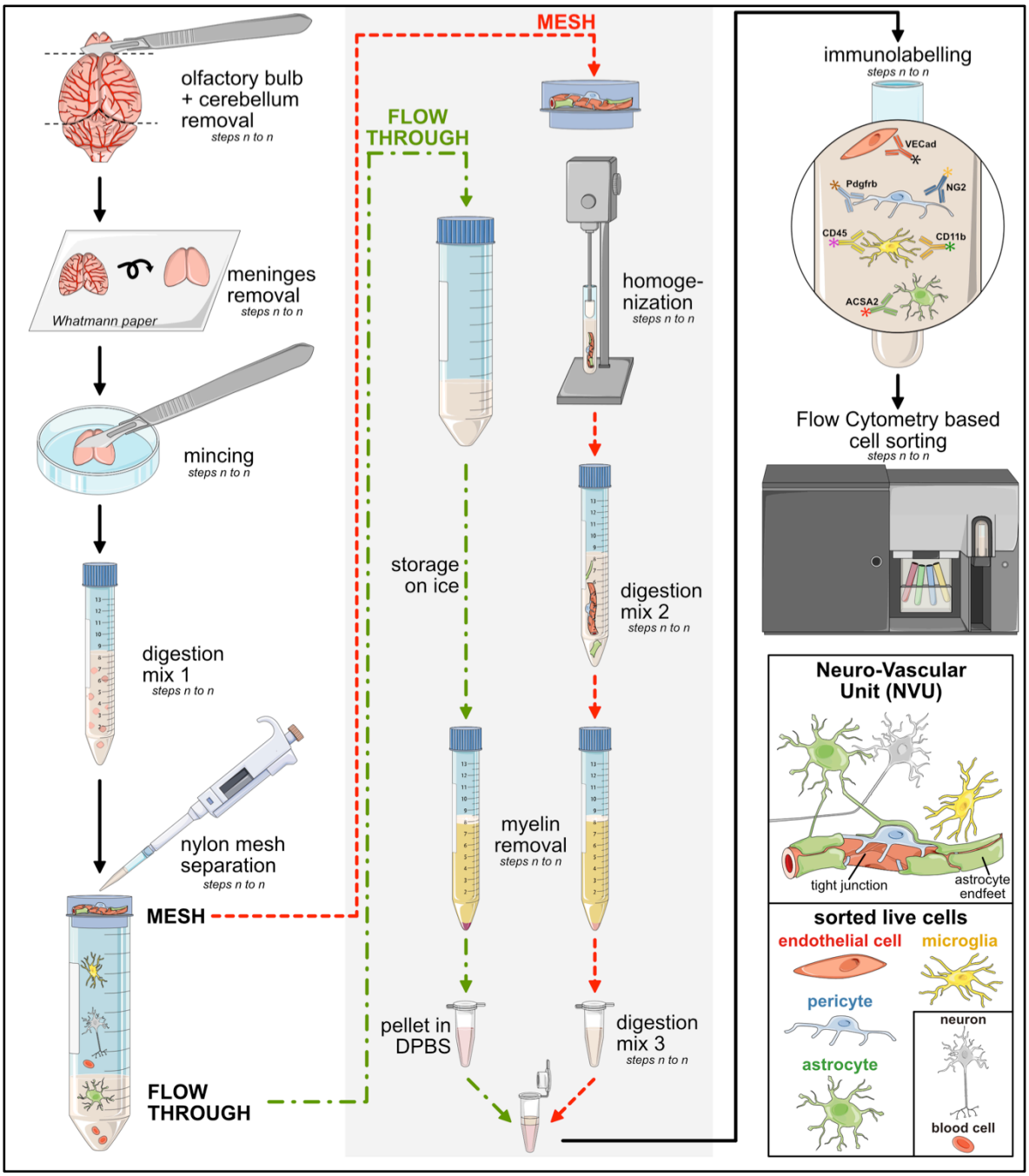

Figure 25: schematic representation of the live cell isolation protocol (cortesy of Dr. Kavi Devraj, unpublished).

The FACS sorting was done in collaboration with Dr. med. Daniel Spitzer, Dr. Sylvaine Guerit, or Dr. Kavi Devraj, who were in charge of the flow cytometer (FACS Aria). They had previously established the gating, and all the sorting experiments were followed according to the same gating strategy. The cells were directly sorted into RLT&DTT buffer (Quiagen) and stored at -80˚C until further use. The gating strategy can be seen in **Figure 26**.

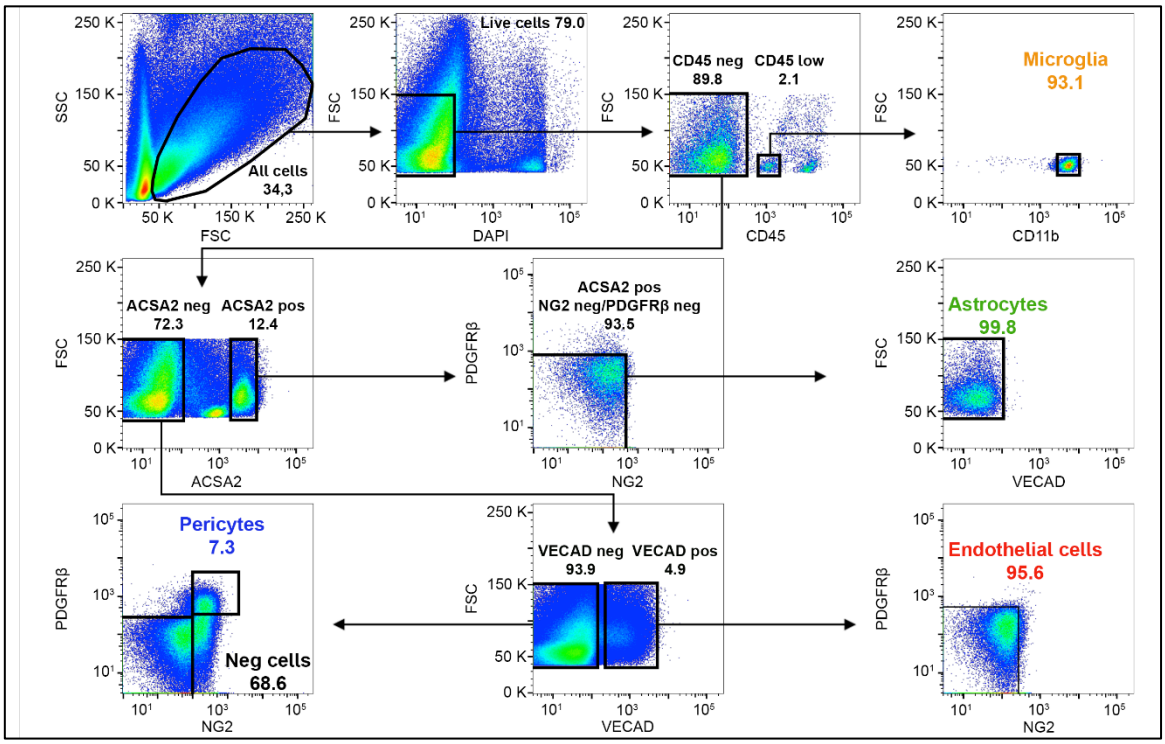

Figure 26: gating strategy for the FACS sorting of CD45^{low} & CD11b^{high} MG, ACSA2^{+} ACs, NG2^{+} & Pdgfrb^{+} PCs, and VECad^{+} (Cdh5^{+}) ECs. Courtesy of Dr. med. Daniel Spitzer (unpublished).

Essentially, live cells were gated as DAPI^{-} cells and divided as CD45^{-} or CD45^{low}. The CD45^{low} population that was CD11b^{high} was defined as MG. The CD45^{low} population was further divided as Acsa2^{-} or Acsa2^{+}. Acsa2^{+} cells were only defined as ACs after gating them Ng2^{-}, Pdgfrb^{-}, and Cdh5^{-} (or VECad^{-}) to exclude PCs or ECs attached to ACs. Acsa2^{-} cells were divided as Cdh5^{-} or Cdh5^{+}. The Cdh5^{-} population served to gate Ng2^{+} & Pdgfrb^{+} PCs, with no ACs or ECs attached. The Cdh5^{+} cells were defined as ECs only after gating Ng2^{-}, Pdgfrb^{-} to exclude PCs and ACs attached to the ECs.

4.7. RNA & DNA isolation

RNA from cell culture experiments was isolated using the RNeasy mini kit from Quiagen. Briefly, the cell lysates in RLT&DTT buffer were mixed with ethanol and added to the provided column. After washing the column, the RNA was eluted with H_2O and either immediately used for cDNA synthesis or stored at -80˚C until further use.

If the RNA to be isolated was coming from other experiments with low quantity, such as FACS-sorted or microvessel samples, the RNeasy micro or RNeasy plus micro kit from Quiagen were used. In short, the sample lysate in RLT&DTT buffer was mixed with ethanol and added to the provided column. Then, an incubation with DNase I was performed for 15 min at room temperaturein the column. Afterwards, the column was washed, and the RNA was eluted with H_2O and either immediately used for cDNA synthesis or stored at -80˚C until further use.

The RNA and DNA from microvessel and FACS-sorted samples used for further RNA-Seq were isolated in collaboration with GenXPro. Although the ZR-Duet DNA/RNA MiniPrep was used for the double isolation, the principle is the same as the Quiagen kit. It's important to notice that the main difference was that ethanol was not mixed at the beginning and the lysate was directly added to the column. The DNA has high affinity for it even in absence of ethanol, and therefore it remained attached while the RNA went through after spinning down the column. Then, ethanol was added to the flow-through (containing the RNA) and the mixture put in a new column. Both columns were washed and eluted with H_2O.

4.8. Quantitative polymerase-chain-reaction (qPCR)

The cDNA synthesis was achieved using the cDNA Synthesis Kit by Thermo Scientific. The following reagents were thawed and added into a sterile, nuclease-free tube on ice in the indicated order:

1. Total RNA (0.1 ng – 5 µg) 11 µl
2. Random hexamer primer 1 µl
3. 5x Reaction Buffer 4 µl
4. RiboLock RNase Inhibitor (20 u/µl) 1 µl

5. 10mM dNTP Mix 2 µl
6. RevertAid H Minus M-MuLV Reverse Transcriptase (200 u/µl) 1 µl

(Total volume 20 µl)

The sample was incubated for 5 min at 25˚C, followed by 60 min at 42˚C. The reaction was terminated by heating at 70˚C for 5 min. The remaining RNA was degraded by an incubation with RNase H for 30 min at 37°C. The final cDNA was stored at -20°C.

For qPCR experiments, the cDNA was diluted with H_2O to a final amount of ~ 3 ng. The qPCR was performed in technical triplicates for each sample using the Absolute qPCR SYBR Green Fluorescein Mix (#AB-1219, Thermo Fisher Scientific) according to the manufacturer's protocol with the program described in the following table (**Table 3**). Rplp0 was used as a housekeeping gene for normalization unless stated otherwise. Expression data was analyzed with the ΔΔct method. Primer sequences used for cDNA amplification by qPCR are listed in the 8.2.6. Primer lists section (page 167).

Table 3: qPCR program for RNA expression analysis.

Step	Temperature (°C)	Time (s)	Repeats
Initial denaturation	95	15 × 60	
Denaturation	95	30	45×
Annealing	61	30	
Elongation	72	35	
Final elongation	72	60	
Melt curve	55 (+0.5 per cycle)	5	80

4.9. 3′ mRNA-Seq & bioinformatics

The library preparation, 3' RNA-sequencing (Massive Analysis of cDNA Ends: MACE-Seq), and bioinformatics were performed by GenXPro. At the end, I obtained an excel table with the list of genes found by the RNA-Seq, and the correspondent statistics. Briefly, RNA was isolated as described in section 4.7 and the quality checked. For the library preparation, the cDNA was fragmented to obtain ~200 nucleotides long fragments and ligated to adaptors before the PCR amplification. The sequencing was made with Illumina Nextseq 500 and the results filtered with

FastQC. Then, PCR duplicates were removed and a second quality control was made. The mapping was performed with Bowtie2, the gene count with HTSeq, and the normalization and statistics with DEseq2. Finally, the pathway enrichment analysis was obtained using g:Profiler to identify over-represented biochemical pathways from 3 databases (KEGG, Reactome and Gene Ontology). A schematic representation of the whole procedure is shown in **Figure 27**.

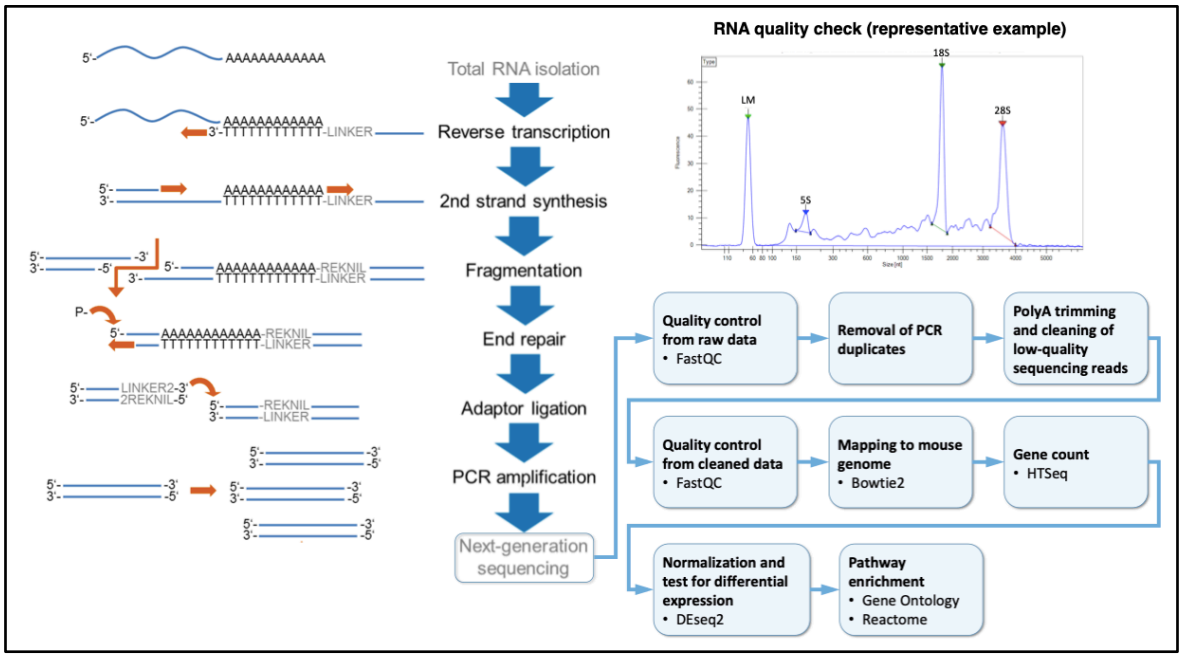

Figure 27: schematic representation of the MACE-Seq protocol by GeneXPro.

4.10. Analysis of marker genes in 3' RNA-Seq datasets

Thanks to the Barres and Betsholtz single-cell RNA-Seq datasets of mouse brains (Zhang et al. 2014; Vanlandewijck et al. 2018), I could define genes that were expressed at least 15 times more in a specified cell-type than in all the others. Only genes with at least 15 reads per million were considered. The list of genes can be read in **Table 4**. Housekeeping genes are named HK for space reasons.

Table 4: list of marker genes

Cell type	Marker gene list
EC	8430408G22Rik Abcb1a Abcc4 Abcc6 Ablim1 Acer2 Acvrl1 Adgrf5 Adgrl4 Afap1l1 AI467606 Akr1c14 Alox12 Ankrd33b Aqp11 Arap3 Arhgef15 Arl15 AU021092 AW112010 Bcl6b Bmx Bsg C130074G19Rik Cavin2 Ccm2l Cd34 Cd93 Cdh5 Cdkn2b Ceacam1 Cldn5 Clec14a Clic5 Ctla2a Cyb561 Ddc Def6 Degs2 Dennd3 Dll4 Dnah6 Edn1 Efr3b Egfl7 Egfl8 Eogt Eps8l2 Erg Far2 Fendrr Fgd5 Flt1 Flt4 Fmo2 Foxq1 Gata2 Gbp5 Gch1 Gimap1 Gimap5 Gkn3 Gm12250 Gm45837 Gm694 Grasp Grb7 Grrp1 Hmcn1 Hmgcs2 Hspa12b Icam2 Igsf5 Il2rg Impdh1 Itm2a Jag2 Jcad Kank3 Kcnq1 Kdr Layn Lef1 Lmo2 Lrp8 Lrrn3 Lsr Ly6a Ly6c1 Ly75 Mcf2l Mecom Megf6 Meox1 Mfsd2a Mmrn2 Myct1 N4bp3 Nos2 Nos3 Nostrin Notum Nxpe2 Nxpe4 Ocln Palmd Paqr5 Pecam1 Pglyrp1 Pik3r6

	Pkn3 Plk2 Pltp Podxl Pomc Prkch Prom1 Proser2 Ptprb Ptprr Rab11fip1 Rad54b Ramp2 Rasip1 Rassf9 Rgs12 Rnf125 Rnf144b Robo4 Rtp3 S1pr4 Samd12 Sema3c Sema7a Sgms1 Sgms2 Sgpp2 She Shroom1 Shroom4 Sigirr Slc16a1 Slc16a4 Slc19a3 Slc1a1 Slc26a10 Slc2a1 Slc30a1 Slc35f2 Slc38a5 Slc39a10 Slc39a8 Slc40a1 Slc52a3 Slc6a6 Slc7a1 Slc7a3 Slc7a5 Slco1a4 Slco1c1 Sox17 Sox18 Sox7 Spock2 St3gal6 St8sia6 Stap2 Stra6 Tbx1 Tdrp Tek Tfrc Thsd1 Tiam1 Tie1 Tmem252 Tmem88 Tnfsf10 Trib3 Trim16 Tspan13 Unc45b Ushbp1 Vil1 Vwf Zap70 Zfp366 Zic3
AC	1500009C09Rik 1700003M07Rik 1700084C01Rik 1810041L15Rik 2210416O15Rik 2610034M16Rik 2610203C20Rik 2900052N01Rik 2900092D14Rik 4833424O15Rik 4930480K15Rik 6330403K07Rik 9330159F19Rik A330076C08Rik Aass Abhd3 Acot11 Acsbg1 Acsl3 Acsl6 Adcy2 Adcy8 Adcyap1r1 Adhfe1 Adra2a Agpat5 Agt AI464131 AI854517 Aifm3 Aldh1l1 Aldoc Ap3b2 Apba2 Aqp4 Aqp9 Arhgef19 Arhgef26 Arhgef4 Arpp21 Arxes1 Arxes2 Asic1 Asphd2 Astn1 Atp13a4 Atp2b2 B230323A14Rik B3galt2 Baalc Bai1 Bai2 Bai3 Bbox1 Bcan Bdh1 Bmpr1b Brinp3 Btbd17 Bzrap1 Cacng5 Cadm2 Caskin1 Cbs Ccdc88c Cdh20 Cdh22 Celsr2 Chil1 Chl1 Chst1 Chst10 Cldn10 Clic6 Clip4 Clu Cml5 Cntn1 Col9a3 Cpe Cpne6 Csdc2 Cspg5 Cth Ctnnd2 Cxcl14 Cyp2j6 Cyp2j9 Cyp4f14 Cyp4f15 Dab1 Dbx2 Dclk1 Ddhd1 Ddo Ddx3y Dlgap1 Dnah7b Dnaic1 Dner Dok7 Dpp6 Drp2 Dtna Dtx1 E130114P18Rik Ednrb Efna5 Egfl6 Eif2s3y Elovl2 Enho Entpd2 Ephb3 Ephx2 Erbb4 Etnppl Etv4 Eva1a Exoc3l4 Extl1 Fabp7 Fads2 Fam107a Fam181a Fam181b Fam184a Fam198a Fam228a Fam228b Fam69c Fat3 Fgfr3 Fjx1 Fmn2 Folh1 Foxb1 Frmpd1 Fut9 Fzd9 Gabbr2 Gabra4 Gabrb1 Gabrg1 Galnt16 Gareml Gcnt4 Gdpd2 Gja1 Gjb6 Gldc Gli1 Gli2 Gm166 Gm2115 Gm266 Gm5607 Gm973 Gm996 Gpc5 Gpld1 Gpm6a Gpr123 Gpr179 Gpr19 Gpr37l1 Gria2 Grin2b Grin2c Grin3a Hepacam Hes5 Hif3a Hrh1 Hsd11b1 Id4 Igdcc4 Igsf1 Igsf11 Irx2 Itih3 Jakmip1 Kcna2 Kcnc4 Kcnd2 Kcne1l Kcng4 Kcnj10 Kcnj16 Kcnk1 Kcnn2 Kcnn3 Kcnt1 Kdm5d Kirrel3 Klhdc7a Lcat Lect1 Lgi1 Lgi4 Lgr6 Lix1 Lrrc9 Lrrn2 Lrtm2 Lsamp Luzp2 Maneal Mapk10 Mdga2 Meis2 Mgat4c Micalcl Mlc1 Mmd2 Mpped1 Mro Msmo1 Mt3 Mtss1l Nat8 Nat8l Ncam1 Ncan Ndp Necab3 Negr1 Nell2 Ngef Nkain4 Nlgn1 Nlgn3 Nnat Npas3 Nr2e1 Nrcam Nrxn1 Ntrk2 Ntsr2 Nwd1 Ogdhl Otx2 P4ha3 Pacrg Pantr1 Paqr6 Paqr8 Pcdh10 Pcdh17 Pcdh7 Pclo Pfn4 Phactr3 Phf21b Phkg1 Phyhipl Pipox Pla2g7 Plcd4 Plekhd1 Pm20d1 Pou3f2 Pou3f3 Ppap2b Ppargc1a Ppil6 Ppp1r1b Ppp2r2b Proca1 Prodh Prss35 Psd2 Ptch1 Ptchd2 Ptprz1 Rap1gap Rarres1 Rasgrf1 Rfx4 Rgs20 Rimklb Rims2 Rnase1 Rnf182 Rorb S100b Sall2 Scg3 Scn8a Scrg1 Sdsl Sel1l3 Sema4a Sema5b Serpina3n Sez6 Sfrp5 Sfxn5 Shisa9 Slc13a5 Slc14a1 Slc1a2 Slc1a3 Slc1a4 Slc22a4 Slc25a18 Slc27a1 Slc2a12 Slc38a1 Slc39a12 Slc4a4 Slc6a1 Slc6a11 Slc6a9 Slc7a10 Slitrk2 Smyd1 Snph Sorcs2 Sorl1 Sox1 Sox2 Sox21 Spag5 Spon1 St8sia5 Stmn3 Sybu Sycp2 Syn2 Tagln3 Tekt1 Timp4 Tlcd1 Tmem47 Tnik Tom1l1 Trim9 Trpm3 Tspan33 Tst Ttll3 Ttpa Ttyh1 Tuba4a Uty Vav3 Vit Wnt7a Wnt7b Wwc1 Zcchc18 Zfp641
MuC	**PC/vSMC:** 2310030G06Rik 4932435O22Rik 5033404E19Rik Abcc9 Ace2 Adamts16 AI593442 Ajap1 Anpep Arhgap42 Art3 Atp13a5 AW549542 Casq2 Cd80 Chst3 Cox4i2 Ecm2 Egflam Enpep Ephx3 Ggt1 Gm14005 Grm7 Higd1b Ifi30 Il2ra Impa2 Iqsec3 Kcnj8 Kctd1 Lin7a Mmp15 Ndufa4l2 Nodal Ntn1 Nts Nxph4 P2ry14 Pde4c Pde8b Pdgfrb Pla1a Plxdc1 Prrt3 Pth1r Ptk7 Ptpn22 Rai2 Sebox Sfrp2 Slc16a12 Slc19a1 Slc30a10 Slc5a5 Slc6a20a Sod3 Stc1 Tbxa2r Tlr12 Tmem178 Trpc3 Trpc4 Uchl1 Vtn Wbscr17. **SMC**: 6330403A02Rik Acta2 Actg2 Adamts14 Adamts8 Alx1 Ano1 Aoc3 Asb2 Atp1b1 Cabp1 Cap2 Cdh6 Cnn1 Crip1 Ctnna3 Cysltr2 Des Dgkb Dgkg Fam81a Fbxl22 Filip1l Gm13889 Gm6249 Gm9199 Gpr20 Gpr21 Grip2 Gucy2g Hrc Hspb2 Hspb7 Jph2 Kcna5 Kcnab1 Kcnb1 Kcnk3 Klhl38 Leprel1 Lmod1 Lrrc10b Mamdc2 Map3k7cl Mlf1 Mustn1 Myh11 Myl9 Mylk Myocd Myom1 Nexn Npy1r Nrip2 Ntf3 Ntn4 Olfr558 Olfr78 Palld Pde3a Pdlim3 Plin4 Pln Pnck Pou2f3 Ppp1r12b Rasl11a Rasl12 Rbm24 Rbpms2 Ryr2 Scn4b Sgca Sh3bgr Slc2a4 Smim5 Sncg Sntb1 Spint2 Srl Susd5 Tagln Tcap Tesc Tgfb3 Tmem255b Tpm2 Trpc6 Wtip Xirp1 Adamtsl1 Cdh4 Fhl5 Grem2 Klhl30 Ldb3 Mrgprh Nxnl2 Otogl Pgam2 Pi15 Ppp1r14c Rasd2 Susd2 Synpo2l. **Common**: Ajuba Asb10 Aspn Atp2a3 Cacna1c Cacna1h Ccdc160 Cd248 Cspg4 Ednra Emid1 Foxs1 Gper1 Gprc5c Gucy1a3 Gucy1b3 Hey2 Heyl Inpp4b Itga7 Kcnj12 Kcnmb1 Klhl23 Mcam Mir143hg Mrvi1 Ndst3 Notch3 Odf3l1 Pcdh18 Perp Pkia Plce1 Ptger3 Rgs4 Rgs5 Rrad Rtn4rl1 Serpini1 Slc38a11 Tbx2
MG	0610040J01Rik 2610203C22Rik 4632428N05Rik 5031414D18Rik 5430427O19Rik 5830444B04Rik 6330407A03Rik A630001G21Rik AB124611 Abcc3 Abi3 Adgb Adora3 Adrb2 AF251705 AI607873 Aif1 Alox5 Alox5ap Ang Aoah Apbb1ip Arhgap19 Arhgap22 Arhgap30 Arhgap4 Arhgap9 Arl11 Arl4c Arrb2 Atf3 Atp8b4 B430306N03Rik Basp1 BC035044 Bcl2a1b Bin2 Blnk Bmp2 Btk C1qa C1qb C1qc C1rl C3ar1 C5ar1 C5ar2 Capn3 Card9 Casp1 Cass4 Cbr2 Ccdc88b Ccl12 Ccl2 Ccl24 Ccl3 Ccl4 Ccl6 Ccl7 Ccl8 Ccl9 Ccr2 Ccr5 Cd14 Cd163 Cd180 Cd200r1 Cd209a Cd209f Cd22 Cd300a Cd300ld Cd33 Cd36 Cd37 Cd48 Cd52 Cd53 Cd68 Cd74 Cd79b Cd83 Cd84 Cd86 Cdh23 Cds1 Cdt1 Cebpa Cfp Clec10a Clec12a Clec4a1 Clec4a2 Clec4a3 Clec4d Clec4n Clec5a Clec7a Coro1a Cotl1 Crybb1 Csf1r Csf2rb Csf2rb2 Csf3r Ctss Cx3cr1 Cxcl2 Cxcr3 Cybb Cyth4 D130043K22Rik Dapp1 Dbpht2 Dennd1c Dock2 Dock8 Dok2 Dok3 Dusp2 E230029C05Rik Ebi3 Emr1 Epsti1 F13a1 F9 Fam102b Fam105a Fam46c Fcer1g Fcgr1 Fcgr2b Fcgr3 Fcrl1 Fcrls Fermt3 Fgd2 Fmnl1 Fndc7 Folr2 Frrs1 Fyb G530011O06Rik Gal3st4 Galnt12 Gcnt1 Glrp1 Gm10790 Gm11346 Gm11545 Gm14023 Gm5086 Gm6377 Gmip Gna15 Gp49a Gpr183 Gpr34 Gpr84 Gsap H2-Aa H2-Ab1 H2-DMa H2-DMb1 H2-Eb1 H2-Ob Havcr2 Hcar2 Hck Hcls1 Hexb Hk2 Hk3 Hmga2-ps1 Hmha1 Hpgd Hpgds Hpn Hrg Hvcn1 Ier5 Ifi202b Igsf6 Ikzf1 Il10ra Il16 Il1a Il1b Il20ra Il21r Inpp5d Iqgap2 Irf5 Irf8 Itgam Itgb2 Klk8 Klra2 Kmo Lacc1 Lag3 Lair1 Laptm5 Lat2 Lcp1 Lcp2 Lgmn Lilra5 Lilrb4 Liph Lpcat2 Lpxn Lrmp Lrrc25 Lrrc3 Lst1 Ltc4s Ly86 Ly9 Lyve1 Lyz2 Maf Man2b1 Map3k15 Map3k9 March1 Marcksl1 Matk Mgl2 Mlph Mlxipl Mmp9 Mpeg1 Mrc1 Ms4a6b Ms4a6c Ms4a6d Ms4a7 Msr1 Myo1f Myo7a Naip2 Naip6 Nav3 Ncf1 Ncf4 Nckap1l Neurl1a Neurl3 Nfam1 Nfatc2 Nfe2 Nfkbid Nfkbiz Nlrp1a Nlrp1c-ps Nlrp3 Npl Nyap2 Oas2 Olfr424 Orai2 Osm P2ry12 P2ry13 P2ry6 Parvg Pde3b Pf4 Pik3ap1 Pik3cg Pirb Pkib Pla2g2d Plbd1 Plcb2 Plcl2 Pld4 Plek Psd4 Ptafr Ptgs1 Ptk2b Ptpn18 Ptpn6 Ptprc Ptpre Ptpro Pvrl4 Rab20 Rab32 Rab3il1 Rac2 Rasa4 Rasal3 Rassf5 Rbm47 Rel Rgs1 Rgs10 Rgs18 Rgs2 Rhoh Rnf128 Rtl1 Runx1 Samsn1 Sash3 Sec16b Selplg Serpina3g Siglec1 Siglece Siglech Sirpa Sla Slamf9 Slc11a1 Slc15a3 Slc2a5 Slc37a2 Slc7a8 Snx20 Spi1 Spint1 Stab1 Stxbp2 Susd1 Susd3 Syk Syngr1 Tagap Tanc2 Tbc1d9 Tbxas1 Tfec Tgfbr1 Themis2 Ticam2 Tifab Timd4 Tlr13 Tlr2 Tlr6 Tlr7 Tmem119 Tmem173 Tnf Tnfaip3 Tnfaip8l2 Tnfrsf17 Tnfsf9 Tns4 Traf3ip3 Trem2 Treml2 Trpm2 Tshr Tyrobp Ubash3b Ugt1a7c Ulbp1 Unc13d Unc93b1 Vav1 Wdfy4 Wfdc17
FB	1500015O10Rik A730020M07Rik Abca6 Abca8a Abi3bp Adam12 Adamdec1 Adcy1 Aebp1 Aff3 Alcam Aldh1a2 Angptl1 Aox3 Apod Art4 Asgr1 BC055402 Bicc1 Bmp7 Bmper Car12 Car13 Car3 Ccbe1 Ccdc80 Ccl11 Cd44 Cd55 Cdh1 Cdo1 Cemip Cilp Clec3b Clmp Coch Col12a1 Col13a1 Col15a1 Col1a1 Col1a2 Col23a1 Col25a1 Col26a1 Col3a1 Col5a1 Col6a1 Col6a3 Col8a1 Col8a2 Colec11 Cpxm1 Cpz Crym Ctxn3 Cubn Cxadr Cxcl1 Cxcl16 Cygb Cyp1b1 Cyp2s1 D630003M21Rik Dapl1 Dcn Dkk3 Dpep1 Dpt Ebf2 Efemp1 Egln3 Emb Emp1 Enpp1 Eya1 Eya2 Fam174b Fam180a Fam26f Fanci Fbln1 Fbln7 Fbn1 Fhl2 Fibin Flnc Flrt3 Fmod Fndc1 Foxd2os Foxp2 Frzb Fxyd6 G630090E17Rik Gata6 Gdf10 Gjb2 Glt8d2 Gpr182 Gpr88 Gria3 Hgf Hpca Igf2 Igfbp2 Igfbp4 Igfbp5 Igfbp6 Igsf10 Inmt Islr Itgbl1 Itih2 Kazald1 Kcnj13 Kcnk2 Kcnt2 Kl Klf5 Lama1 Lamb1 Lbp Loxl1 Loxl2 Lpin3 Lrrc17 Ltbp2 Lum Matn2 Medag Mfap2 Mfap4 Mfap5 Mgp Mme Mmp2 Mmp23 Moxd1 Mpzl2 Mrap Mrc2 Ms4a4d Msln Musk Myoc Necab1 Ngfr Nnmt Nov Npr3 Nr1h4 Omd Osr1 Pamr1 Pdgfra Pdgfrl Pdzk1ip1 Phex Pi16 Piezo2 Plac8 Plekha4 Plekha6 Plk5 Plxnc1 Pnmal2 Podn Postn Ppp1r1a Prg4 Prrx2 Ptgdr Ptgds Ptger2 Ptger4 Ptgfr Ptgs2 Radil Ranbp3l Rbp1 Rbp4 Rnasel Robo1 Rspo3 S100a6 Scara3 Scara5 Scml4 Scn7a Scube1 Serpinf1 Sfrp4 Sgcg Six1 Six3os1 Slc13a4 Slc22a2 Slc22a6 Slc43a3 Slc47a1 Slc6a12 Slc6a13 Slc7a14 Slco5a1 Smoc2

	Sned1 Sphk1 Spon2 Spp1 Sprn Srpx2 Ssc5d St8sia1 Steap4 Sulf1 Svep1 Svopl Syt13 Tbx20 Tcf21 Tgfbi Thbs2 Timp1 Tmem158 Tnfaip2 Wdr86 Wisp1 Wnk4 Wnt2 Wnt4 Wnt6 Zmynd15
OL	1190005I06Rik 1500015L24Rik 1700047M11Rik 1700063D05Rik 2310069G16Rik 2810468N07Rik 4930506C21Rik 4930506M07Rik 9330117O12Rik 9330182L06Rik A230001M10Rik A230009B12Rik Aatk Abca2 Ablim2 Acot7 Adamts20 Adamts4 Adap1 Adssl1 Amph Ank3 Anks1b Ankub1 Anln Aplp1 Arc Arsg Aspa Atcay Atp9a B3galt5 Bcas1 Bcat1 Bfsp2 Bin1 C030029H02Rik Car2 Casq1 Ccdc13 Ccp110 Cdk18 Cela1 Cldn11 Cmtm5 Cnp Cntn2 Cobl Cpox Creb5 Creg2 Crtac1 Cryab Csmd3 Cyp2j12 D7Ertd443e Dbndd2 Depdc7 Desi1 Dlg2 Dlk2 Dnajc6 Dscaml1 Dusp15 Dusp26 Edil3 Efhd1 Efnb3 Elavl3 Enox1 Enpp2 Epb4.1l3 Ephb1 Erbb3 Ermn Evi2a Fa2h Faah Fabp5 Faim2 Fam131b Fam171b Fbxo2 Fcho1 Fez1 Fgfr2 Fsd1 Gabrr2 Gal3st1 Galnt6 Gjb1 Gjc2 Gjc3 Gm13293 Gnai1 Gpm6b Gpr37 Gpr62 Gria4 Hapln2 Hcn2 Hhip Il17rb Il1rap Il33 Inpp5j Itgb4 Jakmip3 Josd2 Jph4 Kcna1 Kcna6 Kcnk13 Kctd13 Kctd4 Kif1a Kif21a Kndc1 Lgi3 Lhfpl3 Lpar1 Lrrn1 Mag Mal Map6d1 Map7 Mapk8ip1 Mapt Mbp Mobp Mog Myh14 Myrf Nacad Ncam2 Neu4 Nfasc Nfe2l3 Ninj2 Nipal4 Nkain1 Nkain2 Nkx6-2 Nmral1 Npsr1 Olig1 Olig2 Omg Opalin Opcml Padi2 Pak1 Pak7 Pcbp4 Pcdh15 Pcdh9 Pcolce2 Pcsk1n Pcyt1b Pde1c Pex5l Pgbd5 Pigz Pik3c2b Pkd2l1 Plagl1 Plekhb1 Plekhh1 Plp1 Pls1 Plxnb3 Pnmal1 Ppp2r2c Prkcq Prkcz Prox1 Prr18 Psat1 Pstpip2 Ptprd Qdpr Qpct Rab33a Rasal1 Rhou Rnf112 Rtkn Rtkn2 S1pr5 Scd2 Scg5 Serpinb1a Serpind1 Sez6l2 Sgk2 Sh3gl3 Shisa4 Slain1 Slc24a2 Slc44a1 Smco3 Sorcs1 Sox10 Sox2ot Sox8 Spock3 Srcin1 Srd5a1 St18 Stmn4 Syt11 Tmeff2 Tmem108 Tmem125 Tmem132b Tmem151a Tmem163 Tmem88b Tnfaip6 Tnni1 Tppp Tprn Trf Trim2 Trim59 Tspan2 Ttc9 Tubb4a Tyro3 Ugt8a Vldlr Wnt3 Wscd1 Zfp239 Zfp488 Zfp536
N	Lhx1os 5330417C22Rik Nyap1 A930038C07Rik Ablim3 Ache Actl6b Amy1 Atp1a3 Plppr3 Bcl11a Bhlhe22 Cacna2d1 Cacna2d2 Cacna2d3 Calb2 Car10 Cd274 Cdh4 Celf4 Celf5 Celf6 Celsr3 Chgb Clstn2 Cnr1 Col6a2 Cpne7 Crabp1 Crmp1 Dact1 Dlx1 Dlx1as Dlx2 Dpysl5 Dync1i1 Ebf3 Ecel1 Elavl2 Erc2 Ripor2 Foxo6 Gabrg2 Gad1 Gad2 Gap43 Gdf5 Gng2 Gprin1 Grem2 Gria1 Grm2 Hcn4 Hspa12a Igfbpl1 Ina Islr2 Kcnc2 Kcnip2 Kcnk9 L1cam Lhx5 Lhx6 Mab21l1 March4 Meg3 Mrap2 Ndrg4 Nell1 Nhlh2 Nos1 Npas4 Nppc Npy Nr2f2 Nrn1 Nrxn3 Nxph4 P2rx5 Penk Plekha7 Pnoc Ppfia4 Rab3c Reln Rem2 Rian Rims3 Robo2 Scg2 Slc17a6 Slc2a13 Slc32a1 Snap25 Snhg11 Spock1 Sst Stk32b Stmn2 Sv2b Syngr3 Synpr Syp Syt1 Syt4 Syt7 Tbr1 Thsd7b Tmem130 Tmem59l Syndig1l Trp73 Tubb3 Vgf Vstm2l Zcchc12 Zic1
HK	Actb B2m G6pdx Gapdh Gusb Pgk1 Ppia Rpl13a Rplp0 Rps18 Sdha Ywhaz

To analyse changes in cell-type content in the MBMV samples, the markers' relative expression was calculated normalizing the tags per million (TPM) of each marker to the mean expression of all groups. Then, the average was calculated for all markers of each cell-type and the values of each sample were introduced in Prism for statistical analysis and graphic design. An example table is shown below (**Table 5**).

Table 5: calculation of average markers' relative expression with example values

Marker gene	Cell-type	TPM WT	TPM AD	Mean	Rel WT	Rel AD
EC_1	EC	200	300	250	0,8	1,2
EC_2	EC	50	90	70	0,7	1,3
AC_1	AC	30	20	25	1,2	0,8
AC_2	AC	60	50	55	1,1	0,9
Average EC	EC				0,75	1,25
Average AC	AC				1,15	0,85

4.11. Histology procedures

4.11.1. Tissue embedding and sectioning

Tissue samples were isolated from mice, embedded in Tissue TEK® O.C.T. compound (Sakura) and frozen on dry ice. 10 μm cryosections (unless stated otherwise) were cut by Microm HM550 microtome at -20°C, placed on Superfrost

Microscope slides and dried on a heating plate set at 37 °C. The sections were stored at -80 °C.

4.11.2. Immunofluorescence staining and imaging

Cryosections were thawed on a 37 °C heating plate for 10 min and washed 3 x in PBS for 5 min. After fixation with 4 % PFA (in PBS) for 10 min at room temperature or ice-cold methanol for 5 min at -20 °C, and repeating the washing step with PBS, sections were blocked in a humidifying chamber for 1 h. The sections were incubated with the primary antibody mix for 2 h at room temperature or overnight at 4°C (for details about the blocking and antibody mix, see 8.2.4. Buffers and solutions on page 165). Following a washing step, they were incubated with the corresponding secondary antibody mix 1 h at room temperature and were washed again with PBS 3 x 5 min. The tissue was counterstained with DAPI, nuclear green or Topro for 10 min at room temperature. Slides were mounted with Aqua PolyMount and left for at least 1 day to dry before using them. Pictures were taken with a confocal laser scanning microscope (Eclipse TE 2000-E, Nikon Instruments) and analysed with the NIS-Elements Microscope Imaging Software AR (Nikon Instruments).

4.11.3. Immunohistochemistry staining and imaging

The IHC procedure was performed on an automated IHC stainer (Leica). In short, the automated steps are:

1. Peroxide block 5 min
2. BOND wash solution 3x
3. Marker (1:100) 15 min
4. BOND wash solution 3x
5. Polymer 8 min
6. BOND wash solution 2x 2 min
7. Deionized water 1x
8. Mixed DAB refine 1x
8. Mixed DAB refine 10 min
9. Deionized water 4x
10. Haematoxylin 10 min

11. Deionized water 1x
12. BOND wash solution 1x

The slides were visualized with a Nikon ECLIPSE 80i microscope.

4.11.4. Tissue preparation and light sheet imaging

Methoxy-X04 was injected IP 24 h and 1 h prior to sacrifice (50 μl, 5 mg/ml). Mouse blood vessels were labelled by intravenous injection (80 µl) of DyLight 488 or 649 labeled Lycopersicon Esculentum (Tomato) Lectin (#DL-1174 or #DL-1178, Vector laboratories), which was dialyzed one day before for at least 4 hours at room temperature, in PBS. After a circulation time of 4 minutes the animals were sacrificed, and the brains collected and left in overnight fixation (4% PFA in PBS) protected from light. After 3x PBS washes, the tissue was embedded in 0.4% low-melt agarose diluted in Millipore water.

The following dehydration and delipidation protocol has been adapted (Renier et al. 2014; Orlich and Kiefer 2018). In brief, methanol (50/70/100%) in PBS was used for dehydration (1 h for each step) in dark-brown glass vials slightly shaking at room temperature, followed by overnight incubation in 100% methanol. To remove lipids, an incubation with dichlormethane (#270997-100ML, Sigma-Aldrich) followed for around 30 min until the tissue sank down. Afterwards, clearing with ethylcinnamate (ECi; #112372, Sigma-Aldrich) was performed (Klingberg et al. 2017). Finally, samples were stored in ECi solution that was renewed one day before the acquisition. Imaging was acquired in ECi solution with an UltraMicroscope II (LaVision, Germany). Data were further processed for visualization with Imaris 9 (BitPlane, Switzerland).

4.12. Plasmid cloning

For the cloning of pLKO.1-SIRT1-ShRNA, pLKO.1-control, and pMD2.G (viral envelope plasmid), ***E. coli*** Stbl3 for unstable DNA were used. For the viral packaging plasmid psPAX2, ***E. coli*** DH5α were used. Briefly, the Stbl3 transformation was made by heat-shock at 42˚C for 45 s, and the DH5α at 42˚C but for 90 s. After that, the bacteria were placed on ice for 2 min, followed by addition of warm (37˚C) S.O.C. Medium. The bacteria were kept at incubation

(37˚C, 220 rpm) for 1 h, and afterwards the medium was spread over bacterial plates (with Ampicillin) and left in overnight incubation.

Alternatively, other plasmids (pCS2-***DKK2***-flag and pcDNA3.1-***Sirt1***-FL) were received already in bacteria as agar stab, and were placed on bacterial plates (with Ampicillin) directly and left in overnight incubation. The next day, the three best-looking colonies of each plasmid were picked for growing in 4 ml LB medium (incubation for 7-8 h at 37˚C, 220 rpm), and afterwards the densest sample of them three was chosen for overnight growing in 300 ml LB medium (37˚C, 220 rpm).

The plasmid-DNA extraction was made with the Plasmid Purification Maxi kit (Quiagen). In short, the bacteria was pelleted by centrifugation (6000 × g, 15 min, 4˚C) and mixed with the provided buffers to lysate the bacteria. After another centrifugation (20000 × g, 30 min, 4˚C), the supernatant containing the plasmid DNA was added to a provided column and washed several times according to protocol. Then, the plasmid DNA was eluted in 15 ml buffer QF, precipitated by adding 10.5 ml isopropanol, and pelleted by 30 min centrifugation (15000 × g, 4˚C). The supernatant was removed and the pellet washed with 70% ethanol, and air-dried. Finally, it was re-suspended in H_2O and stored at -20˚C. The concentration was measured using a spectrophotometer.

4.13. BEnd5-*Sirt1*^{KD} generation and characterization

4.13.1. Viral particles production

The protocol for lentiviral infection of mammalian cells was taken from Addgene (Addgene Plasmid 10878. Protocol Version 1.0. December 2006). 7×10^5 HEK-293T cells in 5 mL of media were plated on a 6 cm tissue culture plate and incubated at 37°C, 5% CO_2 overnight. Although cells should regularly be passaged in DMEM + 10% FBS with penicillin/streptomycin, cells should be plated at this step in DMEM + 10% FBS without antibiotics. The next day the transfection was performed in the late afternoon because the transfection mix should only be incubated with the cells for 12-15 hours. The transfection mix was made in polypropylene microfuge tubes (do NOT use polystyrene tubes) as follows:

- 1 μg pLKO.1 shRNA plasmid
- 750 ng psPAX2 packaging plasmid
- 250 ng pMD2.G envelope plasmid
- to 20 μl serum-free OPTI-MEM

In a separated tube, 74 μl serum-free OPTI-MEM and 6 μl FuGENE were mixed, and incubated for 5 min at room temperature. Then, this was mixed with the transfection mix, and incubated for 20-30 min at room temperature before added to the HEK293T cells. Important note, at this point the cells were kept in a Security level 2 laboratory. 12-15 h after, the media was changed to media containing antibiotics and left further incubating for 24 h. After that, the media was collected and centrifuged (1250 rpm, 5 min), or filtered (0.45 μm) to remove possible cells. Finally, an ultra-centrifugation (90 min, 21000 rpm) was made to pellet the viral particles, which were then re-suspended in 100 μl PBS. This was used to make 10 μl aliquots for immediate use or stored at -80˚C.

4.13.2. Infection of bEnd5 with lentiviral particles

The bEnd5 were ~ 70% confluent before infection and polybrene (8 μg/mL) was added to the MCDB complete media. 20 μl (2 aliquots) of re-suspended viral particles were added to each plate followed by a centrifugation at 1000 rpm for 30 min. Then, the cells were incubated (37°C, 5% CO_2) for 24 h before changing to fresh media containing puromycin (2 μg/ml). They were kept in puromycin containing MCDB complete media.

4.13.3. Proliferation & migration characterization

Plates were always previously coated with 0,1% gelatine. Both bEnd5-***Sirt1***^{KD} and bEnd5-control were maintained in MCDB complete + puromycin media and passaged after the cells reached confluence.

4.13.3.1. Proliferation assay

On 24-well plates, 16000 or 33000 cells/well of each bEnd5-***Sirt1***^{KD} and bEnd5-control lines were seeded and left to grow. Cells were counted at 12 h, 1, 2, 3, 4, and 6 days to obtain a proliferation line.

4.13.3.2. Scratch-wound assay and live-cell microscopy

For the scratch-wound assay the cells were always confluent. With a sterile 1 ml pipette tip, a scratch (wound) was made from top to bottom on the plate surface containing the cells. Pictures were taken before and after the scratch, and the next day. The width and area of the wound were measured with ImageJ.

Alternatively, the cells were left overnight in the live-cell microscope (Okolab), at the same conditions as the cell culture incubator (HERA cell 150, Thermo Electron Corporation), i.e., 37˚C and 5% CO_2. Pictures were programmed to be taken every 15 min. The area of the wound was measured with the NIS-Elements Microscope Imaging Software AR (Nikon Instruments).

The scratch-wound assays that did not require live-cell microscopy were made by Aylin Möckl under my supervision as part of her master program.

4.14. HEK293T transfection

Transient transfection of HEK293T cells was performed following the calcium phosphate-DNA co-precipitation method. Prior to transfection, $\sim 1.5 \times 10^6$ cells were plated into 10 cm culture dishes and incubated for 4 h at 37°C and 5% CO_2. Approximately 2 h before cell treatment with the transfection mix, the complete growth medium was changed to medium without antibiotics. The plasmid DNA was diluted with UltraPure™ DNase/RNase-free distilled water to a final volume of 437.5 μl, following addition of 125 μl 1M $CaCl_2$ and thorough mixing. Additionally, 250 μl of 2x BES (pH = 6.97) were pipetted drop-wise onto the DNA-$CaCl_2$ solution and an incubation at room temperature for 15-20 min allowed for a uniform haze to form, which is critical for the transfection efficiency. Lastly, the Ca_2-PO_4-DNA solution was added drop-wise onto the cells and incubated at 37°C and 5% CO_2 overnight. 15-17 h post transfection, the medium was changed to complete growth medium with antibiotics and the cells were incubated under the appropriate conditions until harvesting for either RNA isolation, protein isolation & western blot, or luciferase assay (i.e. 36 h post transfection).

4.15. Dual luciferase assay

HEK293T cells were transfected as described previously (4.14. Dual luciferase assay) with one of the co-transfection mixes described below. The M50 Super 8x

TOP-FLASH, M51 Super 8x FOP-FLASH, pTRE2-hygromycin, pTRE2-hygromycin-GFP, and pRL-TK-Renilla are referred to as TOP, FOP, Empty Vector (EV), GFP, and Renilla, respectively.

- TOP + Renilla + GFP + DKK2 = TOP-DKK2
- TOP + Renilla + GFP + EV = TOP-EV
- FOP + Renilla + GFP + DKK2 = FOP-DKK2
- FOP + Renilla + GFP + EV = FOP-EV

The transfected cells were seeded in 24-well plates (10^5 cells/well), and 4 hours afterwards treated with either recombinant murine Wnt3a (Peprotech, #315-20) at different concentrations (1.5, 15, or 150 ng/ml), or vehicle (0.1% BSA in PBS). Around 20 hours after treatment, the cells were washed with pre-warmed PBS and lysed using 200 μl/well of 1x Passive Lysis Buffer for dual-luciferase reporter assay systems. The plate was directly placed on an orbital shaker at 300 rpm for 30 min. The cell lysates were transferred into 1.5 ml tubes and centrifuged at 13000 rpm (room temperature) for 10 min. 75 ml of each sample were pipetted into a Corning® 96-well white polystyrene microplate and the activity of Firefly and Renilla was measured using the plate reader (Tecan). For this, 37.5 μl of D-Luciferin was added to 10 ml of Firefly Buffer and 5 μl of Colenterazine were added to 10 ml of Renilla Buffer. Once the substrates were added, the tubes were wrapped with foil and the measurement was conducted.

4.16. Statistical analysis

Statistical tests were conducted with the software of GraphPad Prism 6. All data are represented as mean ± standard error of the mean (SEM). Differences between two groups were evaluated by unpaired two-tailed t-test unless stated otherwise, and statistical significance was determined based on the p value, where $p < 0.05$ is considered significant (*), $p < 0.01$ strongly significant (**) and $p < 0.001$ highly significant (***).

4.17. Contribution of collaborators

The scratch-wound assays were partially done by Aylin Möckl who was a master student under my supervision in the laboratory. She performed the experiments following my instructions.

The FACS-sorting protocol for isolation of ECs, PCs, ACs, and MG was made together with Daniel Spitzer, Sylvaine Guerit, or Kavi Devraj, who supervised the bench part and run the FACS machine for the sorting part.

The RNA-Sequencing was done in collaboration with the company GenXPro GmbH, which is also part of the European network “BtRAIN”. More specifically, I collaborated with Ricardo Figueiredo who developed a protocol for sequencing samples with low RNA quantity, and performed the library preparation and bioinformatics of all my sequencing samples. He also participated in sample analysis and graphic creation.

The whole BtRAIN network including students and principal investigators participated actively in scientific discussions. Their input and feedback contributed greatly to the development of this project.

5. Results

5.1. *Sirt1*-knockdown in bEnd5 cells promotes augmented proliferation/migration properties

SIRT1 is a known modulator of vascular ageing and it has been linked to AD with reports showing a beneficial effect of ***Sirt1*** activation in AD mouse models (Guo, Xu, and Wang 2016). I aimed to investigate the role of murine endothelial ***Sirt1*** by knocking down its expression in the immortalized mouse brain endothelial cell line bEnd5. To do so, I transfected HEK293T cells with the pLKO.1 plasmid containing a murine ***Sirt1*** targeting ShRNA or a scrambled control. The transfection included the viral packaging and envelope plasmids psPAX2 and pMD2.G, respectively, necessary to produce lentiviral particles. The bEnd5 were then infected with the lentiviral particles, as it is presented in **Figure 28 F**. The knockdown efficiency was measured by qPCR. After a few passages with media containing puromycin, the ***Sirt1***-knockdown (***Sirt1***-KD) became stable (**Figure 28 A**). I then measured the proliferation of both bEnd5 control and ***Sirt1***-KD by counting the number of cells at consecutive time points and obtaining the growing equation. At high density, no differences were apparent. However, at low density the ***Sirt1***-KD cells grew more than the control (**Figure 28 B**). This result is not conclusive, as more biological replicates are needed for statistical analysis. Nevertheless, it drove further investigation and thus, scratch-wound assays that measure the proliferation/migration of cells were performed. At this step, Aylin Möckl became my laboratory supervisee and the following experiments were done by her, following my instructions. bEnd5 cells were grown until they reached confluence. At that point, a scratch was made from top to bottom, forming a wound on the cellular layer. Aylin took pictures of the scratched surface before, after, and the next day to compare the reduction of wounded area and width due to migration of ***Sirt1***-KD and control cells. The results indicated that ***Sirt1***-KD cells invaded more area and width of the scratched surface than control cells (**Figure 28 C-D**). Interestingly, this result was only noticeable many passages after the infection, suggesting that the ***Sirt1***-KD was probably still not completely settled in previous passages. To confirm our suspicions, I decided to repeat the scratch-wound assays with further passages of the cells and analyse the migration by live-

cell microscopy. After the wound was made, the cells were placed inside the live-cell microscope chamber and left to grow overnight. Pictures were taken every 15 min and the comparison was made at 14.5 hours post-wound. In all three passages analysed, the ***Sirt1***-KD cells invaded the scratched area faster (**Figure 28 E**). Therefore, the reduced ***Sirt1*** gene expression in bEnd5 cells causes a hyper-proliferating/migrating phenotype.

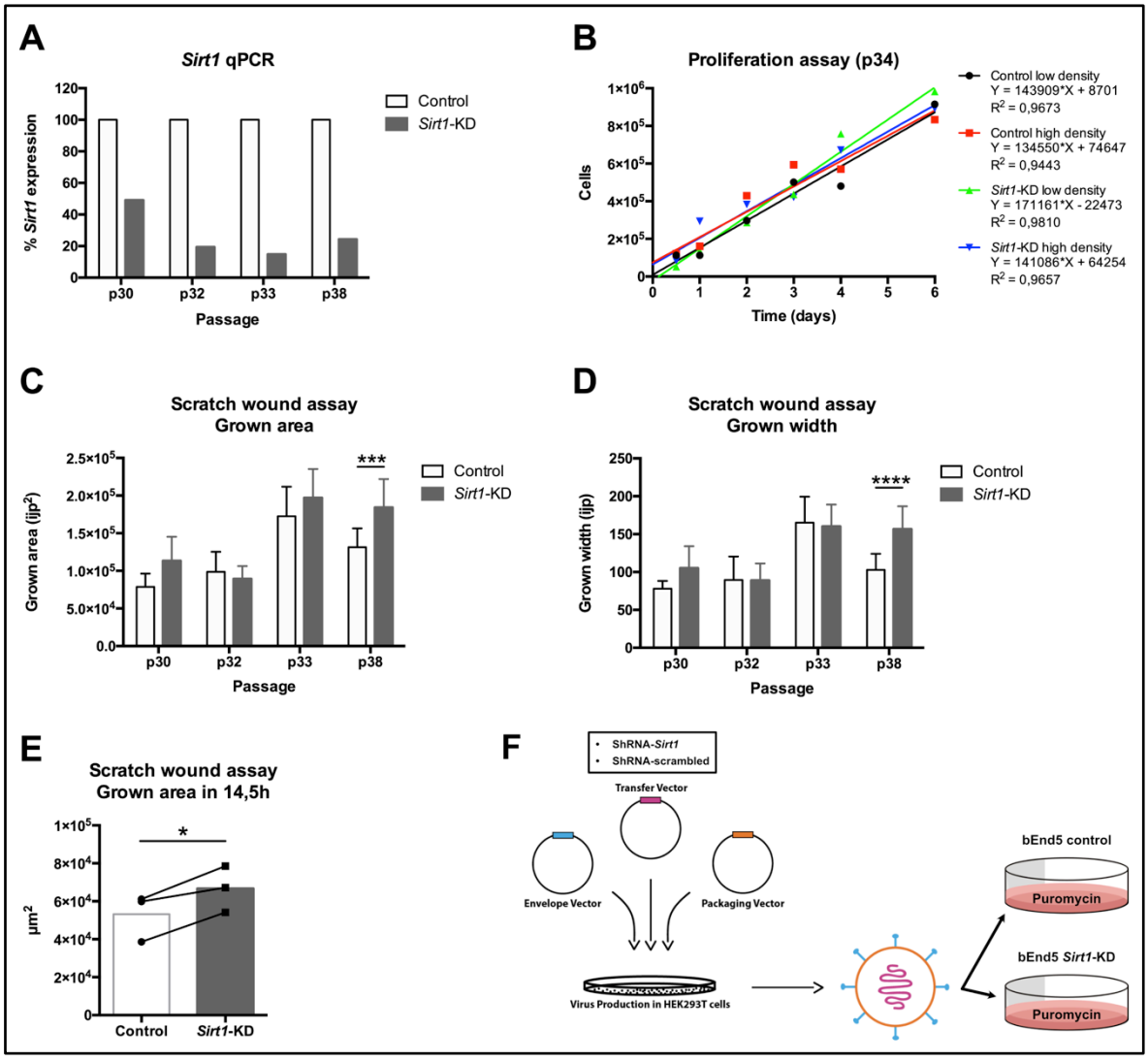

Figure 28: (**A**) quantitative PCRs for ***Sirt1*** in bEnd5 cells, normalized to ***Rplp0***. (**B**) Proliferation assay of bEnd5 cells at passage #34. Low and high density correspond to 1.7×10^4 and 3.3×10^4 seeded cells per 24-well-plate well, respectively. Each measurement was made in duplicates, and the average was used. (**C-D**) Scratch wound assays in bEnd5 cells at passages #30, 32, 33, and 38. The grown area (**C**) and width (**D**) were calculated by substraction of initial to final scratched area/width. N = 4-5 and 12 for p30&32 and p33&38, respectively. "ijp": ImageJ pixels. (**E**) Scratch wound assays in bEnd5 cells at passages #39, 40, and 41. The grown area was measured by substraction of scratched area at time-0 to time-14,5 hours. (**F**) Schematic representation of bEnd5-***Sirt1***-KD/control production.

The ***in vitro*** work proved useful to study the effect of ***Sirt1*** reduction in endothelial cells. However, in order to investigate AD, a higher level of complexity was needed. Therefore, I made use of an animal model that mimics the effects of AD observed in humans.

5.2. The *Thy1-APP*^{SwDI} mouse model develops Aβ plaques and memory loss

The animal model of choice to study AD was the transgenic mouse ***Thy1-APP***^{SwDI} that harvest the human ***APP*** known mutations ***Swedish***, ***Dutch*** and ***Iowa*** under the mouse neuronal promoter ***Thy1***. Previous literature reports indicated that this mouse model develops extensive vascular Aβ depositions (Davis et al. 2004). It was also indicated that the first Aβ plaques appear at three months of age, together with cognitive impairment. To test whether I could observe the same AD hallmarks with our animal-keeping conditions, I analyzed the behavior of wild type (WT), and homozygous and heterozygous ***Thy1-APP***^{SwDI} (AD) by behavioral tests at different ages, and stained mouse brains with methoxy-x04 – a dye with high affinity for Aβ plaques –, CD31 or Tomatolectin to visualize the vessels, and nuclear green – a dye that intercalates in the DNA – to visualize the nuclei. Furthermore, I performed BBB permeability assays and 3' RNA-Seq as pictured in **Figure 29**.

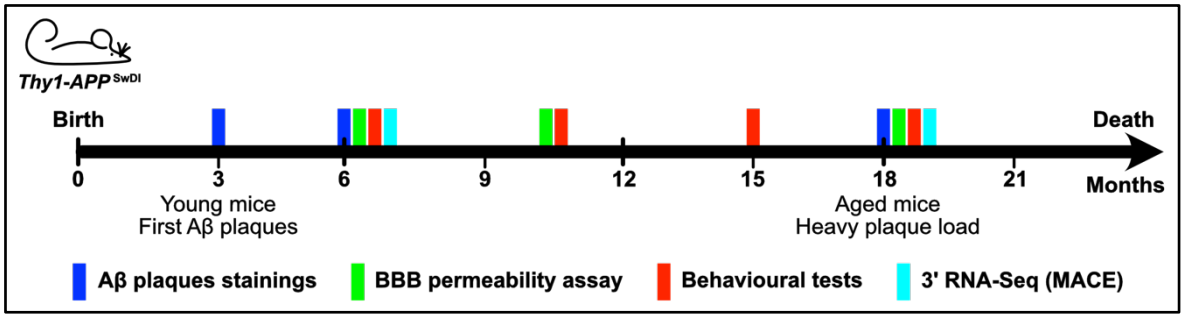

Figure 29: timeline of the AD mouse model's life-span showing onset of Aβ plaques, and time points at which BBB permeability assays, behavioral tests, and 3' RNA-Seq were performed.

The Aβ plaques were visible in AD homozygous mice at three months of age, as reported in the literature. Heterozygous AD mice, however, showed Aβ plaques around six months, although in some cases Aβ depositions were already visible at three months and in other cases, six month old mice had very few or no plaques at all (**Figure 30**).

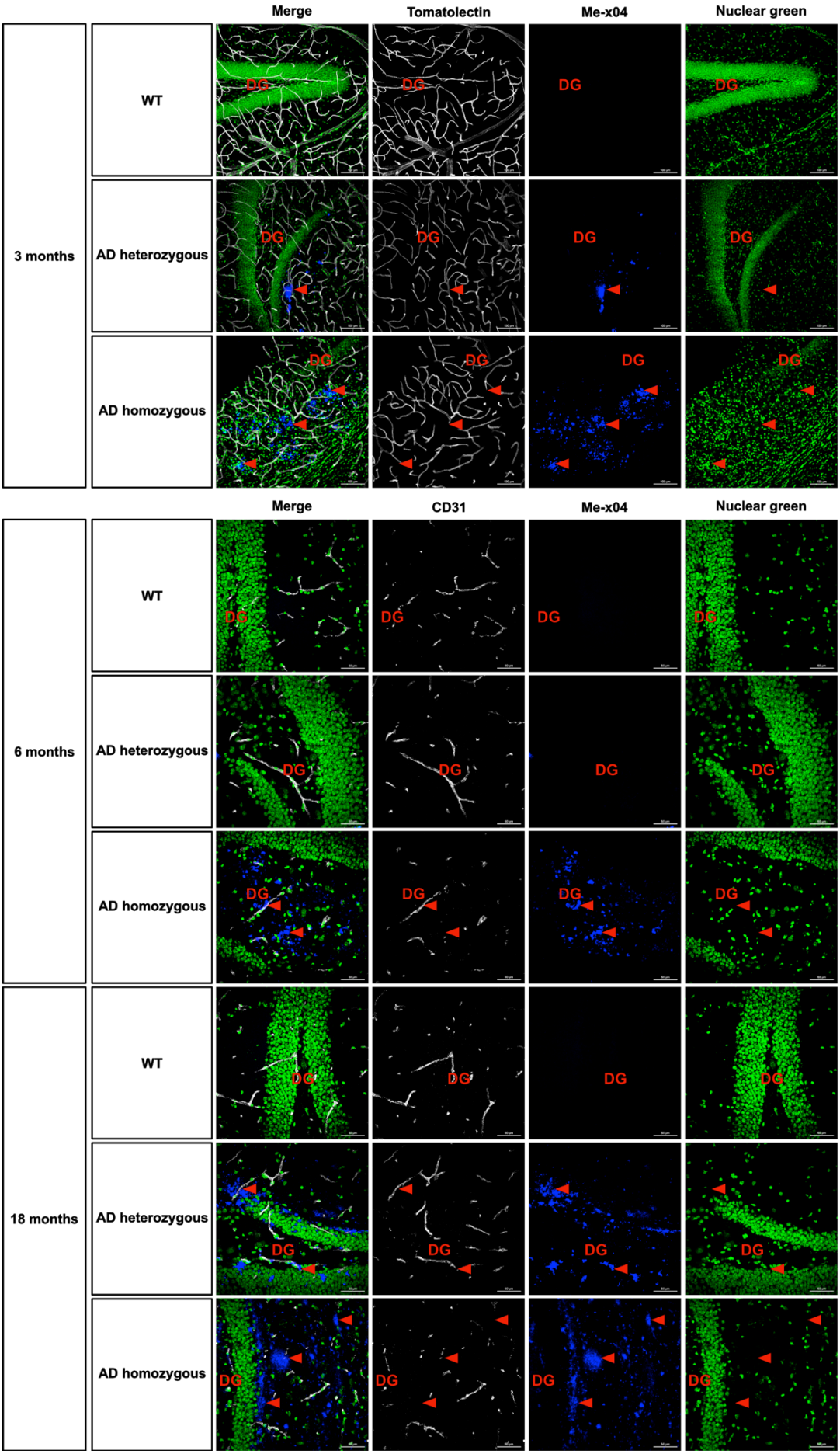
Merge
Tomatolectin
Me-x04
Nuclear green
3 months
WT
AD heterozygous
AD homozygous
DG
Merge
CD31
Me-x04
Nuclear green
6 months
WT
AD heterozygous
AD homozygous
18 months
WT
AD heterozygous
AD homozygous
DG

Figure 30: Hippocampal Aβ plaques and vasculature in 3, 6, and 18 months old WT, heterozygous and homozygous AD mice. Dentate gyrus sections of 30μm and 10 μm from 3 months, and 6 & 18 months old mice, respectively. DG: dentate gyrus. Arrow heads point at Aβ plaques.

The Aβ plaques continued to deposit as mice aged; consequently, at the time when the mice reached an old age (18 months), both homozygous and heterozygous AD mice showed extensive Aβ plaques (**Figure 30**).

As pictured in **Figure 29**, I analysed the behaviour of mice at different ages. I used the nesting test that measures general well-being, the burrowing test that measures general well-being and hippocampal activity, the Y-maze of spontaneous alternations that measures memory, and the elevated-plus maze that measures anxiety. The nesting test and the elevated-plus maze could not detect consistent differences between WT and AD mice. The number of total entries in the elevated-plus maze was low (minimum of 9 is advised), and therefore no reliable results could be obtained from it (**Figure 31 C-F**). Due to the ineffectiveness of using the nesting and elevated-plus maze tests, I stopped their use after the first period of my project. Fortunately, I could continue analysing the hippocampal activity and memory performance with the burrowing test and the Y-maze of spontaneous alternations, the most important behavioural parameters in AD. The burrowing test showed decreased burrowing activity in both heterozygous and homozygous AD mice at young (6-8 months) and old (>18 months) ages (**Figure 31 A**). However, no differences were found at ages 9-16 months (**Figure 31 A**). Interestingly, thanks to the Y-maze test of spontaneous alternations, a decreased memory performance was detected in 9-12 months old homozygous AD mice when compared to age-matched WT mice (**Figure 31 B**). Unfortunately, no differences were found between AD and WT mice in other age groups (**Figure 31 B**).

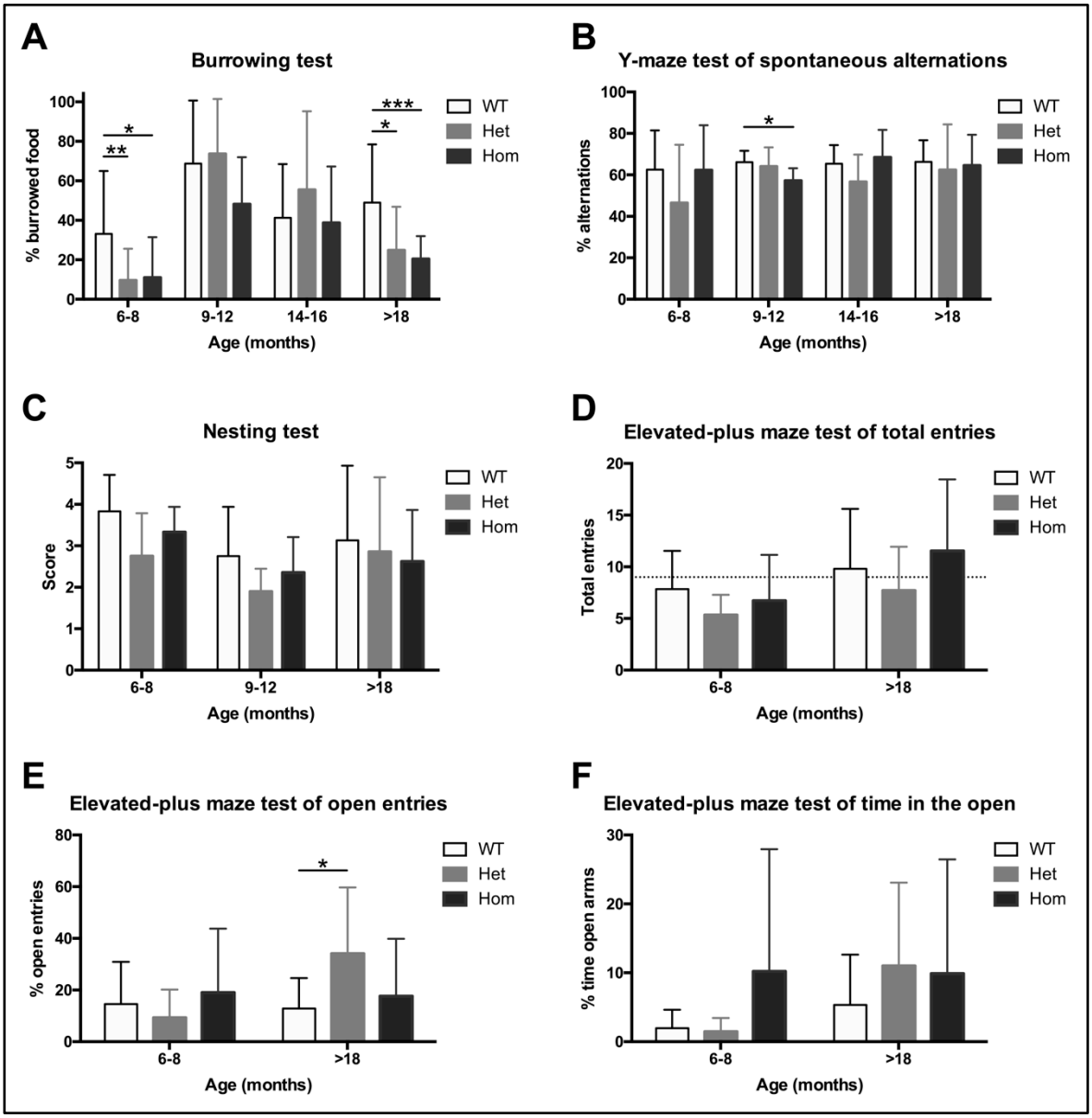

Figure 31: behavioural tests in WT vs AD heterozygous (Het) and homozygous (Hom) mice. (**A**) Burrowing test, (**B**) Y-maze test of spontaneous alternations, (**C**) nesting test, and (**D**) total entries, (**E**) % entries to open arms and (**F**) % time in the open arms of the elevated-plus test. All tests were analysed with the 2-tailed unpaired t-test except for the nesting test (**C**), in which a gaussian distribution cannot be assumed and hence the Mann Whitney test was used. The n numbers for WT6-8, Het6-8, Hom6-8, WT9-12, Het9-12, Hom9-12, WT14-16, Het14-16, Hom14-16, WT>18, Het>18, and Hom>18 are 26, 19, 11, 7, 8, 5, 7, 10, 9, 18, 13, and 17. Six mice of the WT>18 group are mT/mG (no Tamoxifen induction).

5.3. The permeability of the BBB is increased in the AD model

In order to know whether the BBB function was altered in AD, I performed several permeability assays to analyse the extent of unspecific crossing between blood and CNS in AD mice. 3 kDa TMR, or 4 kDa FITC and 20 kDa TMR dextrans

were injected and allowed to circulate for 20 min (IP injection) or 3-5 min (IV injection) before perfusing the mice with PBS. Cerebrum, cerebellum, and kidney were collected, homogenised and the supernatant was used to measure tracer content by fluorometry. The fluorescent readings were normalized to tissue weight and tracer content in serum.

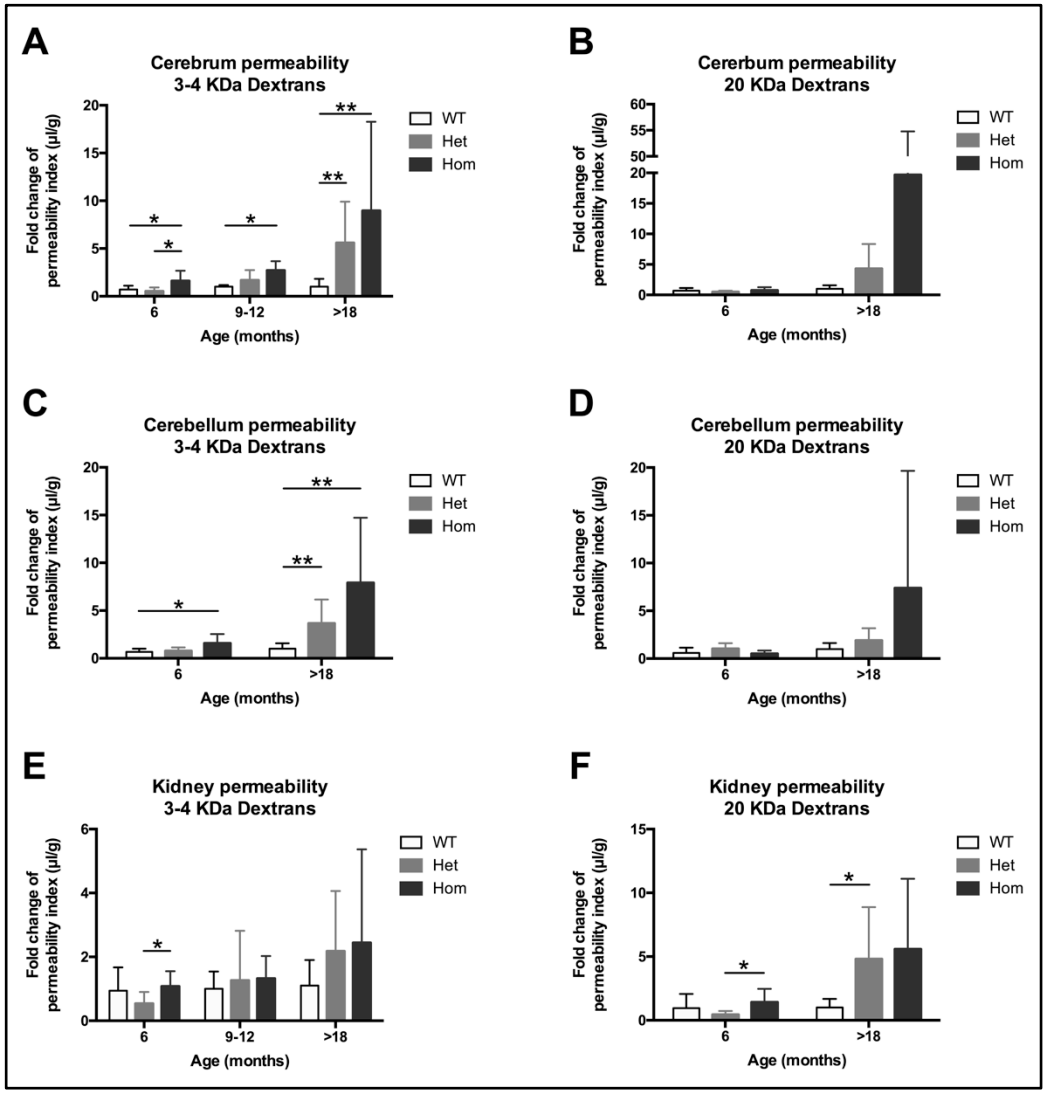

Figure 32: permeability assays in cerebrum, cerebellum and kidney with 3 kDa TMR, 4 kDa FITC and 20 kDa TMR dextrans. Processed data from 3 and 4 kDa dextrans have been combined (**A, C, E**) while data from 20 kDa dextrans is displayed separately (**B, D, F**). The n numbers of WT6, Het6, Hom6, WT9-12, Het9-12, Hom9-12, WT>18, Het>18, and Hom>18 are 9, 7, 5, 4, 4, 5, 12, 9, and 5, respectively.

As depicted in **Figure 32 A**, 3-4 kDa tracer content in cerebrum and cerebellum was higher in all AD homozygous mice compared to their age-matched

WT controls. AD heterozygous mice showed higher 3-4 kDa tracer content in cerebrum and cerebellum at old ages (**Figure 32A, C**). By contrast, 20 kDa tracer content in AD mice was not different from WT controls at any tested age, although a clear increasing trend is visible at old ages (**Figure 32B, D**). Surprisingly, AD homozygous kidney showed higher 3-4 and 20 kDa tracer content than AD heterozygous at 6 months of age. Likewise, AD heterozygous kidney showed higher 20 kDa tracer content than WT controls at old ages (**Figure 32E, F**).

A higher BBB permeability is a sign of BBB dysfunction. However, it gives no information about the cause of the disruption. Consequently, a different approach is needed to investigate that matter.

5.4. Transcriptomic analysis

In order to understand how the BBB is affected by AD, I analysed the transcriptomic profile of MBMVs, and FACS-sorted ECs, MuCs, ACs, and MG (**Figure 33**).

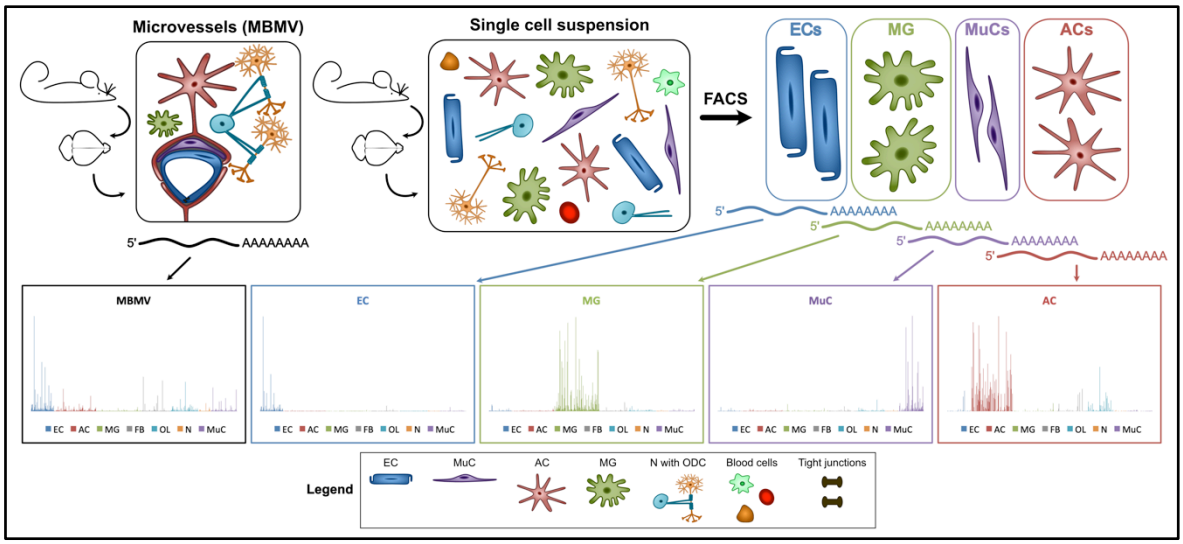

Figure 33: isolation and sequencing scheme of MBMV, ECs, MG, MuCs, and ACs.

5.4.1. Data from MBMVs

MBMVs were isolated from WT, AD heterozygous (Het), and AD homozygous (Hom) male mice of 6 months, and WT and Hom male mice of 18 months (**Table 6**).

Table 6: MBMV samples

Genotype	6 months	18 months
WT	3	3*
AD heterozygous	3	
AD homozygous	3	3

* One mouse in the WT18 group was mT/mG (no Tamoxifen induction).

The MBMV dataset contained a total of 33059 genes from which the p value, corrected p value (false discovery rate or FDR) and log2 fold change (log2FC) were calculated by statistical analysis in the compared groups. The genes that were significantly regulated ($p<0.05$) and had a log2FC>1 or <-1 were called differentially expressed (DE) genes. The summary of MBMV data can be found in Table 7.

Table 7: MBMV data

Comparison	P<0.05 genes	FDR<0.05 genes	DE genes
WT6 vs. Het6	1063	97	162
WT6 vs. Hom6	1057	112	271
WT6 vs. WT18	3547	620	1234
WT18 vs. Hom18	717	20	346

5.4.1.1. Cell-type population changes between groups

In order to analyse the purity of the MBMV isolation, or in other words, the contamination in the MBMV from other brain cells, I created a list of EC, MuC, AC, MG, FB, OL, and neuronal (N) marker genes. Thanks to the Barres and Betsholtz single-cell RNA-Seq datasets of mouse brains (Zhang et al. 2014; Vanlandewijck et al. 2018), I could define genes that were expressed at least 15 times more in a specified cell-type than in all the others.

The analysis of marker genes showed that all MBMV samples were very homogeneous and therefore comparable. All samples revealed a clear high expression of EC genes although MuC, AC, MG, FB, OL, and N genes were also detected, as it was expected (**Figure 34**).

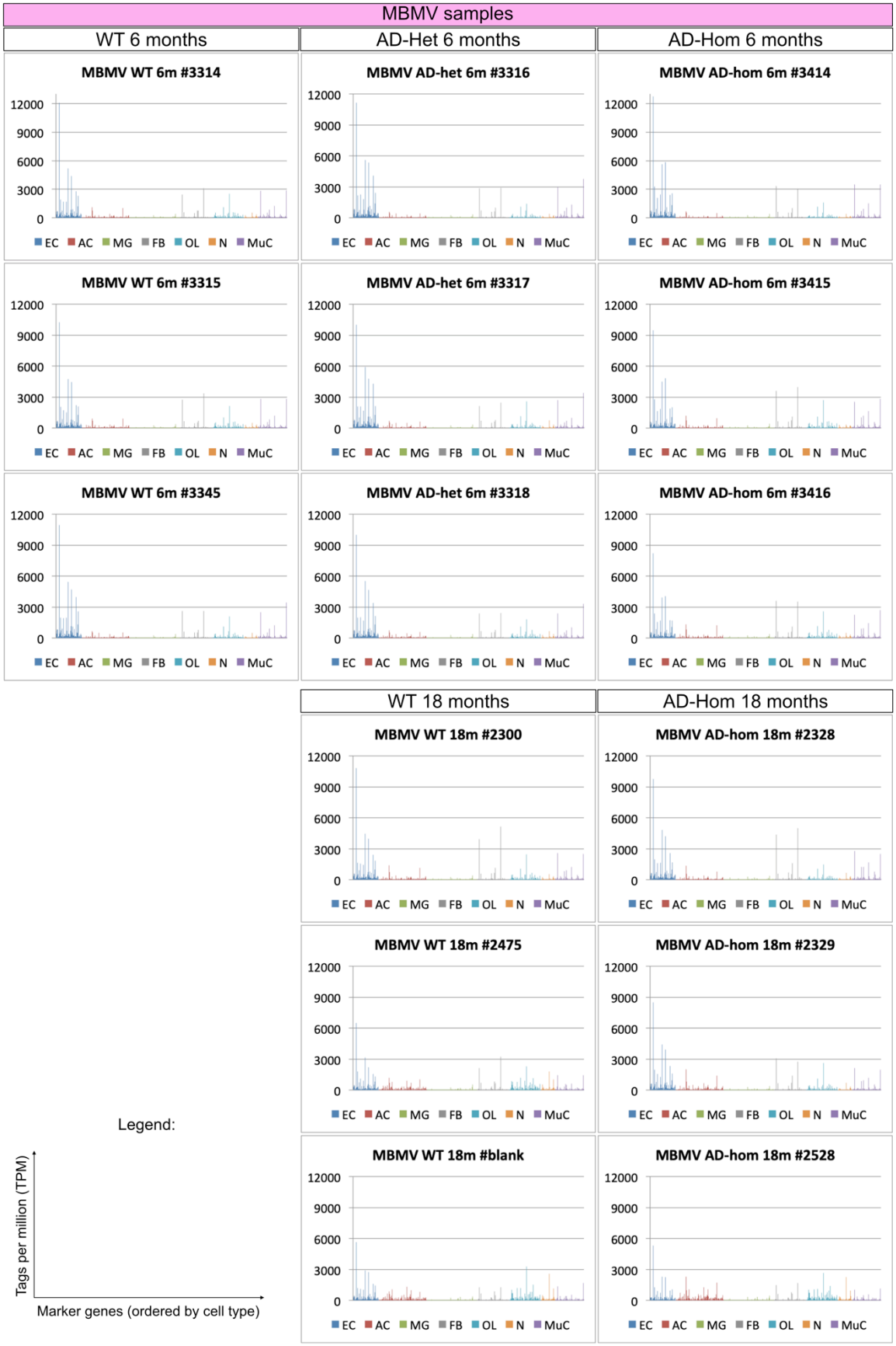

Figure 34: Marker genes of MBMV samples. All samples show homogeneous markers expression and clear EC enrichment and were included in the data analysis. Each bar represents one marker gene.

Additionally, I checked the approximate cell content by choosing the five most expressed markers of each cell-type and plotting them together. **Figure 35 A** visibly exposes the EC enrichment present in all groups, as EC marker genes were the highest. The marker genes of MuCs were separated into PC and SMC markers in order to have a more defined view. Importantly, PCs and venous SMC (vSMCs)

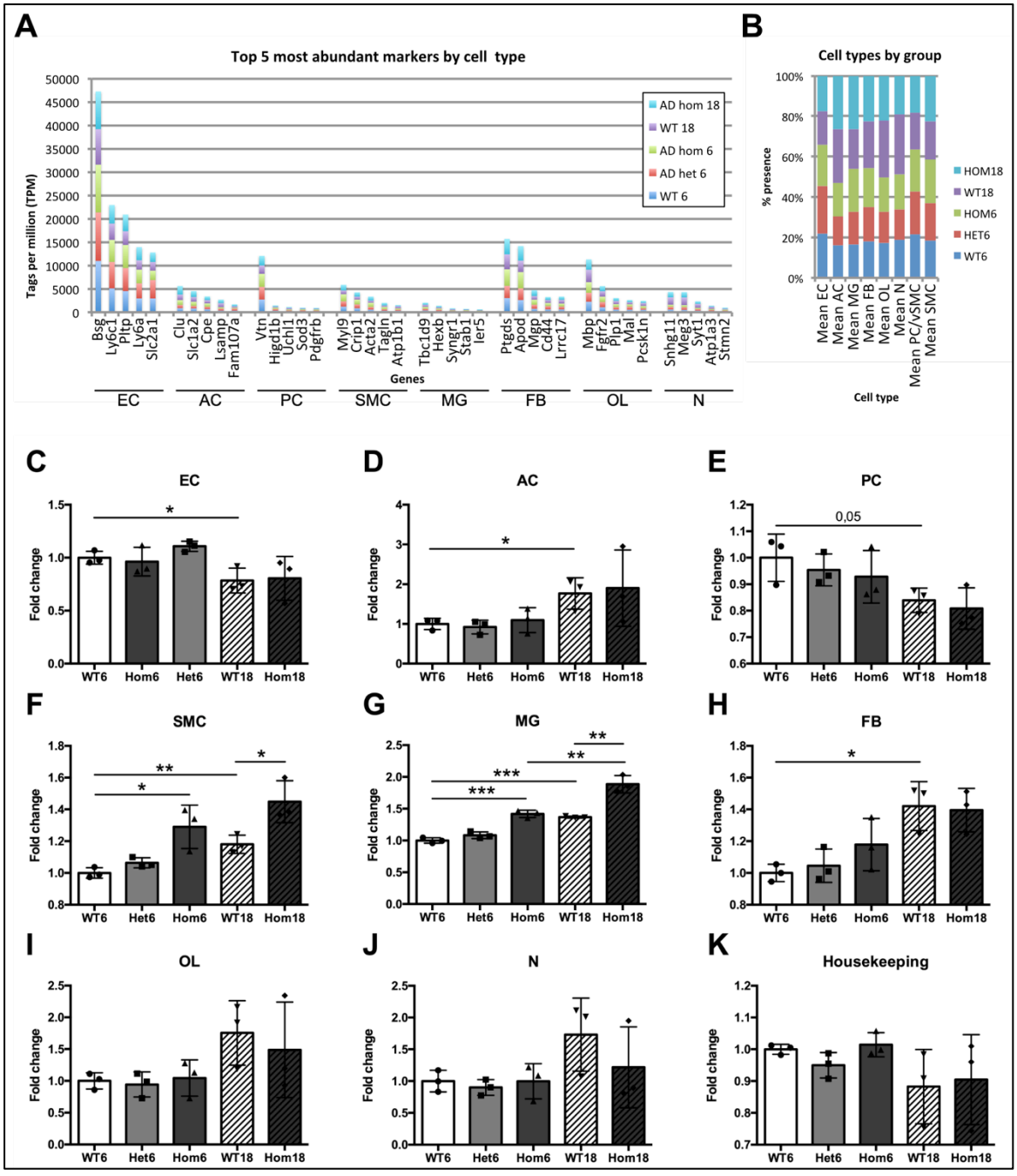

Figure 35: (**A**) top 5 most expressed markers by cell type. Each bar represents the sum of tags per million (TPM) between all groups. (**B**) % group presence in each cell type calculated by the mean of their markers. (C-J) Average of marker genes per group in ECs (**C**), ACs (**D**), PCs (**E**), SMCs (**F**), MG (**G**), FBs (**H**), OLs (**I**), and Ns (**J**). (**K**) Average of housekeeping genes per group.

were, at least transcriptionally, almost identical and consequently, I made no distinction between PC and vSMC marker genes. Interestingly, if I calculated the average of the markers' relative expression and compared the different groups, each group's contribution was not equal, suggesting a swift in the cell-type population between groups (**Figure 35 B**). In order to check if the change in the percentage of cell-type markers was relevant, I statistically analysed the average of the relative expression of the marker genes for each group (**Figure 35 C-J**). Surprisingly, almost all marker genes appeared to be significantly different in at least one comparison. As expected, the housekeeping genes were not significantly different (**Figure 35 K**).

EC markers were lower in WT old mice compared to young ones. In order to check if the change observed in the EC marker genes was real, I stained mouse brain sections with anti-Erg, anti-CD31, nuclear green and me-x04. Then, I counted how many Erg^{+} cells were per vessel length to get the EC/vessel length measure (**Figure 36 A**). The results proved the decrease of EC in the hippocampus of aged mice and moreover, a significant decrease in the hippocampus of Hom6 mice compared to WT6 was found as well (**Figure 36 B**). No changes were observed in the cortex (**Figure 36 C**).

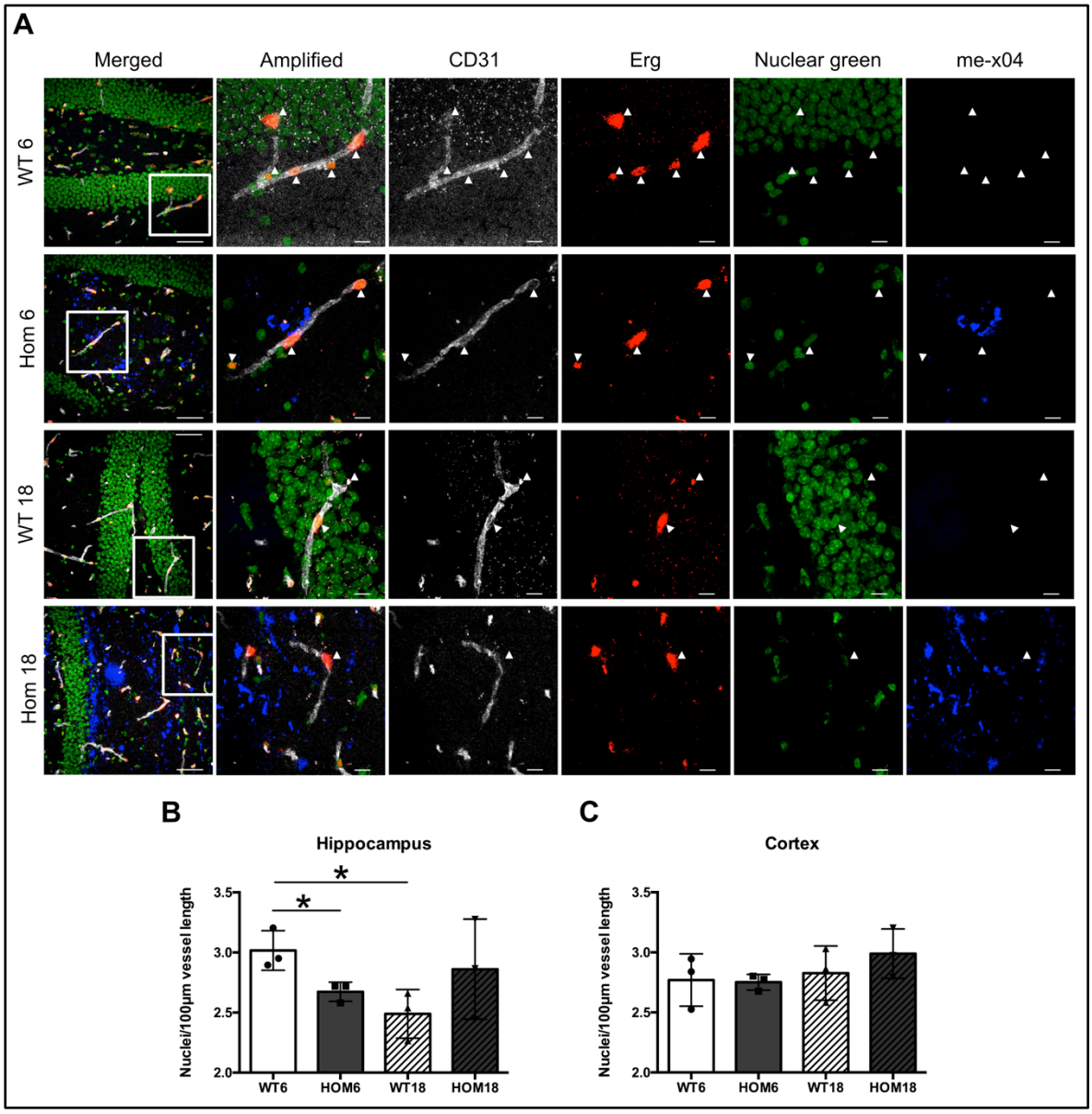

Figure 36: (**A**) 10 μm sections of brain from WT and Hom mice of 6 & 18 months stained with anti-Erg (red), anti-CD31 (white), me-X04 (blue), and nuclear green (green). Arrowheads point at Erg^+ nuclei. (**B-C**) Number of Erg^+ nuclei per 100 μm of vessel length in hippocampus (**B**) and cortex (**C**).

5.4.1.2. *Bace1* and *Sirt1* are not regulated in MBMVs

Previous data from the research group had shown that ***Bace1*** was up-regulated in MBMVs of a different AD mouse model (Devraj et al. 2016). It has also been proven that ***Sirt1*** activation swifts the APP processing from the β-secretase towards the non pathological α-secretase (X. F. Wang et al. 2016). However the MBMVs from the ***Thy1-APP***^{SwDI} AD mouse model revealed no ***Bace1*** or ***Sirt1*** regulation (**Table 8**).

Table 8: *Bace1* and *Sirt1* MBMV sequencing data

	Log2FC				P value			
Gene	WT6-Het6	WT6-Hom6	WT18-Hom18	WT6-WT18	WT6-Het6	WT6-Hom6	WT18-Hom18	WT6-WT18
Bace1	-0,005	0,079	-0,196	0,243	0,962	0,702	0,698	0,627
Sirt1	-0,185	-0,398	-0,399	0,402	0,587	0,186	0,297	0,335

The lack of ***Bace1*** regulation forced me to abandon the original hypothesis, which was centred on the harmful effect of ***Bace1*** upregulation in MBMVs. In order to find the cause of vascular dysfunction observed in AD, I analysed the transcriptomic data to find novel gene regulations.

5.4.1.3. Healthy ageing shows strong transcriptional changes

Despite the stable expression of ***Bace1*** and ***Sirt1***, many genes were identified to be differentially expressed in MBMVs. **Figure 37** offers an overview of the data for each comparison. In the volcano plot, each gene is organized by its p value (Y axis) and log2 fold change value (X axis). Heat maps show the relative expression of selected genes for each sample. For space reasons, I am showing the top 20 differentially expressed genes when comparing WT6 vs. Het6, WT6 vs. Hom6, WT18 vs. Hom18, and healthy ageing (WT6 vs. WT18). Interestingly, the Kruppel Like Factor 2 (***Klf2***) was one of the top DE genes in Hom6 mice compared to age-matched WT (**Figure 37**), indicative of a strong regulation.

In an effort to find common DE genes in AD, I compared both AD6 groups (Het & Hom) to WT6, and both Hom groups (6 & 18 months) to their respective WT age-matched controls (**Figure 38**).

Dkk2 and ***Pttg1*** were up-regulated in both Het6 and Hom6 groups, compared to WT6. This double comparison detected early and consistently regulated genes in AD. As Het6 mice are only starting to be affected by AD (**Figure 30**), some of the genes in this group might only be starting to be regulated and hence, the regulation might still be too weak to be detected. Therefore, I compared common regulated genes in both Hom groups (6 & 18 months) to show strongly regulated genes in AD (**Figure 38**).

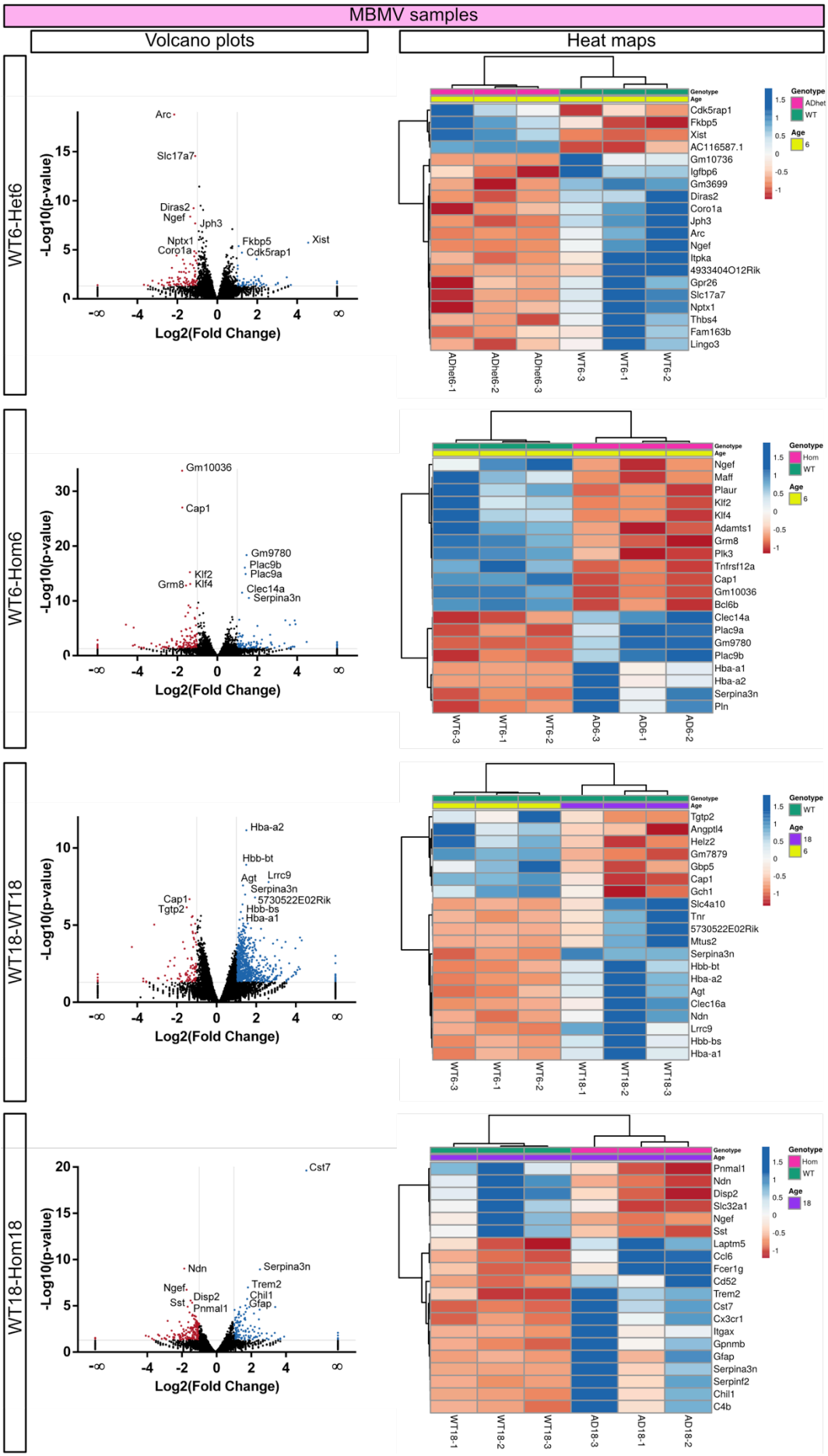
MBMV samples
Volcano plots
Heat maps
WT6-Het6
WT6-Hom6
WT18-WT18
WT18-Hom18
-Log10(p-value)
Log2(Fold Change)
Arc
Slc17a7
Diras2
Ngef
Jph3
Nptx1
Coro1a
Fkbp5
Cdk5rap1
Xist
Gm10036
Cap1
Gm9780
Plac9b
Plac9a
Klf2
Klf4
Grm8
Clec14a
Serpina3n
Hba-a2
Hbb-bt
Agt
Lrrc9
Serpina3n
5730522E02Rik
Hbb-bs
Hba-a1
Cap1
Tgtp2
Cst7
Ndn
Serpina3n
Ngef
Disp2
Sst
Pnmal1
Trem2
Chil1
Gfap
Genotype
Age
ADhet
WT
Hom
6
18
ADhet6-1
ADhet6-2
ADhet6-3
WT6-3
WT6-1
WT6-2
AD6-3
AD6-1
AD6-2
WT18-1
WT18-2
WT18-3
AD18-3
AD18-1
AD18-2

Figure 37: Volcano plots and heat maps of MBMV samples.

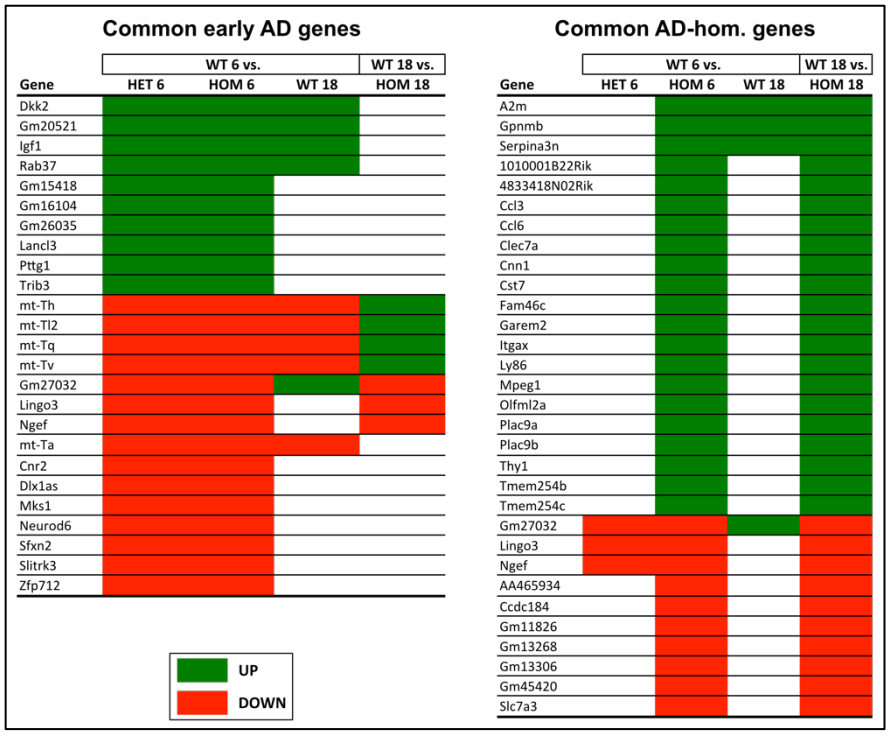

Figure 38: common DE genes in early AD and in Hom groups. Up-regulated (green) and down-regulated (red) genes are $p<0,05$ and $log2FC>1$ or <-1.

Furthermore, when comparing all AD groups to their WT age-matched controls, 18 genes were commonly regulated, suggesting a strong and consistent change (**Figure 39 A**). Noticeably, when I analysed the total number of regulated genes of each group, the healthy ageing comparison (WT6 vs. WT18) was by far the most regulated of them all (**Figure 39 B**). Surprisingly, the early-regulated genes found in common in Het6 and Hom6 mice compared to WT6 mice had more regulated genes in common with healthy aged mice (WT18 vs. WT6) than aged AD mice with healthy aged mice (Hom18 vs. WT18) (**Figure 39 C**). Thus, ageing not only heavily affected the MBMV transcription, but also early changes observable in AD had a strong link with changes associated to ageing. Of note, ***Pttg1*** appeared again in both comparisons suggesting a strong and consistent regulation. Moreover, ***Pttg1*** is involved in angiogenesis, and is regulated by β-catenin/TCF in human colorectal carcinoma (Ishikawa et al. 2001; Hlubek et al. 2006). Therefore, I selected ***Pttg1*** as the top candidate gene, and checked in isolated MBMVs from

female mice the ***Pttg1*** expression by qPCR to know if the regulation was consistent and not due to sex differences. The results confirmed ***Pttg1*** up-regulation in all groups (**Figure 39 D**), supporting the potential of ***Pttg1*** as top candidate gene for further testing.

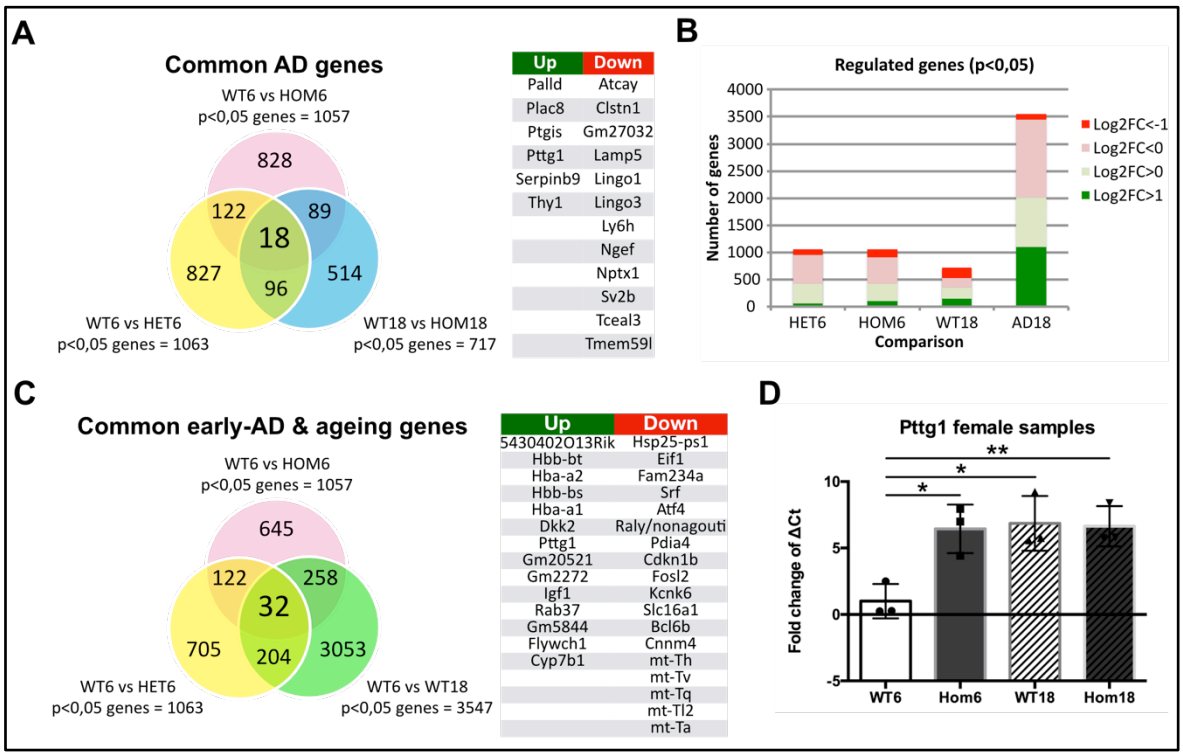

Figure 39: (**A**) regulated genes in common in all three AD groups. (**B**) Number of regulated genes classified by their log2FC in each comparison. Het6, Hom6 and WT18 are compared to WT6, and AD18 to WT18. (**C**) Regulated genes in common in early AD and healthy ageing. (**D**) qPCR in MBMVs from female mice showing ***Pttg1*** up-regulation in ageing and AD. Normalization was made to ***Rplp0***. The WT6 group are mT/mG mice (no Tamoxifen induction).

5.4.1.4. Regulation of Dkk2 and other Wnt/β-catenin genes

In order to obtain an overview of the biological meaning of the regulated genes identified in this MBMV dataset, a pathway enrichment analysis was performed. Essentially, groups of functionally related genes are ordered statistically to highlight the pathways that are most significant. **Figure 40** pictures a selection of the most relevant pathways found.

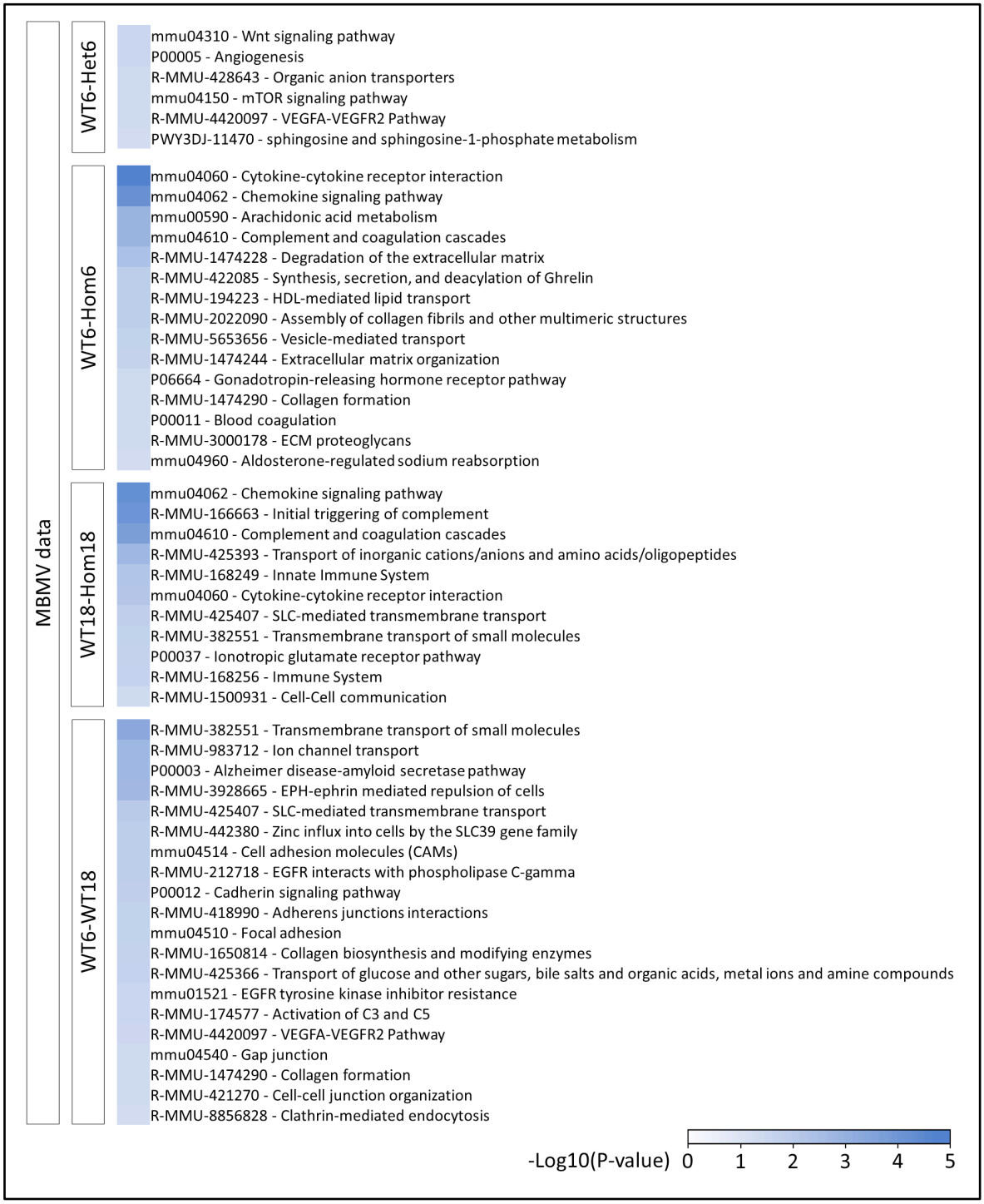

Figure 40: selection of regulated pathways found by pathway enrichment analysis of DE genes in each comparison.

Inflammatory-related pathways were found in all comparisons, but specially in Hom groups or healthy ageing comparisons, such as “chemokine signalling pathway”, and “activation of C3 and C5”. Interestingly, pathways such as “transmembrane transport of small molecules”, “sphingosine metabolism”, “Wnt signalling pathway”, “angiogenesis”, and “cell-cell junction formation” hinted at

changes in BBB properties. Importantly, "Alzheimer disease-amyloid secretase pathway" was among the significant pathways, suggesting that known genes related to AD are regulated in the dataset (**Figure 40**).

In order to identify the specific genes leading to the regulation of pathways observed in **Figure 40**, I looked at known genes involved in AD, BBB properties, and important players in BBB maintenance like the Wnt and S1P pathways (**Figure 41**).

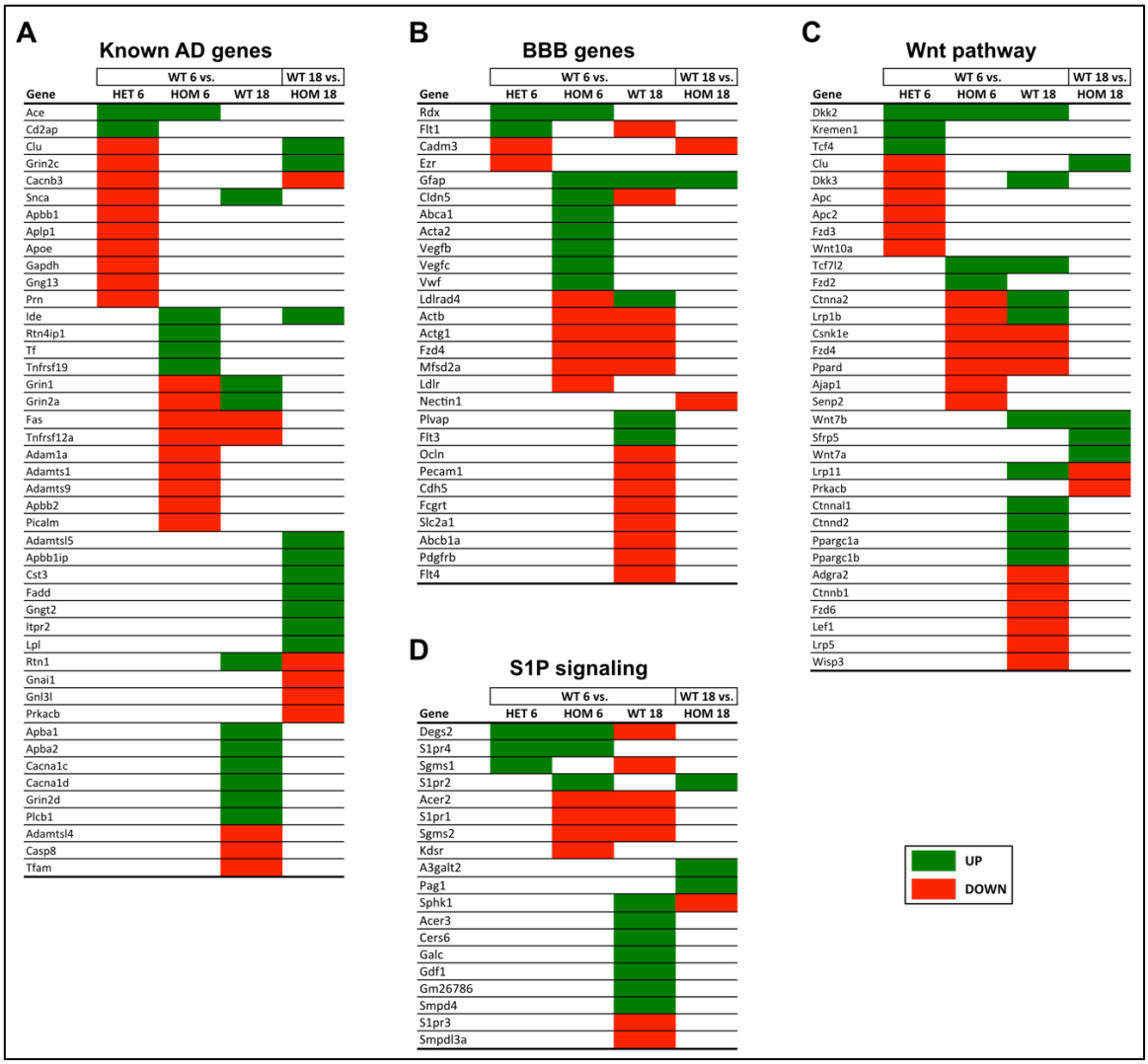

Figure 41: regulated genes in MBMV data grouped by function. Up-regulated (green) and down-regulated (red) genes ($p<0.05$).

Interestingly, ***Dkk2*** appeared up-regulated in three out of the four comparisons suggesting a strong regulation, which is related to the Wnt pathway (**Figure 41**).

Given the high number of regulated BBB-related genes, I checked marker genes of ECs, PCs, SMCs, ACs, and MG to find regulated genes of defined cellular identity (**Figure 42**).

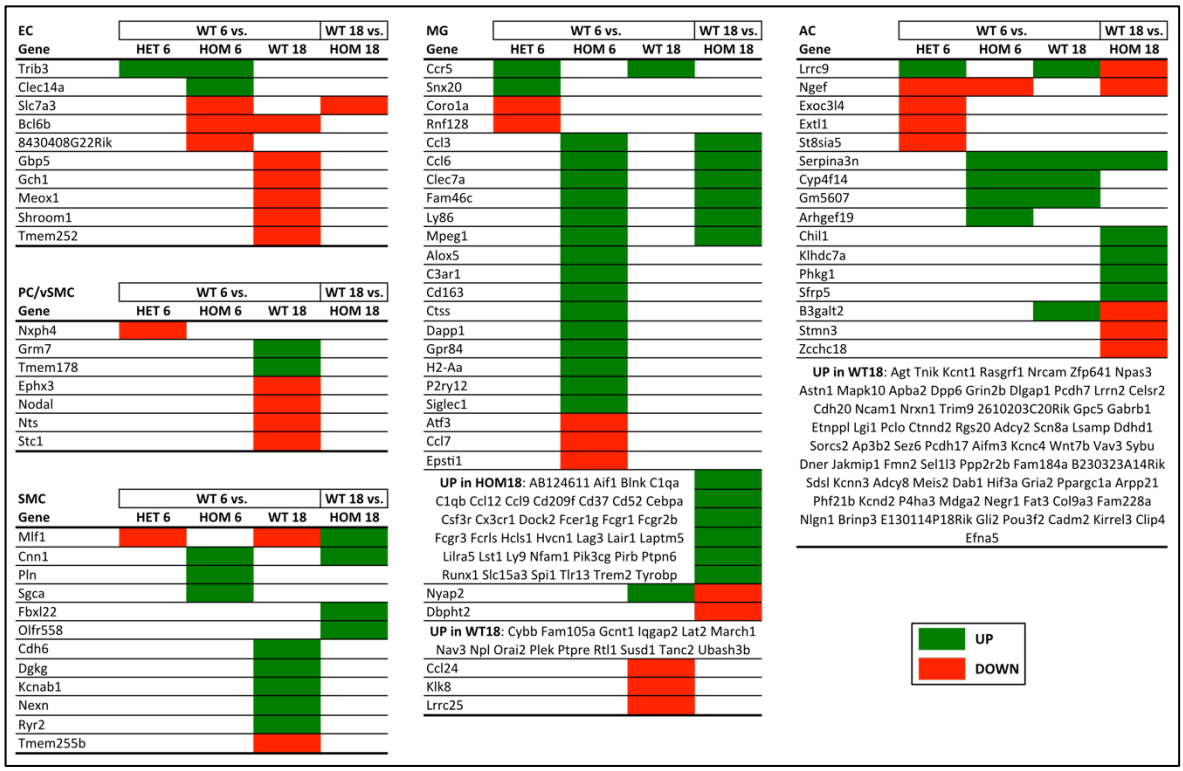

Figure 42: DE marker genes in MBMV data. Up-regulated (green) and down-regulated (red) genes are $p<0.05$ and $log2FC>1$ or <-1.

Many marker genes were differentially expressed, especially in ACs and MG. In ACs, the majority of the regulation was coming from the ageing comparison, whereas in MG, the AD groups showed numerous up-regulated genes, as it would be expected from activated MG. In PCs, only the ***Nxph4*** gene was differentially expressed in an AD group (Het6 vs. WT6). In contrast, SMCs showed a higher number of differentially expressed genes, amongst them ***Cnn1*** emerged again as commonly up-regulated in both Hom groups. Last but not least, differentially expressed EC marker genes showed regulations already seen in previous comparisons such as ***Slc7a3*** and ***Trib3***. ***Bcl6b*** appeared down-regulated in both Hom6 and WT18 when compared to WT6, and ***Clec14a*** rose exclusively in Hom6. Again, ageing had an important effect in ECs as well, although conclusions cannot be made easily as it was already demonstrated that ECs were reduced in healthy aged MBMVs (**Figure 36**).

Overall, the sequencing data from MBMVs reflected transcriptomic changes due to healthy ageing and AD, such as inflammation and Wnt/β-catenin regulation. However, the presence of different cell types in the samples impaired a deeper and more accurate analysis. Hence, I next analysed the transcriptional changes of FACS-sorted samples.

5.4.2. Data from FACS-sorted samples

FACS-sorted ECs, MuCs, ACs, and MG were sequenced and analysed to verify the gene regulation found in MBMVs, to pinpoint their cellular identity, and to find novel gene regulations.

In order to have enough cells, two or three mice were pooled to make one sample, except in old AD-hom mice. ECs, MuCs, ACs and MG were sorted by FACS as $Cdh5^{+}$, $Ng2^{+}$ & $Pdgfrb^{+}$, $Acsa2^{+}$, and $CD45^{low}$ & $CD11b^{high}$ populations, respectively. The cells were isolated from WT and AD mice of 6 and 18 months-of-age (**Table 9**). Het and Hom mice of 18 months-of-age were combined as an AD group for the statistical analysis of their transcriptomes.

Table 9: FACS-sorted samples

Name sample	Genotype	Age (months)	Pooled mice	Sex	Group
2Br	WT	18	2	F/F	WT18
3Br	WT	18	3	F/F/F	
3xWT	WT	18	3	F/F/F	
12_3	WT	18	2	M/M	
9_3	WT	18	2	M/M	
79, 80	HET	18	2	M/M	AD18
99, 02	HET	18	2	M/M	
12_3	HET	18	2	F/F	
9_3	HET	18	2	F/F	
2807	HOM	18	1	M	
2972	HOM	18	1	M	
21	WT	6	2	f/m	WT6
22	WT	6	2	M/M	
A	WT	6	2	M/M	
B	WT	6	2	M/M	
2_3	HOM	6	2	M/M	AD6
4_7	HOM	6	2	f/m	
21	HOM	6	2	f/m	
22	HOM	6	2	F/F	

5.4.2.1. Marker analysis of FACS-sorted samples allows to detect contaminated samples and exclude them from data analysis

The purity of cell-sorted samples was checked by analysing the expression of marker genes. The endothelial and microglial samples showed clear specific genes respectively, with no contamination from other cell types (**Figure 43** and **Figure 44**). The PC sorted samples expressed PCs marker genes, but SMCs markers as well. Therefore, I refer to those samples as mural sorted cells instead (MuCs). Unfortunately, two WT-6 and two AD-6 MuC samples expressed marker genes from other cell types (**Figure 45**), indicating contamination from cells other than MuCs, and consequently had to be excluded from further analysis. Lastly, the majority of AC samples showed very low expression of AC marker genes, with only two WT-18 and four AD-18 samples expressing good amounts of AC markers (**Figure 46**). Although these six samples showed contamination from other cell types, I decided to keep them and to compare the two groups to see if any results could be obtained. Hence, the AC dataset consists of one single comparison between WT-18 vs AD-18.

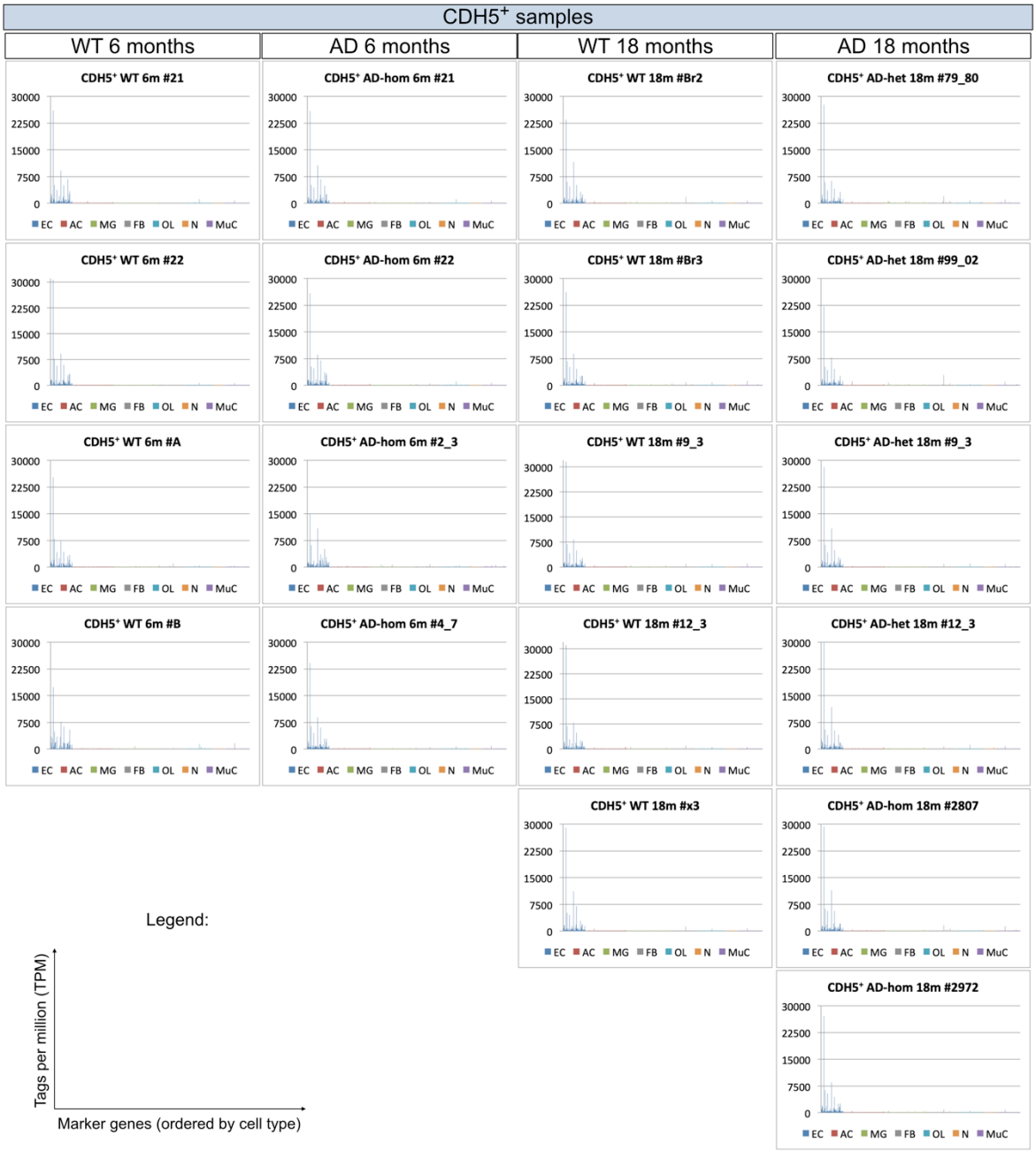

Figure 43: Marker genes of Cdh5$^+$ samples (EC population). All samples show a clear EC specificity and were included in the data analysis.

Figure 44: Marker genes of CD45^{low} & CD11b^{high} samples (MG population). All samples show a clear MG specificity and were included in the data analysis.

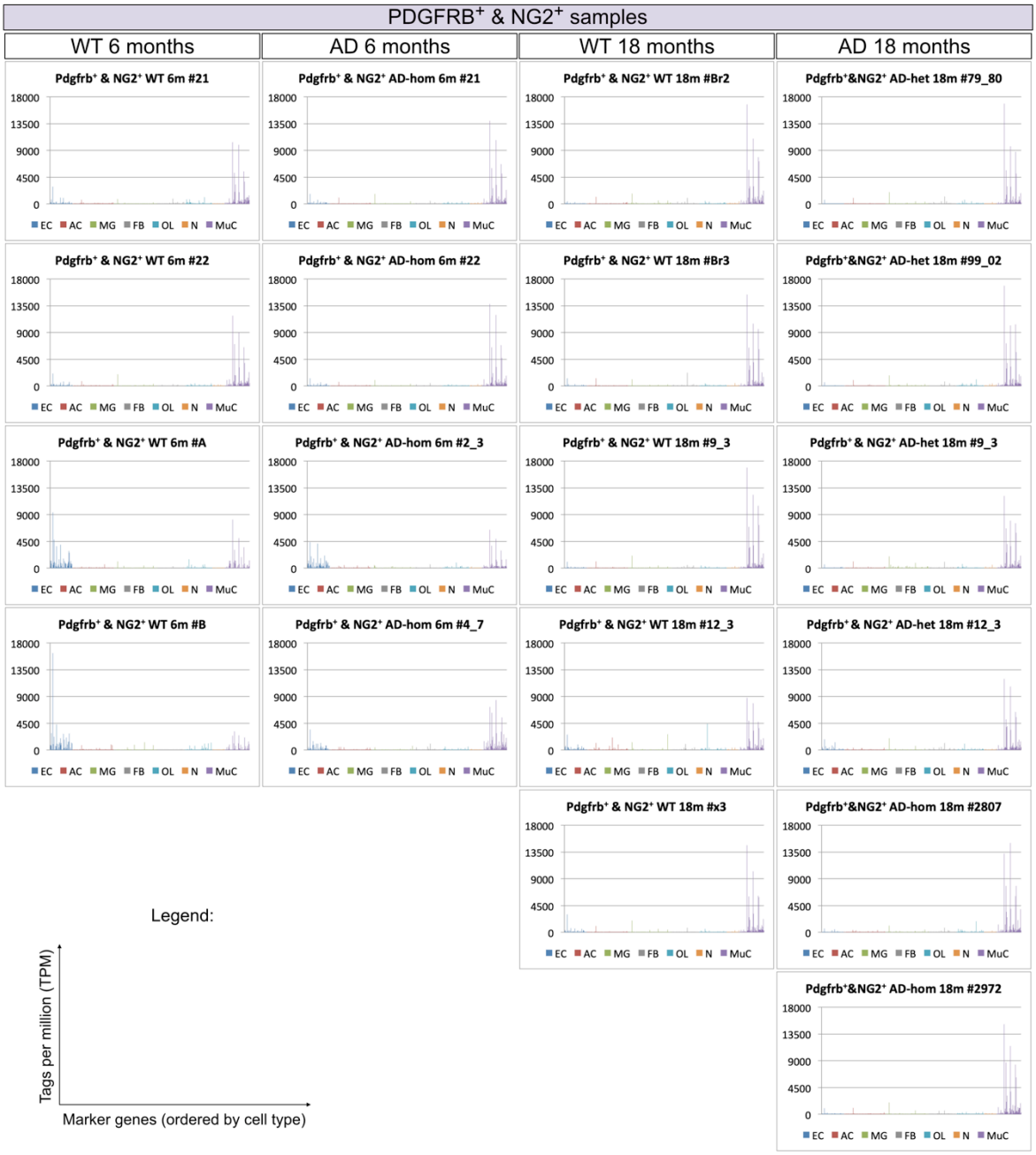

Figure 45: Marker genes of Pdgfrb^{+} & NG2^{+} samples (MuC population). Samples #A & #B from WT-6, and #2_3 & #4_7 from AD-6 were excluded from data analysis due to the presence of EC markers. The rest of the samples show a clear MuC specificity and were included in the data analysis.

Figure 46: Marker genes of Acsa2$^+$ samples (AC population). The expression of AC marker genes is very low in all samples except #Br2 & #Br3 from WT-18, and #79-80, #99-02, #2807 & #2972 from AD-18. Only the mentioned samples were included in the data analysis.

5.4.2.2. The sequencing data from AC samples show unreliable results

As it was revealed in **Figure 46**, the majority of AC samples had to be removed from data analysis due to the low expression of AC-specific marker genes. The remaining samples showed high levels of AC markers but contained

contamination coming from other cell types as well. Nevertheless, I decided to compare the AD-18 samples with their age-matched control WT-18 samples and analyse the results. Unfortunately, because the WT-18 group had only n=2 samples, statistics could not be made and the p value and false discovery rate value (FDR: corrected p value for multiple testing) were an approximation.

The AC dataset contained 23107 detected genes, from which only one gene, ***Xist***, had FDR<0.05 (**Table 10**). Due to the exclusion of contaminated samples, the remaining WT-18 and AD-18 samples were coming from female and male mice, respectively (**Table 9**). This sex difference could explain the lower transcript levels of ***Xist*** in the AD group and more importantly, it added another level of unreliability to the results. Moreover, known genes that were up-regulated in reactive ACs such as ***Gfap*** did not appear regulated.

Table 10: AC-sorted data

Gene	WT18 TPM	AD18 TPM	Log2FC	P value	FDR
Gfap	73.65	103.892	0.496	0.989	0.999
Xist	505.834	1.349	-8.551	1.36E-07	0.001

Taking together, the AC dataset did not offer reliable results and no conclusions could be made from it.

5.4.2.3. The sequencing data from ECs show a Wnt/β-catenin pathway repression

At the data processing step, Ricardo Figueiredo (in charge of generating the dataset) realised that one sample (#B) from the WT6 group had much lower raw reads and was creating high variances in the WT6 group. He tracked the outlier to the initial RNA amount, which was much lower in that sample due to few sorted cells. The WT6 #B sample was then excluded from the analysis.

The EC final dataset contained a total of 28173 genes. The summary of EC data can be found in **Table 11**.

Table 11: EC data

Comparison	P<0.05 genes	FDR<0.05 genes	DE genes
WT6 vs. AD6	1079	41	1059
WT6 vs. WT18	1393	136	1301
WT18 vs. AD18	1077	61	1006

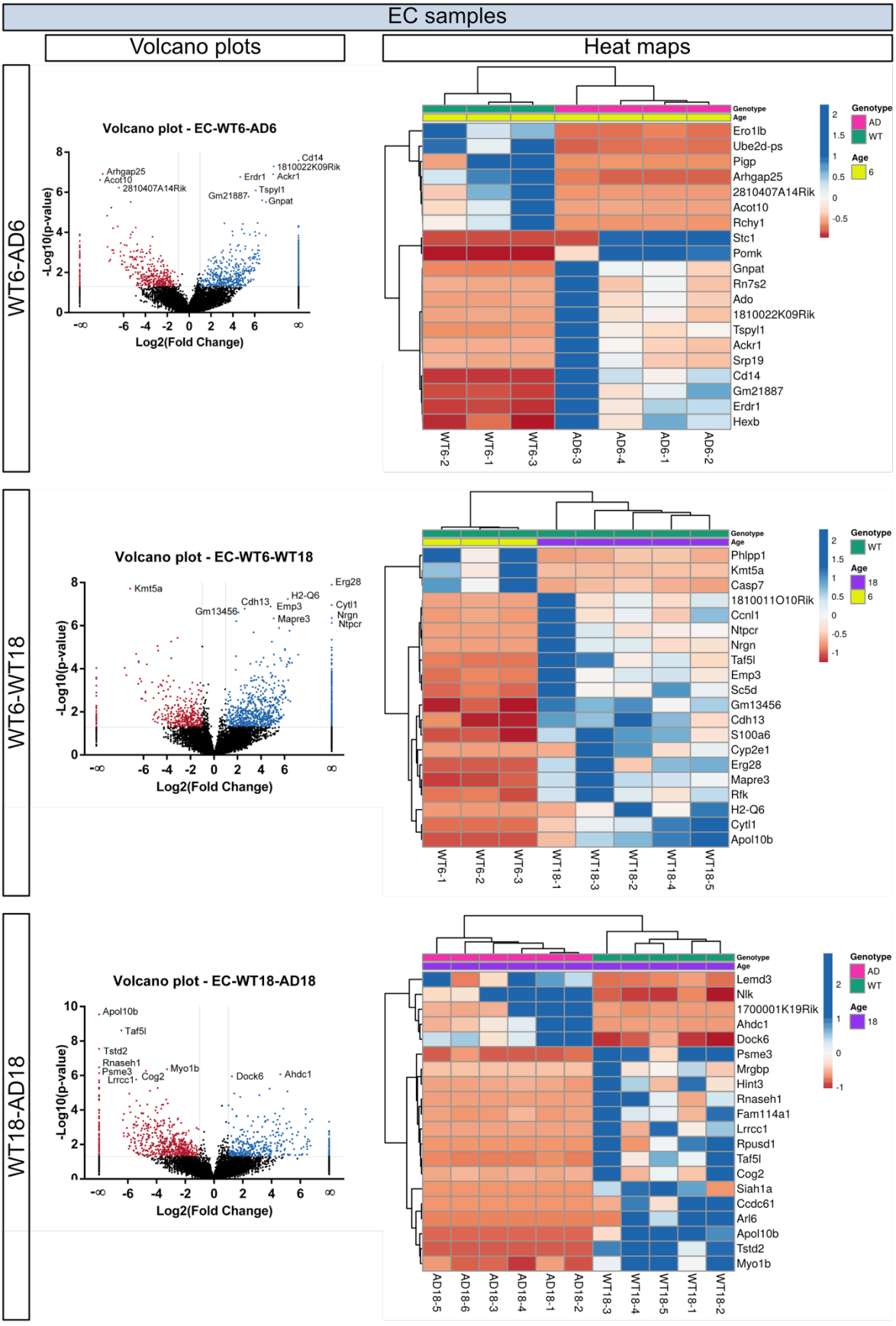

Figure 47: volcano plots and heat maps of EC samples.

It is important to mention that, to the best of my knowledge, this is the first dataset of EC-regulated genes in an AD mouse model and hence, all regulated genes are potentially interesting. In order to reduce the search for interesting genes, I first looked at the top 20 DE genes in each comparison, which can be found in **Figure 47**. Many of the DE genes were involved in metabolic processes, such as ***Acot10***, ***Hexb***, ***Rfk***, and ***Nlk***. Interestingly, genes related to adhesion (***Cdh13***), inflammation (***Cd14***, ***Ackr1*** and ***Cytl1***), cell cycle (***Casp7***, ***Ccnl1***), and protein modification (***Ube2d-ps***, ***Psme3***) also appeared among the top 20 DE genes, suggesting that the mentioned processes were strongly regulated.

Along with the diverse roles of top 20 DE genes, I analysed the pathway enrichment of all DE genes in the three comparisons. The most interesting findings are shown in **Figure 48**.

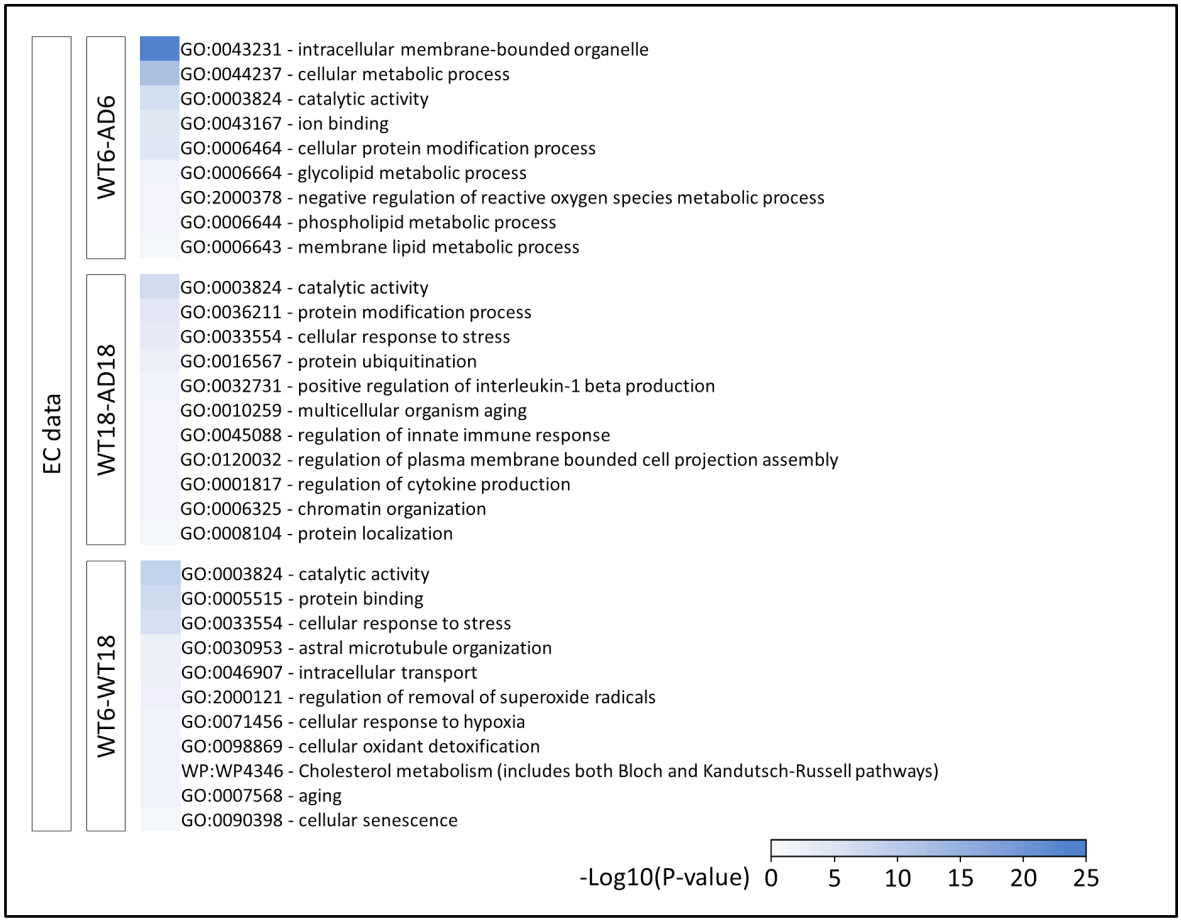

Figure 48: selection of regulated pathways found by pathway enrichment analysis of DE genes in each comparison.

The pathway enrichment analysis also showed regulation of inflammatory ("positive regulation of interleukin-1 beta production", "regulation of innate immune response", "reactive oxygen metabolic process", and "regulation of cytokine production"), metabolic ("glycolipid metabolic process", and "cholesterol metabolism"), and protein modification ("cellular protein modification process", and "protein ubiquitination") processes. Other interesting pathways were "ion binding",", "cellular response to stress", "cellular senescence", and "cellular response to hypoxia" (**Figure 48**). Altogether, important processes for cell and BBB function were found regulated.

In order to look at the specific genes involved in regulated processes, I manually listed the DE genes contained in relevant KEGG pathways (**Figure 49**). Interestingly, the Wnt pathway was highly regulated, with important genes differentially expressed in more than one comparison, such as down-regulated canonical ***Ctnnb1*** or up-regulated suppressors ***Nfatc4***, ***Nkd2***, and ***Ruvbl1***. These changes indicated an overall effect on canonical Wnt pathway repression. Genes related to the immune system/inflammation were highly regulated as well, although the list of genes was too great to show it in this format.

Then, I defined the AD signature in ECs as the differentially expressed genes in common for both AD groups. These "AD genes" play many different roles, which I summarized in **Figure 50**. One gene strongly up-regulated was ***Ccl3***, as it is described in the following section.

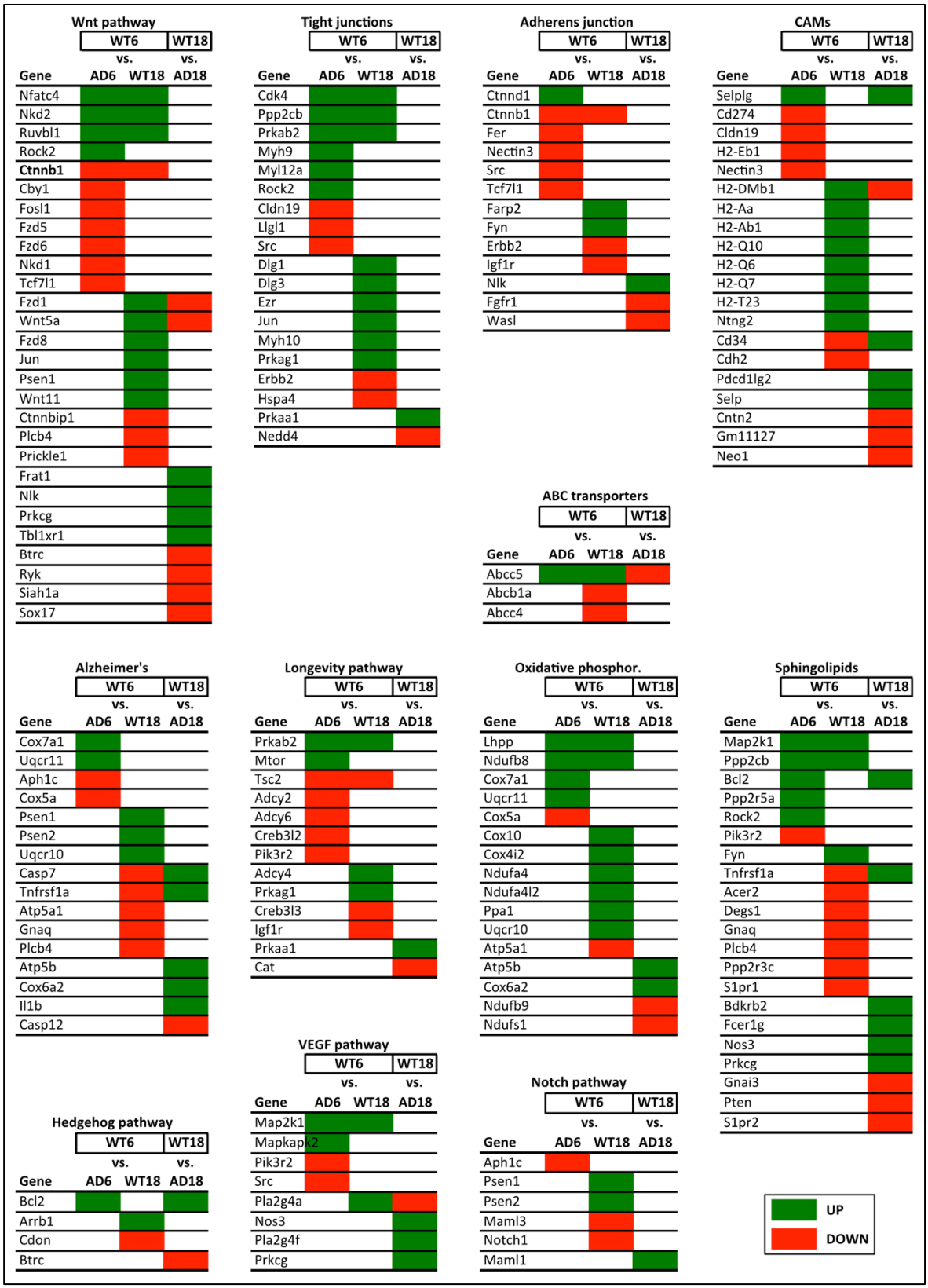

Figure 49: DE genes in KEGG pathways. Up-regulation (green) and down-regulation (red) in AD compared to age-matched WT, and in healthy ageing (WT18 compared to WT6). DE genes here are defined as $p<0.05$ & $log2FC>0,5$ or $<-0,5$.

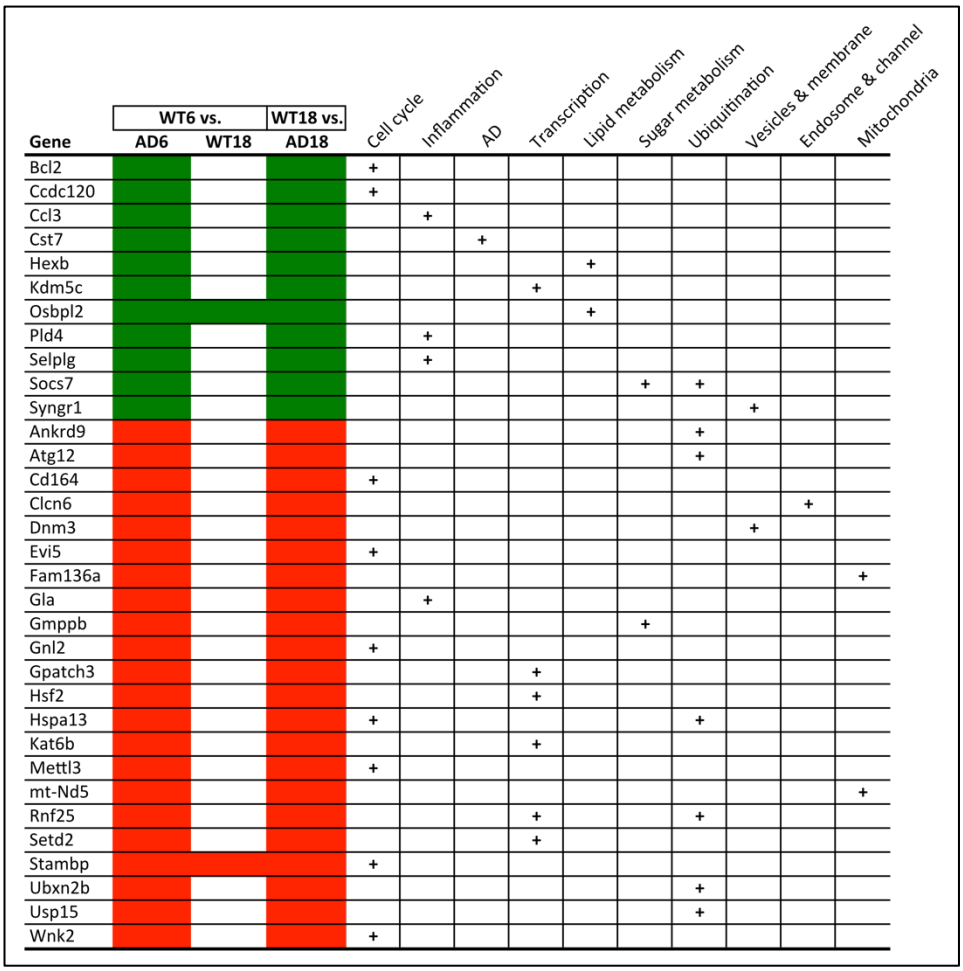

Gene	WT6 vs. AD6	WT6 vs. WT18	WT18 vs. AD18	Cell cycle	Inflammation	AD	Transcription	Lipid metabolism	Sugar metabolism	Ubiquitination	Vesicles & membrane	Endosome & channel	Mitochondria
Bcl2				+									
Ccdc120				+									
Ccl3					+								
Cst7						+							
Hexb								+					
Kdm5c							+						
Osbpl2								+					
Pld4					+								
Selplg					+								
Socs7									+	+			
Syngr1											+		
Ankrd9										+			
Atg12										+			
Cd164				+									
Clcn6												+	
Dnm3											+		
Evi5				+									
Fam136a													+
Gla					+								
Gmppb									+				
Gnl2				+									
Gpatch3							+						
Hsf2							+						
Hspa13				+						+			
Kat6b							+						
Mettl3				+									
mt-Nd5													+
Rnf25							+			+			
Setd2							+						
Stambp				+									
Ubxn2b										+			
Usp15										+			
Wnk2				+									

Figure 50: AD signature genes in ECs. Up-regulated (green) and down-regulated (red) genes are $p<0.05$ and log2FC>1 or <-1 in both AD groups compared to their correspondent WT age-matched controls, and in healthy ageing (WT18 vs. WT6).

5.4.2.4. Common MBMV-EC data: strongly EC-regulated genes

The MBMV samples were enriched with ECs, and therefore a comparison between the MBMV and EC datasets was possible. **Table 12** shows the number of genes with $p<0.05$ and log2FC>0 or <0 in common for each comparison.

Unfortunately, no genes were found in common between all AD groups. In early AD (all AD6), 3 genes were up-regulated in common: ***Gm28177***, ***Ptgis***, and ***Rfk***. In all AD groups except Het6, 3 different genes were found to be up-regulated in common: ***Ccl3***, ***Cst7***, and ***Pld4***.

Table 12: number of regulated genes in common between MBMVs and ECs (nc = not compared)

		MBMV					
		WT6-Het6	WT6-Hom6	WT18-Hom18	WT6-WT18	All AD6	All Hom (no Het6)
EC	WT6-AD6	25	31	nc	nc	3	3
	WT18-AD18	nc	nc	26	nc	nc	
	WT6-WT18	nc	nc	nc	140	nc	nc

In general, the overlap between MBMV and EC datasets was moderate. However, the genes found in common were specific for ECs, and detecting them in the MBMV samples, in which different cell-types were present, indicated a strong gene regulation.

5.4.2.5. The sequencing data from MuCs show novel gene regulations

The MuC dataset contained a total of 25814 genes. Due to the contamination in two WT6 and two AD6 samples, the remaining samples in those groups were n=2 and therefore the p value and FDR were approximates. Thus, I decided to use only the FDR for the comparisons involving those groups. The summary of MuC data can be found in **Table 13**.

Table 13: MuC data

Comparison	P<0.05 genes	FDR<0.05 genes	DE genes
WT6 vs. AD6	–	258	256
WT6 vs. WT18	–	181	180
WT18 vs. AD18	1415	51	1371

Like the EC data, the MuC data is the first dataset of MuC-regulated genes in an AD mouse model and hence, all regulated genes are potentially interesting. Unfortunately, statistics could not be made for the WT6-AD6 and WT6-WT18 comparisons due to the excluded samples in WT6 and AD6 groups. Nevertheless, an approximate p value and FDR were used to analyse the data. The top 20 DE genes in each comparison give an idea of the strongest regulations happening in the cells, pictured in **Figure 51**.

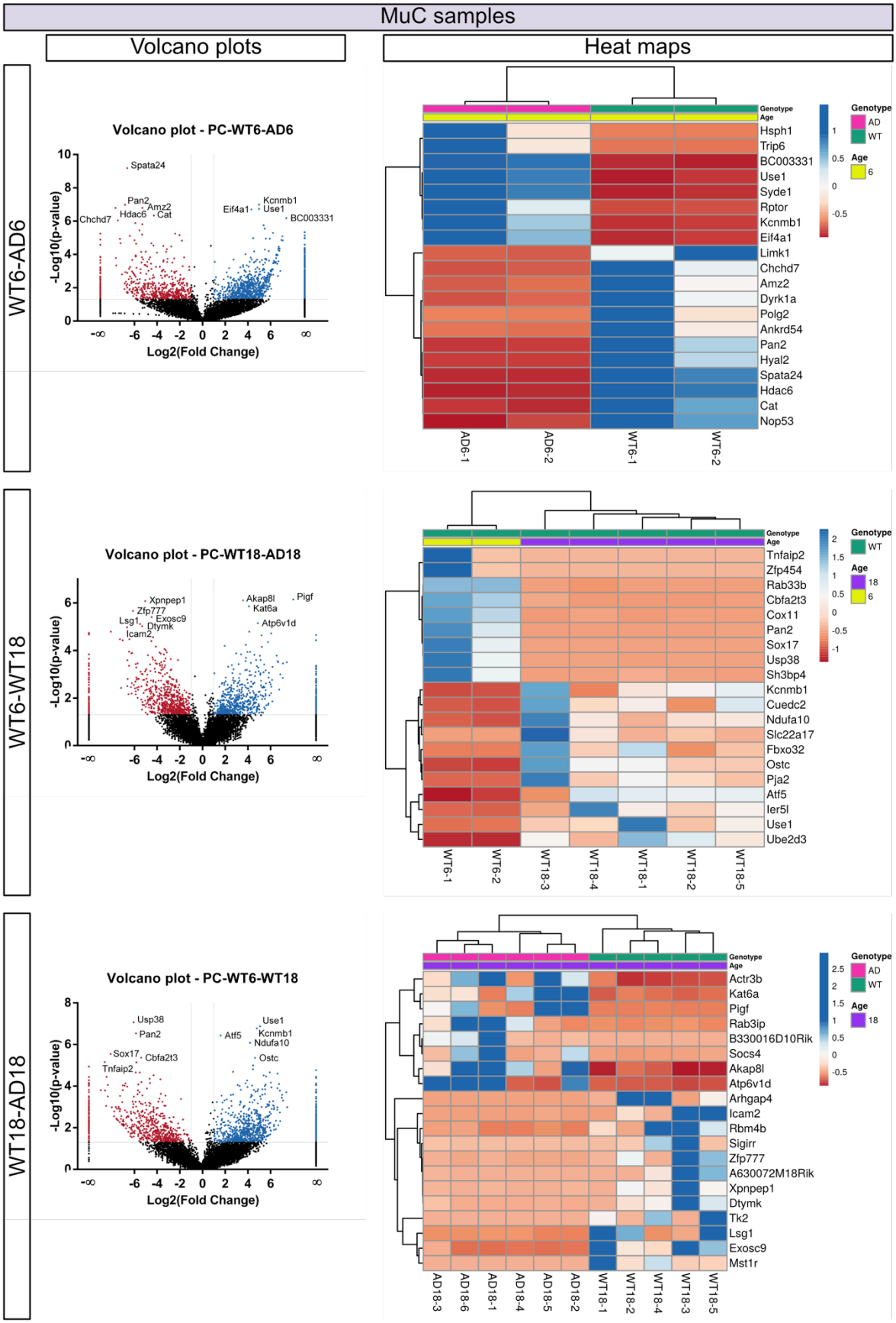

Figure 51: volcano plots and heat maps of MuC samples.

Interestingly, in the late AD comparison, which has the strength for adequate statistical analysis, some inflammation-related genes were down-regulated such as ***Icam2*** and ***Sigirr***, while the suppressor cytokine signalling 4 (***Socs4***) was up-regulated.

The pathway enrichment analysis pictured in **Figure 52** showed abundant vascular-related pathways regulated in both AD groups, such as "regulation of platelet-derived growth factor receptor-beta signalling pathway", "artery development", "blood vessel morphogenesis", and "vasculature development", among others. Also, pathways related to BBB function could be found like "peptide transport", "cell junction assembly", and "regulation of cell adhesion". Among others, some interesting pathways that could be found were "cellular response to

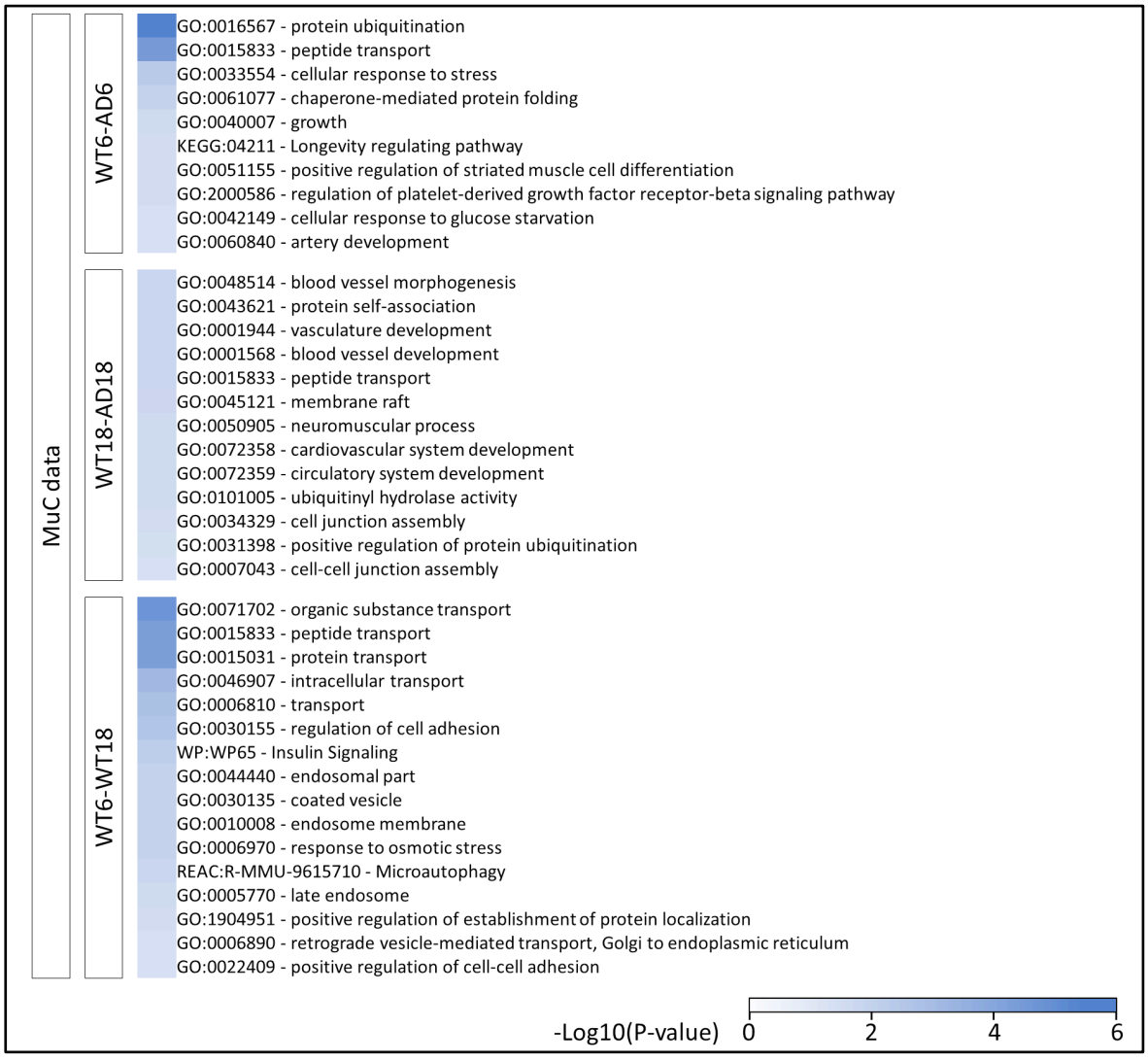

Figure 52: selection of regulated pathways found by pathway enrichment analysis of DE genes in each comparison.

stress", "longevity regulation pathway", "neuromuscular process", and "response to osmotic stress".

Taken altogether, the MuC sequencing results showed important novel genes and pathways regulated. In order to define specific AD regulations, I also created the AD signature in MuCs as the differentially expressed genes in common for both AD groups. **Figure 53** shows the AD genes in MuC with a short description of their related pathways.

AD genes in MuCs

Gene	WT6 vs. AD6	WT6 vs. WT18	WT18 vs. AD18	Information
Cdkn2aip				RNA binding & p53 binding
Mrps10				Mitochondrial translation & Viral mRNA Translation & Organelle biogenesis and maintenance
Naxd				Stress & Metabolism of water-soluble vitamins and cofactors
Nudt14				Post-translational protein modification
Rbck1				Immune System & Necroptosis
Rnf123				Deubiquitination & Immune System & Post-translational protein modification
Amz2				metallopeptidase activity & SMC contraction
Fam117a				
Snx19				insulin secretion & phosphatidylinositol binding
Spata24				
Ubox5				Ubiquitination & Immune System

Figure 53: AD signature genes in MuCs. DE genes in AD6 and WT18 (compared to WT6) are defined as FDR<0.05 & log2FC>1 or <-1. DE genes in AD18 vs. WT18 are p<0.05 & log2FC>1 or <-1. Information about related pathways is provided for each gene except ***Fam117a*** and ***Spata24*** because they are not well known.

The analysis of AD genes in MuCs showed inflammation-related genes previously not detected, such as ***Rbck1***, ***Rnf123***, and ***Ubox5***. Hence, the sequencing data analysis from EC and MuC samples found inflammation- and BBB-related processes, indicating that both might be playing an important role in AD.

5.4.2.6. The sequencing data from MG validates the AD model and the EC & MuC datasets

The MG dataset contained a total of 28024 genes. The summary of MG data can be found in **Table 14**.

Table 14: MG data

Comparison	P<0.05 genes	FDR<0.05 genes	DE genes
WT6 vs. AD6	1466	183	1402
WT6 vs. WT18	1565	215	1502
WT18 vs. AD18	1156	70	1047

As it was expected, the pathway enrichment analysis displayed in **Figure 54** and the top 20 DE genes pictured in **Figure 55** showed inflammatory pathways and genes regulated, such as “inflammatory response to wounding” (**Figure 54**) and ***Ildr2***, ***H2-Ab1***, ***H2-Aa***, and ***Cxcl1*** (**Figure 55**).

The pathway enrichment analysis also found other interesting regulated pathways, such as “negative regulation of vascular endothelial growth factor production”, “response to muscle activity”, positive regulation of amyloid precursor protein biosynthetic process”, and “establishment of blood-retinal barrier” (**Figure 54**).

The fact that all of those pathways are regulated suggested that MG reacted to AD not only by modulating the inflammatory response, but also by modulating the vascular compartment.

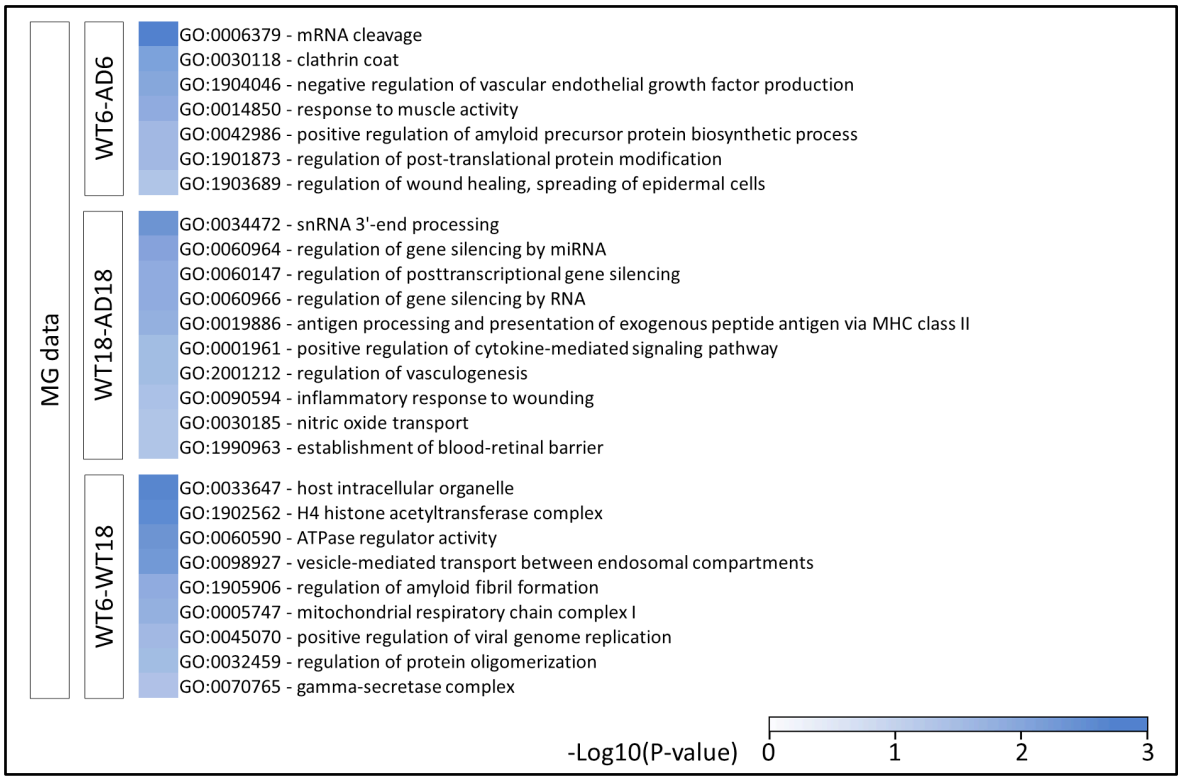

Figure 54: selection of regulated pathways found by pathway enrichment analysis of DE genes in each comparison.

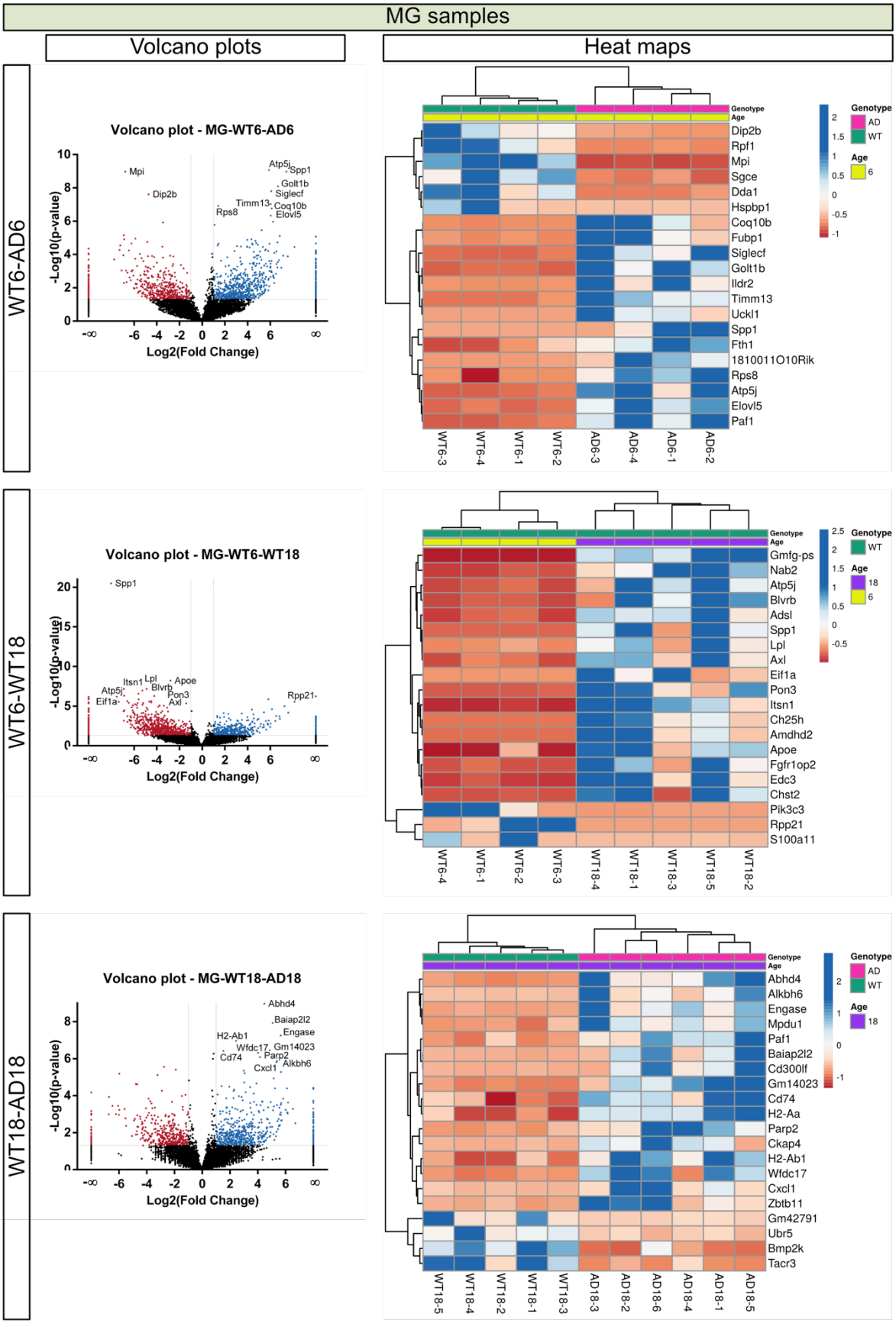

Figure 55: volcano plots and heat maps of MG samples.

Unlike ECs and MuCs, MG has been deeply studied in the context of AD and hence, many sequencing databases are available from mouse models and human patients. Therefore, MG sequencing results could be used to validate the mouse model and the novel databases of ECs and MuCs if the changes observed in the MG from ***Thy1-APP***^{SwDI} were the same as the changes known to happen in the MG of other AD models and patients. I selected three papers from top journals that sequenced single-cell MG (Mathys et al. 2017; Keren-Shaul et al. 2017; Mathys et al. 2019). These studies identified MG genes specifically up-regulated with AD, the information is shown in **Table 15**.

Table 15: scRNA-Seq selected papers

Paper	Samples from	AD up-regulated genes described
Mathys et al. 2017, Cell Reports	CK-p25 mouse MG	515
Keren-Shaul et al. 2017, Cell	5XFAD mouse MG	257
Mathys et al. 2019, Nature	Postmortem human MG from AD patients	77

With the AD-upregulated MG genes found by Mathys et al. 2017, Keren-Shaul et al. 2017, and Mathys et al. 2019, I first analysed how many they had in common, finding that the three datasets do not show a great overlap, with only 27 genes in common (**Figure 56 A**). Then, I compared each dataset to mine and found that most of the regulated genes in common were up-regulated in my dataset (**Figure 56 B**). This finding indicated that even though not all the genes from the published datasets were regulated in mine, most of the genes that did, were up-regulated and therefore followed the published regulation. The list of up-regulated genes in common between the published datasets and mine is pictured in **Figure 56 C**, showing important AD genes such as ***Apoe*** and ***Tyrobp***.

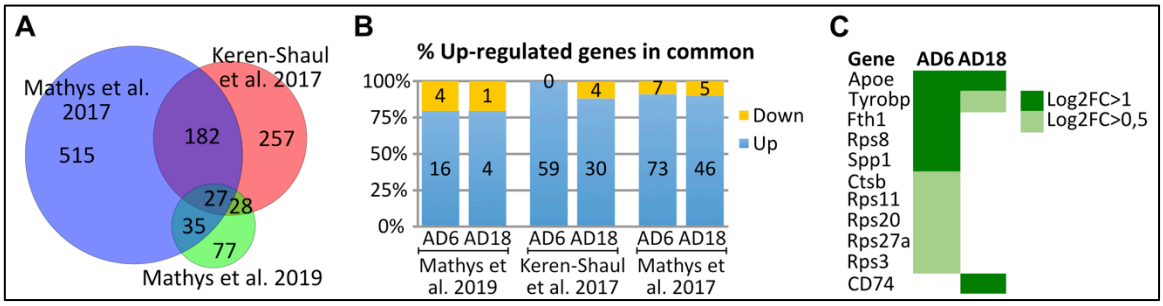

Figure 56: (**A**) Venn diagram with the common AD genes within the published datasets. (**B**) % MG regulated genes in AD6 and AD18 (vs. age-matched WT) that are up-regulated compared to the MG published datasets. (**C**) List of up-regulated MG genes in common with the published datasets and mine.

5.4.2.6.1. MG is the source of Dkk2 up-regulation

Besides blind-comparing published datasets to mine, I manually searched for well-known MG regulated genes in AD. I could find important genes such as ***Trem2*** and ***Apoe*** up-regulated in both AD groups (**Figure 57**). I also found ***Dkk2*** strongly up-regulated exclusively in the AD groups, indicating that the up-regulation detected in the MBMV data was derived from the little MG contamination that those samples had (**Figure 34**). Taking all the MG data analysis together, it appears that the AD-reacting MG might be modulating the brain vasculature, possibly by ***Dkk2*** up-regulation.

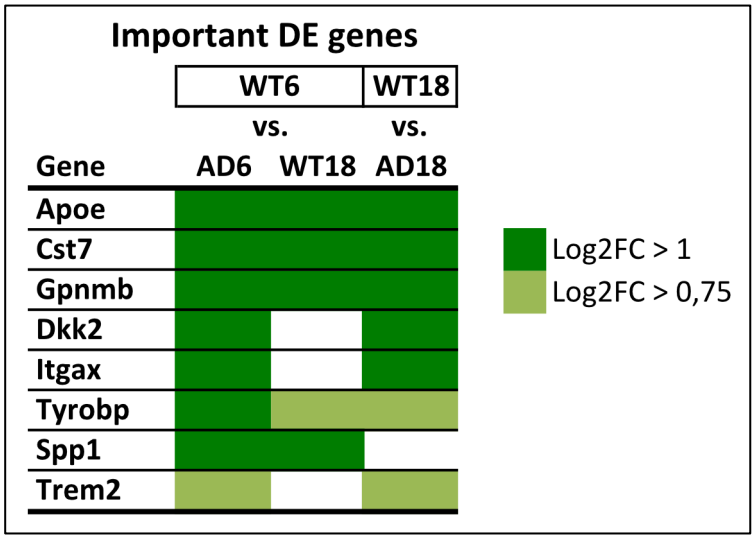

Figure 57: list of important MG genes regulated in AD showing in which group/s they are up-regulated.

Pttg1 was not found to be regulated in any sequencing result from FACS-sorted samples. The cellular source appeared to be neuronal in a preliminary IF staining with anti-Pttg1 (data not shown). Therefore, ***Pttg1*** was discarded as candidate gene and further analysis was continued with ***Dkk2*** as the new top candidate gene for testing.

5.5. DKK2 is present in human AD brain tissue

For the next step of the analysis, I wanted to check the Dkk2 protein expression in WT and AD mouse brains. Although unfortunately anti-Dkk2 antibodies were not available for mouse samples, luckily anti-DKK2 for IHC in human samples was commercially available. I therefore checked the DKK2 presence by IHC in autopsy tissue from a 76 year old male with AD and a control autopsy tissue from a 62 year old male with no AD or mild cognitive symptoms. The AD sample clearly showed stronger DKK2 immunoreactivity than the control (**Figure 58**).

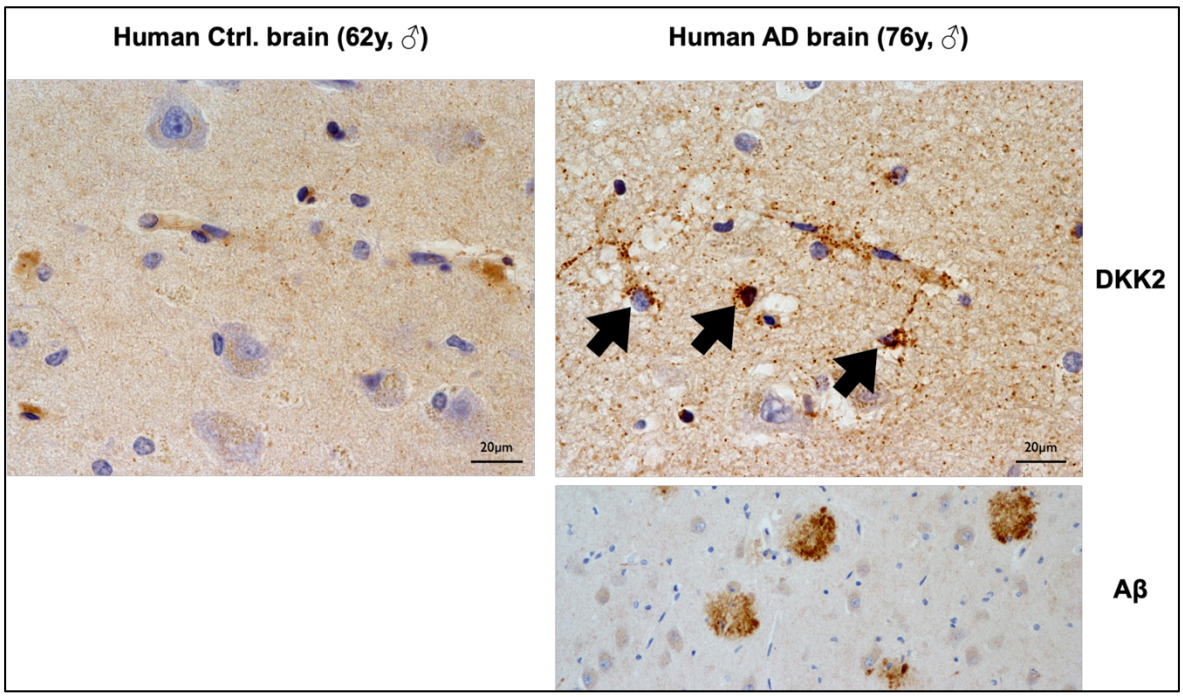

Figure 58: human brain autopsy tissue stained by IHC with (**top**) anti-DKK2 (brown) and hematoxylin (purple-blue), and (**bottom**) anti-Aβ (brown) and hematoxylin (purple-blue). Arrows indicate DKK2 immunoreactivity on the AD sample.

5.6. DKK2 is a Wnt/β-catenin inhibitor

The dickkopf family of secreted proteins are important regulators of the Wnt/β-catenin signalling pathway, with DKK1 the most known member as a Wnt pathway inhibitor. The role of DKK2, however, is not entirely clear and hence, I decided to test if it would have any effect on the Wnt pathway. For this, I co-transfected HEK293T cells with a human-DKK2 (hDKK2) overexpressing plasmid and a β-catenin reporter plasmid (TOP) that contains TCF/LEF sites upstream of a luciferase (firefly) reporter (M50 Super 8x TOP-FLASH, Randall Moon). As control for the hDKK2 overexpression I used the same empty vector, and as control for the β-catenin reporter I used a plasmid with mutated TCF/LEF binding sites (FOP) upstream of the same luciferase reporter (M51 Super 8x FOP-FLASH, Randall Moon). To normalize the transfection efficiency, I co-transfected all plates with a Renilla luciferase plasmid as well (TK-Renilla, Promega). The cells were treated with Wnt3a to induce the Wnt pathway, and the dual luciferase activity measured 20 h afterwards (**Figure 59 A**). The results were obtained by dividing the random fluorescent units of firefly to renilla luciferase. **Figure 59 B** shows the Wnt induction in the absence of DKK2 and a strong DKK2 inhibition of the Wnt-induced luciferase activity. The FOP control showed no difference upon Wnt treatment and/or hDKK2 overexpression.

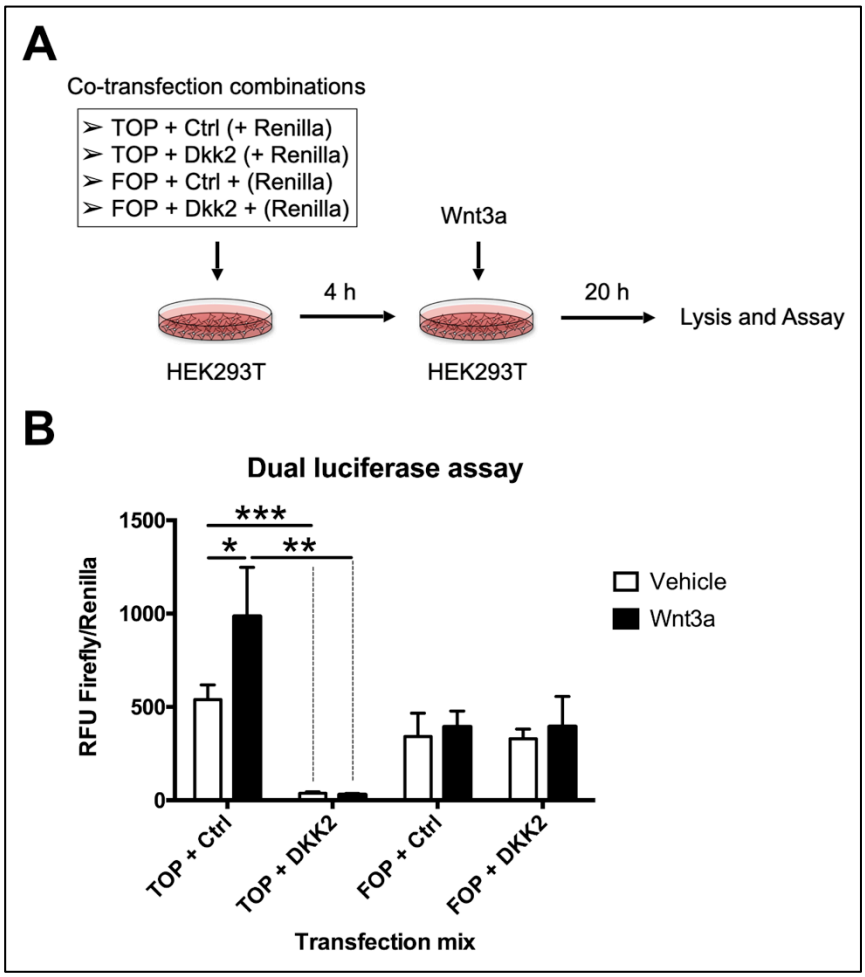

Figure 59: (**A**) schematic representation of the HEK293T co-transfection and Wnt treatment. (**B**) Dual luciferase assay. RFU=random fluorescent units.

5.7. Wnt/β-catenin activation in ECs ameliorates the AD phenotype

In vivo permeability assays showed a higher BBB permeability in AD groups, indicative of BBB dysfunction. EC transcriptomic analysis found, among others, a down-regulation of ***Ctnnb1***, the gene coding for β-catenin. MG transcriptomic analysis confirmed the up-regulation found in MBMV data of ***Dkk2***, a secreted Wnt pathway inhibitor. Given the collective data pointing towards a BBB dysfunction in AD with the possible cause being a Wnt/β-catenin repression in ECs, the question opens: does activation of the canonical Wnt signalling by β-catenin stabilization ameliorate the AD symptoms?

To answer that question, I made use of the tamoxifen inducible ***Cdh5***(PAC)-CreERT2:***Ctnnb1***(Ex3)fl/fl mouse line. In ECs of this line, the exon 3 of ***Ctnnb1*** is cleaved after induction with Tamoxifen, protecting β-catenin from phosphorylation and degradation, thereby creating a GOF mutation. This mouse line was then crossed with the AD line, generating AD/GOF (GOF) and AD/control (control) mice. The control mice lack the CreERT2 enzyme so β-catenin can be phosphorylated and recognized by the degradation complex even after Tamoxifen application.

GOF and control mice were injected with Tamoxifen at different ages to test the effect of induction on disease stage. Mice were sacrificed after induction for 2, 5, or 9.5 months. I performed permeability assays to test whether after inducing the β-catenin GOF, a decrease in BBB permeability could be observed in the GOF group. A statistically significant decrease of BBB permeability was detectable with 3-4 kDa dextrans in the cerebellum of 20-22 months old GOF compared to control mice after two months of induction (**Figure 60 A**). Unfortunately, in the cerebrum there was no significant change of BBB permeability (**Figure 60**).

I also analysed the behaviour of GOF and control mice. Interestingly, the GOF group with lower BBB permeability in the cerebellum also exhibited lower burrowing activity (**Figure 61 A**), although no significant differences could be found with the Y-maze test (**Figure 61 B**). Interestingly, the 9-12 months old GOF group induced for 9.5 months performed better in the Y-maze test of spontaneous alternations than the control group (**Figure 61 F**), indicating an amelioration of memory function. This was the same age at which I could detect a loss of memory in AD mice using the same experimental set-up (**Figure 31**).

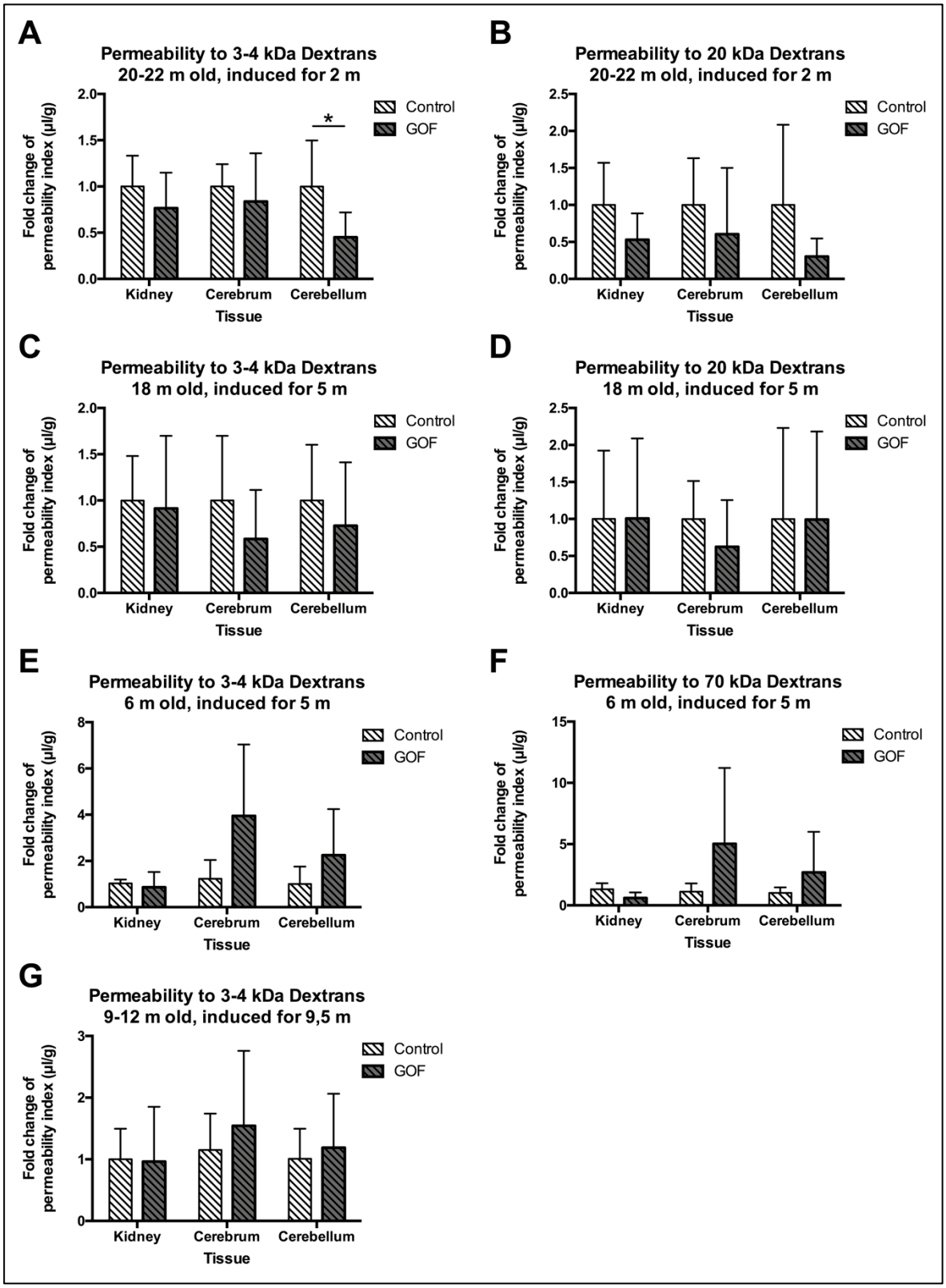

Figure 60: permeability assays in cerebrum, cerebellum and kidney with 3 kDa TMR, 4 kDa FITC, 20 kDa TMR, and 70 kDa FITC dextrans. Processed data from 3 and 4 kDa dextrans have been combined (**A, C, E, G**) while data from 20 kDa and 70 kDa dextrans are displayed separately (**B, D, F**). The n numbers of Ctrl6, GOF6, Ctrl9-12, GOF9-12, Ctrl18, GOF18, Ctrl20-22, and GOF20-22 are 4, 4, 6, 7, 4, 5, 4, and 8, respectively.

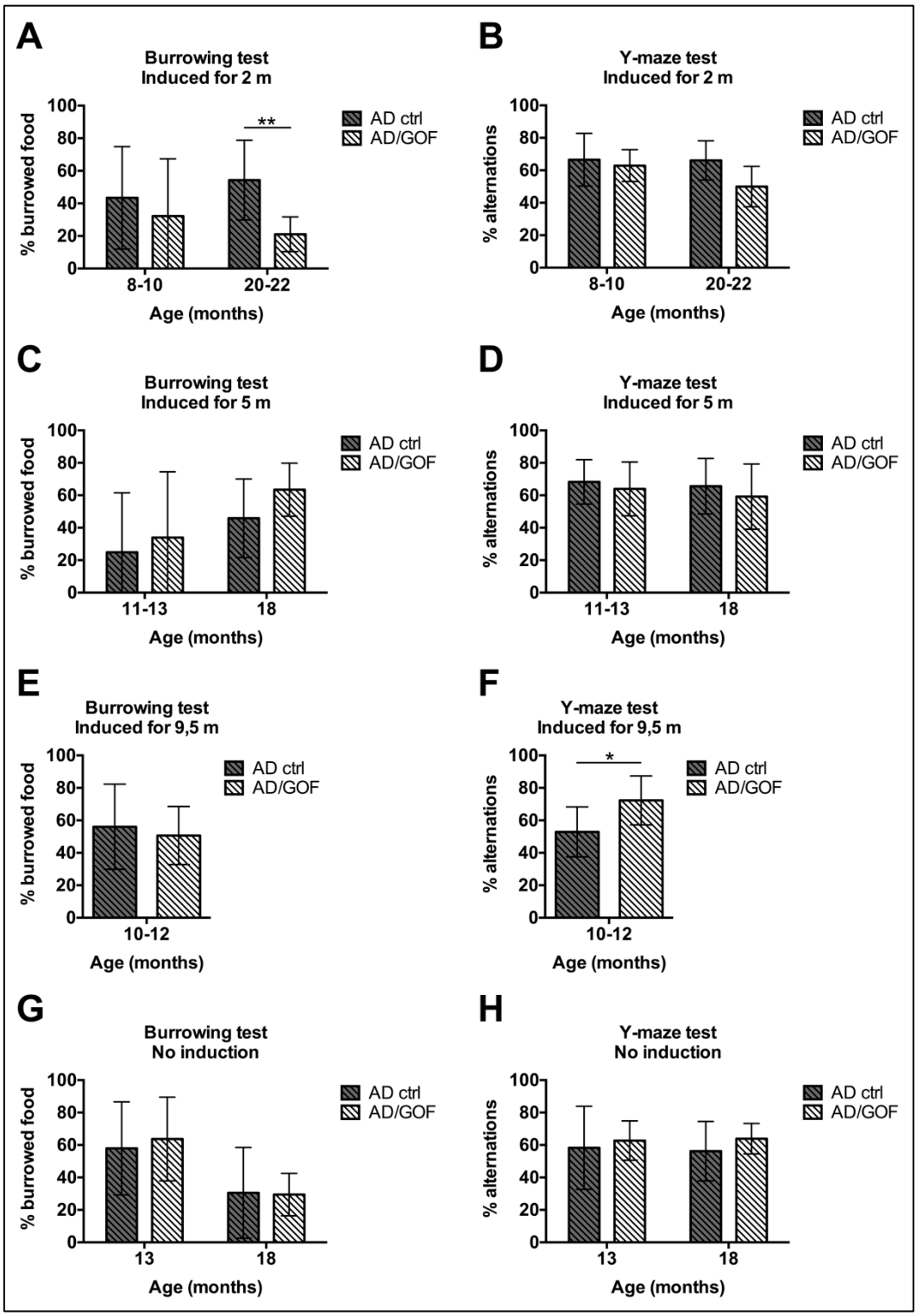

Figure 61: behavioural tests in GOF and control mice. (**A, C, E, G**) Burrowing tests, (**B, D, F, H**) Y-maze tests of spontaneous alternations. Induction for 2 (**A-B**), 5 (**C-D**), 9.5 months (**E-F**), or no induction control (**G-H**). The n numbers for Ctrl8-10, GOF8-10, Ctrl11-13, GOF11-13, Ctrl18 (induced-5), GOF18 (induced-5), Ctrl10-12, GOF10-12, Ctrl13, GOF13, Ctrl18 (no ind.), and GOF18 (no ind.) are 11, 11, 4, 8, 10, 7, 4, 5, 7, 7, 6, 6, 8, and 10.

6. Discussion

This project is composed of a number of experiments aiming to answer the initial research question, what is the contribution of the BBB to AD. At first, I made use of an immortalized mouse brain endothelial line (bEnd5) to knockdown ***Sirt1*** – a known vascular regulator involved in processes such as ageing-related endothelial senescence – and to study properties of the cell line. I also used mouse models of AD and β-catenin GOF to assess BBB permeability, memory performance, and transcriptomic changes in brain microvessels and FACS-sorted cells of the NVU (ECs, MuCs, ACs, and MG).

6.1. *Sirt1* reduction in ECs as a possible cause of BBB dysfunction

The bEnd5-***Sirt1***-KD cells appeared to grow faster than control cells according to the proliferation assay (**Figure 28**). At low density, the cells had more space to grow and therefore differences in proliferation could be seen more easily. However, more biological replicates are needed to confirm this finding. Along the same line, the bEnd5-***Sirt1***-KD cells invaded the scratched surface faster than control cells, indicating elevated proliferation and/or migration properties. ***SIRT1*** has been reported to be reduced in the serum of AD patients (Kumar et al. 2013), with some studies proving evidence that ***Sirt1*** activation has beneficial effects in mouse models of AD (Guo, Xu, and Wang 2016). Here I show that low levels of ***Sirt1*** in a mouse cell line of brain ECs cause a hyper-proliferating/migrating phenotype, opposed to what was reported by Potente et al. (Potente et al. 2007). They showed that Sirt1 protein controls the angiogenic activity of ECs and loss of Sirt1 function blocks sprouting angiogenesis and branching morphogenesis of ECs (Potente et al. 2007). The differences in the effects of reduced Sirt1 on ECs might be due to the usage of brain ECs (bEnd5 line) vs. lung ECs and human umbilical vein ECs (HUVECs; Potente et al. 2007). Thus, the effects of Sirt1 on ECs might differ when the ECs are forming a tight barrier or when they are not.

Augmented proliferation or migration in ECs is associated with angiogenesis and is opposed to barrier formation. Hence, low levels of ***Sirt1*** in brain ECs would be promoting BBB dysfunction and AD progression. The ***APP***^{SwDI} mouse model used

in this thesis showed no change of ***Sirt1*** gene expression in MBMV or FACS-sorted samples. Interestingly, a study comparing ***SIRT1*** levels in both AD patients and a transgenic mouse model of AD found only a decrease in AD patients but not in the AD mouse model (Julien et al. 2009). Preliminary data from this thesis suggest a negative effect of ***Sirt1*** down-regulation in AD, in line with what has been reported in the literature. A more accurate AD model with a significant ***Sirt1*** reduction would be needed to assess its potential as therapeutic target. Thus, possible beneficial effects of vascular ***Sirt1*** activation in AD remain to be evaluated.

6.2. The *Thy1-APP*^{SwDI} mouse line as a model for AD

The ***Thy1-APP***^{SwDI} (AD) mouse model was selected among other AD models due to published properties such as extensive vascular Aβ depositions and early AD symptoms (Aβ plaques and cognitive dysfunction already at 3 months of age; Xu et al. 2007). Given that every animal housing facility has different working procedures and conditions, they can influence the behavior and even Aβ deposition in mice. Therefore, I tested whether I could detect the key AD-hallmarks in the AD mouse model and if they would corroborate published characteristics.

AD-homozygous mice displayed robust AD symptoms, with Aβ plaques already at 3 months-of-age, diminished burrowing activity at 6 and 18 months-of-age, and lower memory performance at 9-12 month-of-age (**Figure 31 B**). AD-heterozygous mice showed more variable AD symptoms, with some animals developing Aβ plaques at 3 months-of-age, and others at 6 months-of-age or older. Nevertheless, 6 and 18 months old Het mice burrowed significantly less food than their WT littermates (**Figure 31 A**). Reduced burrowing activity is an indication of poor well-being but also of weakened hippocampal activity (Deacon 2006). The hippocampus is one of the first areas to be affected in AD, accounting for the memory loss symptoms typical of the disease. Therefore, both burrowing and Y-maze tests serve to measure AD symptoms.

It is important to notice that behavioural tests are very sensitive to changes in noise, odour, movement, light, time, and mouse conditions. The room in the animal facility where I performed the behavioural tests was often filled with different noises and smells of people and other animals. Consequently, obtaining significant

results is an indication of strong changes in behaviour. Moreover, it is difficult to conclude that no differences exist in those AD groups displaying no significant reduction in burrowing activity or spontaneous alternations in the Y-maze. Xu et al. reported cognitive dysfunction in 3, 9 and 12 months old ***Thy1-APP***^{SwDI} mice using the Barnes maze test for learning and memory (F. Xu et al. 2007). Hence, whether lack of differences in the non-significant AD groups owned to less robust tests or to not optimal behavioural conditions is, at this point, not possible to know. Testing in a specialized behavioural laboratory would be needed to draw definite conclusions. Nonetheless, the fact that I could detect Aβ plaques, hippocampal dysfunction, and memory loss proved that ***Thy1-APP***^{SwDI} mice could be used as AD model.

6.3. BBB dysfunction in AD

Whether BBB dysfunction is present in AD has been a matter of debate in the past few years (Profaci et al. 2020). Tracer experiments with dextrans of different molecular size allow for the study of BBB permeability ***in vivo***. In AD cerebra, the permeability assays showed a clear increase of 3-4 kDa dextrans in 6, 9-12, and 18 months-of-age or older Hom mice. In Het mice, the increase was significant in 18 months-of-age or older mice, but not in 6 months old mice. This correlated with the irregular Aβ accumulation seen at 6 months-of-age, indicating that Het mice begin to show the AD phenotype at this time. The BBB permeability increase was not detected with bigger (20 kDa) tracers, suggesting a modest BBB leakage in AD mice (**Figure 32 A-B**). AD is a chronic disease and a BBB dysfunction, although modest, might lead to severe complications over time if it is not repaired, such as brain inflammation.

Interestingly, the permeability increase could also be seen in AD mouse cerebella (**Figure 32 C**). In the cerebellum tissue Aβ plaques did not accumulate, suggesting that the cause of BBB dysfunction was, at least in this tissue, of a different origin. Inflammation is a well-known regulator of vascular permeability. In this AD mouse model, strong transcriptional changes in brain MG were detected that can potentially affect BBB function, such as ***Dkk2*** up-regulation. It would be very interesting to study if similar MG changes can be identified in the cerebellum.

Surprisingly, kidney tissue control also revealed vascular permeability changes (**Figure 32 E-F**). Hom mice of 6 months-of-age exhibited greater permeability than Het mice to both 3-4 kDa and 20 kDa dextrans. Het mice of 18 months-of-age and older showed higher permeability to 20 kDa but not to 3-4 kDa dextrans. Some studies report systemical changes in AD, including renal dysfunction where serum Aβ levels are positively correlated with impaired renal function (J. Wang et al. 2017). Aβ plaques were extensive in old Het mice and already fairly present in 6 month-of-age Hom mice (**Figure 30**). Reasonably, Aβ levels rose in blood as well, which might explain the increase in kidney vascular permeability.

6.4. Marker analysis of MBMV: useful to study population changes

Mice of 6 and 18 months of age were selected for the 3' RNA-Seq analysis. Mice of 6 months-of-age served to capture early changes in AD, and 18 months old mice the late changes. A milder AD phenotype could be observed in young Het mice compared to Hom mice. At 6 months-of-age, Het mice displayed no change in BBB permeability and irregular Aβ accumulation. Therefore, the presence of one or both mutated alleles in the AD model impacted significantly the onset of AD symptoms, as it would be expected. However, at old ages, both Het and Hom mice exhibited strong Aβ accumulation, behavioral deficits, and BBB dysfunction, indicating that the severity of the disease was comparable. Hence, having both AD groups at 6 months-of-age offered a wide view on early AD changes that could be analyzed separately, while Het and Hom groups at old ages could be merged as one single AD group.

The analysis of 3' RNA-sequencing data from MBMVs showed marker genes expression from ECs, MuCs, ACs, MG, FBs, OLs, and Ns (**Figure 34**). It was no surprise to find higher expression of EC marker genes, along with the other BBB-constituting cells (MuCs and ACs). The detection of MG, FB, OL, and N genes however, meant that these cells were in close contact with MBMV and were therefore isolated along with them. Thanks to published single-cell sequenced databases it was possible to identify cell-type specific marker genes and use them to analyse the cell-type content of the MBMV samples. The decrease of EC markers

detected in old WT compared to WT6 was further confirmed by a decrease of Erg^+ cells per vessel length (**Figure 36**). Interestingly, a decrease of ECs in Hom6 compared to WT6 was also revealed. The reduction of ECs in AD and ageing have already been reported in other studies, however mainly as a reduction of capillary density (X. Xu et al. 2018; Sweeney et al. 2019). Nonetheless, the detection of this change with marker genes was a good indication of the validity of the analysis and served to have an overview of large swifts in cell populations.

Other changes in markers that could be observed were an increase of AC genes in WT18 compared to WT6. Again, ageing had a strong effect on cells. Astrogliosis is known to happen in ageing, with already numerous groups reporting a substantial swift in gene expression in aged ACs (Orre et al. 2014; Habib et al. 2020). This astrogliosis might explain why more ACs were isolated together with MBMVs, although confirmation by stainings or other methods is needed to obtain conclusive results.

The decrease of PC markers in WT 18 compared to WT6 did not reach statistical significance ($p=0,05$) although the trend is clear. PC marker genes are not so numerous and are not distinguishable from venous smooth-muscle cells (vSMCs). This mixture could explain why the statistics did not reach significance. The reduction of PCs in ageing has, once more, been described already and interestingly, PC loss leads to EC degeneration in the context of AD (Montagne et al. 2020). It would be interesting to check if this is indeed the case in this AD model.

Both SMCs and MG showed augmented marker expression in AD and ageing groups. This could be due to the loss of ECs, which as a result increased the proportion of attached cells such as SMC and MG. Also, a thickened intima consisting of infiltrating SMCs and MG is known to develop with ageing and might explain the increased marker expression of those cell types (Monk and George 2015).

FBs are a cell-type defined by Vanlandewijck et al. and their function has not been described as of yet (Vanlandewijck et al. 2018). The authors define FBs as a population of cells with a unique gene profile, related to scar-forming cells in spinal cord injury. The increase of FB markers coincided with the increase observed in AC

markers, but whether this correlation has any biological meaning is difficult to judge.

OL and N markers were not significantly changed despite that neuronal degeneration in AD is very well documented. The N and OL genes obtained in the MBMV dataset came from the few N and OL cells that were isolated attached to the MBMVs. Hence, no change in N and OL markers means that no change in the number of N and OL attached cells happened. Whether a decrease of mouse brain total Ns occurred is not possible to define using this MBMV dataset.

As expected, housekeeping genes did not show significant variation, and added an extra level of validation to the analysis.

6.5. Sequencing data

This thesis is the first study showing transcriptional changes occurring in MBMVs, ECs, and MuCs of AD mice, and correlating them to changes in BBB permeability and cognitive decline.

The original hypothesis of the thesis formulated that ***Bace1*** was up-regulated at the BBB and contributed to APP cleavage and Aβ generation around vessels leading to BBB dysfunction and AD aggravation. However, ***Bace1*** was not found to be regulated in MBMV, EC, MuC, and MG sequencing data. ***Bace1*** was reported to be up-regulated in MBMV from $hAPP^{SL}$ mice (Devraj et al. 2016) using qPCR. It is possible that using a different AD mouse model, the regulation would be different. Nevertheless, the original hypothesis had to be discarded.

Fortunately, the sequencing of MBMV and later on the sequencing of FACS-sorted samples, allowed to explore novel gene regulations. The MBMV data proved to be a suitable tool to demonstrate AD-related transcriptomic changes at the microvasculature. The FACS-sorted data not only confirmed some of the gene regulations observed in MBMV, but also added key information about the cellular identity of detected regulated genes.

As seen with the marker gene analysis of MBMV samples, ageing had a strong effect on gene regulation of all sequenced datasets. Although the aim of this thesis was not to identify changes in healthy ageing, the data was produced to be able to discern changes due to ageing, or due to AD. It is very interesting to observe that,

in general for all datasets, alterations in early AD and in healthy ageing shared a lot of regulated genes (**Figure 39**). Furthermore, not that many genes were altered in old AD mice compared to old WT mice, indicating that both groups were transcriptionally close and highlighting the strong relationship between AD and ageing.

In order to identify novel genes and/or pathways to explain the vascular dysfunction observed in AD, I meticulously investigated (in the literature) the role of all top regulated genes in each comparison and of all commonly regulated genes in between groups, for each dataset. Pathway enrichment analysis and pathway gene lists proved to be useful tools to gain an overview of broader regulations.

In MBMV samples, the sequencing results identified a down-regulation of ***Klf2*** in Hom6 mice compared to age-matched WT (**Figure 37**), and in the healthy ageing comparison (data not shown). This gene encodes a transcription factor important for vascular integrity, barrier function, and inflammatory response (SenBanerjee et al. 2004; Lin et al. 2010; Sangwung et al. 2017). The sequencing results from FACS-sorted samples detected a down-regulation of microglial ***Klf2*** in the healthy ageing comparison, and a down-regulating trend in AD6 compared to WT6 ($p=0.086$). Though ***Klf2*** was not regulated in the sequenced FACS-sorted EC samples, the loss of relative ECs in Hom6 and WT18 MBMVs (**Figure 36**) could explain why the ***Klf2*** down-regulation was so strong in those samples. Further studies would be needed to investigate the effects of ***Klf2*** down-regulation in MG.

The pathway enrichment analysis of MBMV samples found inflammatory and BBB-related processes regulated, such as “chemokine signalling pathway”, “activation of C3 and C5”, “Wnt signalling pathway”, “angiogenesis”, and “cell-cell junction formation” (**Figure 40**). Those results could be indicative of the BBB dysfunction observed thanks to the permeability assays. Vascular pathogenesis in AD has been reported already (Di Marco et al. 2015), although a transcriptomic analysis of specific changes is currently missing. The importance of gene regulations found in MBMV and EC samples is discussed further on.

The analysis of MuC DE genes and enriched pathways detected inflammation-related genes and processes. Also, additional analysis of the data identified 11 novel genes exclusively regulated in the AD groups (**Figure 53**). Interestingly, 3 of

those 11 genes (***Rbck1***, ***Rnf123***, and ***Ubox5***) were involved in immune system and ubiquitination, suggesting that in MuCs, inflammation and protein degradation were key changes in response to AD. It would be very interesting to assess the specific changes in PCs and SMCs separately by IF. PC loss in AD has been proposed to occur after Aβ-induced insulin resistance, leading to transcription activation of oxidative stress- and hypoxia-controlled transcription factors, thereby switching on the programmed cell death (Salmina et al. 2019). Interestingly, "cellular response to stress" and "insulin signalling" were among the regulated pathways found in MuC samples (**Figure 52**). Similarly, in the AD genes of the MuC sequencing results, ***Naxd*** and ***Snx19*** were identified as stress- and insulin-related gene, respectively (**Figure 53**). Although this topic was not further investigated in this thesis, it could be very interesting for future studies.

Many studies have been published in the recent past years about bulk or single-cell RNA sequencing of MG in AD from AD mouse models and human patients (Hickman et al. 2013; Keren-Shaul et al. 2017; Krasemann et al. 2017; Mathys et al. 2017; 2019; Sala Frigerio et al. 2019). Thanks to the published data, some MG up-regulated genes in AD are well known and recognized, such as ***Trem2*** and ***Apoe***. Therefore, obtaining similar results in my sequenced MG served as validation for the AD model, and for the other novel sequenced datasets. Interestingly, vascular related pathways were regulated in the MG as well, such as "establishment of blood-retinal barrier" (**Figure 54**). MG has recently been shown to control vascular architecture in the healthy retina (Dudiki et al. 2020), although the role of microglial modulation of the vasculature in AD has not been explored.

6.6. AD-reacting MG secreting Dkk2 in close proximity to vessels might be inhibiting the Wnt pathway

AD-reacting MG might be controlling the AD-brain vasculature via Dkk2 secretion. ***Dkk2*** appears up-regulated in various datasets. Primarily, it was detected in MBMV data and afterwards, MG data confirmed this regulation identifying its cellular origin. Moreover, Dr. Robert Bell from Pfizer had isolated MBMVs from a different AD mouse model (APPPS1) and agreed to share his results with me (data not shown). Dkk2 was one of the regulated genes found in common. Interestingly,

a published dataset of single-cell RNA-Seq of MG from a different AD mouse model (APP^{NL-G-F}) identified ***Dkk2*** as part of the activated response microglia (ARM) subcluster, defined as strongly enriched with AD risk genes (Sala Frigerio et al. 2019). Sala Frigerio et al. detected ***Dkk2*** in a small population of ARM cells defined as the most responsive to AD.

The fact that ***Dkk2*** can be detected in MBMV preparations suggests that the most AD-responsive MG cells are attached or in closed proximity to the vessel wall and hence, potentially affecting vascular function. DKK2 belongs to the Dickkopf family of secreted proteins, known to be inhibitors of the Wnt pathway. The dual luciferase assay confirmed the Wnt inhibiting properties of DKK2 in HEK293 cells in vitro (**Figure 59**). Hence, activated MG secreting Dkk2 in close proximity to the vessels could be inhibiting the Wnt pathway in ECs, leading to BBB dysfunction.

6.7. Repressed canonical Wnt signalling in ECs as a possible cause of BBB dysfunction

The transcriptomic analysis of MBMV data detected important canonical Wnt signalling genes to be down-regulated such as ***Lef1***, ***Fzd6***, ***Lrp5*** in ageing, and ***Fzd4*** in both Hom6 and WT18 compared to WT6. The data needs to be handled with special care, as the detected reduction could be due to the EC loss observed in MBMVs in those groups (**Figure 36**). Similarly, the pathway enrichment analysis identified inflammation- and BBB- related pathways that could explain the BBB dysfunction observed in AD mice. However, it is complicated to obtain conclusive results due to the presence of different cell types in the MBMV samples.

Comparing the MBMV data with the EC data allowed for the discovery of strongly regulated EC genes, as they could be detected in both datasets. Interestingly, ***Ccl3*** is a gene coding for chemokine (C-C motif) ligand 3 (also known as macrophage inflammatory protein 1-alpha or MIP1α), a type of chemo-attractant cytokine known to play an important role in inflammation. The up-regulation of ***Ccl3*** in all AD groups, except Het6 in MBMVs, suggests an inflammatory reaction in ECs in AD. ECs have been described to produce MIP1α upon treatment with TNF-α, IL-1β, or LPS (Chui and Dorovini-Zis 2010) but not in the context of AD. Hence, the discovery of ***Ccl3*** up-regulation in ECs consolidates the barely-explored field of

research about inflammation of ECs in AD, not investigated in this thesis. Inflammation in ECs leads to changes in BBB permeability, and could therefore explain the BBB dysfunction seen in the AD mouse model.

Other groups have reported changes in BBB transporters such as Lrp1, Pgp (***Abcb1***), RAGE (***Ager***), and Glut1 (***Slc2a1***), attributing their dysregulation to a decreased Aβ clearance leading to CAA (Iadecola 2004; Zlokovic 2005). However, the studies show conflicting results, opening a debate about whether the transporters are indeed regulated in AD at the BBB, and in which direction (Donahue et al. 2006; Wijesuriya et al. 2010; Grubman et al. 2019). Shinohara et al. summarize several studies done on the regulation of Lrp1 in AD, concluding that its regulation is dependent on many factors including cell type, Apoe2/3/4 status, CAA, and age (Shinohara et al. 2017). Nonetheless, all the reports are based on protein detection methods, which due to post-transcriptional modifications might show different results. A review by Erickson and Banks compared the expression of Glut1 in different scientific articles, finding a reduction in the expression of Glut1 protein but not a decrease in Glut1 mRNA expression (Erickson and Banks 2013). Consequently, the lack of ***Lrp1***, ***Abcb1***, ***Ager***, and ***Slc2a1*** regulation in my sequencing results does not challenge those reports describing them as regulated at the protein level.

A study by Zenaro et al. (Zenaro et al. 2015) identified increased vascular expression of E-selectin (***Sele***), P-selectin (***Selp***), vascular cell adhesion molecule-1 (VCAM-1) and intercellular adhesion molecule-1 (ICAM-1) in 4-month-old 5xFAD mice and 6-month-old 3xTg-AD mice than in sex- and age-matched WT controls. In the MVMB samples, both ***Vcam1*** and ***Icam1*** were regulated in the Hom groups, and in the EC samples only ***Selp*** was found regulated in the AD18 mice (data not shown). Those variances could be due to the usage of different AD mouse models, or to post-transcriptional modifications. Nevertheless, the novel inflammatory DE genes identified in ECs (***Cd14***, ***Ackr1*** and ***Cytl1***) have not been previously reported in the context of AD. Consequently, their specific contribution to the inflamed phenotype is currently not known and it could be very interesting in future studies.

In both AD6 and WT18 groups compared to WT6 of the EC database, Wnt inhibitor genes ***Nfatc4***, ***Nkd2***, and ***Ruvbl1*** were found to be up-regulated, and the

canonical β-catenin gene, ***Ctnnb1***, down-regulated. Possibly, due to contamination from other cell types, it was not possible to detect the same gene regulation in MBMV and ECs. Nevertheless, both datasets pointed in the same direction towards a canonical Wnt signalling repression. Preliminary unpublished data generated by a colleague demonstrated a reduction in $Lef1^{+}$ cells of AD MBMVs, supporting the hypothesis of a Wnt/β-catenin repression at the BBB in AD.

6.8. Activating the canonical Wnt pathway in ECs ameliorates the AD phenotype

The Wnt/β-catenin signalling pathway is the main regulator of BBB maintenance. The collective data of this thesis point towards a repression of the canonical Wnt signalling, leading to BBB dysfunction. Interestingly, in the study by Munji et al. (Munji et al. 2019), in which they described a core blood-brain barrier dysfunction module, they did not detect a Wnt/β-catenin signalling regulation, suggesting that the Wnt repression is exclusive of AD. Possibly, the difference is due to AD-reactive MG that would be modulating the vascular function and thus differentiating its pathology from others. Along the same line, an activation in ECs of the Wnt pathway by inducing β-catenin stabilization would be expected to rescue, at least partially, the BBB homeostasis.

In Het mice, the increase of BBB permeability was only detectable at old ages (**Figure 32 A**). As both GOF and control groups were Het mice, no change in BBB permeability would be expected in 6 or 9-12 months old mice. The BBB in the cerebellum is more permeable than in the brain (Wilhelm et al. 2016). This difference in permeability might explain why an induced tightening by β-catenin had stronger effects in the cerebellum, where the decrease of permeability to 3-4 kDa dextrans was significant in the oldest GOF group, than in the cerebrum where no significant changes were detected (**Figure 60 A**). The successful BBB tightening in the cerebellum of GOF mice compared to control mice suggests that β-catenin could potentially be a therapeutical target. Still, the fact that the decrease of permeability was not detectable in the brain of 18 months old GOF mice induced for five months implies that either the Wnt pathway is not the only player creating the BBB dysfunction (inflammation might play an important role as well, as the up-

regulation of ***Ccl3*** in ECs suggests), or that part of the repression of the Wnt pathway occurs down-stream of β-catenin.

Induction of the Wnt/β-catenin signalling before AD onset (1-2 months old mice) ameliorated memory function in 9-12 months old mice (**Figure 61 F**), suggesting a protective effect of the Wnt pathway activation. Strikingly, induction of the Wnt/β-catenin signalling at old ages and advanced disease stage created the opposite effect, as 20-22 month old GOF mice displayed reduced burrowing activity than littermate controls (**Figure 61 A**). It would be interesting to analyse the age/disease-stage dependent dual effect of β-catenin activation in further studies. Nevertheless, the collected GOF data suggests that in order to improve AD symptoms, the treatment needs to be administered before neurodegeneration begins. The finding is not an absolute surprise because most of the adult neurons do not divide and thus, neuronal loss cannot be regained.

The beneficial effects of β-catenin activation before disease onset might offer a therapeutic preventive solution in the future when early diagnosis of AD would be possible.

6.9. Conclusions

Here I presented original data from my research on the role of the BBB in AD. The data from in vitro bEnd5-***Sirt1***-KD cells suggests that ***Sirt1*** down-regulation has negative effects on BBB properties, which would contribute to AD worsening. A different AD model that imitates the decrease of SIRT1 observed in patients would be necessary to assess the potential of SIRT1 as a therapeutic target.

The ***Thy1-APP***^{SwDI} AD mouse model developed brain Aβ plaques, weakened hippocampal activity, and memory loss. In addition, increased BBB permeability could be detected in AD, indicating BBB dysfunction. Transcriptomic data from WT and AD mice's MBMVs, ECs, MuCs and MG found known regulated genes in AD, validating the sequenced databases, and novel gene and pathway regulations, such as an increase of inflammation pathways and inflammatory genes like ***Ccl3***. Notably, a repression of the Wnt pathway could be detected in ECs, and an up-regulation of the Wnt inhibitor ***Dkk2*** was identified in MG. Wnt signalling repression could therefore lead to the observed BBB dysfunction in AD.

Importantly, induction of Wnt/β-catenin signalling in ECs of pre-symptomatic AD mice protected them from cognitive decline, highliting the Wnt/β-catenin pathway as a key modulator of brain function via BBB regulation. However, β-catenin induction in ECs of old AD mice worsened the disease phenotype, suggesting detrimental effects of the Wnt/β-catenin signalling in late stage AD. Hence, the Wnt/β-catenin signalling activation might emerge as a potential therapeutic solution for AD prevention.

Figure 62 pictures a summary of NVU changes observed in AD mice, with the proposed mechanism of action explained in this thesis.

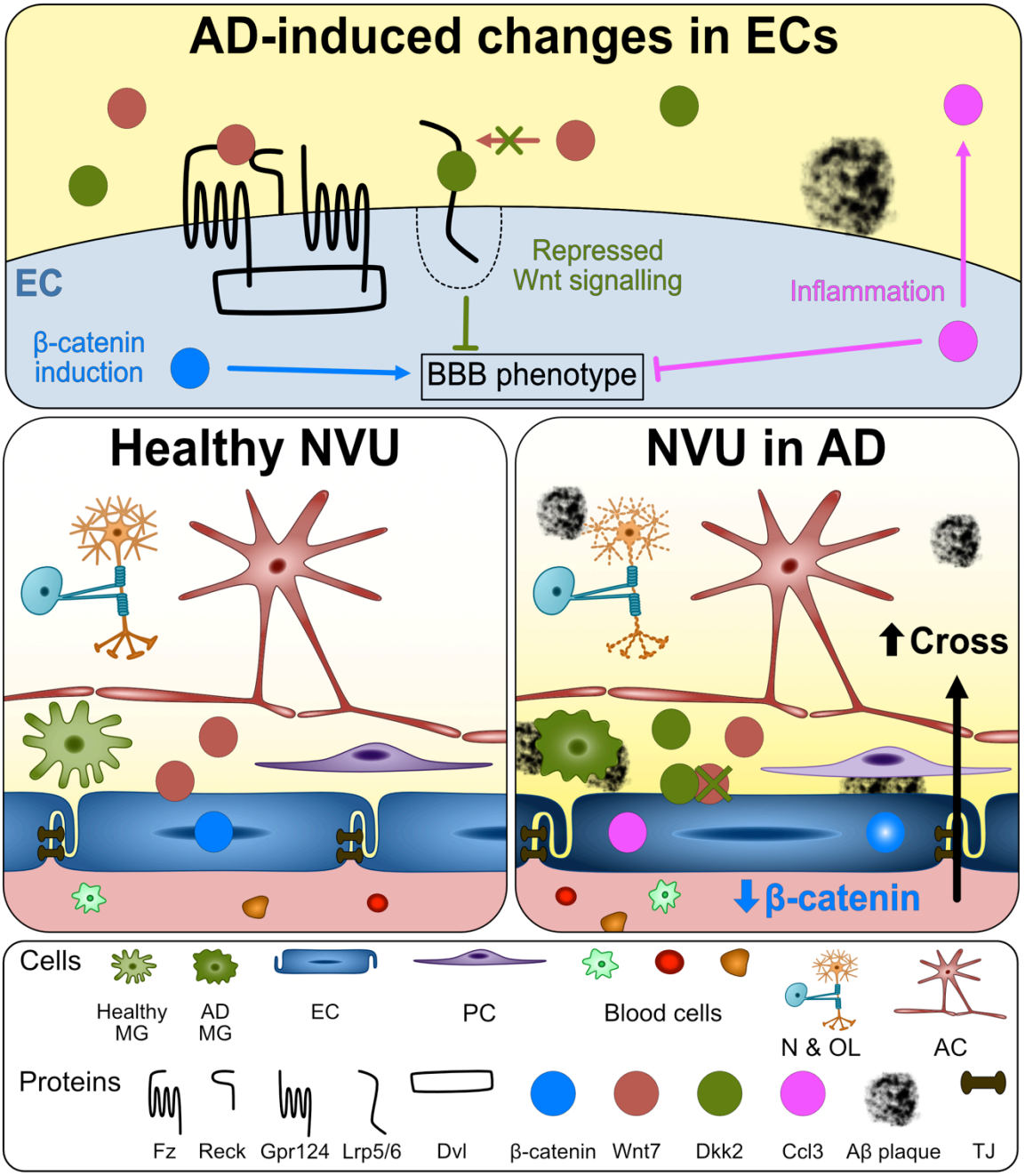

Figure 62: summary of NVU changes observed in AD. **Top**: EC-specific changes showing that inflammation (pink) and repressed Wnt/β-catenin signalling (green) lead to BBB dysfunction, and induced β-catenin (blue) to preserve the BBB phenotype. **Middle**: NVU changes showing Dkk2 up-regulation (green), Wnt/β-catenin repression (blue), Ccl3 up-regulation (pink), and increased BBB permeability (black). **Bottom**: legend.

7. References

Abbott, N. Joan, Lars Rönnbäck, and Elisabeth Hansson. 2006. “Astrocyte-Endothelial Interactions at the Blood-Brain Barrier.” ***Nature Reviews Neuroscience***. https://doi.org/10.1038/nrn1824.

Albensi, Benedict C. 2019. “Dysfunction of Mitochondria: Implications for Alzheimer’s Disease.” In ***International Review of Neurobiology***. https://doi.org/10.1016/bs.irn.2019.03.001.

Alzheimer’s Disease International. 2019. “World Alzheimer Report 2019: Attitudes to Dementia.” ***Alzheimer’s Disease International: London***.

Alzheimer’s Disease International (ADI), A Wimo, M Prince, and Alzheimer’s Disease International. 2015. “World Alzheimer Report 2015, The Global Impact of Dementia.” ***Alzheimer’s Disease International (ADI)***. https://doi.org/10.1111/j.0963-7214.2004.00293.x.

Alzheimer, Alois. 1907. “Uber Eine Eigenartige Erkrankung Der Hirnrinde.” ***Allg Zeitschr f Psychiatrie u Psych-Gerichtl Med***. https://doi.org/10.1002/ca.980080612.

Andreone, Benjamin J., Brian Wai Chow, Aleksandra Tata, Baptiste Lacoste, Ayal Ben-Zvi, Kevin Bullock, Amy A. Deik, David D. Ginty, Clary B. Clish, and Chenghua Gu. 2017. “Blood-Brain Barrier Permeability Is Regulated by Lipid Transport-Dependent Suppression of Caveolae-Mediated Transcytosis.” ***Neuron***. https://doi.org/10.1016/j.neuron.2017.03.043.

Armulik, Annika, Guillem Genové, and Christer Betsholtz. 2011. “Pericytes: Developmental, Physiological, and Pathological Perspectives, Problems, and Promises.” ***Developmental Cell***. https://doi.org/10.1016/j.devcel.2011.07.001.

Armulik, Annika, Guillem Genové, Maarja Mäe, Maya H. Nisancioglu, Elisabet Wallgard, Colin Niaudet, Liqun He, et al. 2010. “Pericytes Regulate the Blood-Brain Barrier.” ***Nature***. https://doi.org/10.1038/nature09522.

Attwell, David, Anusha Mishra, Catherine N. Hall, Fergus M. O’Farrell, and Turgay Dalkara. 2016. “What Is a Pericyte?” ***Journal of Cerebral Blood Flow and Metabolism***. https://doi.org/10.1177/0271678X15610340.

Augustin, Hellmut G., and Gou Young Koh. 2017. “Organotypic Vasculature: From Descriptive Heterogeneity to Functional Pathophysiology.” ***Science***. https://doi.org/10.1126/science.aal2379.

Barker, Warren W., Cheryl A. Luis, Alice Kashuba, Mercy Luis, Dylan G. Harwood, David Loewenstein, Carol Waters, et al. 2002. “Relative Frequencies of Alzheimer Disease, Lewy Body, Vascular and Frontotemporal Dementia, and Hippocampal Sclerosis in the State of Florida Brain Bank.” ***Alzheimer Disease and Associated Disorders***. https://doi.org/10.1097/00002093-200210000-00001.

Bartus, Raymond T., Reginald L. Dean, Bernard Beer, and Arnold S. Lippa. 1982. “The Cholinergic Hypothesis of Geriatric Memory Dysfunction.” ***Science***. https://doi.org/10.1126/science.7046051.

Bell, Robert D., Ethan A. Winkler, Itender Singh, Abhay P. Sagare, Rashid Deane, Zhenhua Wu, David M. Holtzman, et al. 2012. “Apolipoprotein e Controls Cerebrovascular Integrity via Cyclophilin A.” ***Nature***. https://doi.org/10.1038/nature11087.

Ben-Zvi, Ayal, Baptiste Lacoste, Esther Kur, Benjamin J. Andreone, Yoav Mayshar, Han Yan, and Chenghua Gu. 2014. “Mfsd2a Is Critical for the Formation and Function of the Blood-Brain Barrier.” ***Nature***. https://doi.org/10.1038/nature13324.

Benz, Fabienne, and Stefan Liebner. 2020. “Structure and Function of the Blood–Brain Barrier (BBB).” ***Handbook of Experimental Pharmacology***. https://doi.org/10.1007/164_2020_404.

Bielschowsky, Max. 1902. “Die Silberimprägnation Der Achsencylinder.” ***Neurologisches Zentralblatt*** 21 (579): 84.

References

Bien-Ly, Nga, C. Andrew Boswell, Surinder Jeet, Thomas G. Beach, Kwame Hoyte, Wilman Luk, Vera Shihadeh, et al. 2015. "Lack of Widespread BBB Disruption in Alzheimer's Disease Models: Focus on Therapeutic Antibodies." ***Neuron***. https://doi.org/10.1016/j.neuron.2015.09.036.

Biessels, G. J., and L. J. Kappelle. 2005. "Increased Risk of Alzheimer's Disease in Type II Diabetes: Insulin Resistance of the Brain or Insulin-Induced Amyloid Pathology?" ***Biochemical Society Transactions***. https://doi.org/10.1042/BST20051041.

Blennow, K., A. Wallin, P. Fredman, I. Karlsson, C. G. Gottfries, and L. Svennerholm. 1990. "Blood-brain Barrier Disturbance in Patients with Alzheimer's Disease Is Related to Vascular Factors." ***Acta Neurologica Scandinavica***. https://doi.org/10.1111/j.1600-0404.1990.tb01563.x.

Blessed, G., B. E. Tomlinson, and M. Roth. 1968. "The Association between Quantitative Measures of Dementia and of Senile Change in the Cerebral Grey Matter of Elderly Subjects." ***The British Journal of Psychiatry : The Journal of Mental Science***. https://doi.org/10.1192/bjp.114.512.797.

Bolmont, Tristan, Florent Haiss, Daniel Eicke, Rebecca Radde, Chester A. Mathis, William E. Klunk, Shinichi Kohsaka, Mathias Jucker, and Michael E. Calhoun. 2008. "Dynamics of the Microglial/Amyloid Interaction Indicate a Role in Plaque Maintenance." ***Journal of Neuroscience***. https://doi.org/10.1523/JNEUROSCI.4814-07.2008.

Bowen, David M., Carolyn B. Smith, Pamela White, and Alan N. Davison. 1976. "Neurotransmitter-Related Enzymes and Indices of Hypoxia in Senile Dementia and Other Abiotrophies." ***Brain***. https://doi.org/10.1093/brain/99.3.459.

Braak, H., and E. Braak. 1991. "Neuropathological Stageing of Alzheimer-Related Changes." ***Acta Neuropathologica***. https://doi.org/10.1007/BF00308809.

Braak, Heiko, and Kelly Del Tredici. 2011. "The Pathological Process Underlying Alzheimer's Disease in Individuals under Thirty." ***Acta Neuropathologica***. https://doi.org/10.1007/s00401-010-0789-4.

Brenowitz, Willa D., Peter T. Nelson, Lilah M. Besser, Katherine B. Heller, and Walter A. Kukull. 2015. "Cerebral Amyloid Angiopathy and Its Co-Occurrence with Alzheimer's Disease and Other Cerebrovascular Neuropathologic Changes." ***Neurobiology of Aging***. https://doi.org/10.1016/j.neurobiolaging.2015.06.028.

Brion, J.-P., H. Passareiro, J. Nunez, and J. Flament-Durand. 1985. "Mise En Évidence Immunologique de La Protéine Tau Au Niveau Des Lésions de Dégénérescence Neurofibrillaire de La Maladie d'Alzheimer." ***Archives de Biologie***.

Broeckhoven, C. Van, J. Haan, E. Bakker, J. A. Hardy, W. Van Hul, A. Wehnert, M. Vegter-Van Der Vlis, and R. A.C. Roos. 1990. "Amyloid β Protein Precursor Gene and Hereditary Cerebral Hemorrhage with Amyloidosis (Dutch)." ***Science***. https://doi.org/10.1126/science.1971458.

Buée, L., P. R. Hof, C. Bouras, A. Delacourte, D. P. Perl, J. H. Morrison, and H. M. Fillit. 1994. "Pathological Alterations of the Cerebral Microvasculature in Alzheimer's Disease and Related Dementing Disorders." ***Acta Neuropathologica***. https://doi.org/10.1007/BF00294173.

Butterfield, D. Allan, and Debra Boyd-Kimball. 2019. "Redox Proteomics and Amyloid β-Peptide: Insights into Alzheimer Disease." ***Journal of Neurochemistry***. https://doi.org/10.1111/jnc.14589.

Cai, Zhiyou, Nannuan Liu, Chuanling Wang, Biyong Qin, Yingjun Zhou, Ming Xiao, Liying Chang, Liang Jun Yan, and Bin Zhao. 2016. "Role of RAGE in Alzheimer's Disease." ***Cellular and Molecular Neurobiology***. https://doi.org/10.1007/s10571-015-0233-3.

Calignon, Alix De, Manuela Polydoro, Marc Suárez-Calvet, Christopher William, David H. Adamowicz, Kathy J. Kopeikina, Rose Pitstick, et al. 2012. "Propagation of Tau Pathology in a Model of Early Alzheimer's Disease." ***Neuron***.

https://doi.org/10.1016/j.neuron.2011.11.033.
Castro Dias, Mariana, Caroline Coisne, Pascale Baden, Gaby Enzmann, Lillian Garrett, Lore Becker, Sabine M. Hölter, et al. 2019. “Claudin-12 Is Not Required for Blood-Brain Barrier Tight Junction Function.” ***Fluids and Barriers of the CNS***. https://doi.org/10.1186/s12987-019-0150-9.
Chambers, R., and B. W. Zweifach. 1947. “Intercellular Cement and Capillary Permeability.” ***Physiological Reviews***. https://doi.org/10.1152/physrev.1947.27.3.436.
Chen, Ming Kai, Adam P. Mecca, Mika Naganawa, Sjoerd J. Finnema, Takuya Toyonaga, Shu Fei Lin, Soheila Najafzadeh, et al. 2018. “Assessing Synaptic Density in Alzheimer Disease with Synaptic Vesicle Glycoprotein 2A Positron Emission Tomographic Imaging.” ***JAMA Neurology***. https://doi.org/10.1001/jamaneurol.2018.1836.
Chételat, Gaël, Renaud La Joie, Nicolas Villain, Audrey Perrotin, Vincent De La Sayette, Francis Eustache, and Rik Vandenberghe. 2013. “Amyloid Imaging in Cognitively Normal Individuals, at-Risk Populations and Preclinical Alzheimer’s Disease.” ***NeuroImage: Clinical***. https://doi.org/10.1016/j.nicl.2013.02.006.
Cho, Chris, Philip M. Smallwood, and Jeremy Nathans. 2017. “Reck and Gpr124 Are Essential Receptor Cofactors for Wnt7a/Wnt7b-Specific Signaling in Mammalian CNS Angiogenesis and Blood-Brain Barrier Regulation.” ***Neuron***. https://doi.org/10.1016/j.neuron.2017.07.031.
Chuang, Y. F., Y. An, M. Bilgel, D. F. Wong, J. C. Troncoso, R. J. O’Brien, J. C. Breitner, L. Ferruci, S. M. Resnick, and M. Thambisetty. 2016. “Midlife Adiposity Predicts Earlier Onset of Alzheimer’s Dementia, Neuropathology and Presymptomatic Cerebral Amyloid Accumulation.” ***Molecular Psychiatry***. https://doi.org/10.1038/mp.2015.129.
Chui, Ray, and Katerina Dorovini-Zis. 2010. “Regulation of CCL2 and CCL3 Expression in Human Brain Endothelial Cells by Cytokines and Lipopolysaccharide.” ***Journal of Neuroinflammation***. https://doi.org/10.1186/1742-2094-7-1.
Chung, Kyung Min, Nancy Hernández, Andrew A. Sproul, and Wai Haung Yu. 2019. “Alzheimer’s Disease and the Autophagic-Lysosomal System.” ***Neuroscience Letters***. https://doi.org/10.1016/j.neulet.2018.05.017.
Cirrito, John R., Kelvin A. Yamada, Mary Beth Finn, Robert S. Sloviter, Kelly R. Bales, Patrick C. May, Darryle D. Schoepp, Steven M. Paul, Steven Mennerick, and David M. Holtzman. 2005. “Synaptic Activity Regulates Interstitial Fluid Amyloid-β Levels in Vivo.” ***Neuron***. https://doi.org/10.1016/j.neuron.2005.10.028.
Clavaguera, Florence, Tristan Bolmont, R. Anthony Crowther, Dorothee Abramowski, Stephan Frank, Alphonse Probst, Graham Fraser, et al. 2009. “Transmission and Spreading of Tauopathy in Transgenic Mouse Brain.” ***Nature Cell Biology***. https://doi.org/10.1038/ncb1901.
Colomina, Maria Teresa, and Fiona Peris-Sampedro. 2017. “Aluminum and Alzheimer’s Disease.” In ***Advances in Neurobiology***. https://doi.org/10.1007/978-3-319-60189-2_9.
Contestabile, Antonio. 2011. “The History of the Cholinergic Hypothesis.” ***Behavioural Brain Research***. https://doi.org/10.1016/j.bbr.2009.12.044.
Corder, E. H., A. M. Saunders, N. J. Risch, W. J. Strittmatter, D. E. Schmechel, P. C. Gaskell, J. B. Rimmler, et al. 1994. “Protective Effect of Apolipoprotein E Type 2 Allele for Late Onset Alzheimer Disease.” ***Nature Genetics***. https://doi.org/10.1038/ng0694-180.
Corder, E. H., A. M. Saunders, W. J. Strittmatter, D. E. Schmechel, P. C. Gaskell, G. W. Small, A. D. Roses, J. L. Haines, and M. A. Pericak-Vance. 1993. “Gene Dose of Apolipoprotein E Type 4 Allele and the Risk of Alzheimer’s Disease in Late Onset Families.” ***Science***. https://doi.org/10.1126/science.8346443.

References

Croteau, E., C. A. Castellano, M. Fortier, C. Bocti, T. Fulop, N. Paquet, and S. C. Cunnane. 2018. “A Cross-Sectional Comparison of Brain Glucose and Ketone Metabolism in Cognitively Healthy Older Adults, Mild Cognitive Impairment and Early Alzheimer’s Disease.” ***Experimental Gerontology***. https://doi.org/10.1016/j.exger.2017.07.004.

Crowther, R. A., and M. Goedert. 2000. “Abnormal Tau-Containing Filaments in Neurodegenerative Diseases.” ***Journal of Structural Biology***. https://doi.org/10.1006/jsbi.2000.4270.

Cryan, John F., Kenneth J. O’Riordan, Kiran Sandhu, Veronica Peterson, and Timothy G. Dinan. 2020. “The Gut Microbiome in Neurological Disorders.” ***The Lancet Neurology***. https://doi.org/10.1016/S1474-4422(19)30356-4.

Daneman, Richard, Dritan Agalliu, Lu Zhou, Frank Kuhnert, Calvin J. Kuo, and Ben A. Barres. 2009. “Wnt/β-Catenin Signaling Is Required for CNS, but Not Non-CNS, Angiogenesis.” ***Proceedings of the National Academy of Sciences of the United States of America***. https://doi.org/10.1073/pnas.0805165106.

Daneman, Richard, Lu Zhou, Amanuel A. Kebede, and Ben A. Barres. 2010. “Pericytes Are Required for Bloodĝ€"brain Barrier Integrity during Embryogenesis.” ***Nature***. https://doi.org/10.1038/nature09513.

Danielli, J. F. 1940. “Capillary Permeability and Oedema in the Perfused Frog.” ***The Journal of Physiology***. https://doi.org/10.1113/jphysiol.1940.sp003837.

Davies, P., and A. J.F. Maloney. 1976. “SELECTIVE LOSS OF CENTRAL CHOLINERGIC NEURONS IN ALZHEIMER’S DISEASE.” ***The Lancet***. https://doi.org/10.1016/S0140-6736(76)91936-X.

Davis, Judianne, Feng Xu, Rashid Deane, Galina Romanov, Mary Lou Previti, Kelly Zeigler, Berislav V. Zlokovic, and William E. Van Nostrand. 2004. “Early-Onset and Robust Cerebral Microvascular Accumulation of Amyloid β-Protein in Transgenic Mice Expressing Low Levels of a Vasculotropic Dutch/Iowa Mutant Form of Amyloid β-Protein Precursor.” ***Journal of Biological Chemistry***. https://doi.org/10.1074/jbc.M312946200.

Deacon, Robert M.J. 2006. “Burrowing in Rodents: A Sensitive Method for Detecting Behavioral Dysfunction.” ***Nature Protocols***. https://doi.org/10.1038/nprot.2006.19.

Deczkowska, Aleksandra, Ido Amit, and Michal Schwartz. 2018. “Microglial Immune Checkpoint Mechanisms.” ***Nature Neuroscience***. https://doi.org/10.1038/s41593-018-0145-x.

Dejana, Elisabetta, and Fabrizio Orsenigo. 2013. “Endothelial Adherens Junctions at a Glance.” ***Journal of Cell Science***. https://doi.org/10.1242/jcs.124529.

Devanand, D. P. 2018. “Viral Hypothesis and Antiviral Treatment in Alzheimer’s Disease.” ***Current Neurology and Neuroscience Reports***. https://doi.org/10.1007/s11910-018-0863-1.

Devraj, Kavi, Slobodan Poznanovic, Christoph Spahn, Gerhard Schwall, Patrick N. Harter, Michel Mittelbronn, Katia Antoniello, et al. 2016. “BACE-1 Is Expressed in the Blood-Brain Barrier Endothelium and Is Upregulated in a Murine Model of Alzheimer’s Disease.” ***Journal of Cerebral Blood Flow and Metabolism***. https://doi.org/10.1177/0271678X15606463.

Donahue, John E., Stephanie L. Flaherty, Conrad E. Johanson, John A. Duncan, Gerald D. Silverberg, Miles C. Miller, Rosemarie Tavares, et al. 2006. “RAGE, LRP-1, and Amyloid-Beta Protein in Alzheimer’s Disease.” ***Acta Neuropathologica***. https://doi.org/10.1007/s00401-006-0115-3.

Drachman, David A., and Janet Leavitt. 1974. “Human Memory and the Cholinergic System: A Relationship to Aging?” ***Archives of Neurology***. https://doi.org/10.1001/archneur.1974.00490320001001.

Dudiki, Tejasvi, Julia Meller, Gautam Mahajan, Huan Liu, Irina Zhevlakova, Samantha Stefl, Conner Witherow, Eugene Podrez, Chandrasekhar R. Kothapalli, and Tatiana V.

Byzova. 2020. “Microglia Control Vascular Architecture via a TGFβ1 Dependent Paracrine Mechanism Linked to Tissue Mechanics.” ***Nature Communications***. https://doi.org/10.1038/s41467-020-14787-y.

Duff, K., C. Eckman, C. Zehr, X. Yu, C. M. Prada, J. Perez-Tur, M. Hutton, et al. 1996. “Increased Amyloid-B42(43) in Brains of Mice Expressing Mutant Presenilin 1.” ***Nature***. https://doi.org/10.1038/383710a0.

Eberth, Karl Joseph. 1871. ***Handbuch Der Lehre von Den Geweben Des Menschen Und Der Thiere***. Vol. 1 (Leipzig. W. Engelmann.

Ehrlich, P. 1885. “Das Sauerstoff-Bedürfniss Des Organismus: Eine Farbenanalytische Studie.”

Engelhardt, Britta, Peter Vajkoczy, and Roy O. Weller. 2017. “The Movers and Shapers in Immune Privilege of the CNS.” ***Nature Immunology***. https://doi.org/10.1038/ni.3666.

Engelhardt, Britta, and Hartwig Wolburg. 2004. “Mini Review: Transendothelial Migration of Leukocytes: Through the Front Door or around the Side of the House?” ***European Journal of Immunology***. https://doi.org/10.1002/eji.200425327.

Erickson, Michelle A., and William A. Banks. 2013. “Blood-Brain Barrier Dysfunction as a Cause and Consequence of Alzheimer’s Disease.” ***Journal of Cerebral Blood Flow and Metabolism***. https://doi.org/10.1038/jcbfm.2013.135.

Eser Ocak, Pinar, Umut Ocak, Prativa Sherchan, John H. Zhang, and Jiping Tang. 2020. “Insights into Major Facilitator Superfamily Domain-Containing Protein-2a (Mfsd2a) in Physiology and Pathophysiology. What Do We Know so Far?” ***Journal of Neuroscience Research***. https://doi.org/10.1002/jnr.24327.

Eubelen, Marie, Naguissa Bostaille, Pauline Cabochette, Anne Gauquier, Patricia Tebabi, Andra C. Dumitru, Melanie Koehler, et al. 2018. “A Molecular Mechanism for Wnt Ligand-Specific Signaling.” ***Science***. https://doi.org/10.1126/science.aat1178.

Fitzpatrick, Anthony W.P., Benjamin Falcon, Shaoda He, Alexey G. Murzin, Garib Murshudov, Holly J. Garringer, R. Anthony Crowther, Bernardino Ghetti, Michel Goedert, and Sjors H.W. Scheres. 2017. “Cryo-EM Structures of Tau Filaments from Alzheimer’s Disease.” ***Nature***. https://doi.org/10.1038/nature23002.

Franklin, Erin E., Richard J. Perrin, Benjamin Vincent, Michael Baxter, John C. Morris, and Nigel J. Cairns. 2015. “Brain Collection, Standardized Neuropathologic Assessment, and Comorbidity in Alzheimer’s Disease Neuroimaging Initiative 2 Participants.” ***Alzheimer’s and Dementia***. https://doi.org/10.1016/j.jalz.2015.05.010.

Friedman, Brad A., Karpagam Srinivasan, Gai Ayalon, William J. Meilandt, Han Lin, Melanie A. Huntley, Yi Cao, et al. 2018. “Diverse Brain Myeloid Expression Profiles Reveal Distinct Microglial Activation States and Aspects of Alzheimer’s Disease Not Evident in Mouse Models.” ***Cell Reports***. https://doi.org/10.1016/j.celrep.2017.12.066.

Frölich, L., J. Kornhuber, R. Ihl, J. Fritze, K. Maurer, and P. Riederer. 1991. “Integrity of the Blood-CSF Barrier in Dementia of Alzheimer Type: CSF/Serum Ratios of Albumin and IgG.” ***European Archives of Psychiatry and Clinical Neuroscience***. https://doi.org/10.1007/BF02279767.

Frost, Bess, Rachel L. Jacks, and Marc I. Diamond. 2009. “Propagation of Tau Misfolding from the Outside to the inside of a Cell.” ***Journal of Biological Chemistry***. https://doi.org/10.1074/jbc.M808759200.

Furtado, Denzil, Mattias Björnmalm, Scott Ayton, Ashley I. Bush, Kristian Kempe, and Frank Caruso. 2018. “Overcoming the Blood–Brain Barrier: The Role of Nanomaterials in Treating Neurological Diseases.” ***Advanced Materials***. https://doi.org/10.1002/adma.201801362.

Gandy, Sam. 2005. “The Role of Cerebral Amyloid β Accumulation in Common Forms of Alzheimer Disease.” ***Journal of Clinical Investigation***.

https://doi.org/10.1172/JCI200525100.
Gaugler, Joseph, Bryan James, Tricia Johnson, Ken Scholz, and Jennifer Weuve. 2016. "2016 Alzheimer's Disease Facts and Figures." ***Alzheimer's and Dementia***. https://doi.org/10.1016/j.jalz.2016.03.001.
Ghetti, Bernardino, Adrian L Oblak, Bradley F Boeve, Keith a Johnson, Bradford C Dickerson, and Michel Goedert. 2014. "Frontotemporal Dementia Caused by MAPT Mutations: A Chameleon for Neuropathology and Neuroimaging." ***Neuropathology and Applied Neurobiology***. https://doi.org/10.1111/nan.12213.
Glenner, George G., and Caine W. Wong. 1984. "Alzheimer's Disease: Initial Report of the Purification and Characterization of a Novel Cerebrovascular Amyloid Protein." ***Biochemical and Biophysical Research Communications***. https://doi.org/10.1016/S0006-291X(84)80190-4.
Goate, Alison, Marie Christine Chartier-Harlin, Mike Mullan, Jeremy Brown, Fiona Crawford, Liana Fidani, Luis Giuffra, et al. 1991. "Segregation of a Missense Mutation in the Amyloid Precursor Protein Gene with Familial Alzheimer's Disease." ***Nature***. https://doi.org/10.1038/349704a0.
Golgi, Camillo. 1871. "Contribuzione Alla Fina Anatomia Degli Organi Centrali Del Sistema Nervoso." ***Riv. Clin.***
Gottesman, Rebecca F., Andrea L.C. Schneider, Marilyn Albert, Alvaro Alonso, Karen Bandeen-Roche, Laura Coker, Josef Coresh, et al. 2014. "Midlife Hypertension and 20-Year Cognitive Change: The Atherosclerosis Risk in Communities Neurocognitive Study." ***JAMA Neurology***. https://doi.org/10.1001/jamaneurol.2014.1646.
Gottesman, Rebecca F., Andrea L.C. Schneider, Yun Zhou, Josef Coresh, Edward Green, Naresh Gupta, David S. Knopman, et al. 2017. "Association between Midlife Vascular Risk Factors and Estimated Brain Amyloid Deposition." ***JAMA - Journal of the American Medical Association***. https://doi.org/10.1001/jama.2017.3090.
Gras, D., E. Roze, S. Caillet, A. Méneret, D. Doummar, T. Billette De Villemeur, M. Vidailhet, and F. Mochel. 2014. "GLUT1 Deficiency Syndrome: An Update." ***Revue Neurologique***. https://doi.org/10.1016/j.neurol.2013.09.005.
Grubman, Alexandra, Gabriel Chew, John F. Ouyang, Guizhi Sun, Xin Yi Choo, Catriona McLean, Rebecca K. Simmons, et al. 2019. "A Single-Cell Atlas of Entorhinal Cortex from Individuals with Alzheimer's Disease Reveals Cell-Type-Specific Gene Expression Regulation." ***Nature Neuroscience***. https://doi.org/10.1038/s41593-019-0539-4.
Grundke-Iqbal, I., K. Iqbal, Y. C. Tung, M. Quinlan, H. M. Wisniewski, and L. I. Binder. 1986. "Abnormal Phosphorylation of the Microtubule-Associated Protein Tau (Tau) in Alzheimer Cytoskeletal Pathology." ***Proceedings of the National Academy of Sciences of the United States of America***. https://doi.org/10.1073/pnas.83.13.4913.
Guerreiro, Rita, Aleksandra Wojtas, Jose Bras, Minerva Carrasquillo, Ekaterina Rogaeva, Elisa Majounie, Carlos Cruchaga, et al. 2013. "TREM2 Variants in Alzheimer's Disease." ***New England Journal of Medicine***. https://doi.org/10.1056/NEJMoa1211851.
Guo, Yumeng, Aimin Xu, and Yu Wang. 2016. "SIRT1 in Endothelial Cells as a Novel Target for the Prevention of Early Vascular Aging." ***Journal of Cardiovascular Pharmacology***. https://doi.org/10.1097/FJC.0000000000000344.
Haan, Jurre den, Tjado H.J. Morrema, Annemieke J. Rozemuller, Femke H. Bouwman, and Jeroen J.M. Hoozemans. 2018. "Different Curcumin Forms Selectively Bind Fibrillar Amyloid Beta in Post Mortem Alzheimer's Disease Brains: Implications for in-Vivo Diagnostics." ***Acta Neuropathologica Communications***. https://doi.org/10.1186/s40478-018-0577-2.
Haar, Harm J. Van De, Saartje Burgmans, Jacobus F.A. Jansen, Matthias J.P. Van Osch, Mark A. Van Buchem, Majon Muller, Paul A.M. Hofman, Frans R.J. Verhey, and Walter H. Backes. 2016. "Blood-Brain Barrier Leakage in Patients with Early

Alzheimer Disease." ***Radiology***. https://doi.org/10.1148/radiol.2016152244.

Habib, Naomi, Cristin McCabe, Sedi Medina, Miriam Varshavsky, Daniel Kitsberg, Raz Dvir-Szternfeld, Gilad Green, et al. 2020. "Disease-Associated Astrocytes in Alzheimer's Disease and Aging." ***Nature Neuroscience***. https://doi.org/10.1038/s41593-020-0624-8.

Harada, Naomoto, Yoshitaka Tamai, Tomo O. Ishikawa, Brian Sauer, Kazuaki Takaku, Masanobu Oshima, and Makoto M. Taketo. 1999. "Intestinal Polyposis in Mice with a Dominant Stable Mutation of the β-Catenin Gene." ***EMBO Journal***. https://doi.org/10.1093/emboj/18.21.5931.

Hardy, John, and David Allsop. 1991. "Amyloid Deposition as the Central Event in the Aetiology of Alzheimer's Disease." ***Trends in Pharmacological Sciences***. https://doi.org/10.1016/0165-6147(91)90609-V.

Hardy, John, and Dennis J. Selkoe. 2002. "The Amyloid Hypothesis of Alzheimer's Disease: Progress and Problems on the Road to Therapeutics." ***Science***. https://doi.org/10.1126/science.1072994.

Hayden, Melvin R. 2019. "Type 2 Diabetes Mellitus Increases the Risk of Late-Onset Alzheimer's Disease: Ultrastructural Remodeling of the Neurovascular Unit and Diabetic Gliopathy." ***Brain Sciences***. https://doi.org/10.3390/brainsci9100262.

He, Wanxia, Jinxuan Hu, Yuxing Xia, and Riqiang Yan. 2014. "β-Site Amyloid Precursor Protein Cleaving Enzyme 1(BACE1) Regulates Notch Signaling by Controlling the Cleavage of Jagged 1 (Jag1) and Jagged2 (Jag2) Proteins." ***Journal of Biological Chemistry***. https://doi.org/10.1074/jbc.M114.579862.

Hebert, Liesi E., Jennifer Weuve, Paul A. Scherr, and Denis A. Evans. 2013. "Alzheimer Disease in the United States (2010-2050) Estimated Using the 2010 Census." ***Neurology***. https://doi.org/10.1212/WNL.0b013e31828726f5.

Herzig, Martin C., David T. Winkler, Patrick Burgermeister, Michelle Pfeifer, Esther Kohler, Stephen D. Schmidt, Simone Danner, et al. 2004. "Aβ Is Targeted to the Vasculature in a Mouse Model of Hereditary Cerebral Hemorrhage with Amyloidosis." ***Nature Neuroscience***. https://doi.org/10.1038/nn1302.

Hickman, Suzanne E., Nathan D. Kingery, Toshiro K. Ohsumi, Mark L. Borowsky, Li Chong Wang, Terry K. Means, and Joseph El Khoury. 2013. "The Microglial Sensome Revealed by Direct RNA Sequencing." ***Nature Neuroscience***. https://doi.org/10.1038/nn.3554.

Hill, Robert A., Lei Tong, Peng Yuan, Sasidhar Murikinati, Shobhana Gupta, and Jaime Grutzendler. 2015. "Regional Blood Flow in the Normal and Ischemic Brain Is Controlled by Arteriolar Smooth Muscle Cell Contractility and Not by Capillary Pericytes." ***Neuron***. https://doi.org/10.1016/j.neuron.2015.06.001.

Hlubek, F., S. Pfeiffer, J. Budczies, S. Spaderna, A. Jung, T. Kirchner, and T. Brabletz. 2006. "Securin (HPTTG1) Expression Is Regulated by β-Catenin/TCF in Human Colorectal Carcinoma." ***British Journal of Cancer*** 94 (11): 1672–77. https://doi.org/10.1038/sj.bjc.6603155.

Holm, Annegret, Tina Heumann, and Hellmut G. Augustin. 2018. "Microvascular Mural Cell Organotypic Heterogeneity and Functional Plasticity." ***Trends in Cell Biology***. https://doi.org/10.1016/j.tcb.2017.12.002.

Hupe, Mike, Minerva Xueting Li, Susanne Kneitz, Daria Davydova, Chika Yokota, Julianna Kele-Olovsson, Belma Hot, Jan M. Stenman, and Manfred Gessler. 2017. "Gene Expression Profiles of Brain Endothelial Cells during Embryonic Development at Bulk and Single-Cell Levels." ***Science Signaling***. https://doi.org/10.1126/scisignal.aag2476.

Hur, Ji-Yeun, Georgia R Frost, Xianzhong Wu, Christina Crump, Si Jia Pan, Eitan Wong, Marilia Barros, Thomas Li, Pengju Nie, and Yujia Zhai. 2020. "The Innate Immunity Protein IFITM3 Modulates γ-Secretase in Alzheimer's Disease." ***Nature***, 1–6.

Iadecola, Costantino. 2004. “Neurovascular Regulation in the Normal Brain and in Alzheimer’s Disease.” ***Nature Reviews Neuroscience***. https://doi.org/10.1038/nrn1387.

———. 2017. “The Neurovascular Unit Coming of Age: A Journey through Neurovascular Coupling in Health and Disease.” ***Neuron***. https://doi.org/10.1016/j.neuron.2017.07.030.

Iadecola, Costantino, Fangyi Zhang, Kiyoshi Niwa, Chris Eckman, Sherry K. Turner, Elizabeth Fischer, Steven Younkin, David R. Borchelt, Karen K. Hsiao, and George A. Carlson. 1999. “SOD1 Rescues Cerebral Endothelial Dysfunction in Mice Overexpressing Amyloid Precursor Protein.” ***Nature Neuroscience***. https://doi.org/10.1038/5715.

Ishikawa, Hiroki, Anthony P. Heaney, Run Yu, Gregory A. Horwitz, and Shlomo Melmed. 2001. “Human Pituitary Tumor-Transforming Gene Induces Angiogenesis.” ***Journal of Clinical Endocrinology and Metabolism***. https://doi.org/10.1210/jc.86.2.867.

J. Allen, Shelley, Judy J. Watson, and David Dawbarn. 2011. “The Neurotrophins and Their Role in Alzheimers Disease.” ***Current Neuropharmacology***. https://doi.org/10.2174/157015911798376190.

Jawhar, Sadim, Anna Trawicka, Carolin Jenneckens, Thomas A. Bayer, and Oliver Wirths. 2012. “Motor Deficits, Neuron Loss, and Reduced Anxiety Coinciding with Axonal Degeneration and Intraneuronal Aβ Aggregation in the 5XFAD Mouse Model of Alzheimer’s Disease.” ***Neurobiology of Aging***. https://doi.org/10.1016/j.neurobiolaging.2010.05.027.

Jayadev, Ranjay, and David R. Sherwood. 2017. “Basement Membranes.” ***Current Biology***. https://doi.org/10.1016/j.cub.2017.02.006.

Jellinger, Kurt A., and Johannes Attems. 2008. “Prevalence and Impact of Vascular and Alzheimer Pathologies in Lewy Body Disease.” ***Acta Neuropathologica***. https://doi.org/10.1007/s00401-008-0347-5.

Julien, Carl, Cyntia Tremblay, Vincent Émond, Meryem Lebbadi, Norman Salem, David A. Bennett, and Frédéric Calon. 2009. “Sirtuin 1 Reduction Parallels the Accumulation of Tau in Alzheimer Disease.” ***Journal of Neuropathology and Experimental Neurology***. https://doi.org/10.1097/NEN.0b013e3181922348.

Kang, Jie, Hans Georg Lemaire, Axel Unterbeck, J. Michael Salbaum, Colin L. Masters, Karl Heinz Grzeschik, Gerd Multhaup, Konrad Beyreuther, and Benno Müller-Hill. 1987. “The Precursor of Alzheimer’s Disease Amyloid A4 Protein Resembles a Cell-Surface Receptor.” ***Nature***. https://doi.org/10.1038/325733a0.

Katzman, Robert. 1976. “The Prevalence and Malignancy of Alzheimer Disease: A Major Killer.” ***Archives of Neurology***. https://doi.org/10.1001/archneur.1976.00500040001001.

Kelley, Kevin W., Hiromi Nakao-Inoue, Anna V. Molofsky, and Michael C. Oldham. 2018. “Variation among Intact Tissue Samples Reveals the Core Transcriptional Features of Human CNS Cell Classes.” ***Nature Neuroscience***. https://doi.org/10.1038/s41593-018-0216-z.

Kerchner, Geoffrey A., and Tony Wyss-Coray. 2015. ***The Role of Aging in Alzheimer’s Disease***. ***Advances in Geroscience***.

Keren-Shaul, Hadas, Amit Spinrad, Assaf Weiner, Orit Matcovitch-Natan, Raz Dvir-Szternfeld, Tyler K. Ulland, Eyal David, et al. 2017. “A Unique Microglia Type Associated with Restricting Development of Alzheimer’s Disease.” ***Cell***. https://doi.org/10.1016/j.cell.2017.05.018.

Kida, Yujiro, and Michael S. Goligorsky. 2016. “Sirtuins, Cell Senescence, and Vascular Aging.” ***Canadian Journal of Cardiology***. https://doi.org/10.1016/j.cjca.2015.11.022.

Kitchens, Craig S. 2013. “The Consultative Process.” In ***Consultative Hemostasis and***

Thrombosis: Third Edition. https://doi.org/10.1016/B978-1-4557-2296-9.00001-4.

Kivipelto, M., E. L. Helkala, M. P. Laakso, T. Hänninen, M. Hallikainen, K. Alhainen, H. Soininen, J. Tuomilehto, and A. Nissien. 2001. "Midlife Vascular Risk Factors and Alzheimer's Disease in Later Life: Longitudinal, Population Based Study." ***British Medical Journal***. https://doi.org/10.1136/bmj.322.7300.1447.

Klingberg, Anika, Anja Hasenberg, Isis Ludwig-Portugall, Anna Medyukhina, Linda Männ, Alexandra Brenzel, Daniel R. Engel, Marc Thilo Figge, Christian Kurts, and Matthias Gunzer. 2017. "Fully Automated Evaluation of Total Glomerular Number and Capillary Tuft Size in Nephritic Kidneys Using Lightsheet Microscopy." ***Journal of the American Society of Nephrology***. https://doi.org/10.1681/ASN.2016020232.

Krasemann, Susanne, Charlotte Madore, Ron Cialic, Caroline Baufeld, Narghes Calcagno, Rachid El Fatimy, Lien Beckers, et al. 2017. "The TREM2-APOE Pathway Drives the Transcriptional Phenotype of Dysfunctional Microglia in Neurodegenerative Diseases." ***Immunity***. https://doi.org/10.1016/j.immuni.2017.08.008.

Kumar, Rahul, Prasun Chaterjee, Prakash K. Sharma, Abhay K. Singh, Abhishek Gupta, Kamaldeep Gill, Manjari Tripathi, Aparajit B. Dey, and Sharmistha Dey. 2013. "Sirtuin1: A Promising Serum Protein Marker for Early Detection of Alzheimer's Disease." ***PLoS ONE***. https://doi.org/10.1371/journal.pone.0061560.

Lalla, Rakhee, and Gizem Donmez. 2013. "The Role of Sirtuins in Alzheimer's Disease." ***Frontiers in Aging Neuroscience***. https://doi.org/10.3389/fnagi.2013.00016.

Launer, Lenore J., G. Webster Ross, Helen Petrovitch, Kamal Masaki, Dan Foley, Lon R. White, and Richard J. Havlik. 2000. "Midlife Blood Pressure and Dementia: The Honolulu-Asia Aging Study." ***Neurobiology of Aging***. https://doi.org/10.1016/S0197-4580(00)00096-8.

Lee, C. Y.Daniel, and Gary E. Landreth. 2010. "The Role of Microglia in Amyloid Clearance from the AD Brain." ***Journal of Neural Transmission***. https://doi.org/10.1007/s00702-010-0433-4.

Lenhossék, Michael von. 1891. "Zur Kenntnis Der Neuroglia Des Menschlichen Rückenmarkes." ***Verh Anat Ges. 1891;5:193–221***.

Levy, Efrat, Mark D. Carman, Ivan J. Fernandez-Madrid, Michael D. Power, Ivan Lieberburg, Sjoerd G. Van Duinen, Gerard Th A.M. Bots, Willem Luyendijk, and Blas Frangione. 1990. "Mutation of the Alzheimer's Disease Amyloid Gene in Hereditary Cerebral Hemorrhage, Dutch Type." ***Science***. https://doi.org/10.1126/science.2111584.

Lewis, Jada, Eileen McGowan, Julia Rockwood, Heather Melrose, Parimala Nacharaju, Marjon Van Slegtenhorst, Katrina Gwinn-Hardy, et al. 2000. "Neurofibrillary Tangles, Amyotrophy and Progressive Motor Disturbance in Mice Expressing Mutant (P301L)Tau Protein." ***Nature Genetics***. https://doi.org/10.1038/78078.

Li, Yanjun, Yongming Li, Xiaotao Li, Shuang Zhang, Jincheng Zhao, Xiaofeng Zhu, and Guozhong Tian. 2017. "Head Injury as a Risk Factor for Dementia and Alzheimer's Disease: A Systematic Review and Meta-Analysis of 32 Observational Studies." ***PLoS ONE***. https://doi.org/10.1371/journal.pone.0169650.

Liebner, Stefan, Monica Corada, Thorsten Bangsow, Jane Babbage, Andrea Taddei, Cathrin J. Czupalla, Marco Reis, et al. 2008. "Wnt/β-Catenin Signaling Controls Development of the Blood - Brain Barrier." ***Journal of Cell Biology***. https://doi.org/10.1083/jcb.200806024.

Liebner, Stefan, Cathrin J. Czupalla, and Hartwig Wolburg. 2011. "Current Concepts of Blood-Brain Barrier Development." ***International Journal of Developmental Biology***. https://doi.org/10.1387/ijdb.103224sl.

Liebner, Stefan, Rick M. Dijkhuizen, Yvonne Reiss, Karl H. Plate, Dritan Agalliu, and Gabriela Constantin. 2018. "Functional Morphology of the Blood–Brain Barrier in Health and Disease." ***Acta Neuropathologica***. https://doi.org/10.1007/s00401-018-

1815-1.
Liebner, Stefan, and Karl Plate. 2010. “Differentiation of the Brain Vasculature: The Answer Came Blowing by the Wnt.” ***Journal of Angiogenesis Research***. https://doi.org/10.1186/2040-2384-2-1.
Lin, Zhiyong, Viswanath Natesan, Hong Shi, Fei Dong, Daiji Kawanami, Ganapati H. Mahabeleshwar, G. Brandon Atkins, et al. 2010. “Kruppel-like Factor 2 Regulates Endothelial Barrier Function.” ***Arteriosclerosis, Thrombosis, and Vascular Biology***. https://doi.org/10.1161/ATVBAHA.110.211474.
Liu, Li, Valerie Drouet, Jessica W. Wu, Menno P. Witter, Scott A. Small, Catherine Clelland, and Karen Duff. 2012. “Trans-Synaptic Spread of Tau Pathology in Vivo.” ***PLoS ONE***. https://doi.org/10.1371/journal.pone.0031302.
Luchsinger, José A., Ming Xin Tang, Joshua Miller, Ralph Green, and Richard Mayeux. 2007. “Relation of Higher Folate Intake to Lower Risk of Alzheimer Disease in the Elderly.” ***Archives of Neurology***. https://doi.org/10.1001/archneur.64.1.86.
Luft, J. H. 1966. “Fine Structures of Capillary and Endocapillary Layer as Revealed by Ruthenium Red.” ***Federation Proceedings***.
Marco, Luigi Yuri Di, Annalena Venneri, Eszter Farkas, Paul C. Evans, Alberto Marzo, and Alejandro F. Frangi. 2015. “Vascular Dysfunction in the Pathogenesis of Alzheimer’s Disease - A Review of Endothelium-Mediated Mechanisms and Ensuing Vicious Circles.” ***Neurobiology of Disease***. https://doi.org/10.1016/j.nbd.2015.08.014.
Mathiisen, Thomas Misje, Knut Petter Lehre, Niels Christian Danbolt, and Ole Petter Ottersen. 2010. “The Perivascular Astroglial Sheath Provides a Complete Covering of the Brain Microvessels: An Electron Microscopic 3D Reconstruction.” ***GLIA***. https://doi.org/10.1002/glia.20990.
Mathys, Hansruedi, Chinnakkaruppan Adaikkan, Fan Gao, Jennie Z. Young, Elodie Manet, Martin Hemberg, Philip L. De Jager, Richard M. Ransohoff, Aviv Regev, and Li Huei Tsai. 2017. “Temporal Tracking of Microglia Activation in Neurodegeneration at Single-Cell Resolution.” ***Cell Reports***. https://doi.org/10.1016/j.celrep.2017.09.039.
Mathys, Hansruedi, Jose Davila-Velderrain, Zhuyu Peng, Fan Gao, Shahin Mohammadi, Jennie Z. Young, Madhvi Menon, et al. 2019. “Single-Cell Transcriptomic Analysis of Alzheimer’s Disease.” ***Nature***. https://doi.org/10.1038/s41586-019-1195-2.
McCarthy, Ryan C, Yun-Hee Park, and Daniel J Kosman. 2014. “ SAPP Modulates Iron Efflux from Brain Microvascular Endothelial Cells by Stabilizing the Ferrous Iron Exporter Ferroportin .” ***EMBO Reports***. https://doi.org/10.15252/embr.201338064.
McGeer, Patrick L., and Edith G. McGeer. 2013. “The Amyloid Cascade-Inflammatory Hypothesis of Alzheimer Disease: Implications for Therapy.” ***Acta Neuropathologica***. https://doi.org/10.1007/s00401-013-1177-7.
Mesulam, M. M. 1976. “A Horseradish Peroxidase Method for the Identification of the Efferents of Acetyl Cholinesterase Containing Neurons.” ***Journal of Histochemistry and Cytochemistry***. https://doi.org/10.1177/24.12.826585.
Mezzaroba, Leda, Daniela Frizon Alfieri, Andrea Name Colado Simão, and Edna Maria Vissoci Reiche. 2019. “The Role of Zinc, Copper, Manganese and Iron in Neurodegenerative Diseases.” ***NeuroToxicology***. https://doi.org/10.1016/j.neuro.2019.07.007.
Monk, Bethan Alice, and Sarah Jane George. 2015. “The Effect of Ageing on Vascular Smooth Muscle Cell Behaviour - A Mini-Review.” ***Gerontology***. https://doi.org/10.1159/000368576.
Montagne, Axel, Samuel R. Barnes, Melanie D. Sweeney, Matthew R. Halliday, Abhay P. Sagare, Zhen Zhao, Arthur W. Toga, et al. 2015. “Blood-Brain Barrier Breakdown in the Aging Human Hippocampus.” ***Neuron***. https://doi.org/10.1016/j.neuron.2014.12.032.
Montagne, Axel, Daniel A. Nation, Abhay P. Sagare, Giuseppe Barisano, Melanie D.

Sweeney, Ararat Chakhoyan, Maricarmen Pachicano, et al. 2020. “APOE4 Leads to Blood–Brain Barrier Dysfunction Predicting Cognitive Decline.” ***Nature***. https://doi.org/10.1038/s41586-020-2247-3.

Munji, Roeben Nocon, Allison Luen Soung, Geoffrey Aaron Weiner, Fabien Sohet, Bridgette Deanne Semple, Alpa Trivedi, Kayleen Gimlin, et al. 2019. “Profiling the Mouse Brain Endothelial Transcriptome in Health and Disease Models Reveals a Core Blood–Brain Barrier Dysfunction Module.” ***Nature Neuroscience***. https://doi.org/10.1038/s41593-019-0497-x.

Musiek, Erik S., David D. Xiong, and David M. Holtzman. 2015. “Sleep, Circadian Rhythms, and the Pathogenesis of Alzheimer Disease.” ***Experimental & Molecular Medicine***. https://doi.org/10.1038/emm.2014.121.

Muzumdar, Mandar Deepak, Bosiljka Tasic, Kazunari Miyamichi, Ng Li, and Liqun Luo. 2007. “A Global Double-Fluorescent Cre Reporter Mouse.” ***Genesis***. https://doi.org/10.1002/dvg.20335.

Nasrabady, Sara E., Batool Rizvi, James E. Goldman, and Adam M. Brickman. 2018. “White Matter Changes in Alzheimer’s Disease: A Focus on Myelin and Oligodendrocytes.” ***Acta Neuropathologica Communications***. https://doi.org/10.1186/s40478-018-0515-3.

Nation, Daniel A., Melanie D. Sweeney, Axel Montagne, Abhay P. Sagare, Lina M. D’Orazio, Maricarmen Pachicano, Farshid Sepehrband, et al. 2019. “Blood–Brain Barrier Breakdown Is an Early Biomarker of Human Cognitive Dysfunction.” ***Nature Medicine***. https://doi.org/10.1038/s41591-018-0297-y.

Newman, George C., Frank E. Hospod, Clifford S. Patlak, Sean D. Trowbridge, Richard J. Wilke, Mark Fuhrmann, and Keith W. Jones. 2002. “Calcium Compartments in Brain.” ***Journal of Cerebral Blood Flow and Metabolism***. https://doi.org/10.1097/00004647-200204000-00012.

Nguyen, Long N., Dongliang Ma, Guanghou Shui, Peiyan Wong, Amaury Cazenave-Gassiot, Xiaodong Zhang, Markus R. Wenk, Eyleen L.K. Goh, and David L. Silver. 2014. “Mfsd2a Is a Transporter for the Essential Omega-3 Fatty Acid Docosahexaenoic Acid.” ***Nature***. https://doi.org/10.1038/nature13241.

Nichols, Emma, Cassandra E.I. Szoeke, Stein Emil Vollset, Nooshin Abbasi, Foad Abd-Allah, Jemal Abdela, Miloud Taki Eddine Aichour, et al. 2019. “Global, Regional, and National Burden of Alzheimer’s Disease and Other Dementias, 1990–2016: A Systematic Analysis for the Global Burden of Disease Study 2016.” ***The Lancet Neurology***. https://doi.org/10.1016/S1474-4422(18)30403-4.

Nitta, Tekehiro, Masaki Hata, Shimpei Gotoh, Yoshiteru Seo, Hiroyuki Sasaki, Nobuo Hashimoto, Mikio Furuse, and Shoichiro Tsukita. 2003. “Size-Selective Loosening of the Blood-Brain Barrier in Claudin-5-Deficient Mice.” ***Journal of Cell Biology***. https://doi.org/10.1083/jcb.200302070.

O’Brown, Natasha M., Sarah J. Pfau, and Chenghua Gu. 2018. “Bridging Barriers: A Comparative Look at the Blood-Brain Barrier across Organisms.” ***Genes and Development***. https://doi.org/10.1101/gad.309823.117.

Obermeier, Birgit, Richard Daneman, and Richard M. Ransohoff. 2013. “Development, Maintenance and Disruption of the Blood-Brain Barrier.” ***Nature Medicine***. https://doi.org/10.1038/nm.3407.

Orlich, Michael, and Friedemann Kiefer. 2018. “A Qualitative Comparison of Ten Tissue Clearing Techniques.” ***Histology and Histopathology***. https://doi.org/10.14670/HH-11-903.

Orre, Marie, Willem Kamphuis, Lana M. Osborn, Jeroen Melief, Lieneke Kooijman, Inge Huitinga, Jan Klooster, Koen Bossers, and Elly M. Hol. 2014. “Acute Isolation and Transcriptome Characterization of Cortical Astrocytes and Microglia from Young and Aged Mice.” ***Neurobiology of Aging***.

https://doi.org/10.1016/j.neurobiolaging.2013.07.008.
Paloneva, Juha, Tuula Manninen, Grant Christman, Karine Hovanes, Jami Mandelin, Rolf Adolfsson, Marino Bianchin, et al. 2002. “Mutations in Two Genes Encoding Different Subunits of a Receptor Signaling Complex Result in an Identical Disease Phenotype.” ***American Journal of Human Genetics***. https://doi.org/10.1086/342259.
Paolo, Gilbert Di, and Tae Wan Kim. 2011. “Linking Lipids to Alzheimer’s Disease: Cholesterol and Beyond.” ***Nature Reviews Neuroscience***. https://doi.org/10.1038/nrn3012.
Piazza-Gardner, Anna K., Timothy J.B. Gaffud, and Adam E. Barry. 2013. “The Impact of Alcohol on Alzheimer’s Disease: A Systematic Review.” ***Aging and Mental Health***. https://doi.org/10.1080/13607863.2012.742488.
Pike, Christian J. 2017. “Sex and the Development of Alzheimer’s Disease.” ***Journal of Neuroscience Research***. https://doi.org/10.1002/jnr.23827.
Poirier, J., P. Bertrand, J. Poirier, S. Kogan, S. Gauthier, J. Poirier, S. Gauthier, J. Davignon, D. Bouthillier, and J. Davignon. 1993. “Apolipoprotein E Polymorphism and Alzheimer’s Disease.” ***The Lancet***. https://doi.org/10.1016/0140-6736(93)91705-Q.
Porayette, Prashob, Miguel J. Gallego, Maria M. Kaltcheva, Sivan Vadakkadath Meethal, and Craig S. Atwood. 2007. “Amyloid-β Precursor Protein Expression and Modulation in Human Embryonic Stem Cells: A Novel Role for Human Chorionic Gonadotropin.” ***Biochemical and Biophysical Research Communications***. https://doi.org/10.1016/j.bbrc.2007.10.021.
Potente, Michael, Laleh Ghaeni, Danila Baldessari, Raul Mostoslavsky, Lothar Rossig, Franck Dequiedt, Judith Haendeler, et al. 2007. “SIRT1 Controls Endothelial Angiogenic Functions during Vascular Growth.” ***Genes and Development***. https://doi.org/10.1101/gad.435107.
Potente, Michael, and Taija Mäkinen. 2017. “Vascular Heterogeneity and Specialization in Development and Disease.” ***Nature Reviews Molecular Cell Biology***. https://doi.org/10.1038/nrm.2017.36.
Pries, A. R., T. W. Secomb, and P. Gaehtgens. 2000. “The Endothelial Surface Layer.” ***Pflugers Archiv European Journal of Physiology***. https://doi.org/10.1007/s004240000307.
Profaci, Caterina P., Roeben N. Munji, Robert S. Pulido, and Richard Daneman. 2020. “The Blood–Brain Barrier in Health and Disease: Important Unanswered Questions.” ***Journal of Experimental Medicine***. https://doi.org/10.1084/jem.20190062.
Qazi, Talal Jamil, Zhenzhen Quan, Asif Mir, and Hong Qing. 2018. “Epigenetics in Alzheimer’s Disease: Perspective of DNA Methylation.” ***Molecular Neurobiology***. https://doi.org/10.1007/s12035-016-0357-6.
Qiu, Chengxuan, Miia Kivipelto, and Eva Von Strauss. 2009. “Epidemiology of Alzheimer’s Disease: Occurrence, Determinants, and Strategies toward Intervention.” ***Dialogues in Clinical Neuroscience***.
Quon, D., Y. Wang, R. Catalano, J. Marian Scardina, K. Murakami, and B. Cordell. 1991. “Formation of β-Amyloid Protein Deposits in Brains of Transgenic Mice.” ***Nature***. https://doi.org/10.1038/352239a0.
Ramón y Cajal, Santiago. 1911. “Histologie Du Systeme Nerveux de l’homme et Des Vertebres.” ***Paris Maloine***. https://doi.org/10.1109/WiCom.2008.1401.
Reed, Bruce, Sylvia Villeneuve, Wendy Mack, Charles DeCarli, Helena C. Chui, and William Jagust. 2014. “Associations between Serum Cholesterol Levels and Cerebral Amyloidosis.” ***JAMA Neurology***. https://doi.org/10.1001/jamaneurol.2013.5390.
Renier, Nicolas, Zhuhao Wu, David J. Simon, Jing Yang, Pablo Ariel, and Marc Tessier-Lavigne. 2014. “IDISCO: A Simple, Rapid Method to Immunolabel Large Tissue Samples for Volume Imaging.” ***Cell***. https://doi.org/10.1016/j.cell.2014.10.010.

Ricciarelli, Roberta, and Ernesto Fedele. 2017. “The Amyloid Cascade Hypothesis in Alzheimer’s Disease: It’s Time to Change Our Mind.” ***Current Neuropharmacology***. https://doi.org/10.2174/1570159x15666170116143743.

Rouget, C. 1873. “Memoire Sur Le Developpement, La Structure et Les Proprietes Physiologiques Des Capillaries Sanguins et Lymphatiques.” ***Arch. Physiol. Normale Pathol.***

Sagare, Abhay P., Robert D. Bell, Zhen Zhao, Qingyi Ma, Ethan A. Winkler, Anita Ramanathan, and Berislav V. Zlokovic. 2013. “Pericyte Loss Influences Alzheimer-like Neurodegeneration in Mice.” ***Nature Communications***. https://doi.org/10.1038/ncomms3932.

Sajeev, Gautam, Jennifer Weuve, John W. Jackson, Tyler J. VanderWeele, David A. Bennett, Francine Grodstein, and Deborah Blacker. 2016. “Late-Life Cognitive Activity and Dementia: A Systematic Review and Bias Analysis.” ***Epidemiology (Cambridge, Mass.)***.

Sala Frigerio, Carlo, Leen Wolfs, Nicola Fattorelli, Nicola Thrupp, Iryna Voytyuk, Inga Schmidt, Renzo Mancuso, et al. 2019. “The Major Risk Factors for Alzheimer’s Disease: Age, Sex, and Genes Modulate the Microglia Response to Aβ Plaques.” ***Cell Reports***. https://doi.org/10.1016/j.celrep.2019.03.099.

Salmina, Alla B., Yulia K. Komleva, Olga L. Lopatina, and Alexander Birbrair. 2019. “Pericytes in Alzheimer’s Disease: Novel Clues to Cerebral Amyloid Angiopathy Pathogenesis.” In ***Advances in Experimental Medicine and Biology***. https://doi.org/10.1007/978-3-030-16908-4_7.

Sangwung, Panjamaporn, Guangjin Zhou, Lalitha Nayak, E. Ricky Chan, Sandeep Kumar, Dong-Won Kang, Rongli Zhang, et al. 2017. “KLF2 and KLF4 Control Endothelial Identity and Vascular Integrity.” ***JCI Insight***. https://doi.org/10.1172/jci.insight.91700.

Satpute-Krishnan, Prasanna, Joseph A. DeGiorgis, Michael P. Conley, Marcus Jang, and Elaine L. Bearer. 2006. “A Peptide Zipcode Sufficient for Anterograde Transport within Amyloid Precursor Protein.” ***Proceedings of the National Academy of Sciences of the United States of America***. https://doi.org/10.1073/pnas.0607527103.

Saunders, A. M., W. J. Strittmatter, D. Schmechel, P. H. St. George-Hyslop, M. A. Pericak-Vance, S. H. Joo, B. L. Rosi, et al. 1993. “Association of Apolipoprotein E Allele E4 with Late-Onset Familial and Sporadic Alzheimer’s Disease.” ***Neurology***. https://doi.org/10.1212/wnl.43.8.1467.

Schlageter, Kurt E., Peter Molnar, Gregory D. Lapin, and Dennis R. Groothuis. 1999. “Microvessel Organization and Structure in Experimental Brain Tumors: Microvessel Populations with Distinctive Structural and Functional Properties.” ***Microvascular Research***. https://doi.org/10.1006/mvre.1999.2188.

Sekiguchi, Rei, and Kenneth M. Yamada. 2018. “Basement Membranes in Development and Disease.” In ***Current Topics in Developmental Biology***. https://doi.org/10.1016/bs.ctdb.2018.02.005.

Selkoe, Dennis J. 1991. “The Molecular Pathology of Alzheimer’s Disease.” ***Neuron***. https://doi.org/10.1016/0896-6273(91)90052-2.

Selkoe, Dennis J, and John Hardy. 2016. “The Amyloid Hypothesis of Alzheimer’s Disease at 25 Years.” ***EMBO Molecular Medicine***. https://doi.org/10.15252/emmm.201606210.

SenBanerjee, Sucharita, Zhiyong Lin, G. Brandon Atkins, Daniel M. Greif, Ravi M. Rao, Ajay Kumar, Mark W. Feinberg, et al. 2004. “KLF2 Is a Novel Transcriptional Regulator of Endothelial Proinflammatory Activation.” ***Journal of Experimental Medicine***. https://doi.org/10.1084/jem.20031132.

Sengillo, Jesse D., Ethan A. Winkler, Corey T. Walker, John S. Sullivan, Mahlon Johnson, and Berislav V. Zlokovic. 2013. “Deficiency in Mural Vascular Cells Coincides with

Blood-Brain Barrier Disruption in Alzheimer's Disease." ***Brain Pathology***. https://doi.org/10.1111/bpa.12004.

Serrano-Pozo, Alberto, Matthew P. Frosch, Eliezer Masliah, and Bradley T. Hyman. 2011. "Neuropathological Alterations in Alzheimer Disease." ***Cold Spring Harbor Perspectives in Medicine***. https://doi.org/10.1101/cshperspect.a006189.

Sheikh, Bilal N., Sukanya Guhathakurta, Tsz Hong Tsang, Marius Schwabenland, Gina Renschler, Benjamin Herquel, Vivek Bhardwaj, et al. 2020. "Neural Metabolic Imbalance Induced by MOF Dysfunction Triggers Pericyte Activation and Breakdown of Vasculature." ***Nature Cell Biology***. https://doi.org/10.1038/s41556-020-0526-8.

Shi, Haoshen, Yosef Koronyo, Altan Rentsendorj, Giovanna C. Regis, Julia Sheyn, Dieu Trang Fuchs, Andrei A. Kramerov, et al. 2020. "Identification of Early Pericyte Loss and Vascular Amyloidosis in Alzheimer's Disease Retina." ***Acta Neuropathologica***. https://doi.org/10.1007/s00401-020-02134-w.

Shi, Yang, and David M. Holtzman. 2018. "Interplay between Innate Immunity and Alzheimer Disease: APOE and TREM2 in the Spotlight." ***Nature Reviews Immunology***. https://doi.org/10.1038/s41577-018-0051-1.

Shinohara, Mitsuru, Masaya Tachibana, Takahisa Kanekiyo, and Guojun Bu. 2017. "Role of LRP1 in the Pathogenesis of Alzheimer's Disease: Evidence from Clinical and Preclinical Studies." ***Journal of Lipid Research***. https://doi.org/10.1194/jlr.R075796.

Siblerud, Robert, Joachim Mutter, Elaine Moore, Johannes Naumann, and Harald Walach. 2019. "A Hypothesis and Evidence That Mercury May Be an Etiological Factor in Alzheimer's Disease." ***International Journal of Environmental Research and Public Health***. https://doi.org/10.3390/ijerph16245152.

Sims, Rebecca, Matthew Hill, and Julie Williams. 2020. "The Multiplex Model of the Genetics of Alzheimer's Disease." ***Nature Neuroscience***. https://doi.org/10.1038/s41593-020-0599-5.

Snowden, Stuart G., Amera A. Ebshiana, Abdul Hye, Olga Pletnikova, Richard O'Brien, An Yang, Juan Troncoso, Cristina Legido-Quigley, and Madhav Thambisetty. 2019. "Neurotransmitter Imbalance in the Brain and Alzheimer's Disease Pathology." ***Journal of Alzheimer's Disease***. https://doi.org/10.3233/JAD-190577.

Söderholm, Simon, and Claudio Cantù. 2020. "The WNT/B-catenin Dependent Transcription: A Tissue-specific Business." ***Wiley Interdisciplinary Reviews: Systems Biology and Medicine***, e1511.

Starr, John M., Andrew J. Farrall, Paul Armitage, Brian McGurn, and Joanna Wardlaw. 2009. "Blood-Brain Barrier Permeability in Alzheimer's Disease: A Case-Control MRI Study." ***Psychiatry Research - Neuroimaging***. https://doi.org/10.1016/j.pscychresns.2008.04.003.

Stenman, Jan M., Jay Rajagopal, Thomas J. Carroll, Makoto Ishibashi, Jill McMahon, and Andrew P. McMahon. 2008. "Canonical Wnt Signaling Regulates Organ-Specific Assembly and Differentiation of CNS Vasculature." ***Science***. https://doi.org/10.1126/science.1164594.

Stern, L, and R Gautier. 1921. "Recherches Sur Le Liquide Céphalo-Rachidien: I.–Les Rapports Entre Le Liquide Céphalo-Rachidien et La Circulation Sanguine." ***Archives Internationales de Physiologie*** 17 (2): 138–92. https://doi.org/10.3109/13813452109146211.

Strittmatter, Warren J., Ann M. Saunders, Donald Schmechel, Margaret Pericak-Vance, Jan Enghild, Guy S. Salvesen, and Allen D. Roses. 1993. "Apolipoprotein E: High-Avidity Binding to β-Amyloid and Increased Frequency of Type 4 Allele in Late-Onset Familial Alzheimer Disease." ***Proceedings of the National Academy of Sciences of the United States of America***. https://doi.org/10.1073/pnas.90.5.1977.

Summers, William Koopmans, Lawrence Victor Majovski, Gary Martin Marsh, Kenneth

Tachiki, and Arthur Kling. 1986. “Oral Tetrahydroaminoacridine in Long-Term Treatment of Senile Dementia, Alzheimer Type.” ***New England Journal of Medicine***. https://doi.org/10.1056/NEJM198611133152001.

Sweeney, Melanie D., Zhen Zhao, Axel Montagne, Amy R. Nelson, and Berislav V. Zlokovic. 2019. “Blood-Brain Barrier: From Physiology to Disease and Back.” ***Physiological Reviews***. https://doi.org/10.1152/physrev.00050.2017.

Tarbell, J. M., and L. M. Cancel. 2016. “The Glycocalyx and Its Significance in Human Medicine.” ***Journal of Internal Medicine***. https://doi.org/10.1111/joim.12465.

Vanlandewijck, Michael, Liqun He, Maarja Andaloussi Mäe, Johanna Andrae, Koji Ando, Francesca Del Gaudio, Khayrun Nahar, et al. 2018. “A Molecular Atlas of Cell Types and Zonation in the Brain Vasculature.” ***Nature***. https://doi.org/10.1038/nature25739.

Vico Varela, Eva, Guillaume Etter, and Sylvain Williams. 2019. “Excitatory-Inhibitory Imbalance in Alzheimer’s Disease and Therapeutic Significance.” ***Neurobiology of Disease***. https://doi.org/10.1016/j.nbd.2019.04.010.

Wang, Jun, Ben J. Gu, Colin L. Masters, and Yan Jiang Wang. 2017. “A Systemic View of Alzheimer Disease - Insights from Amyloid-β Metabolism beyond the Brain.” ***Nature Reviews Neurology***. https://doi.org/10.1038/nrneurol.2017.111.

Wang, Xia Fei, Dong Xin Liu, Yue Liang, Li Li Xing, Wen Hui Zhao, Xiao Xue Qin, De Shu Shang, et al. 2016. “Cystatin C Shifts APP Processing from Amyloid-β Production towards Non-Amyloidgenic Pathway in Brain Endothelial Cells.” ***PLoS ONE***. https://doi.org/10.1371/journal.pone.0161093.

Wang, Yingdi, Masanori Nakayama, Mara E. Pitulescu, Tim S. Schmidt, Magdalena L. Bochenek, Akira Sakakibara, Susanne Adams, et al. 2010. “Ephrin-B2 Controls VEGF-Induced Angiogenesis and Lymphangiogenesis.” ***Nature***. https://doi.org/10.1038/nature09002.

Wattendorff, A. R., G. Th A.M. Bots, L. N. Went, and L. J. Endtz. 1982. “Familial Cerebral Amyloid Angiopathy Presenting as Recurrent Cerebral Haemorrhage.” ***Journal of the Neurological Sciences***. https://doi.org/10.1016/0022-510X(82)90094-6.

Whitehouse, Peter J., Donald L. Price, Arthur W. Clark, Joseph T. Coyle, and Mahlon R. DeLong. 1981. “Alzheimer Disease: Evidence for Selective Loss of Cholinergic Neurons in the Nucleus Basalis.” ***Annals of Neurology***. https://doi.org/10.1002/ana.410100203.

Wijesuriya, Hasini C., Jocelyn Y. Bullock, Richard L.M. Faull, Stephen B. Hladky, and Margery A. Barrand. 2010. “ABC Efflux Transporters in Brain Vasculature of Alzheimer’s Subjects.” ***Brain Research***. https://doi.org/10.1016/j.brainres.2010.08.034.

Wilhelm, Imola, Ádám Nyúl-Tóth, Maria Suciu, Anca Hermenean, and István A. Krizbai. 2016. “Heterogeneity of the Blood-Brain Barrier.” ***Tissue Barriers***. https://doi.org/10.1080/21688370.2016.1143544.

Willem, Michael, Alistair N. Garratt, Bozidar Novak, Martin Citron, Steve Kaufmann, Andrea Rittger, Bart DeStrooper, Paul Saftig, Carmen Birchmeier, and Christian Haass. 2006. “Control of Peripheral Nerve Myelination by the β-Secretase BACE1.” ***Science***. https://doi.org/10.1126/science.1132341.

Willem, Michael, Sabina Tahirovic, Marc Aurel Busche, Saak V. Ovsepian, Magda Chafai, Scherazad Kootar, Daniel Hornburg, et al. 2015. “σ-Secretase Processing of APP Inhibits Neuronal Activity in the Hippocampus.” ***Nature***. https://doi.org/10.1038/nature14864.

Wingo, Thomas S., James J. Lah, Allan I. Levey, and David J. Cutler. 2012. “Autosomal Recessive Causes Likely in Early-Onset Alzheimer Disease.” ***Archives of Neurology***. https://doi.org/10.1001/archneurol.2011.221.

Winkler, Lars, Rosel Blasig, Olga Breitkreuz-Korff, Philipp Berndt, Sophie Dithmer, Hans C.

Helms, Dmytro Puchkov, et al. 2020. “Tight Junctions in the Blood–Brain Barrier Promote Edema Formation and Infarct Size in Stroke – Ambivalent Effects of Sealing Proteins.” ***Journal of Cerebral Blood Flow and Metabolism***. https://doi.org/10.1177/0271678X20904687.

Wong, Siew Ying, and Bor Luen Tang. 2016. “SIRT1 as a Therapeutic Target for Alzheimer’s Disease.” ***Reviews in the Neurosciences***. https://doi.org/10.1515/revneuro-2016-0023.

Xia, Xian, Quanlong Jiang, Joseph McDermott, and Jing Dong J. Han. 2018. “Aging and Alzheimer’s Disease: Comparison and Associations from Molecular to System Level.” ***Aging Cell***. https://doi.org/10.1111/acel.12802.

Xu, F., A. M. Grande, J. K. Robinson, M. L. Previti, M. Vasek, J. Davis, and W. E. Van Nostrand. 2007. “Early-Onset Subicular Microvascular Amyloid and Neuroinflammation Correlate with Behavioral Deficits in Vasculotropic Mutant Amyloid β-Protein Precursor Transgenic Mice.” ***Neuroscience***. https://doi.org/10.1016/j.neuroscience.2007.01.043.

Xu, Xianglai, Brian Wang, Changhong Ren, Jiangnan Hu, David A. Greenberg, Tianxiang Chen, Liping Xie, and Kunlin Jin. 2018. “Age-Related Impairment of Vascular Structure and Functions.” ***Aging and Disease***. https://doi.org/10.14336/ad.2017.0430.

Yankner, Bruce A., Lawrence K. Duffy, and Daniel A. Kirschner. 1990. “Neurotrophic and Neurotoxic Effects of Amyloid β Protein: Reversal by Tachykinin Neuropeptides.” ***Science***. https://doi.org/10.1126/science.2218531.

Yazdani, Samaneh, Javier R. Jaldin-Fincati, Rafaela V.S. Pereira, and Amira Klip. 2019. “Endothelial Cell Barriers: Transport of Molecules between Blood and Tissues.” ***Traffic***. https://doi.org/10.1111/tra.12645.

Yuan, Sarah Y., and Robert R. Rigor. 2011. “Regulation of Endothelial Barrier Function.” ***Colloquium Series on Integrated Systems Physiology: From Molecule to Function***. https://doi.org/10.4199/c00025ed1v01y201101isp013.

Zenaro, Elena, Gennj Piacentino, and Gabriela Constantin. 2017. “The Blood-Brain Barrier in Alzheimer’s Disease.” ***Neurobiology of Disease***. https://doi.org/10.1016/j.nbd.2016.07.007.

Zenaro, Elena, Enrica Pietronigro, Vittorina Della Bianca, Gennj Piacentino, Laura Marongiu, Simona Budui, Ermanna Turano, et al. 2015. “Neutrophils Promote Alzheimer’s Disease-like Pathology and Cognitive Decline via LFA-1 Integrin.” ***Nature Medicine***. https://doi.org/10.1038/nm.3913.

Zhang, Y., K. Chen, S. A. Sloan, M. L. Bennett, A. R. Scholze, S. O’Keeffe, H. P. Phatnani, et al. 2014. “An RNA-Sequencing Transcriptome and Splicing Database of Glia, Neurons, and Vascular Cells of the Cerebral Cortex.” ***Journal of Neuroscience***. https://doi.org/10.1523/JNEUROSCI.1860-14.2014.

Zhao, Zhen, Amy R. Nelson, Christer Betsholtz, and Berislav V. Zlokovic. 2015. “Establishment and Dysfunction of the Blood-Brain Barrier.” ***Cell***. https://doi.org/10.1016/j.cell.2015.10.067.

Zhong, Li, Ying Xu, Rengong Zhuo, Tingting Wang, Kai Wang, Ruizhi Huang, Daxin Wang, et al. 2019. “Soluble TREM2 Ameliorates Pathological Phenotypes by Modulating Microglial Functions in an Alzheimer’s Disease Model.” ***Nature Communications***. https://doi.org/10.1038/s41467-019-09118-9.

Zhou, Yingyue, Wilbur M. Song, Prabhakar S. Andhey, Amanda Swain, Tyler Levy, Kelly R. Miller, Pietro L. Poliani, et al. 2020. “Human and Mouse Single-Nucleus Transcriptomics Reveal TREM2-Dependent and TREM2-Independent Cellular Responses in Alzheimer’s Disease.” ***Nature Medicine***. https://doi.org/10.1038/s41591-019-0695-9.

Zhou, Yulian, and Jeremy Nathans. 2014. “Gpr124 Controls CNS Angiogenesis and Blood-

Brain Barrier Integrity by Promoting Ligand-Specific Canonical Wnt Signaling." ***Developmental Cell***. https://doi.org/10.1016/j.devcel.2014.08.018.

Zhou, Yulian, Yanshu Wang, Max Tischfield, John Williams, Philip M. Smallwood, Amir Rattner, Makoto M. Taketo, and Jeremy Nathans. 2014. "Canonical WNT Signaling Components in Vascular Development and Barrier Formation." ***Journal of Clinical Investigation***. https://doi.org/10.1172/JCI76431.

Zimmermann, K. W. 1923. "Der Feinere Bau Der Blutcapillaren." ***Zeitschrift Für Anatomie Und Entwicklungsgeschichte***. https://doi.org/10.1007/bf02593544.

Zipser, B. D., C. E. Johanson, L. Gonzalez, T. M. Berzin, R. Tavares, C. M. Hulette, M. P. Vitek, V. Hovanesian, and E. G. Stopa. 2007. "Microvascular Injury and Blood-Brain Barrier Leakage in Alzheimer's Disease." ***Neurobiology of Aging***. https://doi.org/10.1016/j.neurobiolaging.2006.05.016.

Zlokovic, Berislav V. 2005. "Neurovascular Mechanisms of Alzheimer's Neurodegeneration." ***Trends in Neurosciences***. https://doi.org/10.1016/j.tins.2005.02.001.

8. Appendix

8.1. List of abbreviations

Alzheimer's disease (AD) • AD heterozygous (Het) • AD homozygous (Hom) • amyloid precursor protein (APP) • amyloid-β (Aβ) • astrocytes (ACs) • basement membrane (BM) • blood-brain barrier (BBB) • cell adhesion molecule (CAM) • central nervous system (CNS) • cerebral amyloid angiopathy (CAA) • cerebrospinal fluid (CSF) • dentate gyrus (DG) • docosahexaenoic acid (DHA) • endothelial cells (ECs) • ethylcinnamate (Eci) • fibroblasts (FBs) • gain of function (GOF) • genome-wide association studies (GWAS) • housekeeping (HK) • immunofluorescence (IF) • immunohistochemistry (IHC) • knockdown (KD) • lysophosphatidylcholine (LPC) • magnetic resonance imaging (MRI) • Massive Analysis of cDNA Ends (MACE-Seq) • microglia (MG) • microvessel buffer (MVB) • mouse brain microvessels (MBMVs) • mural cells (MuCs) • neuro-vascular unit (NVU) • neuronal (N) • oligodendrocytes (OLs) • pericytes (PCs) • peripheral nervous system (PNS) • positron emission tomography (PET) • quantitative polymerase-chain-reaction (qPCR) • retinoic acid (RA) • smooth muscle cells (SMCs) • sonic hedgehog (Shh) • standard error of the mean (SEM) • tags per million (TPM) • venous SMC (vSMCs) • wild type (WT)

8.2. Materials

8.2.1. Instruments

Table 16: List of instruments

Instrument	Type	Provider
Autoclave	V-150	Systec
Automated IHC stainer	BOND III	Leica
Bacterial incubator	Heraeus function line B12	Kendro Laboratory Products
Binocular microscope	Nikon SMZ 1500	Nikon Instruments
Burrowing test tubes		Self-made according to official directions
Centrifuge	5415 D	Eppendorf
Centrifuge	Labofuge 400	Heraeus instruments
Centrifuge	Labofuge 400 R	Heraeus instruments
Confocal laser scanning microscope	Eclipse TE 2000-E	Nikon Instruments
Cryotom	Ultracut UCT	Leica

Dounce homogenizer	0.025 mm clearance	Wheaton
Eppendorf research	Pipettes	Eppendorf
Flow cytometer (cell sorter)	FACS Aria™	BD© Biosciences
Fluorescence microscope	Microscope ECLIPSE 80i	Nikon Instruments
Freezer –20°C	Comfort	Liebherr
Freezer –80°C	HERAfreeze™ HFU	Thermo Fisher
Heating plate	Drying plate 12895	Medax
Holten horizontal laminar airflow (semi-sterile hood)	Clean bench 1.2	Thermo Fisher
Incubator	HERA cell 150	Thermo Electron Corporation
Light sheet microscope	UltraMicroscope II	LaVision
Liquid Nitrogen storage	CryoCon AFT-3L	Taylor Wharton
Live cell microscope	Eclipse Ti	Nikon Instruments
Live cell set-up		Okolab
Microscope Cover Glasses		MARIENFELD
Microscope slides	SUPERFROST® PLUS	Thermo SCIENTIFIC
Mictrotome	HM550	Microm
Microwave	R-208	Sharp
Mouse Y-maze		Self-made according to official directions
Nestlets	14010	Plexx
Overhead electric stirrer	VOS14	VWR
pH-meter	WTW series	Inolab®
Plate reader	Tecan reader infinite M200	Tecan
qRT-PCR machine	C1000™ Thermal Cycler CFX96™ Real-Time System	BIO-RAD
Refrigerator (4°C)	Premium	Liebherr
RNA & DNA measurer	Qubit™ 4 Fluorometer	Life technologies
Sequencing machine	Nextseq 500	Illumina
Rocking shaker	Duomax 1030	Heidolph
Safety Cabinet	Hera Safe KS Class II	Thermo Electron Corporation
Scale	Scout Pro 2000 g	Ohaus
Shaker	Promax 1020	Heidolph
Special accuracy weighing scale	TE 313S-DS	Sartorius
Stereomicroscope	SMZ745	Nikon
Thermocycler	Robocycler® GRADIENT 96	STRATAGENE®
Vortexer	Vortex-Genie 2	Scientific Industries
Waterbath	TW12	Julabo

8.2.2. Software

Table 17: Software list

Software	Provider
Affinity designer 1.7.2	Serif (Europe) Ltd. The Software Centre Wilford Industrial Estate Nottingham, NG11 7EP
Affinity photo 1.8.3	Serif (Europe) Ltd. The Software Centre Wilford Industrial Estate Nottingham, NG11 7EP
FlowJo FACS analysis 8.8.7	FlowJo, LLC
GraphPad Prism 6	GraphPad Software
ImageJ	Public domain
Imaris 9	BitPlane (Switzerland)
Mendeley desktop	Mendeley, Ltd.
Microsoft Office 2011	Microsoft Deutschland GmbH
NIS-Elements Microscope Imaging Software AR	Nikon Instruments
R studio 0.99.892	RStudio, Inc.

8.2.3. Consumables

Table 18: Consumables list

Consumables	Reference	Provider
1 kb ladder	15015-016	Invitrogen
100 bp ladder	15628-050	Invitrogen
Agarose	A9539	Sigma-Aldrich
Aqua Poly/Mount	18606	Polysciences
BES (N,N-bis(2-hydroxyethyl)-2-aminoethanesulfonic acid) (2x)	A1062.0100	AppliChem GmbH
BSA	8076.5	Carl Roth
$CaCl_2$	A3652	AppliChem
Corn Oil	C8267	Sigma-Aldrich
DAPI for FACS	10236276001	Sigma-Aldrich
DEPC	K028.1	Carl Roth
Dichlormethane	270997-100ML	Sigma-Aldrich
Dimethyl sulphoxide (DMSO)	4720.4	Carl Roth
1,4-Dithiothreitol (DTT)	10 197 777 001	Roche
D-Luciferin	102111	PJK GmbH
DMEM+GlutaMAX™ supplement	10566016	Gibco Invitrogen
DPBS	14190-094	Gibco Invitrogen
dNTPs [10mM]	18427-013	Gibco Invitrogen
EDTA	A3553	AppliChem
Endothelial cell growth serum (ECGS)	-	Self made
Ethanol	459836	Sigma-Aldrich
Ethylcinnamate	112372	Sigma-Aldrich
EZ-Link Sulfo-NHS-LC-Biotin	21335	Thermo Scientific
FACS-tubes	352054	Falcon
FACS sorting collection tubes	72.692.005	Sarstedt

FACS strainer (50 μm)	340604	Becton Dickinson
FBS	S0115	Biochrom
FITC 70 kD-dextran	46945	Sigma-Aldrich
FITC 4 kD-dextran	46944	Sigma-Aldrich
Fluorescein 70 kD-dextran lysine fixable	D1822	Life-technogies
FuGENE® 6 Transfection Reagent	11814443001	Roche Applied Biosciences
Gelatin from bovine skin	G9391	Sigma-Aldrich
Glucose	5996-10-1	Riedel-de Haen
Halt™ Protease & Phosphatase Inhibitor Cocktail (100 x)	1861281	Thermo Scientific
Heparin	H4784	Sigma-Aldrich
KCl	A1164	AppliChem
Ketavet	B1830-12	Pfizer
L-Glutamine	G7513	Sigma-Aldrich
LB-agar	X969.1	Carl Roth
LB-medium	X968.1	Carl Roth
Low melt agarose	6351.5	Carl Roth
MCDB131 medium	10372-019	Gibco
Mesh 40 μm (nylon)	352340	Corning
Mesh 100 μm (nylon)	352360	Corning
Methanol	67-56-1	Fisher Scientific
Methoxy-X04	ab142818	Abcam
Microvette® 500 µl, K3 EDTA (plasma collection)	20.1341.100	Sarstedt
Midori^{Green} Advance	MG04	NIPPON Genetics
Multiwell-culture-plate	CELLSTAR. 6-well-plate	GBO
NaCl	3957	Roth
Sodium bicarbonate ($NaHCO_3$)	27778.293	VWR Chemicals
Sodium phosphate dibasic (Na_2HPO_4)	7558794	Sigma-Aldrich
Nuclear Green LCS1	ab138904	Abcam
O.C.T. Compound	4583	Sakura
OPTI-MEM® serum-free media	31985	Invitrogen
PBS	10010-023	Gibco Invitrogen
PCR-tubes	Sprout™	Kisker
Penicillin / Streptavidin	P4333	Sigma-Aldrich
PFA	252549-1L	Sigma-Aldrich
Recombinant Murine Wnt-3a	315-20	PeproTech Inc.
RNase H	10786349001	Roche
Rompun 2 %	ICP06BW1	Bayer
Serum separating tubes	41.500.005	Sarstedt
SDS	4360.1	Roth
SOC-medium	15544-034	Invitrogen
Sterile butterfly 21Gx3/4”	85.1638.235	Sarstedt
Sucrose	4621.1	Carl Roth
SYBR Green Fluorescein Mix	AB-1219/B	Thermo Scientific

Syringe 1ml 25Gx5/8”	SS+01T25161	Terumo
Syringe no dead volume 1ml 29Gx1/2”	BS-N1H2913	Terumo
TAMOXIFEN FREE BASE	156738	MP Biomedicals
TMR 3 kD-dextran lysine fixable	1838004	Molecular Probes
TMR 20 kD-dextran	73766	Sigma-Aldrich
Tomato-lectin (488)	DL-1174	Vector Laboratories
Tomato-lectin (649)	DL-1178	Vector Laboratories
Triton-X100	T8787	Sigma-Aldrich
Trypsin	T4049	Sigma-Aldrich
Whatman paper		Schleicher-Schuell

8.2.4. Buffers and solutions

Table 19: buffers and solutions list

Buffer	Composition
Antibody incubation buffer (pH 7.2)	• BSA 0.5 % • Triton-X 100 0.25 % • ad PBS 100 ml
BES buffer 2x	• BES (N,N-bis(2-hydroxyethyl)-2-aminoethanesulfonic acid) 50mM • NaCl 280mM • Sodium phosphate buffer (pH 6.95) 1.5mM • UltraPure™ DNase/RNase-free distilled water up to 80 ml
Buffer A (pH 7.4)	• NaCl 153 mM • KCl 5.6 mM • $CaCl_2$ 1.7 mM • $MgCl_2$ 1.2 mM • HEPES 15 mM • BSA 10 g • ad $dH_2$01000 ml
FACS buffer	• PBS • FCS 5%
Firefly buffer	• Glycylglycin 25 mM • K2HPO4 (pH = 8:0) 25 mM • EGTA 4mM • ATP 2 mM • DTT 1 mM • $MgSO_4$ • $7H_2O$ 15 mM • CoA 0.1 mM • D-Luciferin 75 μM
HEK293 complete medium	• DMEM-GlutaMAX™ supplement (500 ml) • Sera Plus (10%) • P/S (1%)

HEK293 transient transfection solution	• $CaCl_2$ 1 M • Sodium phosphate buffer (pH 6.95) 0.1 M • BES buffer 2x
HES buffer	• HEPES 10 mM • EDTA 1 mM • Sucrose 250 mM
MCDB131 complete medium (50ml)	• MCDB131 medium 37,5 ml • FBS 10 ml • L-Glutamine 0.5 ml • Penicillin / Streptavidin 0.5 ml • 1 % Heparin 0.5 ml • ECGS 0.5 ml • $NaHCO_3$ 0.5 ml
MV buffer (1 x; pH 7.4)	• HEPES 15 mM; pH 7.4 • NaCl 147 mM • KCl 4 mM • BSA 0.5% • Glucose 5 mM • $CaCl_2$ 3 mM • ad dH_20 / DEPC-Water
PBS 20x (2l)	• NaCl: 327,2 g • KCl: 8,0 g • Na_2HPO_4 (x2 H_20): 71,2 g • KH_2PO_4: 9,8 g
Permeabilization / blocking buffer (pH 7.4-7.6)	• BSA 1 % • Triton-X 100 0.5 % • ad PBS 100 ml
PFA	• 4% PFA • 5% 20x PBS • ad dH_20, pH=7.4
Renilla buffer	• NaCl 1.1 M • Na_2-EDTA 2.2 mM • KH_2PO_4 (pH 5.1) 220 mM • BSA 0.44 mg/ml • NaN_3 1.3 mM • Coelenterazine 1.43 μM
Tail lysis buffer	• 50 mM KCL • 1.5 mM MgCl2 • 10 mM Tris • 0.15% NP-40 • 0.45% Tween20 • ad dH_20, pH=8
10x TBE buffer	• 0.89 M Tris Base • 0.89 M boric acid • 0.01 EDTA • pH=8

8.2.5.Antibody lists

Table 20: IF antibody list

Antibody	Host	Company	Catalog	Dilution	Fixation
Anti-CD31	Rat	BD Pharmingen	553370	1:100	PFA
Anti-Erg	Rabbit	Abcam	Ab92513	1:500	PFA
Anti-rabbit DyLight 550	Donkey	Thermo Fisher Scientific	SA5-10039	1:500	PFA/metOH
Anti-rat DyLight 650	Donkey	Thermo Fisher Scientific	SA5-10029	1:500	PFA/metOH

Table 21: FACS antibody list

Target	Conjugate	Clone	Company	Catalog	Dilution
ACSA2	APC	IH3-18A3	Miltenyi Biotec	130-102-315	1:50
CD11b	BV510	M1/70	BD Bioscience	562950	1:100
CD45	PerCp-Cy5.5	30-F11	eBioscience	45-0451-82	1:100
NG2	PE	1E6.4	Miltenyi Biotec	130-097-458	1:20
Pdgfrb	APC-Vio-770	REA634	Miltenyi Biotec	130-109-870	1:25
VE-Cad	PE-Cy7	BV13	Bio Legend	138016	1:50

8.2.6. Primer lists

Table 22: PCR primer list for genotyping

Primer	Sense	Antisense
β-catenin Ex3 (fl)	5'- GAC ACC GCT GCG TGG ACA ATG -3'	5'- GTG GCT GAC AGC AGC TTT TCT -3'
β-catenin no Ex3	5'- GCT GCG TGG ACA ATG GCT AC -3'	5'- TGA GCC CTA GTC ATT GCA TAC -3'
APP^{SwDI}	5'- AGG ACT GAC CAC TCG ACC AG -3'	5'- CGG GGG TCT AGT TCT GCA T -3'

Table 23: qPCR primer list

Primer	5' to 3' (sense)	3' to 5' (antisense)
Pttg1	5'- AAC AGC CGA CCT TGA CTG GGA -3'	5'- GGG TCA TGA GAG GCA CGC CAT -3'
Rplp0	5'- CTT TGG TCG CTC GCT CCT C -3'	5'- CTG ACC GGG TTG GTT TTG AT -3'
Sirt1	5'- CCA GAC CTC CCA GAC CCT CAA -3'	5'- TGA CAC AGA GAC GGC TGG AAC T -3'

8.2.7. Kits

Table 24: Kits list

Kit	Reference	Provider
ZR-Duet™ DNA/RNA MiniPrep	D7001	Zymo Research
Plasmid maxi kit	12162	Qiagen
Qubit® dsDNA BR Assay Kit	Q32850	Thermo Scientific
Qubit® dsDNA HS Assay Kit	Q32851	Thermo Scientific
Qubit® RNA BR Assay Kit	Q10210	Thermo Scientific
Qubit® RNA HS Assay Kit	Q32852	Thermo Scientific
RevertAid H Minus First Strand cDNA Synthesis Kit	K1632	Thermo Scientific
RNeasy Micro Kit	74004	Qiagen
RNeasy Mini Kit	74106	Qiagen
RNeasy Plus Micro kit (50)	74034	Qiagen

8.2.8. Plasmids

Table 25: plasmids list

Plasmid	Backbone	Provider
hDKK2-flag	pCS2	Addgene
Hygromycin	pTRE2	Clontech
Hygromycin-GFP	pTRE2	Clontech
M50 Super 8x TOP-FLASH	pTA-Luc	Randall Moon
M51 Super 8x FOP-FLASH	pTA-Luc	Randall Moon
SIRT1-FL	pcDNA 3.1	Addgene
SIRT1-ShRNA	pLKO.1	T. Braun
SIRT1-ControlShRNA	pLKO.1 puro	D. Shulter
TK-Renilla	pRL	Promega
Viral envelope	pMD2.G	S. Liebner
Viral packaging	psPAX2	S. Liebner

8.2.9. Enzymes

Table 26: enzymes list

Enzyme	Reference	Provider
Collagenase II	C2-28	Biochrom
Collagenase/Dispase	10269638001	Roche
DNase I	LS006333	Worthington
Papain	LS003126	Worthington

8.2.10. Mammalian cell lines

Table 27: mammalian cell lines list

Cell line	Info	Source
bEnd5	Mouse brain EC inmortalized	S. Liebner
HEK293T	Human embryonic kidney cells	ATCC®
MBE	Mouse brain EC inmortalized	S. Liebner

8.2.11. Bacterial strains

Table 28: bacterial strains list

Bacterial strain	Info	Reference	Source
DH5α	***E. coli, standard***		S. Liebner
Stbl3	***E. coli, for unstable DNA cloning***	C7373-03	Invitrogen

8.4. Declaration and author's declaration

Declaration

I herewith declare that I have not previously participated in any doctoral examination procedure in a mathematics or natural science discipline.

Frankfurt am Main, 17.12.2020

Author's declaration

I herewith declare that I have produced my doctoral dissertation on the topic of

The role of the blood-brain barrier in a mouse model of Alzheimer's disease

independently and using only the tools indicated therein. In particular, all references borrowed from external sources are clearly acknowledged and identified.

I confirm that I have respected the principles of good scientific practice and have not made use of the services of any commercial agency in respect of my doctorate.

Frankfurt am Main, 17.12.2020